

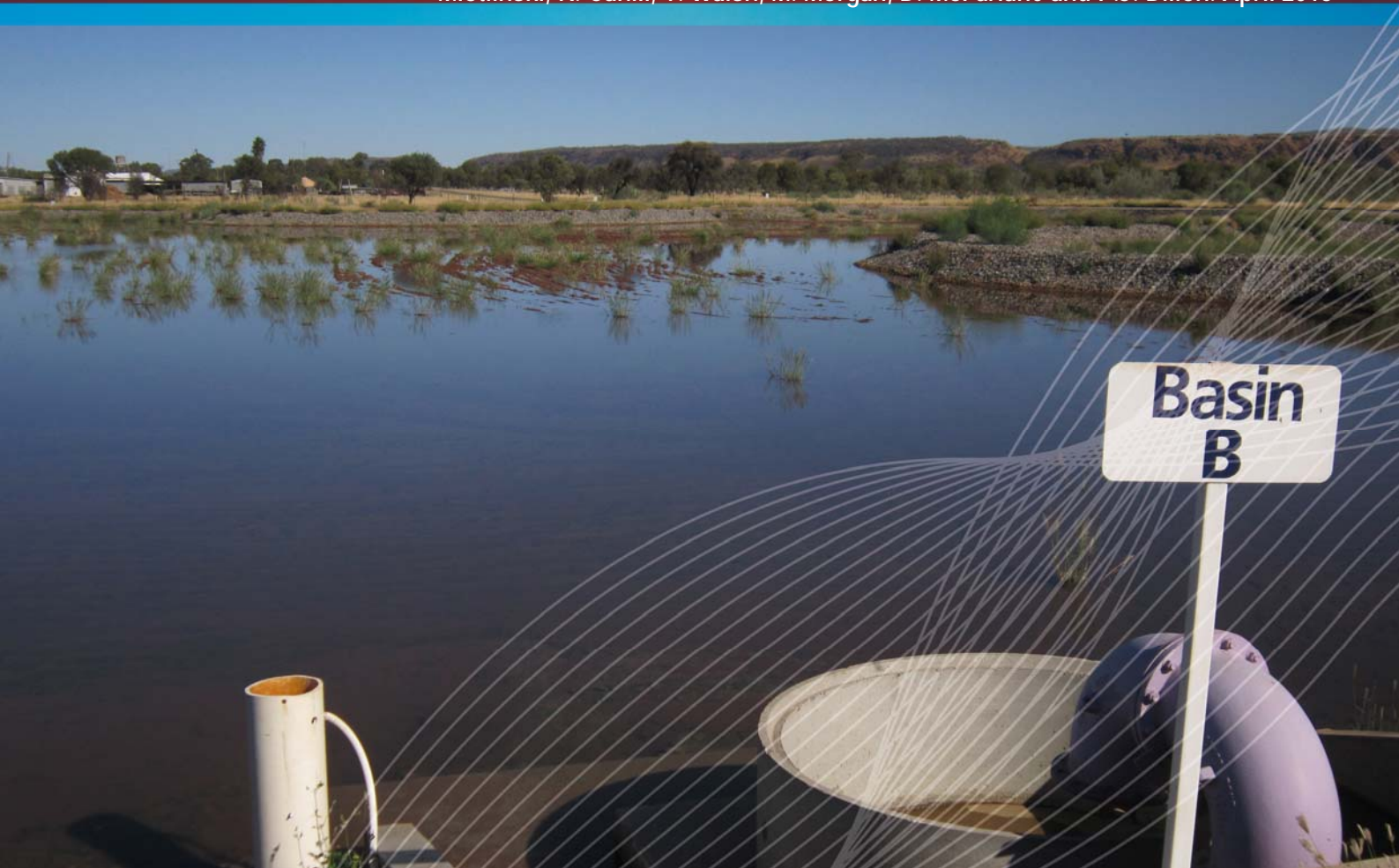
Australian Water Recycling
Centre of Excellence



Managed Aquifer Recharge and Recycling Options: Understanding clogging processes and water quality impacts

A report of a study funded by the
Australian Water Recycling Centre of Excellence

E.B. Bekele, M.J. Donn, K.E. Barry, J.L. Vanderzalm, A.H. Kaksonen, G.J. Puzon, J. Wylie, K. Miotlinski, K. Cahill, T. Walsh, M. Morgan, D. McFarlane and P.J. Dillon. April 2015



Managed Aquifer Recharge and Recycling Options (MARRO)

Project Leader

Joanne Vanderzalm
CSIRO Land and Water
PMB2
Waite Road
Urrbrae SA 5064 AUSTRALIA
Telephone: +61 8303 8505
Report Contact: Elise Bekele

Joanne.Vanderzalm@csiro.au
Elise.Bekele@csiro.au

Citation

Bekele, E.B., Donn, M.J., Barry, K.E., Vanderzalm, J.L., Kaksonen, A.H., Puzon, G.J., Wylie, J., Miotlinski, K., Cahill, K., Walsh, T., Morgan, M., McFarlane, D. and Dillon, P.J. (2015). Managed Aquifer Recharge and Recycling Options (MARRO): Understanding clogging processes and water quality impacts, Australian Water Recycling Centre of Excellence, Brisbane, Australia.

Partners

CSIRO Land and Water
Power Water Corporation
Water Corporation
City West Water
Barwon Water

About the Australian Water Recycling Centre of Excellence

The mission of the Australian Water Recycling Centre of Excellence is to enhance management and use of water recycling through industry partnerships, build capacity and capability within the recycled water industry, and promote water recycling as a socially, environmentally and economically sustainable option for future water security.

The Australian Government has provided \$20 million to the Centre through its National Urban Water and Desalination Plan to support applied research and development projects which meet water recycling challenges for Australia's irrigation, urban development, food processing, heavy industry and water utility sectors. This funding has levered an additional \$40 million investment from more than 80 private and public organisations, in Australia and overseas.

ISBN 978-1-922202-44-4

© Australian Water Recycling Centre of Excellence

This work is copyright. Apart from any use permitted under the Copyright Act 1968, no part of it may be reproduced by any purpose without the written permission from the publisher. Requests and inquiries concerning reproduction right should be directed to the publisher.

Date of publication: April 2015

Publisher:

Australian Water Recycling Centre of Excellence
Level 5, 200 Creek Street, Brisbane, Queensland 4000
www.australianwaterrecycling.com.au

This report was funded by the Australian Water Recycling Centre of Excellence through the Australian Government's National Urban Water and Desalination Plan.

Disclaimer

Use of information contained in this report is at the user's risk. While every effort has been made to ensure the accuracy of that information, the Australian Water Recycling Centre of Excellence does not make any claim, express or implied, regarding it.

Cover Photograph

Description: Soil Aquifer Treatment Basin (Basin B) after filling phase, in 2012.

Photographer: Mike Donn, CSIRO.

Contents

Contents	i
Figures	iii
Tables	ix
Glossary	x
Acknowledgments	xii
Executive summary	xiii
Introduction	1
Floreat Infiltration Galleries	2
Site description	2
Sequence of development	4
MAR system configuration	6
Methods	7
Soil column infiltration experiments	7
Floreat field experiment	11
Results – Soil column infiltration experiments	13
Secondary treated wastewater	13
Filtered secondary treated wastewater	14
Extended duration with filtered secondary treated wastewater	17
Results – Floreat field experiment	23
Cumulative inflow of wastewater to the Floreat site	23
Groundwater levels, infiltration gallery water levels and soil moisture	23
Modelling of soil water retention characteristics	26
HYDRUS model of wastewater Infiltration	30
Geochemistry	34
Microbial communities	40
Floreat summary	42
Clogging	42
Groundwater quality	43
Microbial communities	43
Recommendations	44
Alice Springs Soil Aquifer Treatment	45
Site description	46
Sequence of development	47
MAR system configuration	49
Methods	50

Infiltration rates	50
Soil compaction tests	50
Soil sampling and characterisation.....	51
Geophysical survey	54
Thermal probes	55
Water quality.....	56
SAT Basin operation	58
Influence of drying time	58
Hydraulic performance	61
Thermal Fluxes.....	66
Recharge water quality.....	68
Soil and groundwater characterisation	76
Compaction tests.....	76
Basin soil profiles.....	78
Soil carbon and nitrogen	82
Microbial communities	84
Schmutzdecke characterisation and microbial communities	84
Geophysical characterisation	88
Groundwater quality and level response.....	91
Alice Springs summary	97
Clogging	97
Groundwater quality	97
Microbial communities.....	97
Recommendations	98
References.....	99
Appendix 1 Floreat experimental plan as executed	104
Appendix 2 Floreat MAR site installation and dismantling.....	112
Appendix 3 Soil water retention characterisation of Spearwood Sand for the Floreat MAR site.....	124
Appendix 4 Appearance of SAT basins over time	127
Appendix 5 Guidance of SAT Basin operation (Breton 2009).....	129
Appendix 6 Geophysics results SAT basins	130

Figures

Figure 1 Location map showing the geomorphology and soils of the Swan Coastal Plain (after McArthur and Bettenay, 1974) and the CSIRO Infiltration site in Floreat, Western Australia.	3
Figure 2 Daily rainfall and evaporation at the Subiaco STP (Source: SILO patched point data courtesy of the Queensland Department of Environment and Resource Management and the Australian Bureau of Meteorology).	4
Figure 3 The Floreat MAR site showing the location of the new infiltration gallery, the former (defunct) galleries from a previous study, and monitoring wells that were sampled and used to infer the direction of groundwater flow. There were not enough bores between MB1 and FLGRND1 to delineate groundwater flow paths between these bores; however, groundwater flow to the west was determined at the MAR site using the bores labelled MB and BH.	5
Figure 4 Schematic of column setup showing the 60 cm of Spearwood Sand, and the locations of tensiometers and breather holes for (a) pre-clogging showing water introduction through a flow diffuser and (b) post-clogging showing the constant head conditions (40 cm) imposed and (c) the PVC columns.	9
Figure 5 Infiltration rate test with synthetic wastewater in Spearwood Sand columns (left) matrix potential measured under saturation conditions prior to application of synthetic wastewater and (centre-right) changes in matrix potential during the unsaturated experiment (following column draining) with step changes in application rate (indicated at the top). The location of the tensiometers is given in cm below the top of the soil.	11
Figure 6 Locations of water level logging within the infiltration gallery. The diagram on the right (not to scale) shows the design of the PVC tubes used to monitor water levels in the gallery. Geofabric (not shown) was used to cover the top and sides of the gallery to lessen the opportunity for roots to grow into the gallery.	12
Figure 7 Infiltration of secondary treated wastewater from the Subiaco wastewater treatment plant in Spearwood Sand columns (left) matrix potential measured at saturation, and (centre-right) changes in matrix potential upon the application of wastewater at 5 m/d.	14
Figure 8 Infiltration of filtered secondary treated wastewater from the Subiaco sewage treatment plant in Spearwood Sand columns matrix potential measured at saturation (a – column A, c – column B), and changes in matrix potential upon the application of filtered treated wastewater at 5 m/d (b – column A, d – column B).	16
Figure 9 Filtered secondary treated wastewater column effluent flow rates (a) and comparison of column influent and effluent (b) pH, (c) electrical conductivity (EC), (d) total dissolved nitrogen (TDN), and (e) dissolved organic carbon (DOC) for columns A and B.	17
Figure 10 Effluent flow rate for columns A and B following infiltration of recycled water through Spearwood Sand columns, showing initial rates of 5 m/d and the effect of clogging on flow rates and soil matrix potential measured at 2, 5 and 10 cm below the soil surface. A constant head of water (40 cm above the soil surface) was applied following the observance of ponding of the recycled water.	18
Figure 11 Recycled water and column effluent physio-chemical characteristics (a) electrical conductivity (EC) and calculated total dissolved solids, (b) pH and (c) total suspended solids. The legend for (a) also applies to (b). The column effluent flow rates are shown for comparison.	19
Figure 12 Accumulation of suspended solids (TSS) and cumulative effluent following recycled water infiltration. Non-measured TSS and flow data interpolated between measurements.	20
Figure 13 Nutrient concentrations in influent recycled water and column effluent.	21
Figure 14 Comparison of soil moisture data from the a) North, b) Middle, c) South and d) Offset probes at the CSIRO infiltration gallery site. Note the frequent interruptions of wastewater flow until late December due to equipment problems at the Subiaco STP, and absence of 15 cm soil moisture data at the North probe location due to sensor malfunction.	24
Figure 15 Groundwater measured in the monitoring bores. FLBGRND1 is located farthest from the MAR site (177 m northeast of the site).	25

Figure 16 Level of wastewater in the gallery monitored in the three PVC wells. Elevation of gallery base was 12.10-12.19 m AHD.	25
Figure 17 Soil moisture retention function for Spearwood Sand sampled from the zone through which wastewater infiltrated. The van Genuchten model was fitted using RETC software.	27
Figure 18 Soil moisture retention data and the van Genuchten model for Spearwood Sand based on data from Vermooten (2002), representing initial conditions at the infiltration site prior to any wastewater infiltration (dashed line). The model of post-experiment data from Figure 17(solid line) is plotted for comparison.	29
Figure 19 Unsaturated hydraulic conductivity predicted by the van Genuchten-Mualem model with HYDRUS.	29
Figure 20 Finite element mesh for the HYDRUS flow model through a cross-section of the gallery from 0 to 7 m below ground level. The close-up view shows the six observation points for examining model output that correspond to the approximate locations of soil moisture probes.	30
Figure 21 Predicted distribution of soil water contents for the cross-section model on Days 10 and Day 14.	31
Figure 22 Close-up view of model output at several times, showing a predicted time series of soil water content from the HYDRUS model. Superimposed on the model results are point measurements. Note, MAR commenced on Day 6.	31
Figure 23 Comparison of HYDRUS model results and observed data from soil moisture probes. The hydraulic model is based on soil hydraulic properties derived from the analysis of soil moisture retention data from Vermooten (2002) for Perth, Western Australia.	33
Figure 24 Comparison of Hydrus model results and observed data from monitoring the Offset probe located 5 cm below the base of the gallery. Soil moisture retention data to underpin the hydraulic model were obtained by analysing Spearwood samples collected from the Floreat MAR site, post-experiment.	34
Figure 25 Piper diagram illustrating the transition in major ion chemistry (shown by arrow) in the groundwater down-gradient of the infiltration gallery (MB2) from ambient groundwater (FLBGRND1, FLBGRND2, MB1) toward the infiltration gallery source water (Influent WW).	36
Figure 26 (a) Chloride, (b) potassium, (c) calcium, (d) dissolved organic carbon (DOC), (e) nitrate-N, and (f) total suspended solids concentrations in the infiltration gallery source water (Influent WW), groundwater down-gradient from the infiltration gallery (MB2) and ambient groundwater (FLBGRND1, FLBGRND2, MB1).	37
Figure 27 Fluorescence excitation-emission matrices (EEMs) of dissolved organic carbon for: groundwater sampled from the background bores (FLBGRND1 and FLBGRND2), up-gradient monitoring bore (MB1), down-gradient monitoring bore (MB2) and influent recycled water (Source Water), where A = humic-like, C = humic- and fulvic-like, T1 and T2 = typtophan-like fluorescence. The colours represent the fluorescence intensity expressed in Raman units. Note the different fluorescence intensity scales are used to enable comparison of samples. The white areas mask the Rayleigh scatter peaks of water.	39
Figure 28 Relative abundance (mean) of selected bacterial families present in the filtered Subiaco wastewater and pre-infiltration and post-infiltration soil samples taken from the Floreat infiltration gallery. Error bars represent one standard deviation.	41
Figure 29 Soil Aquifer Treatment System infiltrating water to an unconfined aquifer (MAR Guidelines NRMCC-EPHC-NHMRC 2009).	45
Figure 30 Location of the Alice Springs SAT scheme.	46
Figure 31 Daily Rainfall and evaporation at the Alice Springs Airport, Bureau of Meteorology Station #15590.	47
Figure 32 SAT basin RB1 during filling on 22 July 2009.	48
Figure 33 Expansion of old recharge basins 1, 2, 3, 4, 5 (highlighted), into basins A, B, C, D, E.	49
Figure 34 Sampling locations for geotechnical study. Nuclear densometer tests were done at locations: 4C in Basin A; 1, 2, 3 in Basin B; 5, 5A, and 5B in Basin C; 6A, 6B and 7 in Basin D; and	

8, 9, ZA, ZB and ZC in Basin E. Cone penetrometers tests were done at locations 5, 5A, 5B in Basin B; 6C, 6D, 6E in Basin C and DCP1, DCP2, DCP3 in Basin E (Source: Alice Materials Testing).	51
Figure 35 Overview of soil sampling, instrument locations and near basin monitoring bores used throughout the study.	54
Figure 36 Geophysical survey locations November 2013 and August 2014; black circles represent NanoTEM quadrants in 2013 and black squares represent NanoTEM quadrants in 2014. The red line represents DC Resistivity run in 2013 and repeated in 2014.	55
Figure 37 Stream A of Alice Springs Waste Stabilisation Ponds.	57
Figure 38 Relationship between infiltration rate and drying time for Basins A and C.	59
Figure 39 Relationship between infiltration rate and drying time for Basins D and E.	59
Figure 40 Relationship between infiltration rate and wetting time for Basins A and C.	60
Figure 41 Relationship between infiltration rate and wetting time for Basins D and E.	60
Figure 42 Total volume of water released to the SAT system in its history (Jun 2008- Sep 2014).	61
Figure 43 Volumes of recharge water released to the individual basins from October 2011 to September 2014. Interruptions in inflow for all basins relate to treatment plant stoppages (August 2013, November 2013) and loss of data (March 2014). Additional interruptions in inflow for Basin B represent periods when the basin was not in use.	62
Figure 44 Infiltration rates and lengths of drying and wetting cycles in Basin A.	63
Figure 45 Infiltration rates and lengths of drying and wetting cycles in Basin B.	64
Figure 46 Infiltration rates and lengths of drying and wetting cycles in Basin C.	64
Figure 47 Infiltration rates and lengths of drying and wetting cycles in Basin D.	65
Figure 48 Infiltration rates and lengths of drying and wetting cycles in Basin E.	65
Figure 49 Overall flux comparison at T2 (Basin A) (Gunatunge 2014). The grey shaded area denote recharge events.	67
Figure 50 Overall flux comparison at T6 (Basin E) (Gunatunge 2014). The grey shaded area denote recharge events.	68
Figure 52 Water quality of recharge water sampled at the SAT site. The vertical dashed line marks the WRP upgrade to DAFF treatment in September 2013.	70
Figure 53 Fluorescence excitation-emission matrices (EEMs) of dissolved organic carbon during wastewater treatment for: sewer inlet (Saa001), facultative pond AN2/3 (Saa010), maturation pond A2 (Saa025), maturation pond A4 (Saa030), DAFF source water (Saa040) and SAT source water (Sar080) sampled in September 2014, where A = humic-like, C = humic- and fulvic-like, T1 and T2 = typtophan-like fluorescence. The colours represent the fluorescence intensity expressed in Raman units. Note the different fluorescence intensity scales are used to enable comparison of samples. The white areas mask the Rayleigh scatter peaks of water.	75
Figure 54 Dynamic cone penetrometers results for Basin D (6C, 6D, 6E), C (5, 5A, and 5B) and E (DCP1, DCP2, DCP3) (Source: Alice Materials Testing).	77
Figure 55 Average soil moisture to 1.5 m depth in basin A and D and at locations BA, C18 and D12 from samples collected in 2014.	79
Figure 56 Soil texture previously determined by Costean Trench (C1-C24) (Knapton and Lennartz 2005).	80
Figure 57 Comparisons of organic carbon (OrgC), calcium carbonate (CaCO ₃) and total nitrogen (Total N) in the top 2.5 cm layer over three successive years.	82
Figure 58 Nitrogen species (NO ₃ -N and NH ₄ -N) determined on KCl soil extracts from soil profiles beneath the basins. An average of multiple samples is presented for Basins A and E and individual profiles for Basins B, C and D (locations BA, C18 and D12).	83

Figure 59 a) Accumulated matter near inlet of basin; and b) dried schmutzdecke on surface of basin.....	86
Figure 60 SEM image of schmutzdecke from Basin A (location A_5) indicating the presence of iron oxyhydroxide and organic material.	86
Figure 61 SEM image of schmutzdecke from Basin A (location A_5) indicating the presence of quartz and organic material.....	87
Figure 62 SEM image of accumulated algal material from the inlet of Basin A.....	88
Figure 63 Groundwater flow beneath Basins A and E interpreted from time-domain EM (NanoTEM).....	89
Figure 64 Interpreted CMD (apparent electromagnetic conductivity) survey results for Basins A, B, C and E at 6-6.5 m depth below basin surface after recent wetting (week prior) August 2014. The black line shows the location of the resistivity transect and this line represents the location of high resistivity at surface and at 10 m depth. The blue line represents groundwater flow which occurs at a depth of ~20m. The arrow represents a possible flow direction based on lower conductivities on Lines 1000, 3000 and the resistivity transect and the interpolated groundwater hydraulic gradient.	90
Figure 65 Resistivity transect across Basins E and D.	90
Figure 66 Salinity (EC) in groundwater monitoring bores in response to SAT operation.	92
Figure 67 Chloride concentrations in groundwater monitoring bores in response to SAT operation.	92
Figure 68 Nitrate-N and concentrations in groundwater monitoring bores in response to SAT operation.	93
Figure 69 Dissolved organic carbon (DOC) concentrations in groundwater monitoring bores in response to SAT operation.	93
Figure 70 Fluorescence excitation-emission matrices (EEMs) of dissolved organic carbon in groundwater for: RN17938 (600 m up-gradient), RN17936 (1000 m down-gradient), RN17947 (on site) and RN17942 (200 m down-gradient) sampled in June 2014, where A = humic-like, C = humic- and fulvic-like, T1 and T2 = typtophan-like fluorescence. The colours represent the fluorescence intensity expressed in Raman units. Note the different fluorescence intensity scales are used to enable comparison of samples. The white areas mask the Rayleigh scatter peaks of water.....	94
Figure 71 Average annual stable isotopes of water in groundwater sampled from April 2008 to December 2014 compared to the recharge water (AZRI SAR100) and the meteoric water line.....	95
Figure 72 Groundwater levels (mAHD) of monitoring bores up-gradient from the SAT basin operation.	95
Figure 73 Groundwater levels (mAHD) of monitoring bores down-gradient from the SAT basin operation.	96
Figure 74 Groundwater levels (mAHD) of open hole monitoring bores next to Basin B and in Basin C during SAT operation.....	96
Figure 75 Schematic of proposed installation of six Atlantis Flo-Tank® modules. The dimensions of the linear gallery are approximately 4.0 m by 0.4 m. Vertical slices taken along the long dimension of the gallery will be used for HYDRUS modelling.....	109
Figure 76 Cross-section view of an Atlantis Flo-Tank® modules below the ground surface depicting the excavation depth and details for the placement of geofabric.....	109
Figure 77 Plan view of the field installation at CSIRO relative and the connection to Subiaco STP.	110
Figure 78 Cross-section view depicting the placement of soil moisture probes relative to the base of the gallery. For the probes directly under the gallery, the lateral distances relative to the edge of the gallery are approximate and varied (~2 to 4 cm) for the North, Middle and South sets of probes and the three depths.	111

Figure 79 ARKAL manual disc filter showing mode of filtration (Source: NETAFIM™, http://www.netafimusa.com/landscape/products/disc-filters-tech).	112
Figure 80 Trench excavation for the infiltration gallery (top) and assembly of the reticulated system for dispersing treated wastewater within the Atlantis Flo-Tank® modules (bottom).	113
Figure 81 Close up view of the south end of the gallery, showing the inflow poly pipe connecting to three sections of poly pipe, each approximately 10 cm apart. This photo was taken before the 42 Netafim drippers were inserted and shows the gallery upside down. Three lengths of poly pipe pass laterally through incisions in the partitions within the Atlantis® modules and are terminated at the distal end of the gallery (4m to the north). The pipes were cable-tied to the top panels on the underside of the tanks.	113
Figure 82 Arrangement of Netafim™ pressure-compensating drippers within the Atlantis Flo-Tank® modules. The image shows the placement of drippers relative to the internal partitions within each of the 6 tanks that were assembled.	114
Figure 83 Locations where microbial samples were collected prior to MAR.	114
Figure 84 Locations of water level logging within the infiltration gallery. The diagram on the right (not to scale) shows the design of the PVC tubes used to monitor water levels in the gallery. Geofabric (not shown) was used to cover the top and upper few cm of the gallery to lessen the opportunity for roots to grow into the gallery.	115
Figure 85 Michael Donn standing on a spare Atlantis® plate to distribute his weight while installing the soil moisture probes below the intended base level of the gallery. The foot plates indicate the approximate location of the gallery relative to the sensors. He is standing at a depth of 105 cm below ground. Small temporary trenches were used to insert the probes laterally from the sidewall by first augering a hole using a small piece of PVC tubing (shown on the left) and which were then backfilled. Soil moisture probes at 5 cm, 15 cm and 40 cm below base level were installed at slightly offset positions to avoid side-wall collapse.	116
Figure 86 Placement of South, Middle and North soil moisture probes buried below the base level of the gallery with logging cables extending to the ground surface. The cables connect to a Campbell logger in a weather-proof box. Offset Probes # 12, 10 and 11 located 45, 55 and 65 cm, respectively west of the gallery were installed by augering at an angle to depths of 110, 120 and 145 cm, respectively below ground at roughly the position marked in the photo.	116
Figure 87 Close up view of charred material observed while developing the trench for the infiltration gallery.	117
Figure 88 Sand removed from the trench during installation of the infiltration gallery.	117
Figure 89 Backfilled site on 17-September 2013, showing the skid-mounted control system that regulates flow to the gallery. The PVC tubes for monitoring water levels are shown in the foreground. The tensiometers failed to provide reliable results once installed and are no longer being monitored. The grass has been allowed to grow back over the surface.	118
Figure 90 Photo of the excavated surface of the infiltration gallery and a close up of the roots embedded in the geofabric.	119
Figure 91 View of crate 1 (numbered consecutively with respect to the south end of the gallery).	120
Figure 92 View of the soil layer below one of the crates.	120
Figure 93 Root mat sample collected for microbial analysis.	121
Figure 94 Discolouring or mottled appearance of soil below the gallery.	121
Figure 95 Variations in soil moisture content observed during excavation to remove the gallery.	122
Figure 96 Dye-stained surface showing darker coloured soil due to organic debris and fairly uniform (matrix) flow in the vertical direction.	122
Figure 97 Close-up view of the dye-stained profile looking south, following application of dye to the base of the gallery. Note the movement of dye laterally away to the east.	123

Figure 98 Basin E after the first infiltration event in 2012 showing a) the recharge water inlet and a pipe where the pressure transducer is installed and b) a black substance on the soil attributed to the presence of a water treatment polymer (photo 23/10/2012).	127
Figure 99 The inlet and pipes distributing recharge water in Basin A, which is covered with self-seeding Love Grass (<i>Eragrostis spectabilis</i>) (photo 23/10/2012).	127
Figure 100 Vegetation in Basin D a) ~1.5 m high woody vegetation in July 2013 and b) spreading vegetation with channels forming in between for water flow in November 2013.	127
Figure 101 Basin B vegetation cover a) July 2013 b) November 2013.	128
Figure 102 Best bed surface. Bare dry soil to 3 cm depth – deep cracking (Breton 2009).	129
Figure 103 Acceptable bed surface. Bare dry soil to 3 cm depth – small cracking – complete crumbling of clogging layer to brownish thin material (Breton 2009).	129
Figure 104 Tolerable bed surface. Bare dry soil to 3 cm depth – complete crumbling of clogging layer to flaky thin greenish material (Breton 2009).	129
Figure 105 Inadequate bed surface. Inefficient cracking – thick white greenish algae with fibrous texture that do not break down or crumble during drying period and cover most of the basin area – soil moist for extended periods (Breton 2009).	129
Figure 106 2013 Basin A (line 1000) 3 x 20m NanoTEM stations.	130
Figure 107 2013 Basin E (line 2000) 4 x 20m NanoTEM stations.	131
Figure 108 2013 Basin C (line 4000) 2 x 20m and 3 x 10m NanoTEM stations.	132
Figure 109 2014 Basin A (line 1000) 10 x 10m NanoTEM stations.	133
Figure 110 2014 Basin B (line 2000) 9 x 10m NanoTEM stations.	134
Figure 111 2014 Basin D (line 3000) 5 x 10m NanoTEM stations.	135
Figure 112 2014 Basin E (line 4000) 10 x 10m NanoTEM stations.	136
Figure 113 2014 approximately 500m down-gradient, near bore RN17999 (line 5000) 7 x 20m NanoTEM stations.	137
Figure 114 Map of project monitoring bores and locations of down-gradient NanoTEM surve.	138

Tables

Table 1 Subiaco secondary treated wastewater water quality (Jan 2009 to Feb 2012). All parameters in mg/L except pH (-) and EC (mS/m) and are based on weekly measurements.	6
Table 2 Description of water monitoring bores.	12
Table 3 Total microbial cell abundance in Spearwood Sand before (virgin soil) and after infiltration of wastewater (Column A and B)	22
Table 4 Infiltration gallery source water quality (October 2013-March 2014). Source water is secondary effluent from Subiaco Sewage Treatment Plant with addition filtration. All parameters in mg/L except pH (-) and EC (μ S/cm).....	35
Table 5 Performance of four recharge basins operating in 2008 and 2009 and average/total performance of the SAT site.	48
Table 6 Summary of soil sampling events and equipment installation undertaken at the Alice Springs SAT site.	52
Table 7 Sample locations in Alice Springs Reclamation Plant used to evaluate nutrient reactivity.	56
Table 8 Analysis suite to evaluate nutrient reactivity.	56
Table 9 Summary of infiltration rate, drying time and wetting time (average \pm standard deviation) for basins based on source water treatment (DAF or DAFF). Basin B with DAF treated source water was not included due to the impact of soil compaction on infiltration rate.	58
Table 10 Water quality for raw wastewater and source water for SAT basins.	71
Table 11 Water quality for wastewater train A1.	72
Table 12 Water quality for wastewater train A2.	73
Table 13 Density ratio (%) determined at various depths for locations in Figure 34 (Source: Alice Materials Testing).....	76
Table 14 Average basin bulk density at 0 – 5 cm and water content at 0 – 2.5 cm depth for samples collected July 2012 and July-August 2013.	78
Table 15 Soil texture variability in Basin A.	81
Table 16 Soil texture variability in Basin E.	81
Table 17 Relative change in paleochannel groundwater levels (Δ m) measured from before start of infiltration in June 2007 to September 2013.	96
Table 18 Inflow rates for supplying recycled water to the Atlantis Flo-Tank [®] modules calculated based on the surface area of the gallery base and the target infiltration rate.....	107
Table 19 Bulk density and soil moisture retention characteristics for Spearwood Sand samples collected from the Floreat Infiltration Gallery site. Soil analyses were conducted by the University of Western Australia.	124
Table 20 Summary of statistical P values from performing paired Student’s t-test on groups of soil moisture retention characteristics from fourteen sampled locations at the Floreat infiltration gallery site, post-experiment. Abbreviations: G=Gallery; N=North; S=South; Adj=Adjacent; depth intervals relative to the base of the gallery.	126

Glossary

ADWG	Australian Drinking Water Guidelines; undergoes rolling revision to ensure it represents the latest scientific evidence on good quality drinking water.
Anammox	Anaerobic ammonium oxidation.
ANZECC	Australian and New Zealand Environment Conservation Council
<i>Archaea</i>	A phylogenetic domain of prokaryotes distinct from <i>Bacteria</i> .
Atlantis Flo-Tank® module	A modular tank constructed of recycled polypropylene with a void space of over 90% that is buried below ground and used to enhance the percolation of water (e.g. stormwater, recycled water) into the subsurface. A single tank has dimensions (L x H x W) of 685 mm x 450 mm x 408 mm).
aquifer	A geological formation or group of formations capable of receiving, storing and transmitting significant quantities of water. Aquifer types include confined, unconfined and artesian.
<i>Bacteria</i>	A phylogenetic domain of prokaryotes distinct from <i>Archaea</i> .
BGL	Below ground level.
bore	"bore" means a bore, hole, well, excavation or other opening in the ground, or a natural or artificially constructed or improved underground cavity, which is or could be used for the purpose of intercepting, collecting, obtaining or using groundwater or for the purpose of disposing of water or waste below the surface of the ground, or which extends to an aquifer.
chemoorganotroph	An organism that depends on organic chemicals for its energy and carbon.
CSIRO	Commonwealth Scientific and Industrial Research Organisation
disinfection	The process designed to kill most microorganisms, including essentially all pathogenic bacteria. There are several ways to disinfect; chlorine is most frequently used in water treatment.
DNA	Deoxyribonucleic acid
EC	Electrical conductivity
eukaryote	A cell or organism having a unit membrane-enclosed nucleus and usually other organelles.
irrigation	Provision of sufficient water for the growth of crops, lawns, parks and gardens; can be by flood, furrow, drip, sprinkler or subsurface water application to soil.
labile organic carbon	Fraction of organic carbon that is easily biodegradable.
managed aquifer recharge (MAR)	The intentional recharge of water to aquifers for subsequent recovery or environmental benefit.
mid infrared (MIR)	Mid infrared spectrometry, which can be used to analyse soil properties.
monitoring	Systematically keeping track of something, including sampling or collecting and documenting information.
pathogen	A disease-causing organism (e.g. bacteria, viruses, protozoa).
pre-treatment	Any treatment (e.g. detention, filtration) that improves the quality of water before injection.

prokaryote	A cell or organism lacking a nucleus and other membrane-enclosed organelles, usually having its DNA in a single circular chromosome. Prokaryotes can be divided into <i>Bacteria</i> and <i>Archaea</i> .
quality	The totality of characteristics of an entity that bear on its ability to satisfy stated and implied needs; the term 'quality' should not be used to express a degree of excellence.
recycled water	Water generated from sewage, grey water or stormwater systems and treated to a standard that is appropriate for its intended use.
retention basin	A stormwater management basin that captures storm water runoff and does not discharge directly to a surface water body. The water is "discharged" by infiltration or evaporation.
reuse	Using water that would otherwise be discharged to wastewater or stormwater systems, for domestic, commercial, agricultural or industrial purposes.
salinity	The presence of soluble salts in soil or water. Electrical conductivity and total dissolved salts are measures of salinity.
SAT	Soil aquifer treatment, a MAR technique involving water passing through both soil and an aquifer which combines their treatment compared with direct aquifer injection.
schmutzdecke	Over a slow sand filter, the reddish-brown sticky coating formed on top of the sand, consisting of micro-organisms, partly decomposed organic matter, iron, manganese, aluminium and silica.
sewage or wastewater	Material collected from internal household and other building drains; includes faecal waste and urine from toilets, shower and bath water, laundry water and kitchen water.
soak well	An innovation which collects rain water from a dwelling roof or impermeable ground area via storm water piping and enables it to infiltrate into the soil. They are typically made of concrete, polypropylene, PVC or plastic and may be found with or without concrete pavers or lids to resist pressure from above.
source water	The water pumped or fed by gravity into a managed aquifer recharge scheme.
turbidity	The cloudiness of water caused by the presence of fine suspended matter.
water recycling	A generic term for water reclamation and reuse. Can also describe a specific type of reuse where water is recycled and used again for the same purpose (e.g. recirculating systems for washing and cooling), with or without treatment in between.

Acknowledgments

The work described in this report was supported by the Australian Water Recycling Centre of Excellence, CSIRO Land and Water Flagship, Power Water Corporation, Water Corporation, City West Water and Barwon Water. The assistance of Chris Higgs, Pippa Hepburn, Craig MacDonald, Simon Adams, Pardeep Kumar, Ray Trinder and Stefan Leutenegger (all with the Water Corporation), David George, Will Cormack, Kathleen Hocking, Jordan Phasey and Ganesh Sharma (Power Water Corporation) and Bob Williams (NT Government) are sincerely appreciated in providing information and advice and in facilitating sampling and analyses. The authors gratefully acknowledge the assistance of T. Lambert of the CSIRO in the collection of field data, S. Leiva and H. Urriola of Atlantis Corporation for donating Atlantis Flo-Tank® modules and geofabric for the Floreat infiltration gallery and J. Shaw and S. Wright of CHS Engineering for their technical advice and services contracted to install and commission equipment for the MAR experiment. Advisory Committee Members, Warren Traves, Judy Blackbeard, Chris Hertle, Ed Hauck and John Radcliffe have also provided valuable advice over the course of the project, which is gratefully acknowledged.

Executive summary

Australia has tremendous potential for supplementing groundwater resources using managed aquifer recharge (MAR), the practice of intentionally recharging aquifers under controlled conditions. Highly porous surface and shallow sub-surface sedimentary deposits of sand, gravel and limestone comprise a large proportion of the Australian landscape and, if not within a proclaimed public drinking water catchment or protected area for other purposes, could become designated as water treatment catchments via MAR. Infiltration of usually treated wastewater and the consequent decreases in suspended solids, pathogens and nutrients as it travels through the aquifer is akin to large-scale, slow sand filters commonly used in wastewater treatment schemes. The utilisation of sedimentary deposits for MAR is not without technological challenges; for example, the presence of lower permeability, fine-grained sediments, such as silt and clay, interspersed within a host aquifer, and/or limited treatment of wastewater prior to recharge can promote clogging that is detrimental to the infiltration process. Moreover, the potential for clogging in superficial aquifers used for MAR will depend on the system being operated (e.g. infiltration via underground galleries or soil aquifer treatment). Gaining better insight into how clogging develops and how it can be prevented from small-scale field trials should enable future MAR schemes to advance with fewer obstacles.

To further investigate clogging and changes in water quality during MAR, a research project was funded through the Australian Water Recycling Centre of Excellence, CSIRO Land and Water Flagship, Power and Water Corporation (Northern Territory), Water Corporation (Western Australia), City West Water and Barwon Water. The project was divided into two related field investigations to cover the major issues that were initially identified as impediments to MAR on a national scale. The first component focused on MAR via an infiltration gallery located in predominantly medium-grained Aeolian sand deposits typical of the coastal plain of Western Australia at the Floreat Infiltration Gallery site. The second component focused on MAR via soil aquifer treatment (SAT) using recharge basins located within a mixture of fine- and coarse-gradient riverine deposits in Alice Springs, NT. An infiltration gallery is a covered percolation trench that contains a medium or supporting structure with internal void spaces to facilitate infiltration and thus opportunities for passive treatment of water during passage through the unsaturated zone. SAT involves intermittently filling recharge basins with wastewater to allow infiltration into unconfined aquifers. As a result of cycling between wetting and drying periods, the soils beneath the basins are intermittently aerobic and anaerobic, which are conditions that promote biodegradation and thus removal of nutrients, pathogens, some non-aromatic organic chemicals (including polysaccharides and proteins) and trace metals.

In addition to the field studies, experiments using sediment-filled columns were undertaken at the CSIRO laboratories in Floreat and Adelaide. The laboratory columns were intended to allow closer inspection and monitoring of factors leading to clogging of pore spaces using sediments and wastewater representative of field conditions at Floreat and Alice Springs. A numerical model of variable-saturated flow in the vadose zone was developed for the Floreat Infiltration Gallery site using HYDRUS software and soil water retention characteristics to gain insights into observed changes in the soil moisture and hydraulic performance.

The two sets of experimental results, Floreat Infiltration Gallery and Alice Springs Soil Aquifer Treatment, are discussed below followed by a synthesis of conclusions.

The third component of this project, an economic analysis and review of MAR implementation experiences is reported separately as a compendium of case studies of water recycling via the aquifer in Australia (Vanderzalm *et al.* 2015).

Floreat Infiltration Gallery

The research in this component focused on investigating recharge into Spearwood Sand, using an infiltration gallery designed to infiltrate at a high rate, secondary treated wastewater with only additional filtration to reduce total suspended solid levels; assessing changes in the quality of receiving groundwater from passage of the treated wastewater through the unsaturated zone of the

Spearwood Sand and the underlying Tamala Limestone aquifer; and quantifying changes in the water retention characteristics of soil impacted by wastewater and the consequences for vertical migration of wastewater through the soil profile.

The impetus for this research came from a proposal in 2011 to manage water levels in the hydraulically-connected Perry Lakes. It involved infiltration galleries to recharge Spearwood Sand with high volumes of wastewater. Whilst a three-year pilot study conducted at the Floreat Infiltration galleries site demonstrated that a low wastewater application rate of 1 m/d was feasible, groundwater flow modelling for the Perry Lakes proposal indicated higher infiltration rates (3 to 5 m/d) were required to increase lake levels. The sustainability of using high rates of wastewater in infiltration galleries had not been field-tested in a rigorously monitored study, adding uncertainty to future maintenance costs for the Perry Lakes MAR scheme, which ultimately did not proceed. There is also considerable interest in using high wastewater infiltration rates to manage aquifers for other purposes (e.g. prevention of salt water intrusion, managing levels in groundwater connect lakes, and management of existing contaminant plumes) in Perth's superficial aquifers. Other concerns involved with high wastewater application rates are higher rates of nutrient loading and consequences for clogging and the quality of receiving groundwater in MAR schemes. For these reasons, well-documented field studies are needed to provide guidance and confidence in techniques of recharging treated wastewater into sedimentary deposits typical of a large proportion of Australia.

The research outcomes demonstrated that an infiltration gallery constructed of Atlantis Flo-Tank® modules in Spearwood Sand can recharge the aquifer using secondary treated wastewater applied at an average rate of 4 m/d over a 5 month period. A total of 750 kilolitres was recharged to the Tamala Limestone aquifer over this period (average rate of 6.7 kL/d over a surface area of 1.7 m²), but the watertable elevation only changed in response to the seasonal pattern of rainfall instead of MAR due to the highly conductive sand and limestone at this site. In contrast, infiltration experiments conducted using similar wastewater quality and application rates in columns filled with Spearwood Sand led to clogging and significantly reduced effluent outflows from 5 to 0.2 m/d after 3.5 weeks that led to wastewater ponding at the surface. Whilst high rates of recharge to the aquifer were sustained over the entire duration of the field experiment, changes occurred spatially in gallery wastewater levels and soil moisture contents surrounding the gallery after 14 weeks. These observations support the theory that heterogeneous clogging developed locally within the gallery and promoted increased flow of wastewater laterally away from the gallery.

Results from the column experiment relative to the field trial highlight the limitations of relying solely on a one-dimensional interpretation of flow. Whilst effluent outflow from columns may represent vertical flow to the watertable in a MAR experiment, sediment-filled columns with predominantly unidirectional flow produce a high ratio of wastewater to sediment surface area and hence greater opportunity for trapping of particulates, biofilm growth due to presence of light (even at low levels) and ultimately clogging that severely impedes outflow. This approach provides a minimum estimate of the time until clogging becomes problematic for recharge; however, it is not realistic to extrapolate time estimates derived from column experiments to the field. Setting water quality objectives to avoid clogging based on column experiments may be unnecessarily restrictive due to the greater potential for clogging in this setting.

Field trials of MAR using infiltration galleries are also not without drawbacks and present difficulties of extrapolating to a larger scale as demonstrated in the Floreat study: it was difficult to maintain consistent inflows of wastewater due to malfunctioning of the equipment used to supply wastewater to the site and limited resources to address maintenance and equipment problems as they arose. These issues were specific to this trial and are not inherent in operating a gallery. To maintain a fairly consistent level of TSS required bi-weekly, if not more frequent monitoring and maintenance of the filtration equipment. Despite attempts to frequently maintain consistent wastewater inflow and filtration, TSS ranged from <1 to 52 mg/L (average of 8.7 mg/L) during the 5 month experiment. The field trial revealed changes in wastewater levels in the gallery and soil moisture contents surrounding the gallery after a period of higher than average TSS and the installation of a new supply pump. Consistent maintenance of a high ratio of wastewater to sediment surface area over the entire

duration of the experiment, and the presence of sediment spikes, would presumably lead to clogging within a shorter time frame than that observed in the Floreat field trial.

To extrapolate results from the Floreat field trial to new sites for MAR requires several caveats. It is anticipated that a gallery located in sands with similar hydraulic properties with no lateral restrictions to the outflow of wastewater could recharge the aquifer. To ensure satisfactory hydraulic performance, filtration equipment should be frequently monitored to maintain a target level of TSS of 5 mg/L. Based on this study, an infiltration gallery sized similarly and receiving wastewater of similar quality should provide satisfactory hydraulic performance for a minimum of 5 months. This represents a period of operation that is comparable to that of operating infiltration basins, prior to the need for maintenance. Allowing galleries to periodically dry may reduce clogging due to oxidation of organic material. Evaluation of recovery of hydraulic conductivity following drying is recommended to determine if this may prolong the effectiveness of infiltration galleries.

Changes in the quality of receiving groundwater from passage of wastewater through the Spearwood Sand and the underlying Tamala Limestone aquifer were assessed by comparing the concentrations in the treated wastewater entering the infiltration gallery with water sampled from a monitoring bore located 2 m down-gradient and slotted < 2 m below the watertable. Potassium was used as a tracer to estimate the percentage of wastewater (source water) in groundwater sampled from the down-gradient monitoring bore. While potassium is a reasonable marker of wastewater, it is not a conservative tracer to assess initial breakthrough due to cation exchange. The predominant water type in the Tamala Limestone aquifer is Ca-Na-HCO₃-Cl. The infiltration of secondary treated wastewater gradually changed the composition of the receiving groundwater to that of the Na-Cl dominated source water. The proportion of source water in groundwater sampled from down-gradient increased to 100% after approximately 250 kL of wastewater recharge to the Tamala aquifer (after 60 days of the MAR experiment). The reduction in phosphate from passage of wastewater through the subsurface was 100%, whereas the reduction in Dissolved Organic Carbon (DOC) was 69% throughout the MAR trial. Changes in the groundwater concentrations of calcium, alkalinity and phosphorus suggest carbonate dissolution and phosphorus adsorption occurred during MAR.

There was no evidence of nitrate removal. Aerobic conditions in the unsaturated zone and aerobic source water were not conducive to denitrification. An unexpected source of nitrate was discovered up-gradient from the MAR site, which confounded estimates of nitrate removal.

An investigation of spatial variability in soil moisture retention characteristics of Spearwood Sand from the Floreat field site revealed that non-uniform flow characteristics developed at several locations at shallow depths relative to the base of the gallery due to wastewater infiltration over 5 months. The majority of the samples collected below and adjacent to the gallery were not significantly (statistically) different from each other in terms of their soil moisture retention characteristics; therefore, a single hydraulic function was used to represent sand impacted by wastewater infiltration in the HYDRUS model. A different soil moisture characteristic curve was needed for Spearwood Sand unaffected by wastewater as the range of measured soil moisture contents in response to applied suctions was lower. This suggests that passage of wastewater through the sands near the base of the gallery variably added fine material and suspended solids from wastewater, thereby enabling the soil matrix to retain more moisture and lowered hydraulic conductivity affecting the direction of migration pathways for wastewater.

A HYDRUS model based on unaltered Spearwood Sand could not reproduce the soil moisture data for the entire duration of the MAR trial. A steadily increasing discrepancy between modelled and observed soil moistures for the MAR trial was observed and correlated to just after a period of higher than average TSS and the installation of a new supply pump for wastewater. These changes in water quality and the consistency of wastewater inflow would have likely promoted clogging. A single soil moisture characteristic curve for the Spearwood Sand in the HYDRUS model could not accurately reproduce the time-dependant spatially-varying changes in soil moisture that were observed over the 5 month field trial; instead, temporally varying hydraulic properties in response to changes in wastewater quality are needed in the model.

The total number of microbial cells in soil increased as a result of infiltration of treated wastewater in both column and infiltration gallery experiment. Deoxyribonucleic acid (DNA) sequence analysis showed clear differences in the bacterial communities in sand before and after infiltration. The presence of both bacterial families associated with the influent recycled water and increased abundance of native bacterial families may have contributed to the clogging observed in the columns.

The dominant group of archaea in the Spearwood Sand used for the column studies was methanogens, with ammonia-oxidising archaea also being abundant. These two groups were also consistently observed in the preliminary and extended column experiments. Methanogens represented the most dominant archaeal families in the treated wastewater used in Floreat infiltration gallery with minor populations of ammonia oxidising and symbiotic archaea also present. Most of the soil samples from the Floreat infiltration gallery were dominated by ammonia oxidising archaea, although in some samples methanogens or symbiotic archaea were more abundant.

The column and infiltration gallery studies showed clear differences in the eukaryotic communities in sand before and after infiltration. The eukaryotic communities in Spearwood Sand were dominated by fungi. The samples from the preliminary columns after infiltration were mostly dominated by protists except for top layer (depth 0-5 mm) in one column where algae were most dominant. The relative abundance of the fungi, algae, plasmodial slime molds, and some protists decreased with increasing depth in both columns, whereas the relative abundance of members of other protists increased with increasing depth in both columns. The samples taken from the infiltration gallery before infiltration and the adjacent samples from 140-150 cm distance of the gallery after infiltration had lower overall diversity of eukaryotic families with over 2% abundance than the samples taken from the crates after infiltration. In the Floreat infiltration galleries, the relative abundance of some algae, fungi and protists decreased as a result of infiltration, whereas the abundance of grass, oomycetes, worms, plasmodial slime molds and other algae, protists and fungi increased.

Alice Springs Soil Aquifer Treatment

The research in this component focused on wastewater infiltration at a soil aquifer treatment (SAT) site with variable soil characteristics in five recharge basins overlying an alluvial aquifer; characterising key factors that affect clogging rates (i.e. length of drying and wetting cycles in the recharge basins, the quality of recharge water, vegetation and algal growth in the basins); comparing the hydraulic performance of the recharge basins using wastewater derived from different treatments; and determining changes in the quality of receiving groundwater from recharge operations at the SAT site.

The Alice Springs study was driven by a need to provide better guidance to SAT operators on factors that affect development of a clogging layer at a site. Operation commenced in 2008, was subsequently expanded in 2011 and experienced an upgrade in wastewater treatment from Dissolved Air Flotation (DAF) to Dissolved Air Flotation and Filtration and Ultraviolet disinfection (DAFF + UV) in September 2013. In addition, this research was driven by a need for better knowledge of impacts of SAT operations on receiving groundwater quality as recovered groundwater could be used for agriculture or non-potable domestic purposes in the future. Operation of the SAT since its expansion in 2011 has resulted in recharge of approximately 1.9 ML/d, comparable to the design target of 600 ML/yr. The Alice Springs Water Reclamation Plant has a capacity to treat approximately 6 ML/d. Treated effluent is currently recycled via irrigation of Blatherskite Park and is available for further recycling by non-residential end users.

The research outcomes demonstrated that field-based experimentation was necessary to gain useful insights into clogging mechanisms and spatial variations in infiltration. Sediment-filled column experiments were conducted in the laboratory, but field soil conditions could not be reproduced due to heterogeneity and soil dispersion that obfuscated observations of clogging at a fine-scale. At the larger field scale, it was possible to estimate infiltration rates in individual recharge basins based on measured changes in wastewater levels over the period of time when inflow ceased and the basin floor was fully covered with wastewater. Another technique that was trialled at the Alice Springs SAT

site was using wastewater temperature as a tracer. Estimates of infiltration rates from thermal probes deployed in the subsurface below two of the recharge basins provided results comparable to estimates derived from water level changes in the basins.

Groundwater flow beneath the SAT basins interpreted from geophysical survey data (NanoTEM[®] time-domain electromagnetic and CMD electromagnetic conductivity metering) revealed spatially distinct zones of higher infiltration and lateral gradational changes in infiltration. Using wastewater temperature as a tracer of recharge illustrated the suitability of using thermal probes to determine spatially and temporally variable infiltration rates. In one basin (Basin E) temperature derived infiltration performance varied considerably between two locations, only 20 metres apart.

Results from investigating the chemistry and mineralogy of soil profiles through the SAT recharge basins revealed variations in the type and quantity of carbon present and the interrelationship with algae. The presence of large quantities of filamentous algae trapped on the bottom of a basin contributes to clogging directly and indirectly by inducing greater mineral cementation via precipitation of calcium carbonate and possibly metal oxides by increasing the pH of the recharge water during photosynthesis. Although the organic carbon content of surface soil in one of the SAT basins was the highest, the hydraulic performance did not appear to be compromised. Other factors, such as the construction of the basin in permeable sands, reduced the potential for clogging.

Soil compaction evaluated from geotechnical surveying (nuclear densometer and dynamic core penetrometer methods) of the SAT basins revealed a correlation with the use of heavy machinery during levelling the floor of one of the basins, which negatively affected the infiltration rate in this basin. The hydraulic performance of this basin was improved after approximately 50% of the floor material was turned over to a depth of 700 mm. This isolated experience provided important lessons regarding the impact of heavy machinery on infiltration and also on measures to remediate soil compaction.

An investigation of changes in the hydraulic performance of the SAT basins in response to an upgrade in wastewater treatment from DAF to DAFF revealed that additional filtration and reductions in algae and nutrient concentrations, and turbidity levels improved infiltration rates in all basins, by at least 40%. The hydraulic performance of basins receiving DAF-treated wastewater that had low infiltration rates improved considerably after recharge with DAFF-treated wastewater commenced (e.g. Basin C improved from 140 ± 50 mm/d to 250 ± 100 mm/d).

Results from comparing infiltration rates with the duration of drying periods revealed a positive correlation for two of the SAT basins. These results are compatible with the literature (e.g. Bouwer et al. 1974; 1980), which recommends that basin maintenance include extended dry periods to allow sufficient time for the floor of the basins to crack and expose fresh soil surfaces. Moreover, there is evidence that vegetation growth in the SAT basins acts as mulch, reducing the effectiveness of drying cycles, particularly in the winter in some of the basins. Although there are recommended lengths of drying periods for the winter from the literature (i.e. 5 to 10 days), analysis of operational data for the SAT site suggests that general rules for drying times should be supported by visual inspection of the basin surface condition. The drying period for all SAT basins at the site should be increased to a minimum of 5 days, preferably up to 10 days in winter.

Whilst the maximum length of the wetting period for SAT basins is 7 days (a restriction set by the Department of Health to prevent successful mosquito breeding), water quality data from the site showed that greater reductions in nitrogen were achieved by anoxic conditions that prevailed during longer wetting periods. This study suggests increasing the wetting periods for the recharge basins with the higher infiltration rates may enhance the potential for water quality improvements.

Characterisation of the clogging layer ("schmutzdecke") at multiple locations in the recharge basins indicates high variability in microbial counts and a mixture of clay, quartz, organic material with amorphous iron oxyhydroxide in some samples, whilst in other samples there was predominantly algal material with some aluminium, possibly derived from the coagulant used in wastewater treatment. The most abundant bacterial families identified in three of the basins can reduce nitrate (e.g. *Pseudomonaceae*, *Rhodocyclaceae*) and harbour pathogenic species (e.g. *Pseudomonaceae*).

Deeper in the soil profiles (at 10-50 cm and 90-130 cm depths) the most abundant bacterial families were *Oxalobacteraceae*, *Comamonadaceae* and *Nitrospiraceae*. Some members of *Oxalobacteraceae* family can fix nitrogen, some members of *Comamonadaceae* reduce nitrate and some members of *Nitrospiraceae* family can oxidize nitrite. Some members of the *Oxalobacteraceae*, *Comamonadaceae* families are pathogenic.

The archaeal families in the soil samples obtained from the top layer of the Alice Springs MAR site were dominated by methanogens at the sites close to the water inlets, whereas the sites further away from the inlets were dominated by ammonia-oxidising archaea. Ammonia oxidising and methanogenic families were also dominant in the depth profiles at 10-50 cm and 90-130 cm depths of the basins.

The eukaryotic communities in the top clogging layer of the Alice Springs MAR site were heavily dominated by algae. Other abundant families in the top layer were worms, fruit flies and protists. The most abundant families in the depth profiles were algae, plants, with also large populations of fungi, protists, worms and oomycetes.

A key outcome from the DNA-analysis of microbes sampled within a 1.5 m soil profile below two of the recharge basins was the detection of genes relevant for denitrification and ANaerobic AMMonium Oxidation (anammox). Greater knowledge of the abundance of these species relevant for nitrogen removal has implications for wastewater treatments that alter the concentrations of electron donors. Anammox bacteria convert ammonium and nitrite directly to nitrogen anaerobically and do not require organic carbon or other electron donors unlike denitrifying bacteria, which reduce nitrate to nitrogen with the input of suitable electron donors. Since DAFF treatment reduces the concentrations of labile dissolved organic carbon in wastewater, this is likely to limit the activity of denitrifying bacteria.

Changes in the quality of receiving groundwater in a Quaternary alluvial aquifer down-gradient from the SAT site were assessed from passage of wastewater through soils within the basin and through aquifer material consisting of fine grained clayey silts, clays and sands coarse grained sediments overlying coarse grained sediments. Groundwater on site and down-gradient from the Alice Springs SAT scheme was influenced by the recharge operation. Chloride and electrical conductivity indicated some freshening has occurred, which is an important consideration when assessing the beneficial uses of this groundwater supply. Nitrate concentrations in groundwater varied, with a general increase in response to recharging the aquifer with recycled water. Tracing of SAT recharge water using changes in chemical composition, stable isotope analyses, and EEM fluorescence spectrums of groundwater, clarified the extent to which down-gradient bores were impacted by recharge; however, stable isotopes indicated the presence of recharge water 1000m down-gradient which was not apparent with some of the less sensitive environmental tracers.

Conclusions

The research undertaken in this project is intended to assist water service providers considering different types of MAR with wastewater in areas that have unconfined aquifers suitable for in-situ treatment, storage and transmission. The recommendations and outcomes will hopefully encourage and generate more confidence to enable appropriate use of these types of water recycling schemes in the future.

1. In-situ sediments and pre-treatment of wastewater by filtration directly impact the hydraulic performance of both infiltration galleries and SAT basins:
 - Infiltration galleries can be used to infiltrate secondary treated wastewater into predominantly medium-grained sands, typical of Perth's coastal plain with saturated hydraulic conductivities ≥ 20 m/d at relatively high recharge rates (4 m/d), but hydraulic performance will depend on maintaining TSS below a target level (e.g. 5 mg/L) to reduce the potential for clogging. Periodic drying of the galleries may also reduce clogging problems.

- SAT basins in Alice Springs constructed in sediments of variable grain sizes showed that infiltration was higher (>300 mm/d) in more permeable loamy sands. In heterogeneous soils, described as loamy sand to sandy clay loam, clay dominated lenses influenced infiltration rates. Another factor influencing infiltration was soil compaction. Heavy machinery used to level the floor of recharge basins can compact soils and negatively affect infiltration rates. Moreover, additional pre-treatment by DAFF improved infiltration, but variability within basins remained dependent on the sediment type and on soil compaction history.
 - In infiltration galleries conditions in the soil remained aerobic whereas beneath the SAT basins the soil was mainly aerobic but occasionally at the end of the longer wetting periods evidently anoxic niches occurred. The clogging layer in the infiltration gallery where sunlight was excluded was composed principally of biofilm, roots and solids removed from wastewater during passage through the soil. In the SAT basins where the surface was exposed to sun (and in some cases shaded by vegetation) this clogging layer was composed principally of biofilm, algae, clay, quartz, calcium carbonate and iron oxyhydroxide.
2. Non-uniform infiltration (spatially and temporally) can be expected in both of the MAR designs investigated as the development of the schmutzdecke depends on a variety of factors:
 - Heterogeneous clogging developed locally within the infiltration gallery and promoted increased flow of wastewater laterally away from the gallery. Analysis of modelling results conducted with HYDRUS revealed that changes in soil moisture did not develop instantaneously, but instead gradually altered as passage of wastewater through the sands near the base of the gallery filtered out fine material that assisted in retaining more moisture and likely affected the direction of migration pathways for wastewater.
 - At the Alice Springs SAT site, spatially distinct zones of higher infiltration and laterally gradational changes in infiltration were detected using geophysical methods and recharge water temperature as a tracer. Factors affecting the spatial variations are the chemistry and mineralogy of the SAT basin soils, type and quantity of carbon present and the interrelationship with algae and plant growth on the basin floor which contributes to clogging both directly and indirectly.
 - The duration of drying periods directly impacts infiltration rates. The drying period for all SAT basins at the site should be increased to a minimum of 5 days, preferably up to 10 days in winter.
 3. Different water quality improvements can be anticipated from infiltration galleries and SAT basins:
 - In Perth's Spearwood Sand, large reductions in phosphate and dissolved organic carbon can be expected, but the magnitudes of concentration reduction will depend on the recharge rate relative to rates of biodegradation and adsorption. Application of recharge at higher rates than the rate tested in the field experiment would likely result in lower percentage reductions for phosphate and DOC.
 - At the Alice Springs SAT site, groundwater freshening resulted from wastewater recharge and there were increases in nitrate concentrations. Future use of groundwater will depend on water quality targets for the intended use. It is possible that the salinity of the groundwater will be a greater concern for use in irrigation than nitrate concentrations. This study recommends increasing wetting periods for some recharge basin to as much as 4 days as it may lead to greater nitrate removal. It should be noted that anoxic conditions, which are favourable for nitrogen removal, may increase the mobility of metal species.
 4. Whilst this project focused largely on outcomes from two field-based studies, experimental work conducted in the lab with sediment-filled columns and modelling achieved results that added useful insights:
 - Column experiments using Spearwood Sand provided a minimum estimate of the time until clogging became problematic, leading to ponding of water at the surface.

However, setting water quality objectives to avoid clogging based on column experiments could be unnecessarily restrictive if natural unclogging processes occur. Column studies to guide MAR should be considered as a complement to pilot studies conducted at the field scale.

- Difficulties encountered with the Alice Springs sediment-filled columns highlights that it may be unreasonable to expect columns to reproduce field conditions where fine-scale heterogeneity and dispersive clays are present.
- The HYDRUS model for the infiltration gallery confirmed non-uniform flow characteristics developed due to changes in hydraulic properties, arising from water quality changes. Comparison of predicted and observed soil moisture data demonstrated that it may not be possible to accurately model flow conditions below a gallery *a priori* if there are significant changes in wastewater quality, leading to temporally and spatially varying clogging. However, modelling provides useful insights that can guide positioning of monitoring equipment in the subsurface.

Introduction

Increasing demand on water resources due to population growth and climate variability has led to increased uptake of water recycling. Water recycling via the aquifer, or Managed Aquifer Recharge (MAR), has the potential to significantly increase the portion of water recycled in Australia. In 2012-13, forty three non-major urban utilities (servicing < 50,000 people) collected a total of 283 GL/yr of sewage, and treated and recycled 22% of it. In the same period, 24 major water utilities (servicing > 50,000 people) collected 1314 GL/yr of wastewater and recycled only 12% (NWC, 2014). Rural areas have advanced faster than major cities in water reuse because of a lack of alternative water supplies and the close proximity of municipal and agricultural demands for irrigation water.

There is great potential for increasing the proportion of water that is recycled in water-stressed areas using MAR. MAR provides storage to:

- i) increase the resilience of supplies;
- ii) provide water in seasons and years of high demand;
- iii) replenish over-exploited aquifers;
- iv) prevent saline intrusion;
- v) reduce evaporative losses;
- vi) avoid the need for new dams;
- vii) further treat the water;
- viii) to allow time for 'naturalisation' of water from a public perspective, and
- ix) help meet the needs of groundwater dependent ecosystems (Dillon *et al.* 2009).

Infiltration techniques for water recycling can be particularly attractive as they are generally lower cost than well injection techniques and they take advantage of the potential for natural treatment during infiltration through the unsaturated zone.

Despite the numerous benefits that MAR offers for water recycling, the uptake of this water resource management technique has been lower than expected (Parsons *et al.* 2012). Uncertainty regarding the impact of clogging on infiltration or injection rate, the water quality impacts on the receiving groundwater and the overall economic feasibility of the scheme can influence decisions to construct and commission MAR systems. To date, such uncertainty has impeded the uptake of water recycling.

Therefore, this report aims to address these knowledge gaps by evaluating and documenting the impact of clogging and the fate of nutrients and organic carbon in two water recycling MAR schemes employing novel infiltration techniques. The first of these MAR schemes used buried galleries at Floreat in Perth (section 2). Their closed nature may improve safety and acceptance in an urban setting while also excluding sunlight to inhibit algal growth. This requires higher quality water to be used because access for maintenance is harder than for open basins. The second scheme used soil aquifer treatment (SAT) (section 3), where open basins are operated intermittently to prevent mosquito breeding and with the intent to reduce nitrogen accessions to groundwater at Alice Springs. Each project has wide applicability across Australia. Floreat and Alice Springs are national demonstration projects for recycling via unconfined aquifers for non-potable uses, generally the cheapest form of recycling and hence rapid uptake is expected once proven and documented.

A companion report, *Economics and experiences of managed aquifer recharge (MAR) with recycled water in Australia* (Vanderzalm *et al.* 2015), presents a national compilation of MAR experience in water recycling, including lessons learnt through experience and evaluation of economic feasibility. This research was undertaken within a three year Australian Water Recycling Centre of Excellence research project on 'Raising the national value of water recycling by overcoming impediments to managed aquifer recharge'.

Floreat Infiltration Galleries

This body of work was to investigate the ability of sandy soils located on the Swan Coastal Plain to transmit and modify infiltrated recycled water derived from treated sewage. This follows on from previous field trials of infiltration galleries at the Floreat Infiltration Galleries (FIG) located on the CSIRO site in Western Australia. The FIG site was previously run at a low wastewater application rate of 1 m/d. Testing at a higher rate (between 2.9 and 3.8 m/d; 3.5 m/d on average) in the Atlantis® gallery over a two month period produced rising water levels in the central discharge chamber, which may have been indicative of clogging. Computer modelling indicated that groundwater levels may be raised in the vicinity of hydraulically connected wetlands if rates of 3 to 5 m/d were able to be maintained over long periods. The soils were known to be able to infiltrate very high rates of stormwater in retention basins and soak wells below roof downpipes over short periods but whether this was sustainable using water with higher suspended solids and nutrient loadings and over longer periods was to be assessed. The aim of this study was to understand the impacts of operating at higher infiltration rates (3.5 to 5.0 m/d) including clogging and nitrogen cycling associated with differing water qualities, such as unfiltered and filtered secondary treated wastewater.

Site description

The study was conducted at an experimental field site at the CSIRO Centre for Environment and Life Sciences in Floreat, Perth, Western Australia where there was an existing supply pipe and infrastructure for secondary treated wastewater. The site was located in a 31 m thick unconfined superficial aquifer underlain by a regional aquitard. The upper 7 m of calcareous sand, referred to as the Spearwood Sand grades into carbonate-cemented sand and limestone (Tamala Limestone). The calcareous sand is typical of unconfined aquifers on the western part of the Swan Coastal Plain and Perth Basin of Western Australia (Figure 1).

The site is characterised by a semi-arid climate with an annual average rainfall of 641 mm and an annual average pan evaporation of 1916 mm over the past decade (Figure 2, Station: 9151 SUBIACO TREATMENT PLANT, Lat: -31.96, Long: 115.70, elevation: 20m).

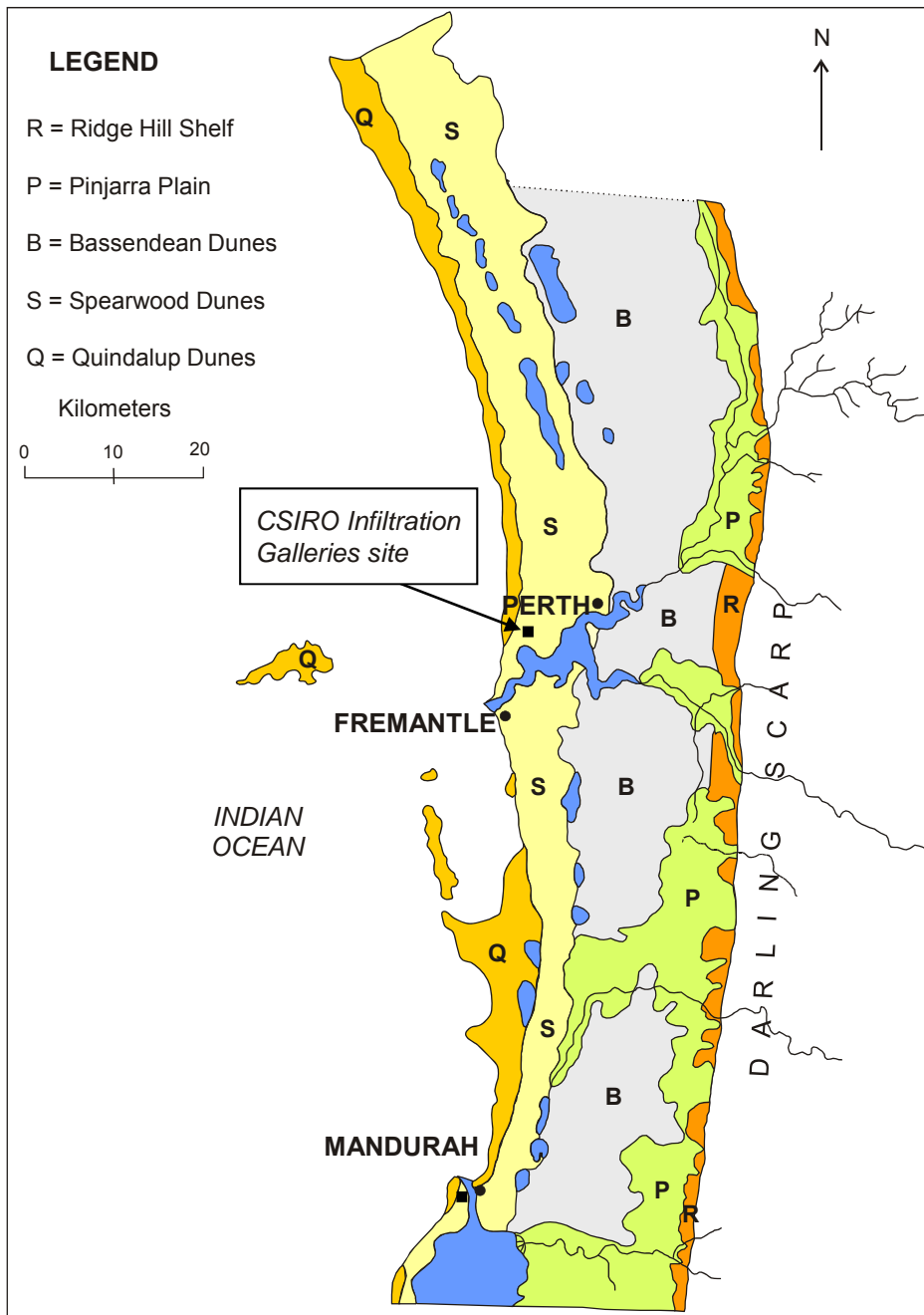


Figure 1 Location map showing the geomorphology and soils of the Swan Coastal Plain (after McArthur and Bettenay, 1974) and the CSIRO Infiltration site in Floreat, Western Australia.

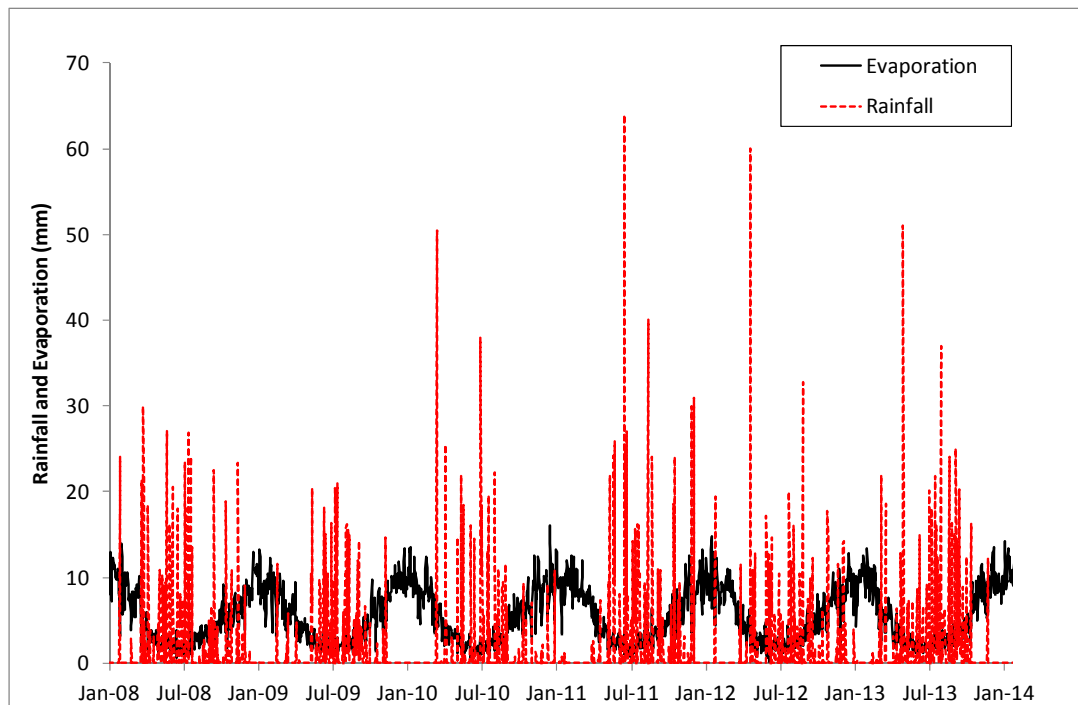


Figure 2 Daily rainfall and evaporation at the Subiaco STP (Source: SILO patched point data courtesy of the Queensland Department of Environment and Resource Management and the Australian Bureau of Meteorology).

Sequence of development

Previous experience from operating infiltration galleries was obtained during the Floreat Infiltration Galleries trial, which operated for 39 months, beginning in October 2005 (Bekele *et al.* 2011; 2013). Figure 3 shows the location of the new infiltration gallery relative to the former, now defunct, pair of infiltration galleries located 10 m to the south. It was not feasible to re-use the older galleries as they had not been maintained since 2009 and would require costly repairs. Moreover, the pair of older galleries was not designed to rigorously monitor clogging and the soil had been impacted by the previous trial. Thus, a new gallery was purpose-built for the present study and the existing supply pipe and infrastructure for controlling the inflow of secondary treated wastewater were reused.

A brief review of the major features of the previous MAR trial is provided herein to explain how and why the current project was conceived: The pair of infiltration galleries at the site, each with dimensions of 25 m x 1 m x 0.5 m (L x W x H), received secondary treated wastewater via a central discharge chamber and were buried below 0.5 m of sand. In the east gallery, the wastewater flowed laterally out through short (<1 m) slotted sections of PVC pipe on either side into Atlantis Flo-Tank® modules (Atlantis gallery), whilst the west gallery contained gravel with a slotted PVC pipe that extended the length of the trench to discharge wastewater (Bekele *et al.* 2013). Midway through the experiment, the west gallery clogged due to grass roots and the gallery was replaced with Atlantis Flo-Tank® modules in the same configuration as the east gallery. Water level measurements were made only at the central water entry location within each gallery, and given the low infiltration rate and highly permeable sands, the recycled water almost certainly was not evenly distributed throughout the galleries as it infiltrated. Nominally 1 m/d of infiltration through the base of the gallery was maintained over a period of up to 3 years. Testing at a higher rate (between 2.9 and 3.8 m/d; 3.5 m/d on average) in the Atlantis® gallery over a two month period produced rising water levels in the central discharge chamber, which may have been indicative of clogging.

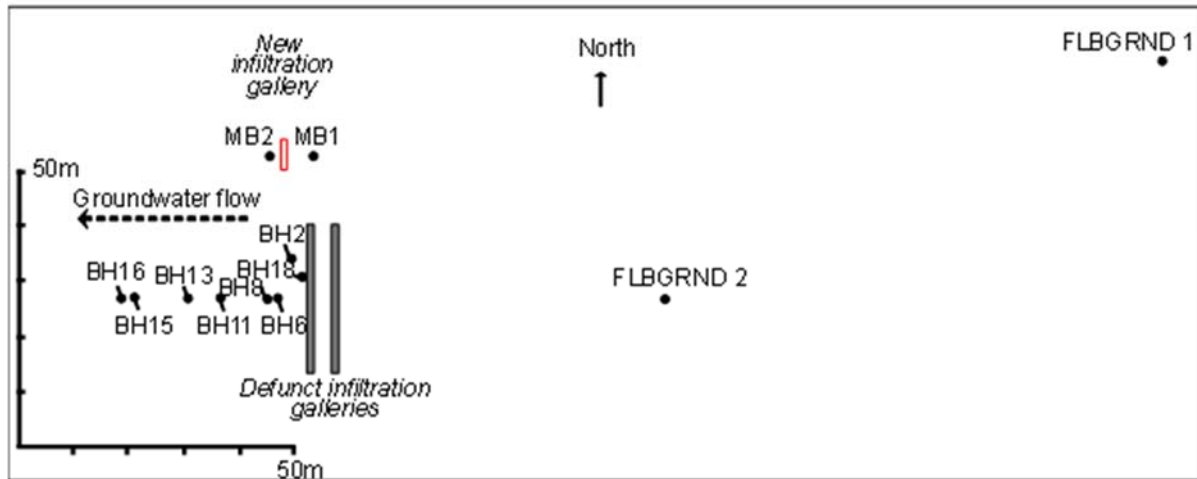


Figure 3 The Floreat MAR site showing the location of the new infiltration gallery, the former (defunct) galleries from a previous study, and monitoring wells that were sampled and used to infer the direction of groundwater flow. There were not enough bores between MB1 and FLGRND1 to delineate groundwater flow paths between these bores; however, groundwater flow to the west was determined at the MAR site using the bores labelled MB and BH.

Regarding the chemistry and water quality transformations at the previous MAR trial, the following results were obtained (Bekele *et al.* 2011): Reductions of 30% for phosphorus and 51% for total organic carbon were achieved by passage of recycled water through up to 10 m of unsaturated thickness at an infiltration rate of 1 m/d. Aerobic recycled water and aerobic conditions in the vadose zone were not conducive for denitrification (total N in recycled water remained unchanged despite passage through the vadose zone). Nitrification occurred in the vadose zone with nitrate produced by the oxidation of ammonia and organic nitrogen.

The new MAR project was conceived by CSIRO in 2011 in response to a proposal developed several years prior to replenish the Superficial Aquifer to provide ecological benefits to Perry Lakes, a flow-through wetland located 500 m north of the Floreat MAR trial (McFarlane *et al.* 2009). Perry Lakes has experienced declining lake levels since 1965 due to the drying climate and increased groundwater abstraction from bores in the vicinity. An alignment of infiltration galleries adjacent to Perry Lakes, covering an infiltration area of 1,300 m² was proposed. The thickness of the vadose zone beneath the proposed infiltration galleries varied between 1.5 and 9 m. The results from preliminary steady-state modelling by CSIRO suggested an infiltration rate of **4 m/d** would raise groundwater levels under Perry Lakes by 1 m compared with current levels (McFarlane *et al.* 2009). The consulting services of GHD were engaged by the proponents to develop a concept design. According to the GHD study, which used a transient groundwater flow model to predict flow paths and water level changes, 1.2 m/d of infiltration through the base of the galleries covering a total infiltration area of 2,500 m² would restore the periodic presence of water in Perry Lakes (GHD, 2011); however, this rate was adjusted to account for the operational efficiency of resting galleries to enhance aerobic conditions and a safety margin, hence a design flow rate of 5 ML/d, equivalent to an infiltration rate of **2 m/d** through the base of the gallery was given in their final recommendation (GHD, 2011).

Whilst the proposal was withdrawn due to inability to reach agreement between the local council and the Water Corporation about funding the supply of wastewater and/or maintenance costs (Thomas and Bennett, 2010), the proponents and the study by GHD identified a need for more research on the frequency and severity of clogging as it affects estimates of ongoing maintenance costs. The experimental plan as executed for the Floreat infiltration gallery site is provided in Appendix 1. Modifications and improvements to the design were made in response to discussions with the contractor, CHS Engineering. Appendix 2 documents the installation of the infiltration gallery in October 2013.

MAR system configuration

The source water was from a secondary clarifier at the Subiaco Wastewater Treatment Plant (WWTP), which then passed through a skid-mounted filtration system. Details of the Amiad® multi-media filtration system at the treatment plant are in Bekele *et al.* (2013). Additional pre-treatment occurred at the field site using an in-line ARKAL® disc filter (2" Dual).

The Subiaco WWTP is designed to treat up to 61.4 ML/d and services a population of 350,000 (Water Corporation 2009). The treatment train involves screening of large materials at the inlet to the plant; primary sedimentation treatment which removes 90% of the remaining solids; advanced secondary treatment processes incorporate a conventional activated sludge process with biological nutrient removal (Water Corporation 2009). The majority of the final wastewater is currently pumped to the Swanbourne Ocean Outlet 1 km offshore. A small quantity of secondary treated wastewater undergoes further treatment (filtration and chlorination) and is diverted for reuse to irrigate a nearby sporting oval.

The composition of the unfiltered secondary treated wastewater is shown in Table 1 (data courtesy of WA Water Corporation). No water quality parameters were available for the filtered secondary treated wastewater produced at the Subiaco WWTP. According to the environmental licence to operate the Subiaco WWTP no additional water quality sampling is required for the 'emissions to land' beyond that of the unfiltered secondary treated wastewater (DER, 2014).

Table 1 Subiaco secondary treated wastewater water quality (Jan 2009 to Feb 2012). All parameters in mg/L except pH (-) and EC (mS/m) and are based on weekly measurements.

	No. of samples	Mean	Standard deviation	Median	Minimum	Maximum
pH	163	7.3	02	7.3	6.8	8.0
Electrical Conductivity (EC)	163	126	13	127	92	176
Total Dissolved Solids (TDS)	163	751	124	748	331	1104
Total Suspended Solids (TSS)	163	23	22	15 ^a	<1	138
Biological Oxygen Demand (BOD)	152	8.4	5.9	6.2	2.2	39
Filtered BOD	150	2.4	1.5	1.9	0.1	10
Ammonium (NH ₄ ⁺ -N)	163	1.8	1.7	1.2	<0.01	114
Nitrate (NO ₃ ⁻ -N)	162	7.9	1.5	7.8	4.4	16.5
Nitrite (NO ₂ ⁻ -N)	163	0.76	0.42	0.68	<0.01	2.22
Total TKN	160	5.0	2.8	4.2	0.5	14.8
Total nitrogen (TN)	162	14	3.1	13	7.9	24
Total phosphorus (TP)	163	7.4	1.6	7.4	1.8	11

^a Note: daily measurements of TSS were also taken, this dataset shows greater variability and a higher median TSS = 20 mg/L (range 0.8 to 280 mg/L) than the weekly measurement sampled at the same time as the other parameters above. Source: WA Water Corporation

The hydrogeology of the site was previously characterised from core and well logs (Bekele *et al.* 2013). The study site is in Spearwood Sand which is derived from the in-situ weathering of the Tamala Limestone (Tapsell *et al.* 2003). The soil mineralogy is dominated by quartz (>88.5%) with the remainder feldspar minerals (microcline and plagioclase) (Bekele *et al.* 2011) and minor quantities of aluminium and iron oxyhydroxides and halloysite clay that forms coatings on the sand grains. Generally goethite gives these sands a yellow colour (Bastian 1996; Bekele *et al.* 2011). Particle size analysis at the FIG site indicates that sand size fractions dominate with 63-66% medium sand (0.18-0.50 mm), 14-21% fine sand (0.063-0.18 mm) and 14-20% coarse sand (0.5-1.0 mm) (Rümmler *et al.* 2005). Bulk density at 1.0 m BGL was 1.6 g/cm³ which corresponds to a porosity of 40%.

Recharge targeted the 31 m-thick unconfined Superficial Aquifer comprised of the Spearwood Sand and Tamala Limestone, which is underlain by a regional aquitard. The upper 7 m of Spearwood Sand grades into carbonate-cemented sand and limestone. The sediments excavated during installation of the gallery trench to a depth of 1 m consisted of fairly undisturbed and relatively uniform sand. Regional groundwater flowed from east to west, approximately perpendicular to the north-south orientation of the infiltration gallery with a gradient of 0.1% based on watertable measurements (Figure 3). The depth to groundwater varies seasonally between 10 and 11 m below ground.

Recovery of groundwater could be used as a non-potable water supply, but further approval by the Department of Water, Department of Health and the Department of Environmental Conservation/EPA would need to be sought as the site was only allowed to operate for the duration of the study in a research capacity with no intended beneficial uses of the infiltrated recycled water.

Methods

Soil column infiltration experiments

Soil column experiments were undertaken to evaluate the feasibility of achieving the target infiltration rate of approximately 5 m/d.

Soil characterisation

A bulk soil sample was collected from a depth of 1.0 to 1.1 m below ground level (m BGL) which corresponds to the typical infiltration gallery depth used previously at Floreat (Bekele *et al.* 2011) and proposed elsewhere (McFarlane *et al.* 2009). The soil was air-dried, mixed and sieved to <2 mm to ensure a consistent source of soil for use in column experiments.

Intact soil cores (10 cm diameter x 15 cm depth) were also collected from 1.0 m BGL to measure the saturated hydraulic conductivity (K_{sat}) of the soil. A 5 cm layer of soil was removed from the top of the soil cores to create space for a constant water head to be applied. A synthetic wastewater solution was used to determine the saturated hydraulic conductivity. This solution had a similar major cation composition and ionic strength (0.7 mM Ca²⁺, 0.5 mM Mg²⁺, 0.6 mM K⁺, 8.3 mM Na⁺ and 11.3 mM Cl⁻) to the secondary treated wastewater produced at the Subiaco WWTP. This solution contained no suspended solids as they would adversely affect the K_{sat} measurements. The reason for using the synthetic wastewater solution was to assess the K_{sat} at the higher Na concentrations of the wastewater (which may promote dispersion) rather than solutions more typical of K_{sat} measurement (5-10 mM CaCl₂ or CaSO₄).

The saturated hydraulic conductivity ranged from 10.0 to 13.5 m/d decreasing with increasing volume of water passing through the cores. These values are greater than in-situ disc permeameter measurements of K_{sat} (1.82 to 5.69 m/d) in Spearwood Sand subsoils (40-50 cm) (Salama *et al.* 2005). Though the measured Spearwood Sand K_{sat} values are similar to those used for subsoil (0.5-50 m BGL) in the Perth groundwater region vertical flux model (10 m/d) (Silberstein *et al.* 2009). The K_{sat} measured values were also comparable to those estimated from particle size analysis of soils from the FIG site (9.3 to 21.8 m/d, Rümmler *et al.* 2005). Groundwater modelling assumes higher hydraulic conductivities than these point measurements. Some of this will be in the Tamala Limestone which is known to be very conductive.

Recycled water

Two water types were used in the column experiments: (i) secondary treated wastewater, and (ii) filtered secondary treated wastewater. A synthetic solution with comparable salinity and sodium adsorption ratio but without nutrients or suspended solids was also used in initial experiments to avoid the possibility of physical and biological clogging related to recycled water application. This solution consisted of 0.7 mM Ca^{2+} , 0.5 mM Mg^{2+} , 0.6 mM K^+ , 8.3 mM Na^+ and 11.3 mM Cl^- which has a similar ionic strength and major cation composition to the secondary treated wastewater used in later parts of the experiment.

Recycled water was collected weekly from the Subiaco WWTP and refrigerated in the dark at 4°C to limit microbial/algal growth and nutrient transformations for up to 7 days until required. This water was allowed to equilibrate to ambient temperature before application to the columns. To limit algal growth in the wastewater, light was excluded from the columns (due to their opaque walls) and from the water delivery system (opaque tubing and aluminium foil covering of the influent diffuser). This mimics the application expected for subsurface galleries which are not exposed to sunlight.

Setup

Infiltration of recycled water in galleries was expected to occur initially under unsaturated flow conditions. To simulate these conditions a column setup was designed where water was introduced at the top and allowed to infiltrate under gravity (or unit gradient flow) through the initially unsaturated soil profile (Figure 4). The columns were made from PVC pipe (5.5 cm diameter x 70 cm long) with two stainless steel meshes (5.0 mm and 0.2 mm) at the base held in place by a PVC cap to prevent the soil from exiting the column. Tensiometers made from porous stainless steel discs (diameter ~5 mm, 12S-HXX Ambit Instruments) were inserted through the side wall of the columns before packing. The tensiometers were attached to pressure sensors (Honeywell HSCDANT005PGAA5) that were logged every 15 to 60 min using a data logger (DataTaker 505). Water inflow to the columns was distributed over the soil surface by a diffuser consisting of seven needles. Flow rates to each column were controlled by a piston pump (Masterflex L/S drive/FMI piston pump head) that drew water from a reservoir.

Two duplicate columns were packed with Spearwood Sand by sprinkling the air-dried soil into a small head (5 mm) of synthetic wastewater solution. After each increment of soil was added the overall water head in the column was raised such that the soil remained saturated during packing and until the unsaturated infiltration experiments were started. The soil was packed to a depth of 60 cm with a mean bulk density of 1.6 g/cm³. Tensiometers were placed at 2, 5, 10, 20 and 40 cm below the soil surface and air breather holes at 3.5, 15, 25, 35, 45 and 55 cm below the upper soil surface to prevent air entrapment. The location of the shallowest tensiometer was chosen to avoid potential inferences caused by the close proximity to the infiltration surface. The columns were kept under saturated conditions initially to test the tensiometers and measure matrix pressures under saturated conditions.

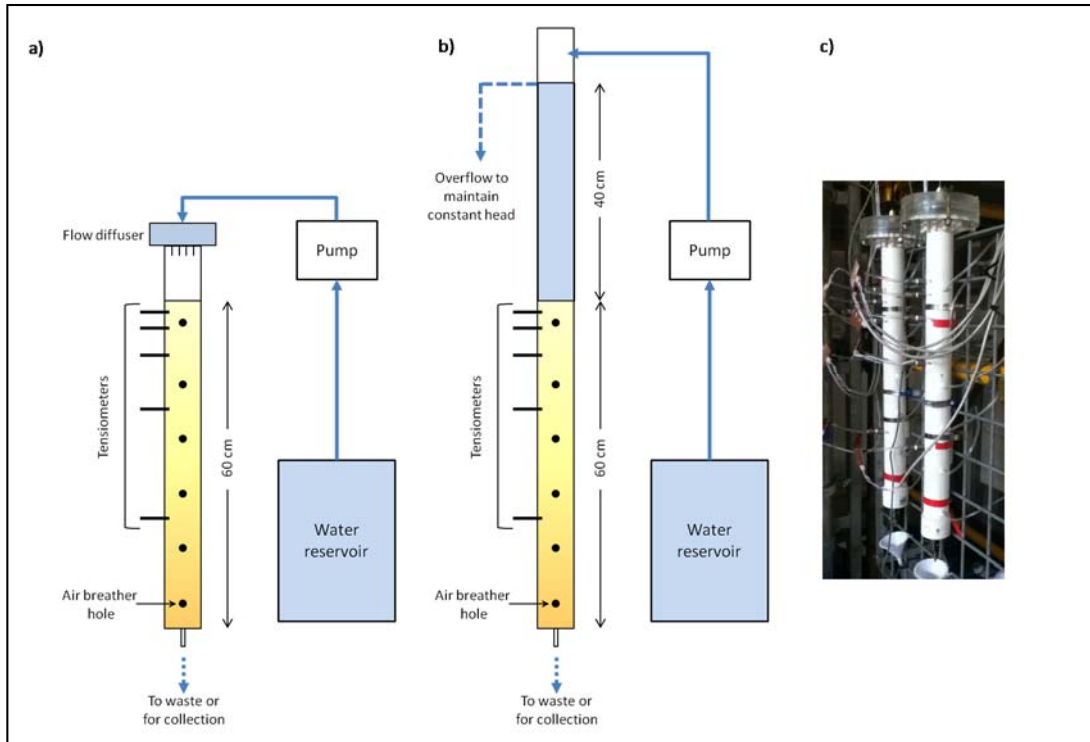


Figure 4 Schematic of column setup showing the 60 cm of Spearwood Sand, and the locations of tensiometers and breather holes for (a) pre-clogging showing water introduction through a flow diffuser and (b) post-clogging showing the constant head conditions (40 cm) imposed and (c) the PVC columns.

Following this initial test period the columns were drained under gravity until effluent ceased to flow from the base of the columns (<-30 cm of water (suction) was measured at all sensors, corresponding to the lower limit of the pressure sensors). Initial equilibration matrix potentials were measured at the application flow rates between 1.0 and 7.5 m/d that were conducted using the synthetic wastewater before switching to Subiaco WWTP recycled water. Note that application rates are less than the measured K_{sat} (at least initially) thus no head of water was present above the soil surface at the beginning of each experiment. Experiments were conducted with differing water types, a synthetic recycled waste water solution, unfiltered Subiaco WWTP recycled water and filtered Subiaco WWTP recycled water to investigate the impact of different water quality on clogging. Freshly packed soil columns were used for each experiment.

For the extended duration experiment, the initial setup was identical to the previous experiment (Figure 4a) with light exclusion enhanced by covering the flow diffuser and painting the columns black. Initially a synthetic recycled water solution (0.7 mM Ca^{2+} , 0.5 mM Mg^{2+} , 0.6 mM K^+ , 8.3 mM Na^+ and 11.3 mM Cl^-) was used during the wet packing and initial flow testing. Prior to commencement of the experiment, a blue dye tracer test was conducted at an application rate of 5 m/d, using synthetic recycled water solution spiked with 50 mg/L Brilliant Blue FCF applied to the soil surface. Once breakthrough had occurred unspiked synthetic recycled water was applied and the wash out of the dye measured. Aliquots of column effluent were collected and analysed for the tracer breakthrough.

Filtered recycled water from the Subiaco WWTP (collected weekly) was introduced at a rate of 5 m/d using a piston pump and a flow diffuser which dripped water directly onto the soil surface. Once clogging was evident, that is ponding of water had occurred, the column length was extended to accommodate up to 40 cm of water head above the soil surface (Figure 4b) which was chosen based on the depth of the void space provided by an infiltration gallery of one Atlantis Flo-Tank® (45 cm). The 40 cm of head was maintained by ensuring the pumping rates were greater than effluent flow rates with the excess water allowed to overflow and directed to waste.

The following monitoring of the columns was undertaken:

- Soil matrix potential – tensiometers placed at 2, 5, 10, 20 and 40 cm below the soil surface (Figure 4) measured soil matrix potential on an hourly basis
- Column effluent flow rate – measured daily (Monday to Friday; M-F) either over a short time period when flow rates were high (i.e. before clogging) and then as a composite sample collected over 1 to 3 days
- Influent, effluent and head water were monitored for pH, EC and temperature daily (M-F)

Water samples of the influent and effluent were collected daily (M-F). Later head water was collected twice weekly (Tue, Fri). These samples were filtered (0.45 μm) and analysed for major ions (Ca, Mg, K, Na, Cl, SO_4), nitrogen (as total dissolved, nitrate and ammonium), phosphorus (as phosphate) and dissolved organic carbon. Total suspended solids were measured for the influent recycled water on the day of collection for both freshly sampled and stored samples from the previous sampling. Samples of the sand before and after column testing were taken for microbial studies and analysed as described by Kaksonen *et al.* (2015).

Infiltration rate testing

Initial testing was conducted using columns without air-breather holes and an additional filter mesh of 10 μm nylon material. The filter fabric enabled a suction (15 cm of water) to be applied at the base of the column using a hanging tube. Synthetic wastewater was applied sequentially starting at 1 m/d then increasing to 2 m/d, 3.5 m/d and 5 m/d following an equilibration time of at least 24 h at each rate.

Infiltration was successful at 1, 2 and 3.5 m/d with matrix pressures stabilising within 1 hour of each step change in rate. However approximately 2 hours after increasing to 5 m/d in both columns the application rate exceeded the infiltration rate and water ponded on the soil surface. Given the saturated hydraulic conductivity was at least double this application rate it was assumed that an unknown clogging process was hindering infiltration. As the synthetic wastewater was free of particulates, physical clogging caused by the infiltrating water was discounted along with dispersion of the soil particles as the same synthetic wastewater composition was used for the saturated hydraulic conductivity testing. It is also unlikely that biological clogging had taken place due to the short duration of the synthetic wastewater application and the absence of additional nutrient and organic carbon sources.

The inability to infiltrate at 5 m/d was thought to be caused by air-entrapment in the soil which was initially unsaturated at the beginning of infiltration at 1 m/d. To prevent air-entrapment in subsequent experiments, air breather holes were installed in the side wall of the columns at six locations (as outlined above). These consisted of a threaded nylon fitting packed with glass wool to prevent soil exiting the column, and a vent tube. As a precaution the 10 μm filter mesh was also removed to prevent clogging by particulates at the base of the columns. Following the removal of the 10 μm filter mesh it was not possible to apply suction to the base of the columns, thus all subsequent experiments were conducted with free drainage at the base of the columns as shown in Figure 4.

Following the changes to the column setup and re-packing with fresh soil, 5 m/d of synthetic wastewater was successfully applied for 24 hours and up to 7.5 m/d applied over a shorter period (Figure 5). Differences in the matrix potential measured at saturation (Figure 5a) probably arise from the slight differences in column packing and these differences translate to measurements under unsaturated conditions (Figure 5b). The differences in the packing may also be responsible for the higher potential measured in column A compared to column B at the 7.5 m/d infiltration rate.

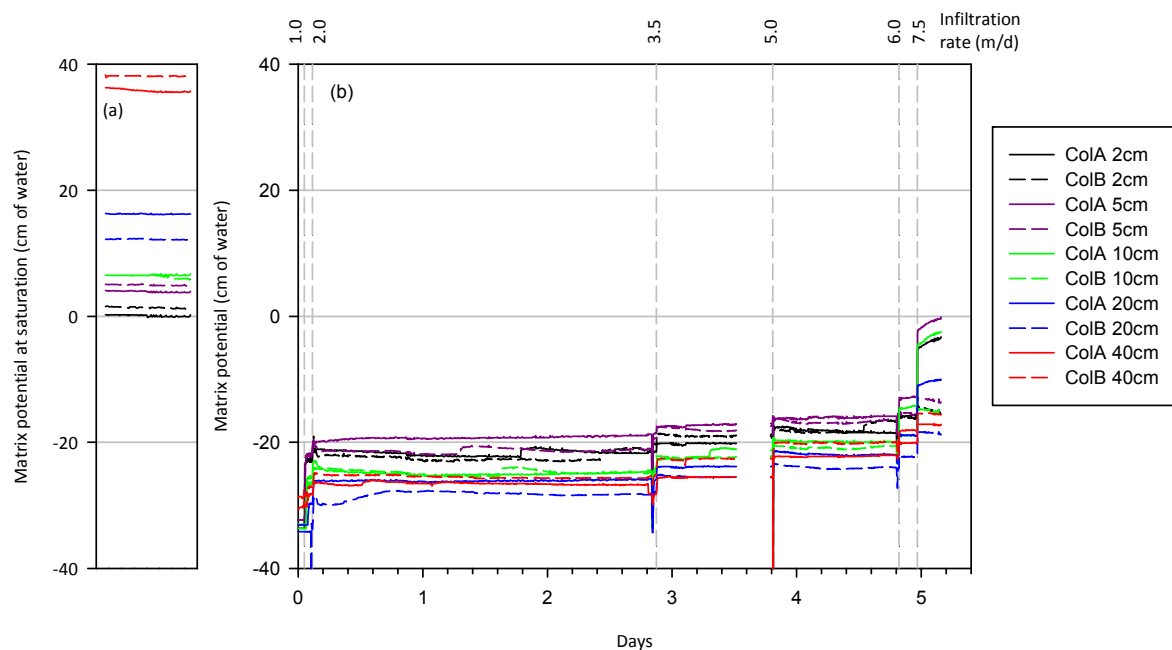


Figure 5 Infiltration rate test with synthetic wastewater in Spearwood Sand columns (left) matrix potential measured under saturation conditions prior to application of synthetic wastewater and (centre-right) changes in matrix potential during the unsaturated experiment (following column draining) with step changes in application rate (indicated at the top). The location of the tensiometers is given in cm below the top of the soil.

Floreat field experiment

Description of the field site

During the August 2013-January 2014 reporting period, the new Floreat infiltration gallery site was established using some of the infrastructure and mechanical equipment that remained from the previous MAR experiment that last operated in 2008. There were components of the system located at Subiaco WWTP, i.e. a skid-mounted, media filtration system with three pumps referred to as filter-feed, filtered water and backwash pumps, and there was the CSIRO Floreat Laboratories site consisting of the MAR infiltration gallery and skid-mounted control system with telemetry back to the WWTP. The engineering services of a private contractor, CHS Engineering, were hired to repair components and install new equipment for the field study.

Details of the installation of the purpose-built infiltration gallery for this study are provided in Appendix 2. Briefly, the site consisted of a series of 6 Atlantis Flo-Tank® modules, each with dimensions of approximately 685 mm x 450 mm x 408 mm (L x H x W) and internal partitions approximately every 340 mm (Figure 6). Small sections of the Atlantis® modules were cut away to allow the reticulated system for dispersing treated wastewater to pass through laterally. Three lengths of 25 mm-diameter polyethylene pipe were used to disperse the wastewater from a 4-way joiner at the inflow (south) end of the gallery and 42 Netafim™ pressure-compensating irrigation drippers were pierced into the pipe at fairly regular intervals. Fourteen drippers were inserted at an average distance of 27 cm apart along each of the 3 pipes. The drippers selected for the study have a nominal flow rate of 8.5 L/hour and working pressure range of 50 to 400 kPa. The distribution of drippers was to provide an application rate of 5 m/d over the extent of the gallery base (411 cm x 40.8 cm). The network of polyethylene pipes rested on the internal framework of the Atlantis® modules rather than the soil surface. This design allowed biofilm to develop in the soil below the base of the gallery with minimal contact with the surrounding gallery structure.

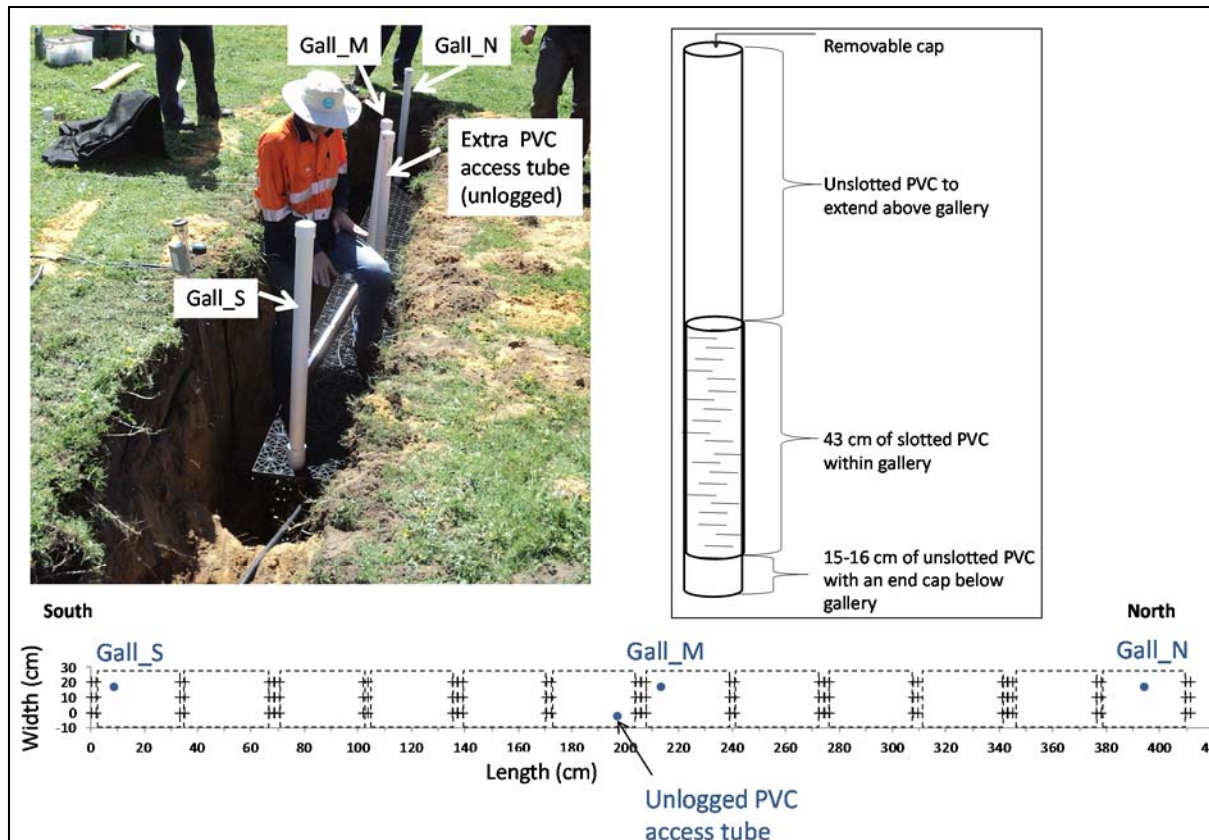


Figure 6 Locations of water level logging within the infiltration gallery. The diagram on the right (not to scale) shows the design of the PVC tubes used to monitor water levels in the gallery. Geofabric (not shown) was used to cover the top and sides of the gallery to lessen the opportunity for roots to grow into the gallery.

Five months prior to installation of the gallery, two monitoring bores were installed: MB1, located 5 m east and MB2, located 2 m west of the future location of the gallery. Loggers to record water levels on a 30-minute basis were installed in these two bores and in two additional bores (FLBGRND1 and FLBGRND2 bores) that are located up-gradient from the gallery site (Table 2). All of the bores, except FLBGRND1 were located in paddocks. FLBGRND1 was located in bare ground near CSIRO storage sheds. The latter two were used to provide background information to compare with changes in water level due to MAR. Prior to installing loggers, water samples were collected from MB1 and MB2 and analysed for water chemistry.

Table 2 Description of water monitoring bores.

Bore	Ground level (m AHD)	Total depth (m below ground)	Slotted interval (m below ground)	Distance and direction from the gallery (m)
MB1	13.12	12.25	11.25-12.25	5 m east
MB2	13.22	12.15	11.15-12.15	2 m west
FLBGRND1	15.93	15	NA*	177 m northeast
FLBGRND2	11.83	12.23	11.23-12.23	75 m east

* FLBRND1 is a CSIRO monitoring bore installed more than 20 years ago with no available record about the casing or slotted interval.

In addition to the field experiment, computer modelling of unsaturated flow was undertaken using the HYDRUS software package (Šimůnek *et al.* 2011). The model was used to assist with field planning and then refined with additional data obtained from field sampling. Soil moisture retention characteristics, which are a critical input to the model were obtained for uncontaminated Spearwood Sand from a previous study (Vermotten 2002). At the end of the infiltration experiment, sediment

samples exposed to effluent and from different depths below the gallery were collected and analysed to determine soil moisture retention characteristics. Soil and treated wastewater samples were also taken for microbial studies and analysed as described by Kaksonen et al. (2015).

Commencement of MAR trial and problems encountered

Once the installation of the field site and logging equipment was completed, the MAR trial was delayed by about one week to record ambient soil moisture conditions and to collect additional water samples prior to infiltrating treated wastewater to the site. The official start to the MAR trial was on 8-October 2013 whereupon treated wastewater flowed to the site from the Subiaco WWTP and infiltrated to the gallery at CSIRO. Wastewater flow to the site continued until 11-March 2014.

The supply of treated wastewater was regularly monitored as it was intended to have a continuous supply for the duration of the MAR trial. The CSIRO skid had an electromagnetic flow meter and instantaneous flow rates and the cumulative volume of treated wastewater supplied to the site were recorded during regular site visits. However, there were frequent problems with maintaining a continuous supply with stoppages of flow occurring at unpredictable and irregular times. CSIRO and staff at the Subiaco WWTP restarted the electronic panel at the Plant, which occurred almost daily during November 2013. After a series of meetings to address this problem, no definitive cause could be identified. Pippa Hepburn, Senior Wastewater Recycling Consultant from the Water Corporation, reviewed the mechanical equipment failure and provided written advice that acknowledged the problem was related to the age and condition of equipment that had been re-used from the 2005-2009 MAR trial. The backwash pump was replaced on 20-December 2013 which led to the continuous operation of the MAR trial until completion of the experiment.

Due to the frequent interruptions in the flow of treated wastewater for the MAR trial, it was difficult to accurately determine flow rates at unmonitored times. Infiltration rates to the gallery were estimated based on instantaneous measurements of cumulative volume and the recorded time between measurements, but this is not very accurate if there were intervening interruptions of flow. A method was developed based on analysing the soil moisture data, which involved identifying interruptions in flow based on sudden declines and increases in soil moisture, due to flow stopping and starting, as well as using the manually recorded observations of flow interruptions to determine the duration of flow. The cumulative volume measured by the skid (electromagnetic flow meter) was then used to calculate a flow rate assuming that flow only occurred during periods of high moisture content.

Results – Soil column infiltration experiments

Secondary treated wastewater

The columns used for the successful infiltration test were used to test the impact of the unfiltered secondary treated wastewater on infiltration. The columns were rested for seven days at low flow rates (1 m/d synthetic wastewater) following the infiltration rate testing. After allowing the columns to drain under gravity, recycled water was applied at a rate of 5 m/d. Ponding of water on the column surface and changes in matrix potential (Figure 7) were indicative of physical clogging. Soon after the initiation of the experiment the matrix potential measurements in the duplicate columns diverged. The differences in matrix potential between the columns are likely to be related to the depth at which the clogging occurred. For example, if clogging were to form then it would be expected that the matrix potential would increase above the clogging layer as the soil became increasingly saturated, whereas the matrix potential would be expected to decrease (become more unsaturated) below the clogging layer as less water passes the observation point. Initially all tensiometers in column A indicated that unsaturated conditions (< 0 cm of water) existed at all measurement locations (Figure 7). However only the 20 cm and 40 cm tensiometers showed similar matrix potentials as those measured for synthetic wastewater (Figure 5 and Figure 7). Greater matrix potentials observed at the other three locations indicate that water contents were higher with respect to the synthetic wastewater suggesting that a degree of clogging had occurred at these locations. The matrix potential continued to rise throughout the experiment until ponding was observed at the end of experiment (~1.8 days). At this

time the soil at 10 cm was still unsaturated as the matrix potential was marginally lower than the matrix potential at saturation (Figure 7). However the matrix potential indicated that saturation was occurring at 2 cm and 5 cm below the soil surface. From this experiment it appeared that clogging occurred in the upper 10 cm of the soil profile in column A.

Following wastewater application the matrix potentials measured in column B as shown in Figure 7 were initially (up to 0.11 days or 2.5 hours) similar to those measured at 5 m/d when infiltrating with synthetic wastewater (Figure 5). Following this infiltration began to decline as evidenced by the decreasing matrix potential recorded at all tensiometer locations. Surface ponding was also observed in this column less than one day after infiltration started and flow was stopped after 17 hours or 0.72 days. Clogging in column B probably occurred at a depth <2 cm as no evidence of saturation was observed at any of the tensiometers unlike column A.

Infiltration of recycled water at 5 m/d application rate quickly clogged both columns such that water ponded on the surface of the soil within two days of starting application. The clogging mechanism probably relates to physical clogging of the soil pores given the high suspended solid concentrations in the secondary treated wastewater (20 mg/L) and the short duration of infiltration prior to ponding (the time scale for biological clogging to occur is typically longer due to the time required for microbial growth). It is unclear why the columns behaved so differently and it may be due to a number of factors such as column packing and colloid movement, however the mechanism was not pursued as the experiment indicated that the secondary treated wastewater from the Subiaco WWTP, without any further treatment would be unsuitable for use in infiltration galleries due to the high potential for clogging. Thus further experiments were conducted using filtered secondary treated wastewater.

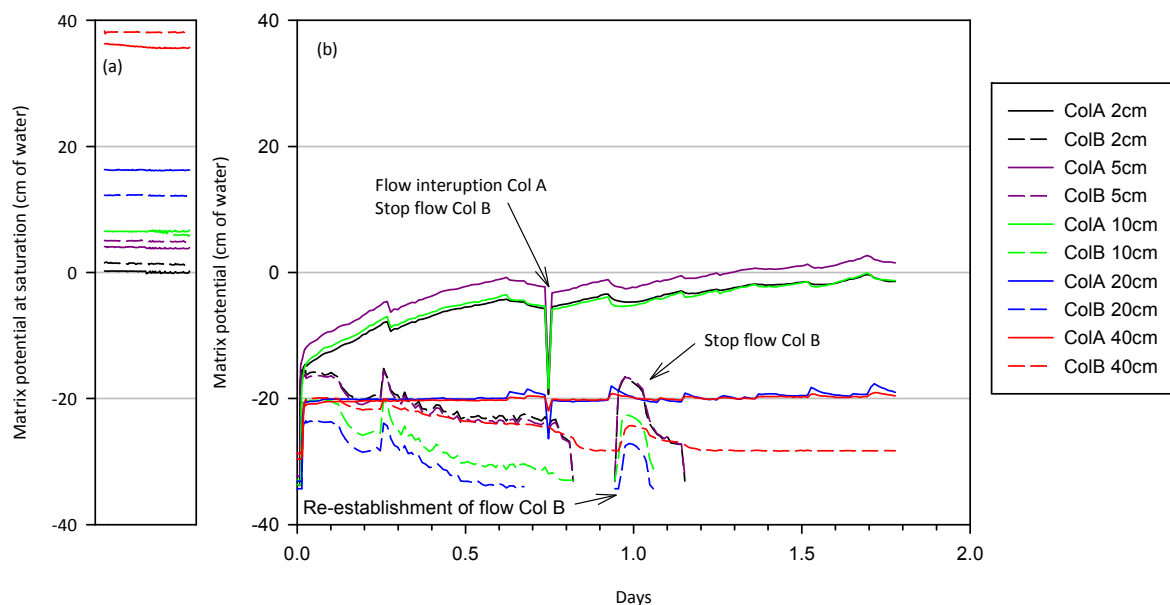


Figure 7 Infiltration of secondary treated wastewater from the Subiaco wastewater treatment plant in Spearwood Sand columns (left) matrix potential measured at saturation, and (centre-right) changes in matrix potential upon the application of wastewater at 5 m/d.

Filtered secondary treated wastewater

Fresh soil was used to repack two duplicate columns using the procedure described above. The columns were kept at saturation until the infiltration experiment was started. Matrix potential was measured with the tensiometers to provide baseline measurements of the saturated conditions. The columns were allowed to drain under gravity prior to the infiltration of synthetic wastewater at a rate of 5 m/d. The tensiometers were tested during the synthetic wastewater addition and column effluent flow rates measured. Following initial testing the influent solution inlet was switched to filtered secondary treated wastewater without allowing the column to drain and application continued at 5

m/d. A short lag period would have occurred between switching water sources and application to the column as the synthetic wastewater was replaced in the pump lines and dispenser reservoir. As part of this experiment water quality measurements were taken for both the column influent and effluent.

Changes to the matrix potential upon application of filtered wastewater are shown in Figure 8. While every effort was undertaken to ensure that the packing of the columns was undertaken in the same manner, small differences in packing and contact with the tensiometers are likely to exist. This results in slightly different signals from the tensiometers at different depths. The matrix potential is relatively stable throughout most of the experiment up to day 13 (except for the period where wastewater application was interrupted and the columns drained). This is reflected in the consistent column effluent flow rates observed (Figure 9 a). The matrix potential indicates that at the measuring depths the soil remains unsaturated throughout the experiment even after ponding occurred in column A, which was maintained at 10 cm above the sediment for several days following the first observation of ponding. Therefore the clogging that resulted in the ponding in column A was located within 2 cm of the infiltration surface since no increase in the matrix potential was observed at 2 cm or deeper. Clogging in column A induced a decrease in the flow rate from the column (Figure 9a) and a corresponding decrease in the matrix potential (Figure 8b) indicating that the soil became increasingly unsaturated below the clogging layer. The consistent flow rate and matrix potential in column B indicated that clogging had not occurred (Figure 8d and Figure 9b).

The chemistry of column influent and effluent (Figure 9) is dominated by a step change related to the switch of influent water batches. Overall there is little difference between the influent and effluent chemistry for either of the columns especially the electrical conductivity (EC) and total dissolved nitrogen (TDN). There is a slight (0.2 units) increase in pH between the influent and effluent which may suggest that carbonate mineral dissolution may be occurring. A strong reduction in the dissolved organic carbon (DOC) between the column influent and effluent was observed at the beginning of the experiment, however by day 6, the influent and effluent concentrations were similar (Figure 9). Sorption of the DOC may account for the initial removal of DOC as the fresh subsoil is low in organic matter (<0.3% as C, Bekele unpublished data).

Microbial communities

Investigations of the cause of clogging in this experiment suggested that algae growth in the wastewater delivery lines and flow diffuser may have caused the clogging of column A. Attempts were made to exclude light (aluminium foil covering of the diffuser and opaque tubing) though algae was still observed and probably grew in the reservoir of the flow diffuser (~350 mL). While attempts were made to identify if algae were responsible for the clogging of column A the 18S rRNA gene pyrosequencing showed that 75-77% of the eukaryotic 18S rRNA genes in the shallow surface layer (0–5 mm) were not identifiable with the remainder (20-22%) protists of the *Stephanocidae* family (flagellates) (Kaksonen *et al.* 2015). The eukaryotic communities in Spearwood Sand were dominated by fungi of the *Sordariomycetes* (33-46%) and *Nectriaceae* (12-27%) families.

Microbial abundance in the shallow surface layer (0–5 mm) was higher ($4.4 \times 10^7 \pm 3.0 \times 10^7$ cells/g) following infiltration than that of the virgin Spearwood Sand ($4.0 \times 10^5 \pm 3.1 \times 10^5$ cells/g) suggesting that microorganisms were either introduced with the filtered wastewater and/or multiplied in-situ (Kaksonen *et al.* 2015). Prior to infiltration the bacterial communities in the Spearwood Sand were dominated by families *Gaiellaceae* (9-12 % relative abundance), *Hyphomicrobiaceae* (5 %), unknown family *Solirubrobacterales* order (4 %), *Rhodospirillaceae* (3-4 %), *Syntrophobacteraceae* (2-3 %) and *Nitrospiraceae* (2 %). After infiltration, bacterial families *Xanthomonadaceae* (17-18 %), *Chitinophagaceae* (10-14 %), unknown *Alphaproteobacteria* (6 %), *Sphingobacteriales* (5-6%), and *Hyphomicrobiaceae* (3 %) were dominant (Kaksonen *et al.* 2015). A number of these families have been previously detected at sewage treatment plants, e.g. *Sphingobacteriales* (Zhang *et al.* 2012; Wang *et al.* 2012), *Hyphomicrobiaceae* (Zhang *et al.* 2012; Wang *et al.* 2012), *Rhodospirillaceae* (Zhang *et al.* 2012), *Syntrophobacteraceae* (Kuever 2014), *Xanthomonadaceae* (Wang *et al.* 2012), *Chitinophagaceae* (Wang *et al.* 2012), *Alphaproteobacteria* (Wang *et al.* 2012), and *Nitrospiraceae* (Daims 2014). The increase in microbial abundance and change in the bacteria communities

suggests that the low flow rates observed in column A in this experiment are likely to be associated with biological (biofilm) clogging.

The most dominant identified archaeal family in the Spearwood Sand was methanogenic *Methanomassiliicoccaceae* (51-53 % relative abundance), with members of ammonia-oxidising *Nitrososphaeraceae* also high in relative abundance (30-31 %) (Kaksonen *et al.* 2015). In the initial, short duration column experiment at depth 0-5 mm, the most dominant archaeal families were methanogenic *Methanobacteriaceae* (26-32 %) (Horn *et al.* 2003) and *Methanosaetaceae* (8-10%) (Boone *et al.* 2001), and ammonia-oxidising *Nitrososphaeraceae* (6-11 %) (Kaksonen *et al.* 2015).

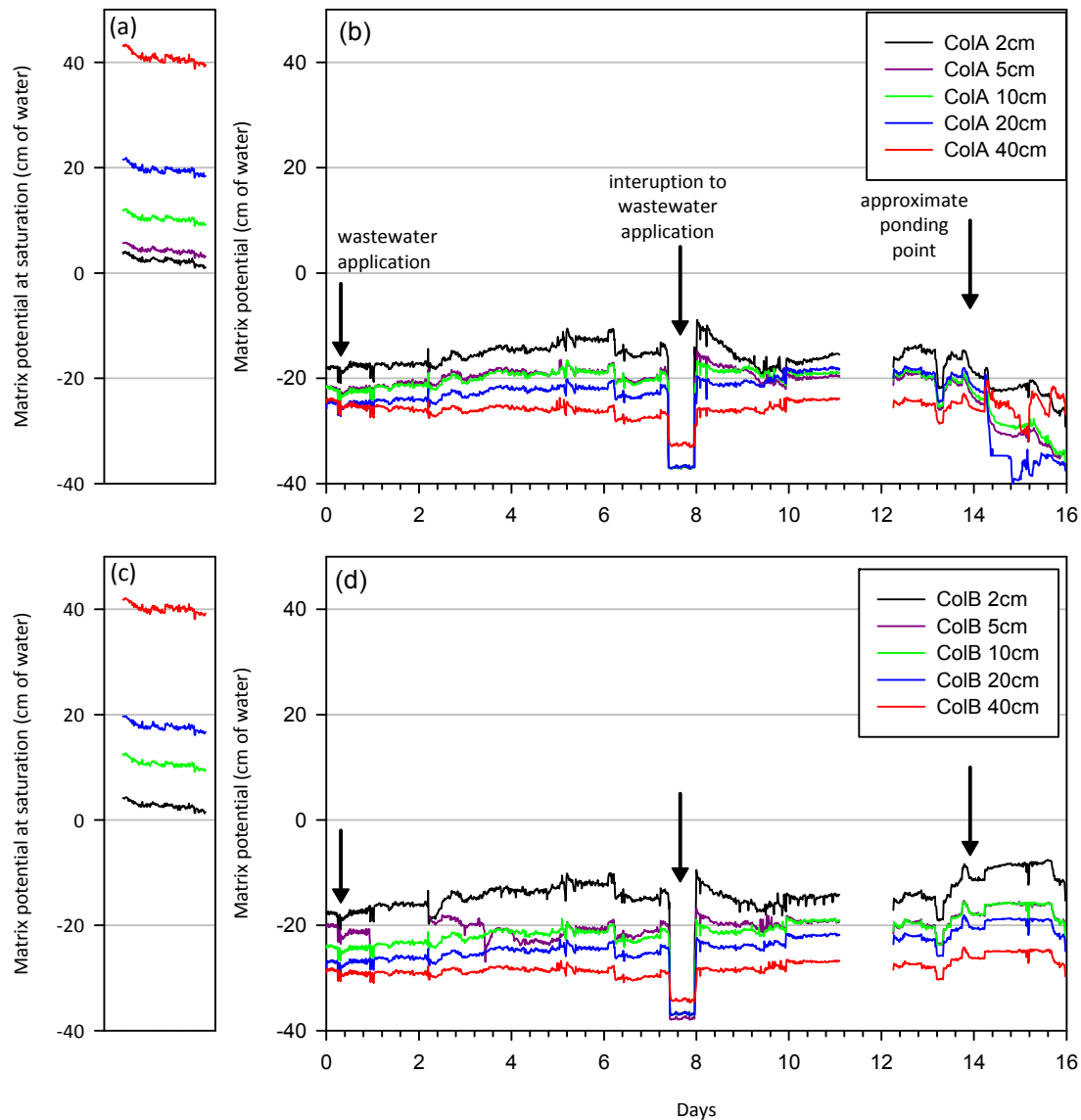


Figure 8 Infiltration of filtered secondary treated wastewater from the Subiaco sewage treatment plant in Spearwood Sand columns matrix potential measured at saturation (a – column A, c – column B), and changes in matrix potential upon the application of filtered treated wastewater at 5 m/d (b – column A, d – column B).

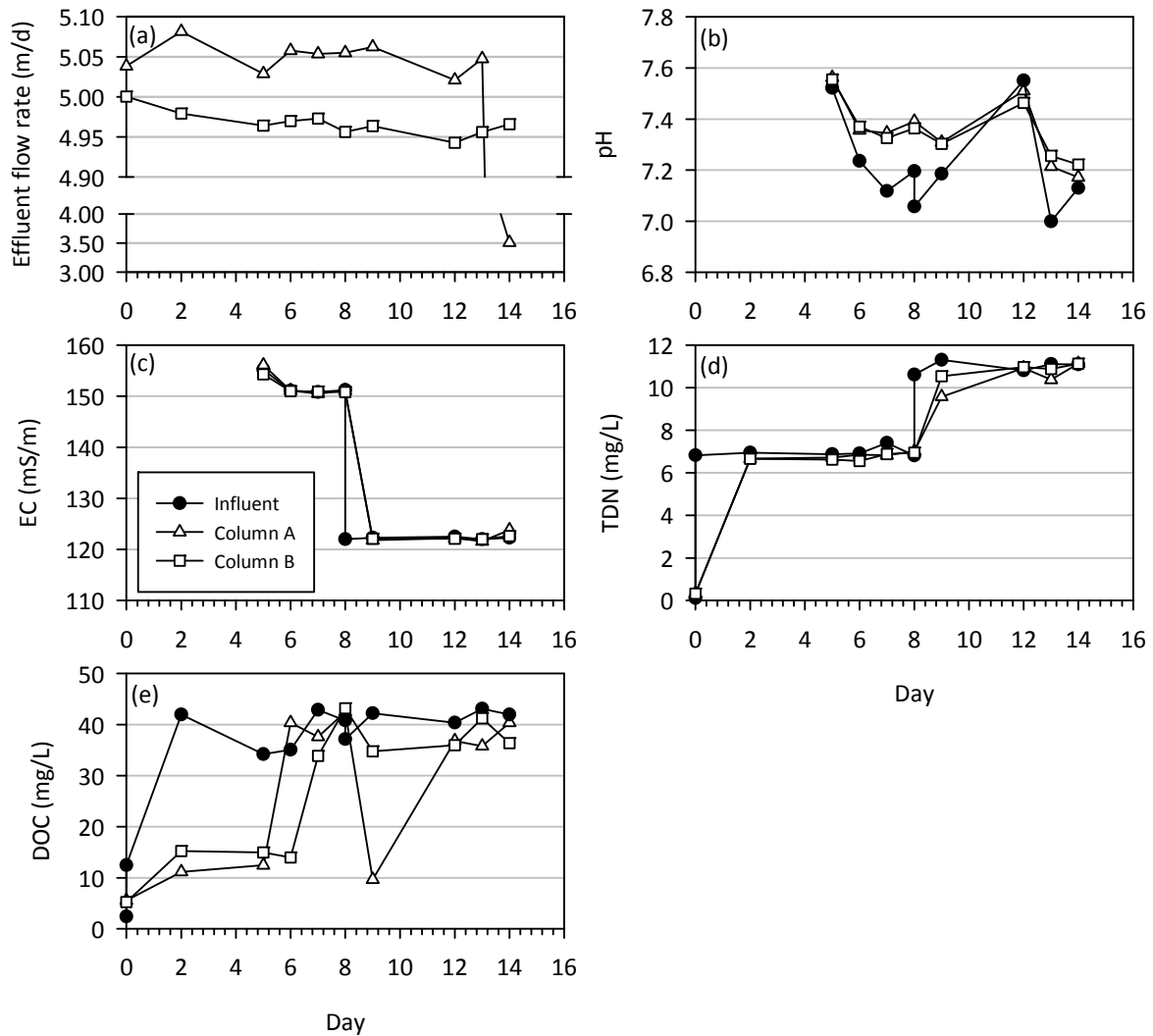


Figure 9 Filtered secondary treated wastewater column effluent flow rates (a) and comparison of column influent and effluent (b) pH, (c) electrical conductivity (EC), (d) total dissolved nitrogen (TDN), and (e) dissolved organic carbon (DOC) for columns A and B.

Extended duration with filtered secondary treated wastewater

Previous column studies indicated that even with filtered recycled water clogging would occur approximately two weeks after the application began. This resulted in ponding of water above the soil surface. Due to the short-term nature of the experiment it was unlikely that the clogging layer would be well developed in terms of the microbiological populations. As such it was decided that further experiments should be conducted for a longer duration. This was achieved by imposing a head of water above the soil once clogging was initiated in the columns to investigate the hydraulic and chemical properties during development of the clogging layer.

Water fluxes

The tracer tests conducted at the beginning of the recycled water infiltration experiment indicated that residence time in the 60 cm long columns was 90 min at an application rate of 5 m/d. At these input rates the soil within the columns remained unsaturated (i.e. the soil matrix potential was < 0 cm of water) in both columns (Figure 10). Similar to the previous experiment clogging (as evidenced by ponding) was observed after approximately 2 weeks of recycled water application (Figure 10) as indicated by the increase in head. As a non-intentional consequence of the alteration of the column setups following the initial clogging the flow rates were artificially increased as a result of the application of the water head. These high flow rates resulted in disturbance of the clogging layer

leading to a temporary improvement of column flow rates back to the 5 m/d influent application rate. However this was short lived and by days 19 and 20 for column A and B, respectively, clogging resulted in the rise in head. On day 24 both columns reached the designated constant head of 40 cm and column effluent rates decrease to approximately 0.18 m/d by day 31 (Figure 10).

During the clogging period (day 19 to 28) the soil profile remains unsaturated and disconnected from the head of water overlying the soil surface as indicated by the negative soil matrix potentials in Figure 10. At some depths the matrix potential decreases during this time reflecting the decrease in effluent water volumes due to the increased clogging. The exception to this is the 2 cm tensiometer in column A which reach positive matrix potentials after day 66, though measurements are still less than that expected if it was fully connected to the overlying water column in which a pressure of ~42 cm of water would be expected (2 cm soil water plus 40 cm of head water).

The hydraulics of these soil columns seems to suggest that the clogging layer thickness is initially small, though it may be increasing as suggested by the rising matrix potential at 2 cm in column A. The thin nature of the clogging layer, and hence saturated zone, produced upon application of recycled water has implications for nitrogen transformations. The low residence time in the saturated zone, approximately 7 hours assuming a 2 cm thick clogging layer (minimum column flow rate was 0.07 m/d or 166 mL/d), is unlikely to result in significant denitrification and hence nitrogen removal.

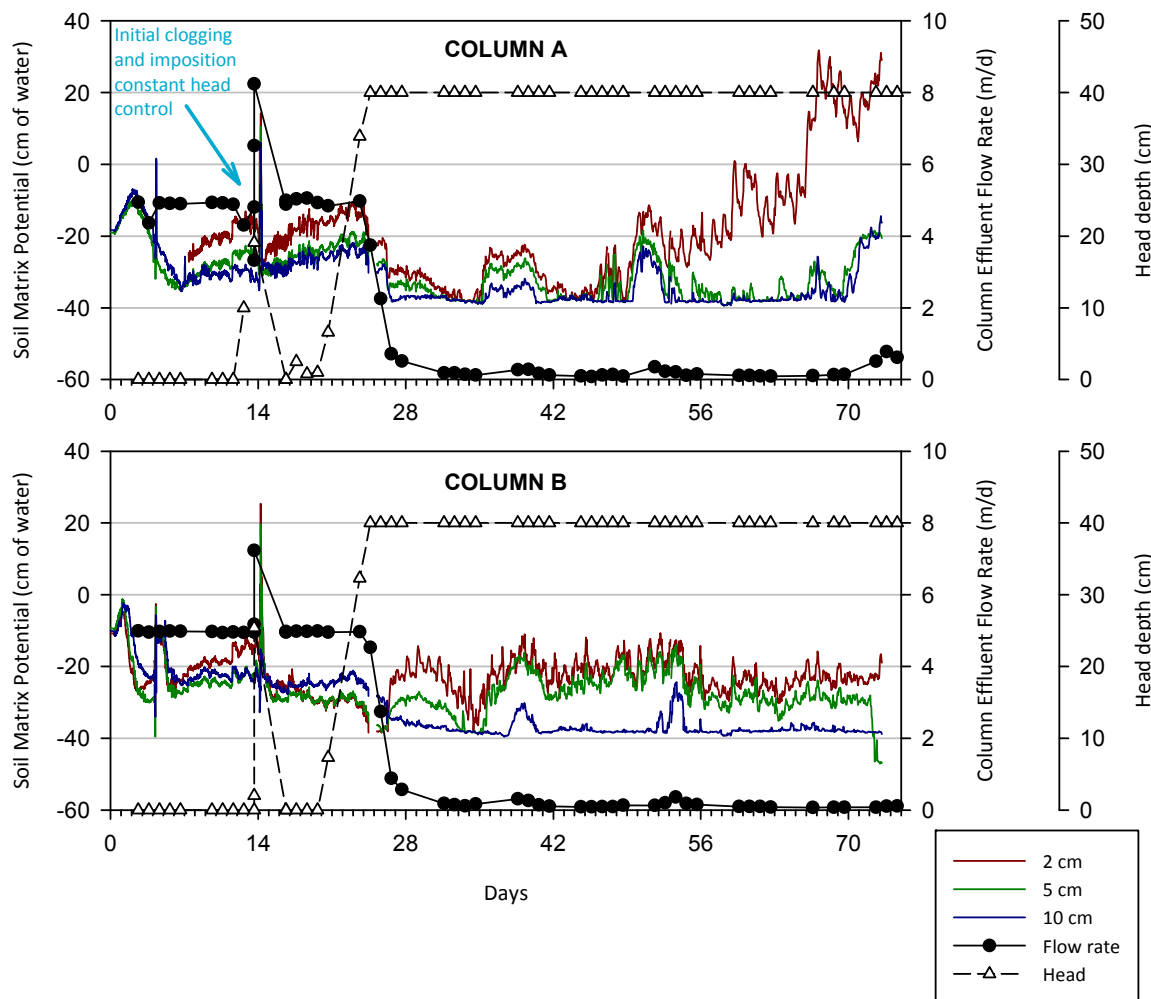


Figure 10 Effluent flow rate for columns A and B following infiltration of recycled water through Spearwood Sand columns, showing initial rates of 5 m/d and the effect of clogging on flow rates and soil matrix potential measured at 2, 5 and 10 cm below the soil surface. A constant head of water (40 cm above the soil surface) was applied following the observance of ponding of the recycled water.

Water chemistry

Influent recycled water for the experiment was collected from the Subiaco sewerage treatment plant once a week and is reflected in the stepped nature of the influent electrical conductivity (EC) changes with time (Figure 11a). Column effluent EC follow that of the influent until a head of water accumulates following clogging (after day 28, Figure 11a). Changes in EC are masked by insufficient mixing of the new batch of influent water with the 40 cm of ponded water maintained above the soil surface. Samples of the ponded water confirm this and the column effluent resembles more closely the ponded water EC.

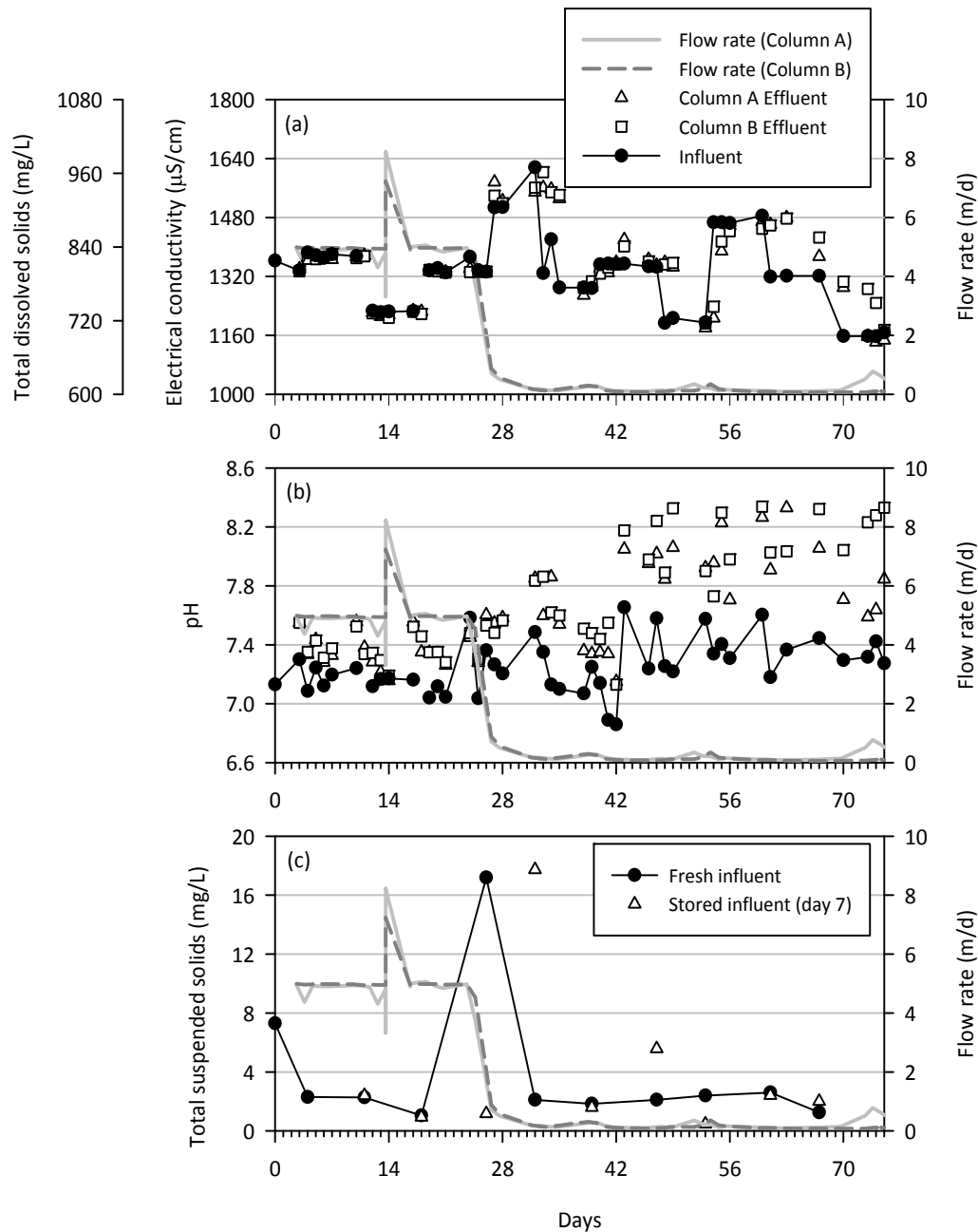


Figure 11 Recycled water and column effluent physio-chemical characteristics (a) electrical conductivity (EC) and calculated total dissolved solids, (b) pH and (c) total suspended solids. The legend for (a) also applies to (b). The column effluent flow rates are shown for comparison.

Similar to the previous experiment the pH shifts to higher values following passage through the columns and varies from approximately 0.2 pH units during high flow rates to between 0.6 and 0.9 pH units during the lower flow rates following clogging. As the soil contains minor amounts of carbonate minerals, the pH increase is likely to be associated with the dissolution of these minerals with the greater pH increase the result of greater water residence times within the soil column under clogged conditions.

Filtration generally maintains the suspended solid concentration around 2 mg/L, though some batches had higher concentrations (e.g. 17 mg/L on day 26). This is low compared to the long-term average of the unfiltered secondary treated wastewater TSS of 23 mg/L. While clogging began to occur prior to the application of the high TSS wastewater batch (initially on day 14 and secondly after day 19) it may have contributed to further enhancement of the clogging. Prior to clogging when collection of column effluent of sufficient volume (1 L) was possible, TSS measurements indicated that the majority of the suspended solids were retained by the columns (effluent measurements were at or below the detection limit of 0.1 mg/L). Due to the low influent TSS concentrations less than a gram of particulates have been introduced into each column (23.75 cm² area) associated with approximately 320 L of recycled water infiltrated per column (Figure 12).

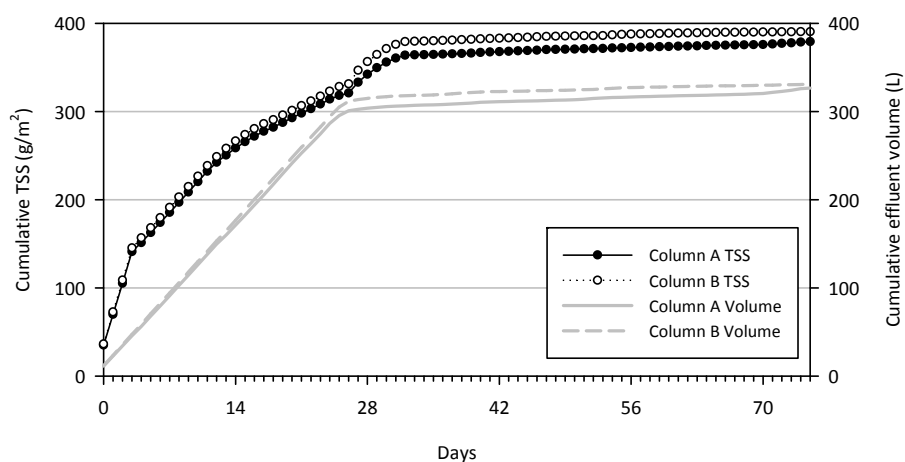


Figure 12 Accumulation of suspended solids (TSS) and cumulative effluent following recycled water infiltration. Non-measured TSS and flow data interpolated between measurements.

The nutrient data during the initial high flow period shows little change between the influent recycled water and the effluent following infiltration through the columns (Figure 13). This is potentially due to the low residence time reducing the potential for transformations to occur during passage through the soil. Effluent concentrations of nitrate and phosphate during the low flow period show that (i) nitrate concentrations increase (Figure 13b) and (ii) phosphate concentrations decrease with respect to the influent concentrations (Figure 13c). The increased residence time may lead to the oxidation of ammonium and organic nitrogen to nitrate and removal of phosphate by adsorption to metal oxides or precipitation with calcium. Further investigation of the adsorption capacity and potential for desorption is required to assess the potential for phosphate removal especially where calcite concentrations increase with depth (up to 30% w/w) within the unsaturated zone.

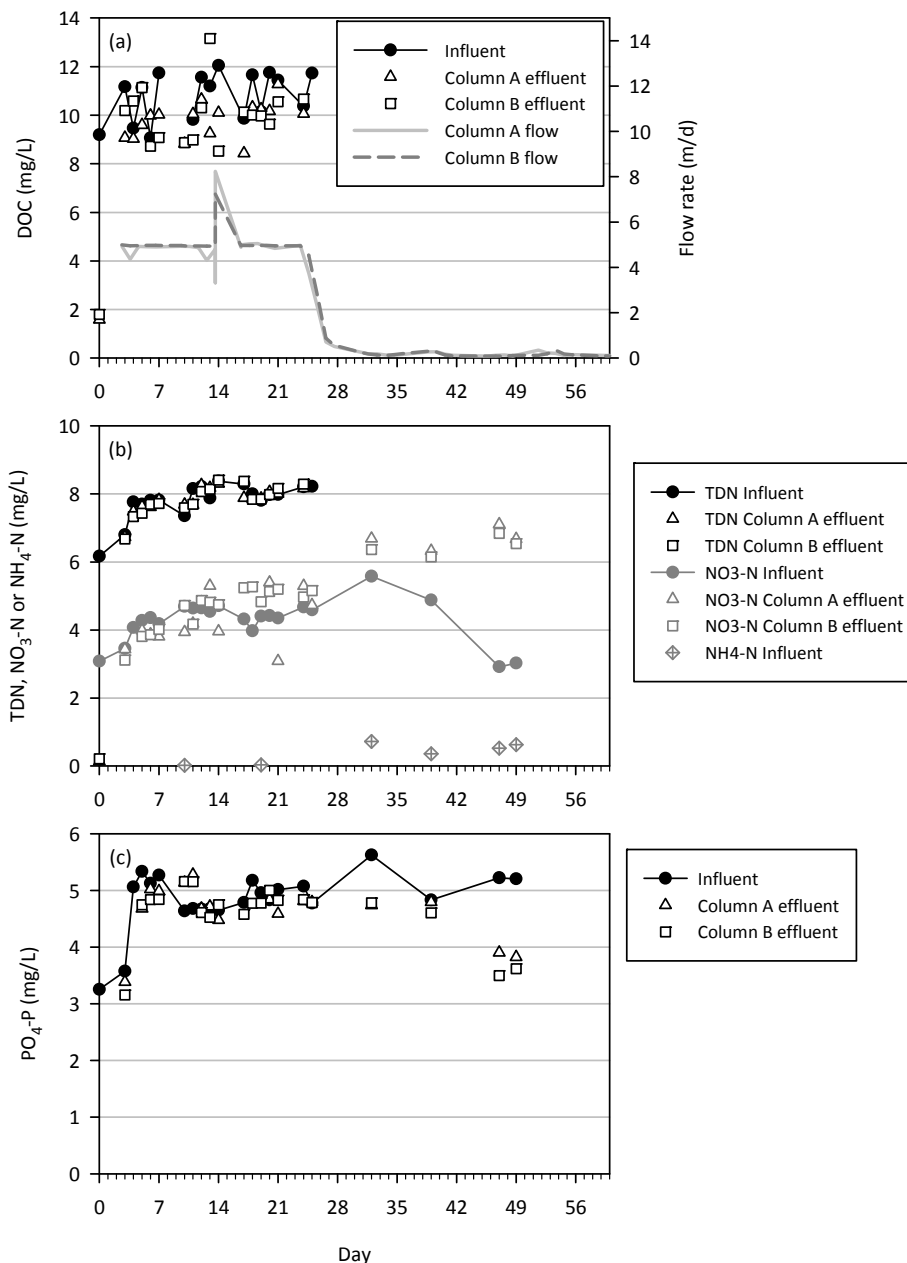


Figure 13 Nutrient concentrations in influent recycled water and column effluent.

Microbial communities

Total microbial cell counts in the extended filtered secondary treated wastewater column experiment ($2.5 \times 10^7 \pm 1.9 \times 10^7$ cells/g soil) were similar to the final column dissections of the initial filtered secondary treated wastewater column experiment (Kaksonen *et al.* 2015). Bacterial community analysis was conducted on three subsamples, 0–5 mm, 5–10 mm and 190–210 mm (relative to the infiltration surface) from both columns A and B following the completion of the experiment on day 75. The total microbial cell abundances of the soil impacted by wastewater infiltration were at least one order of magnitude greater than the virgin Spearwood Sand (Table 3) suggesting that microbial cells were introduced with or grew in response to the application of wastewater. A greater abundance was also observed in the 0–5 mm sample with respect to the 5–10 mm, however different responses were observed in the deeper sample (190–210 mm) with decreasing abundance in column B while in column A the abundance was similar to the 0–5 mm sample.

The shallower depths were dominated by bacterial families associated with natural and human impacted environments, including sewage treatment (*Xanthomonadaceae* (5–11 % relative

abundance), *Rhodocyclaceae* (7-9 %), *Comamonadaceae* (5-7 %), *Saprospiraceae* (2-5 %), and *Chitinophagaceae* (3-4 %) (Wang *et al.* 2012; Zhang *et al.* 2012; Oren 2014; Willems 2014; McIlroy and Nielsen 2014) similar to that observed in the shorter duration column experiment (Kaksonen *et al.* 2015). A number of these families were shown to decrease in relative abundance with depth (*Xanthomonadaceae*, *Chitinophagaceae*, *Saprospiraceae*, along with *Caldilineaceae* (3-6%)) to between <1-2% (Kaksonen *et al.* 2015) suggesting that they were likely removed through filtration and were not mobile in the soil column.

Table 3 Total microbial cell abundance in Spearwood Sand before (virgin soil) and after infiltration of wastewater (Column A and B)

Virgin soil (cells/g soil)	Depth (mm)	Column A (cells/g soil)	Column B (cells/g soil)
4.1x10 ⁵ ± 2.2x10 ⁵	0 – 5	3.6x10 ⁷ ± 0.2x10 ⁷	5.7x10 ⁷ ± 0.2x10 ⁷
	5 – 10	1.2x10 ⁷ ± 0.4x10 ⁷	1.8x10 ⁷ ± 0.4x10 ⁷
	190 – 210	2.3x10 ⁷ ± 0.9x10 ⁷	0.3x10 ⁷ ± 0.2x10 ⁷

Increase in relative abundance of the members of the *Solimonadaceae* (from 0-2% to 11-25%), *Rhodospirillaceae* (from 3% to 4-8%) and *Gaiellaceae* (from 0% to 1%) families was observed with depth. As these families were present in the virgin Spearwood Sand (1%, 3-4 % and 9-12%, respectively), it is likely that they originate from the soil used to pack the columns. However they behave differently with *Solimonadaceae* increasing substantially, *Rhodospirillaceae* slightly increasing and *Gaiellaceae* decreasing rapidly relative to the virgin soil (Kaksonen *et al.* 2015). *Solimonadaceae* and *Rhodospirillaceae* bacterial families are chemoorganotrophs and are likely responding to the increased organic carbon supplied with the infiltrated recycled water. Although members of the *Gaiellaceae* family are also a chemoorganotrophs it is not clear why the relative abundance decreased with respect to the virgin soil. The presence of both bacterial families associated with the influent recycled water and increased abundance of native bacterial families may have contributed to the clogging observed in these columns.

The most abundant archaeal family in the columns A and B was ammonia-oxidising *Nitrososphaeraceae* (3-35 %), and some depths also had populations of methanogenic *Methanobacteriaceae* (0-9 %), *Methanosaetaceae* (0-2 %), and symbiotic *Cenarchaeaceae* (0-6 %). The relative abundance of the members of the above mentioned methanogenic families was highest in the top 0-5 mm of the columns and decreased with depth. This is consistent with the thin saturated clogging layer on the top of the columns that would have created anoxic conditions and thus facilitated the growth of strictly anaerobic methanogens. The overall diversity of archaeal families with ≥ 2% relative abundance in the column samples was rather low (Kaksonen *et al.* 2015).

Based on the sequencing of eukaryotic genes, the soils from 190-210 mm depth of the columns A and B were dominated by protists from the family *Heteromitidae* (29-79%). The two most dominant eukaryotic families in the 5-10 mm depths were *Oxytrichidae* (protists) (10-49%) and *Thaumatostigidae* (protists) (20-36%). *Oxytrichidae* was also dominating the 0-5 mm depth in column A (29-32%) whereas in column B *Licmophoraceae* (diatoms, algae) (14-26%) was the dominant eukaryotic family. The relative abundance of the members of the families *Amoebidiceae* (protists), *Euglyphidae* (protists), *Cryptosporidiidae* (parasitic protists), *Ichthyophonida* (parasitic protists), *Tremellales* (fungi), *Gigasporaceae* (fungi), *Stemonitidae* (plasmodial slime molds), *Licmophoraceae* (algae) and *Chromulinaceae* (algae) decreased with increasing depth in both columns. The relative abundance of members of the family *Codonosigidae* (protists) increased with increasing depth in both columns (Kaksonen *et al.* 2015).

Results – Floreat field experiment

Cumulative inflow of wastewater to the Floreat site

Due to frequent interruptions in the wastewater supply to the MAR site, particularly within the first few months of operation, the procedure outlined in the methods section was used to estimate the flow rates at unmonitored times between flow interruptions. For the period between commencement and cessation of MAR, a total of 750 kL of wastewater were recharged to the Superficial Aquifer. The frequency of flow interruptions is shown by the white shaded bands within the grey-shaded pattern on the plots in Figure 14. Note fairly lengthy periods of stable inflow after 20-December 2013 when the new supply pump was installed at Subiaco WWTP.

Groundwater levels, infiltration gallery water levels and soil moisture

Groundwater levels monitored at the site responded largely to seasonal changes in rainfall (Figure 15). The commencement of MAR on 8-October 2013 occurred just prior to the seasonal peak in groundwater level. Following the seasonal peak and as rainfall became less frequent, groundwater declined for the remainder of the experiment. The water level logger measurements in Figure 15 were confirmed with manual measurements. The highly regular pattern and consistent drawdown of water levels measured in FLBGRND1 is likely due to groundwater abstraction from an irrigation bore located near this monitoring bore.

Water levels were monitored in the three PVC wells (north, middle and south locations) within the gallery. These showed an initial increase due to commencement of MAR and responsive changes due to frequent interruptions of inflow until approximately mid-January 2014 whereupon there was a steady rise in the water levels recorded in the middle and north observation points (Figure 16). This is approximately one month after the new supply pump was installed at Subiaco WWTP providing the site with a more stable supply of wastewater. It seems feasible that a more continuous supply of wastewater provided to the site led to there being greater loading of the soil matrix with suspended solids removed from wastewater that would have altered the hydraulic properties of the Spearwood Sand. Approximately one month after the new supply pump was installed, there were observed changes in soil moisture from some of the probes below the gallery (Figure 14). It is interesting to note the divergent pattern of water levels monitored at the south point (Figure 16). This divergence appears to be related to the infiltration gallery shifting vertically after installation as noted while re-surveying the elevation after the experiment. The southern end was 6 to 8 cm above the middle and northern end of the gallery. Thus ponding of water would most likely occur in the middle and northern end of the gallery before reaching the water level sensor at the southern end. Although water levels declined in the Gallery_South PVC well in late January, all three probes showed about a 6 cm increase in mid-February after the wastewater supply was restored after an interruption of supply from the WWTP for a few days. It is not clear why there is apparent clogging following the interruption of wastewater supply; however, one possible explanation is that particulates or biofilm were dislodged from the supply pipe.

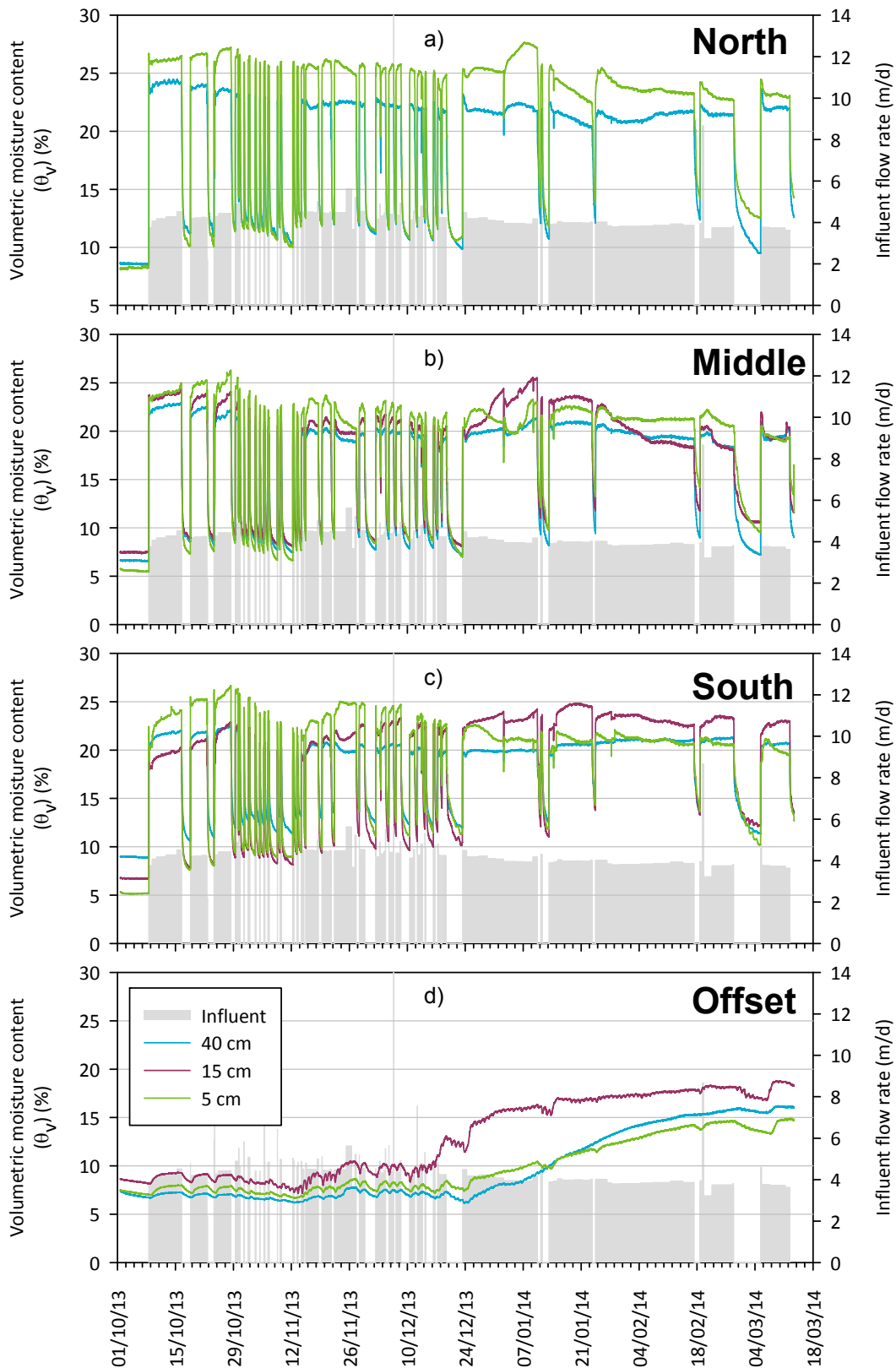


Figure 14 Comparison of soil moisture data from the a) North, b) Middle, c) South and d) Offset probes at the CSIRO infiltration gallery site. Note the frequent interruptions of wastewater flow until late December due to equipment problems at the Subiaco STP, and absence of 15 cm soil moisture data at the North probe location due to sensor malfunction.

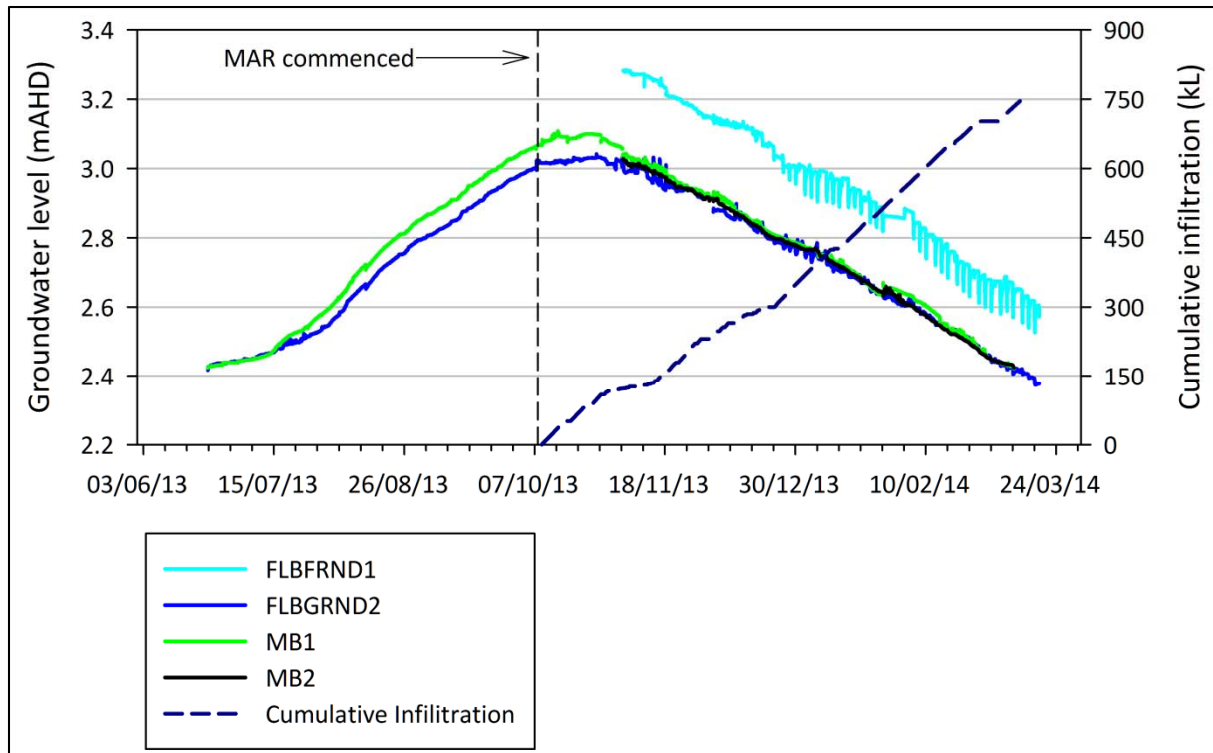


Figure 15 Groundwater measured in the monitoring bores. FLBGRND1 is located farthest from the MAR site (177 m northeast of the site).

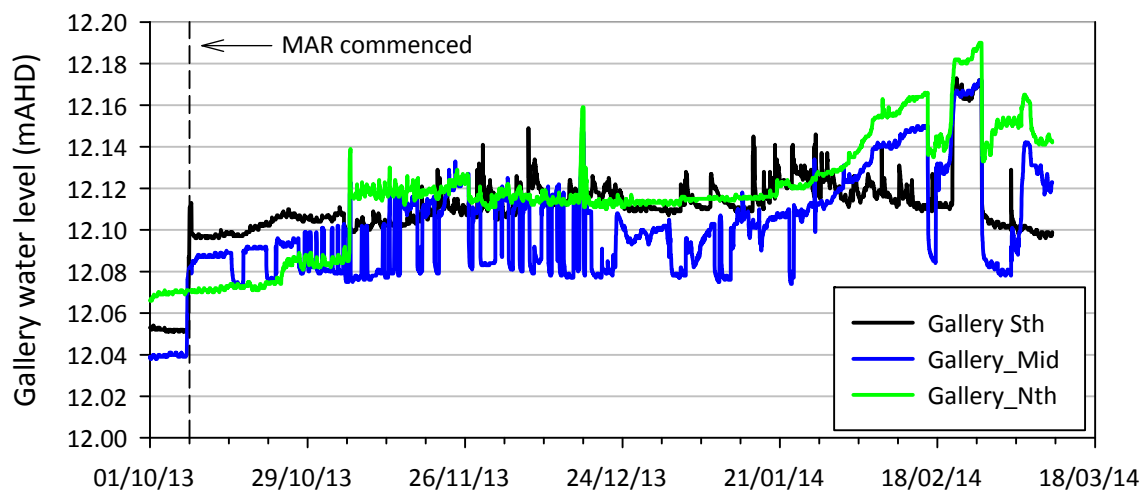


Figure 16 Level of wastewater in the gallery monitored in the three PVC wells. Elevation of gallery base was 12.10-12.19 m AHD.

The soil moisture data for the North, Middle, South and Offset probes (refer to Figure 85 in Appendix 2 for locations) are indicated in Figure 14. Note the 15 cm North probe appears to be malfunctioning from the end of October. Due to malfunctions with wastewater delivery the gallery only received water for 66% of the time between 8th October and 16th December. Due to the high infiltration capacity and low moisture holding capacity of the Spearwood Sand there is a fast response in soil moisture to starting and stopping the application of wastewater.

The North, Middle and South probes responded to the start of the MAR trial with soil moisture contents increasing to between 17 and 30% within the first few weeks. The Offset probes adjacent to the middle probes at lateral distances between 45 and 65 cm from the western edge of the gallery

were slower to respond until the middle of November after a period of frequent interruptions of flow of treated wastewater to the site. This increase in soil moisture content may indicate that the lateral spread of the wastewater plume beneath the gallery was expanding. Since these soils quickly respond to the application of wastewater, the increased lateral spread was potentially due to a reduction in the infiltration rate at the base of the gallery as a result of clogging and greater infiltration through the side walls of the gallery. This can clearly be observed during the extended period of application in January where the moisture content adjacent to the gallery (offset sensors) rose to between 11.5% and 16.8% with the differences between the sensor depths likely due to the distance the sensors were from the gallery. However, the clogging appears to have been minor as the soil moisture below the gallery remained constant or marginally declined over the remaining 80 days of the experiment. If soil porosity is about 40%, 17% water content indicates that the soil was less than half saturated and the hydraulic conductivity was only a fraction of what it would be at saturation (given a normal log normal relationship between water content and hydraulic conductivity).

Modelling of soil water retention characteristics

The water retention function is a relationship between the soil moisture content and the soil water suction, which is essential for predicting flow through variably saturated porous media. In this study, changes in soil moisture were evaluated in response to wastewater recharge to the infiltration gallery. The water retention function was derived from Spearwood Sand samples using the RETC software (van Genuchten *et al.* 2009) and then applied in unsaturated flow models developed with the HYDRUS software package (Šimůnek *et al.* 2011; Šejna *et al.* 2013). The details of this procedure are described in this section.

To determine the water retention function, fourteen sediment samples of Spearwood Sand were collected from different depths, either adjacent or below the infiltration gallery. These were analysed to determine soil moisture content in response to different applied suctions (Figure 17). These analyses were conducted by research staff at the School of Earth and Environment at the University of Western Australia under the direction of Dr Matthias Leopold, using the procedure described in Cresswell (2002). The procedure involves placing an initially saturated sample on a water-filled porous pressure plate and desorbing water from the sample by applying suction. Water drained from the sample through the porous plate to a water outlet system until equilibrium was reached between the soil matrix forces retaining water and the applied suction. Further details of the procedure are given in Cresswell (2002). It should be noted that hysteresis was assumed to be a negligible factor in the field study; thus a model for hysteresis was not developed. Triplicate samples were prepared by repacking sediments into retainer rings, aiming for a bulk density comparable to the average bulk density of four samples collected previously from the site (1.53 g cm^{-3}). The bulk densities of the repacked samples were between 1.461 and 1.536 g cm^{-3} . The suctions applied to the samples were 0.1, 5, 10, 35, 100 and 200 kPa. The suction or matric pressure potential of the soil water may be expressed in terms of force per unit area (kPa) or an equivalent height of a water column. 1 kPa of suction is equivalent to 10.197 cm hanging column of water. The air entry pressure was about 30 cm, suggesting that at least 30 cm suction was required to drain the soil; otherwise the soil remained saturated.

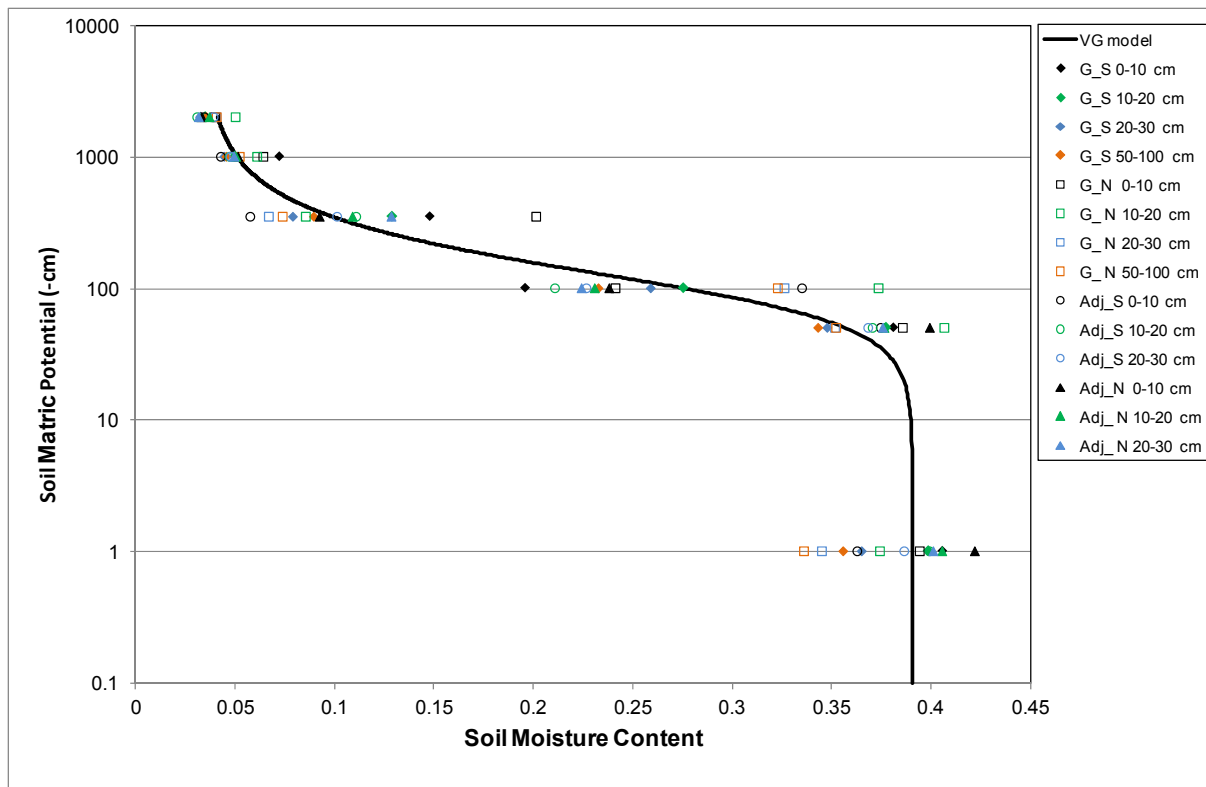


Figure 17 Soil moisture retention function for Spearwood Sand sampled from the zone through which wastewater infiltrated. The van Genuchten model was fitted using RETC software.

Statistical evaluation of spatial variability in soil water retention characteristics

The RETC code for quantifying the hydraulic functions of unsaturated soils was used to analyse the soil water retention function (van Genuchten *et al.* 1991; 2009). The analysis was conducted using the average of triplicate soil moisture data from each location (Appendix 3, Table 19 Bulk density and soil moisture retention characteristics for Spearwood Sand samples collected from the Floreat Infiltration Gallery site. Soil analyses were conducted by the University of Western Australia.). A single hydraulic function was derived based on the samples collected from the fourteen locations, rather than separate hydraulic functions for each location. The decision to use a single hydraulic function was based on a statistical analysis of the results using paired observations and the Student's two-tailed t-test: datasets of measured soil moisture resulting from different applied suctions from the soil water retention experiments were compared for each of the 14 locations. For the Student's t-test, the null hypothesis was that there was no difference between the means of the two datasets. Microsoft Excel was used to calculate the probability (P) that the results were due to chance and the null hypothesis was rejected if $P < 0.05$.

As shown in Table 20 (Appendix 3), there are only a few paired sample locations that have $P < 0.05$, meaning there is a statistically significant difference in the soil moisture retention characteristics between these groups. This occurred at the Gallery South location for the sample collected from the depth interval 10 to 20 cm below the gallery relative to samples collected below this interval between 20 to 30 cm and 50 to 100 cm below the gallery. This also occurred at the Gallery North location for samples collected over the same depth intervals. It remains unknown whether this was due to flow of wastewater causing spatially-dependent changes to the soil properties. Interestingly, there is no statistically significant difference between samples from the shallower depth interval that were collected at the North and South locations (0 to 10 cm below the gallery) relative to samples collected from deeper intervals. It is plausible that suspended solids from the infiltrating wastewater were filtered out of solution during passage through the soil. If this was the case, then the statistical comparison of soil moisture retention characteristics from these groups of samples suggests this mostly impacted the soil 10 to 20 cm below the gallery rather than within the 10 cm vertical profile

immediately below the gallery. There is also a statistically significant difference between the Gallery North sample collected from the depth interval 10 to 20 cm below the gallery and the sample collected at the Adjacent South location from the depth interval 0 to 10 cm relative to the base of the gallery, but not with deeper samples collected from the Adjacent South location. Again, the reason remains uncertain, but could suggest that the post-experiment soil moisture retention characteristics for the Adjacent South sample (0 to 10 cm relative to the base of the gallery) are due to non-uniform infiltration and the filtration of solids from wastewater variably altering soil hydraulic properties to a larger or smaller extent than the other locations sampled.

The majority of the sample groups of soil moisture retention characteristics were not significantly (statistically) different from each other; therefore, a single hydraulic function was used to characterise the post-experiment soil profile.

The RETC program solves an analytical expression for an assigned soil water retention function. For this data set, a van Genuchten model (1980) was selected as it represented the data better than alternatively functions (e.g. the Brooks-Corey function). A nonlinear least-squares parameter optimization method is used by RETC to estimate the unknown coefficients in the hydraulic model (van Genuchten *et al.* 1991). The software produced a model fit with an R^2 of 0.96 based on the following estimates for the soil parameters and model coefficients:

- Saturated soil water content = 0.39078 [-]
- Residual soil water content = 0.03525 [-]
- Parameter α in the soil water retention function = 0.0098 cm^{-1}
- Parameter n in the soil water retention function = 2.35943 [-]

As the soil samples described above were collected at the conclusion of the infiltration experiment from locations in the immediate path of infiltrating wastewater, it is assumed that the soil properties may have altered during the course of the experiment. To test this hypothesis, the results were compared with the water retention function for Spearwood Sand samples from sites that were not subjected to wastewater infiltration. The Spearwood Sand soil moisture retention data from a previous study by Vermooten (2002) are shown in Figure 18. These samples were not from the infiltration site and there may be some natural variability in the Spearwood Sand; however, these data were considered representative of the coastal plain and utilised in the Perth Regional Aquifer Modelling System developed for the Department of Water of Western Australia (Silberstein *et al.* 2009). The parameters determined for the hydraulic model of the data from Vermooten (2002) were:

- Saturated soil water content = 0.357 [-]
- Residual soil water content = 0.04 [-]
- Parameter α in the soil water retention function = 0.057 cm^{-1}
- Parameter n in the soil water retention function = 3.24 [-]

Parameter values for the tortuosity and the hydraulic conductivity required for the HYDRUS unsaturated flow model were not fitted using RETC. RETC software cannot be used to estimate tortuosity. Tortuosity was assigned a value of 0.5 [-] based on the literature and saturated hydraulic conductivity was assigned a value of 20 m/d from previous experimental data from the Floreat Infiltration Galleries site from Rümmler *et al.* (2005). Unsaturated soil hydraulic conductivity was estimated by HYDRUS using the van Genuchten-Mualem model (van Genuchten *et al.* 1991; Figure 19).

The soil moisture retention characteristic curve for the post-experiment data shows higher soil moisture contents for any given suction than the curve representing initial Spearwood Sand conditions at the site (Figure 18). It seems plausible that passage of wastewater through the soil added fine material to the soil matrix, thereby enabling it to retain moisture more than the medium grain texture of the original Spearwood Sand.

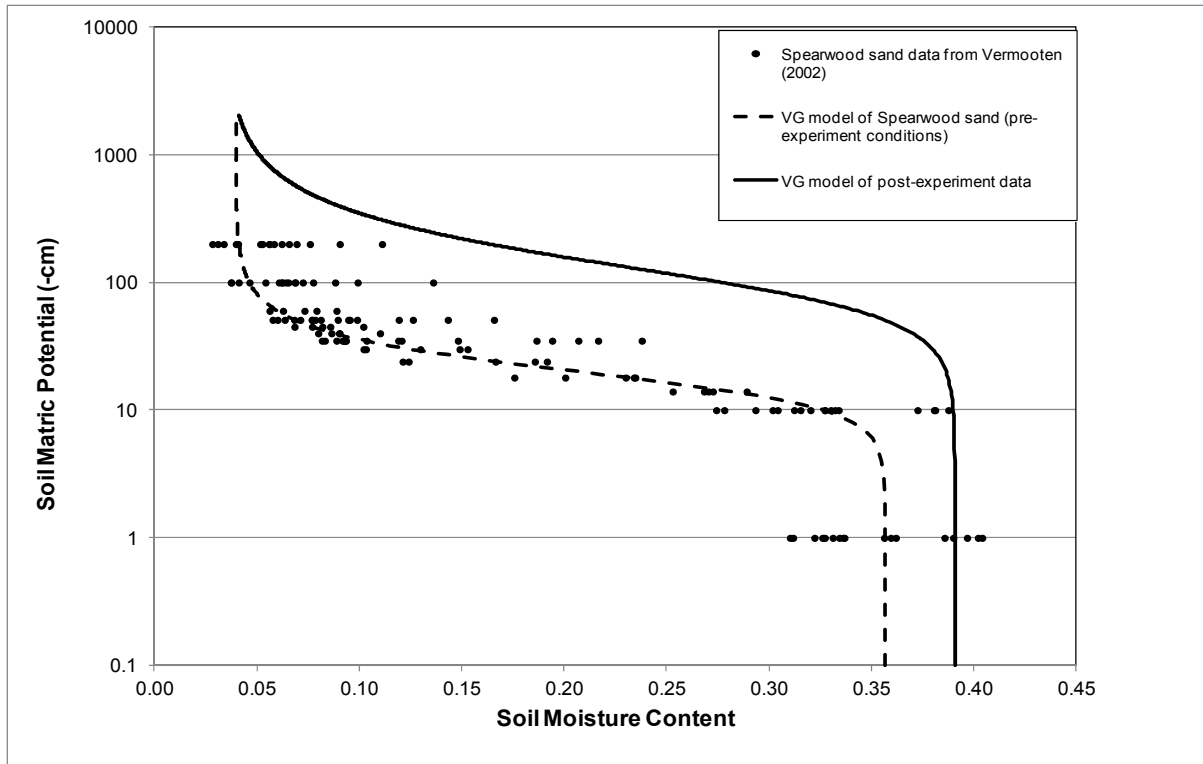


Figure 18 Soil moisture retention data and the van Genuchten model for Spearwood Sand based on data from Vermooten (2002), representing initial conditions at the infiltration site prior to any wastewater infiltration (dashed line). The model of post-experiment data from Figure 17 (solid line) is plotted for comparison.

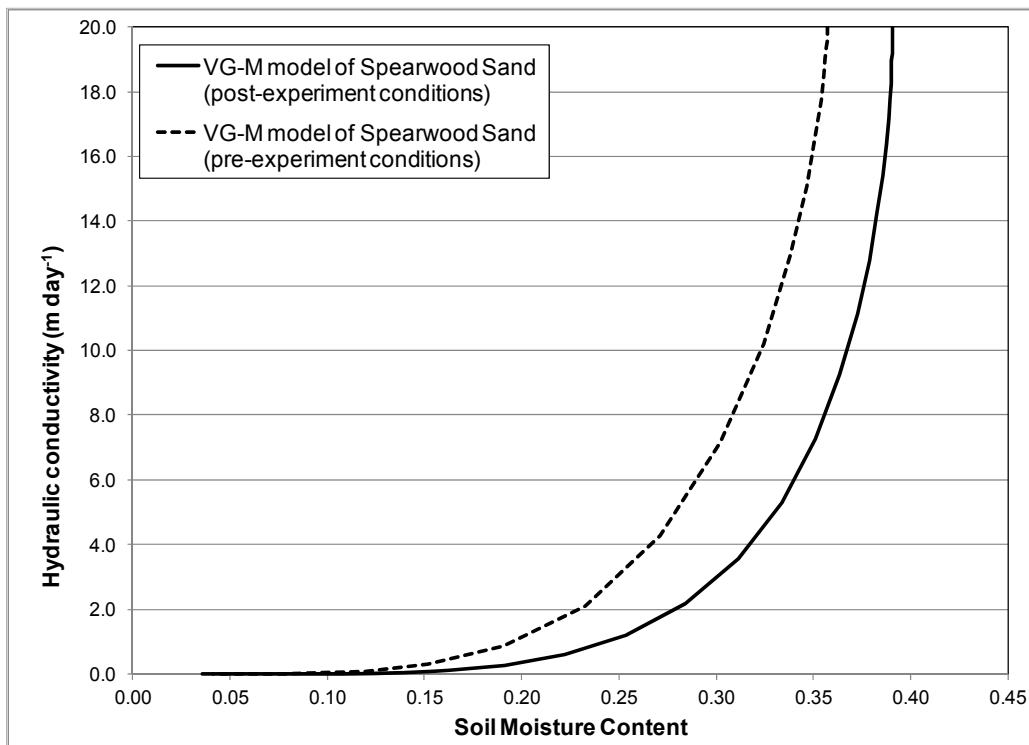


Figure 19 Unsaturated hydraulic conductivity predicted by the van Genuchten-Mualem model with HYDRUS.

The spatial extent of the unsaturated flow model for the Floreat infiltration gallery site was 7 m (depth) by 5 m (width), representing a cross-sectional slice through half the 40.8 cm width of the shortest dimension of the gallery (Figure 20). The boundary conditions for the simulation were as follows: the base of the model was assigned as a free drainage boundary (unit total vertical hydraulic gradient), which is applicable where the watertable is situated several metres below the domain of interest (Šimůnek *et al.* 2011; Šejna *et al.* 2013). The base of the gallery was assigned a variable flux boundary corresponding to the monitored influent flow rates to the gallery depicted in Figure 20. All other boundaries were assigned as zero flux boundaries. It is assumed that geofabric along the top and sides of the gallery prevented outflow along these boundaries, which were thus assigned no flux boundary conditions in the model. The soil moisture probes at depths of 5, 15 and 40 cm (relative to the base of the gallery) at the North, South and Middle locations roughly correspond to observation points #1, 3 and 5, respectively (Figure 20). Observation points # 2, 4 and 6 correspond to the Offset probes at depths 5, 15 and 40 cm, respectively relative to the base of the gallery (Figure 20).

Different versions of the model were tested to ensure that the finite element grid spacing, spatial extent of the model domain, and the assumption of symmetry in cross-section to reduce the model computational time for running the model were appropriate. The target size for the finite element mesh was 10 cm spacing, but grid refinement around the base of the gallery was used to produce smaller grid spacing. The mesh contains 9143 nodes (17,986 2D elements). Six nodes corresponding to the approximate locations of the soil moisture probes were assigned as observation points.

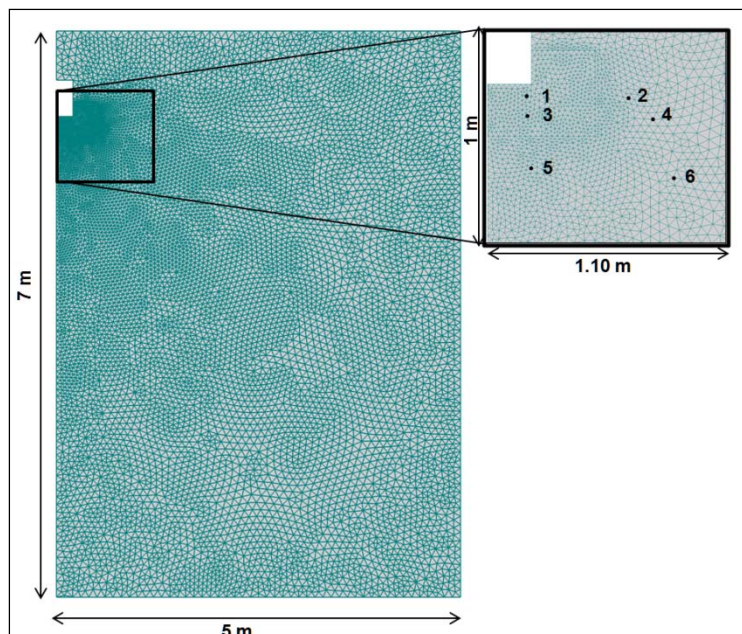


Figure 20 Finite element mesh for the HYDRUS flow model through a cross-section of the gallery from 0 to 7 m below ground level. The close-up view shows the six observation points for examining model output that correspond to the approximate locations of soil moisture probes.

HYDRUS model of wastewater Infiltration

The transient model simulated the 5 month duration of the MAR experiment, beginning 1-October 2013 (one week before recharge commenced) until the experiment concluded in March 2014. As depicted in Figure 21, the water content of the soil zone near the base of the gallery increased over the first 14 days of monitoring until a fairly stable profile of soil moisture was achieved between Days 10 and 14. The maximum predicted water content below the gallery was 0.29 [-]. The model predicted that the soil water content farther away from the gallery (i.e. 3 to 5 m to the west) continued to drain. As shown in the time series of close-up views, water content below the gallery rapidly decreased in response to a stoppage of wastewater inflow from the WWTP between Days #14 and 15 to values between 0.07 to 0.13 (Figure 22). After the inflow of wastewater to the site was restored, water contents below the gallery increased to the previous distribution of values as shown for Day 20. The

results for later in the experiment (Day 120) are shown for comparison. The model takes into account variations in the rates of wastewater inflow to the gallery via the variable flux boundary condition assigned to the base of the gallery. The distribution of water contents predicted for Day 120 are slightly lower due to lower rates of wastewater inflow to the gallery at this time.

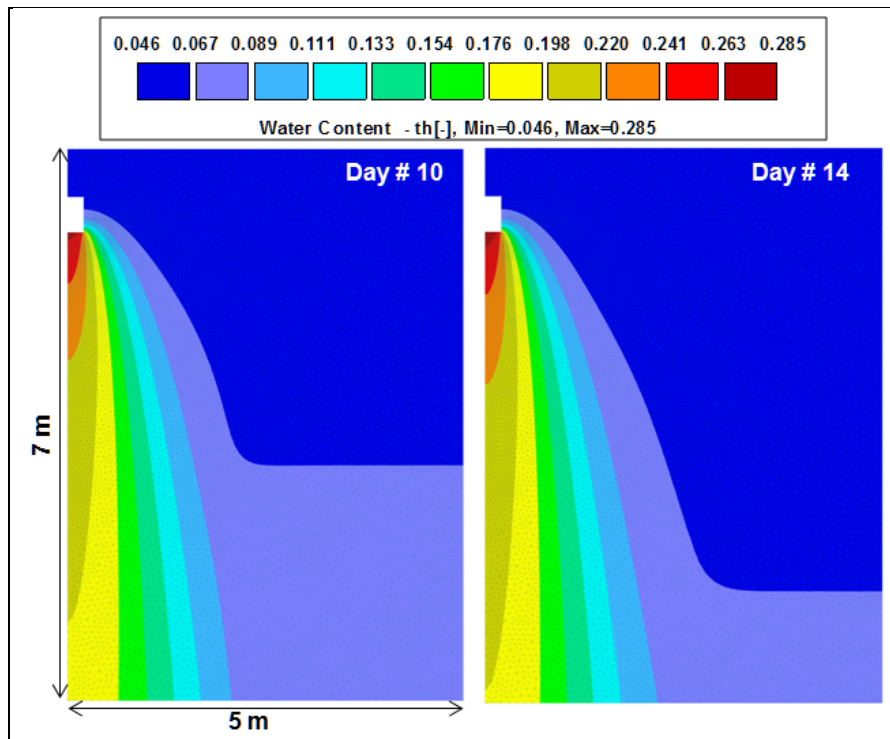


Figure 21 Predicted distribution of soil water contents for the cross-section model on Days 10 and Day 14.

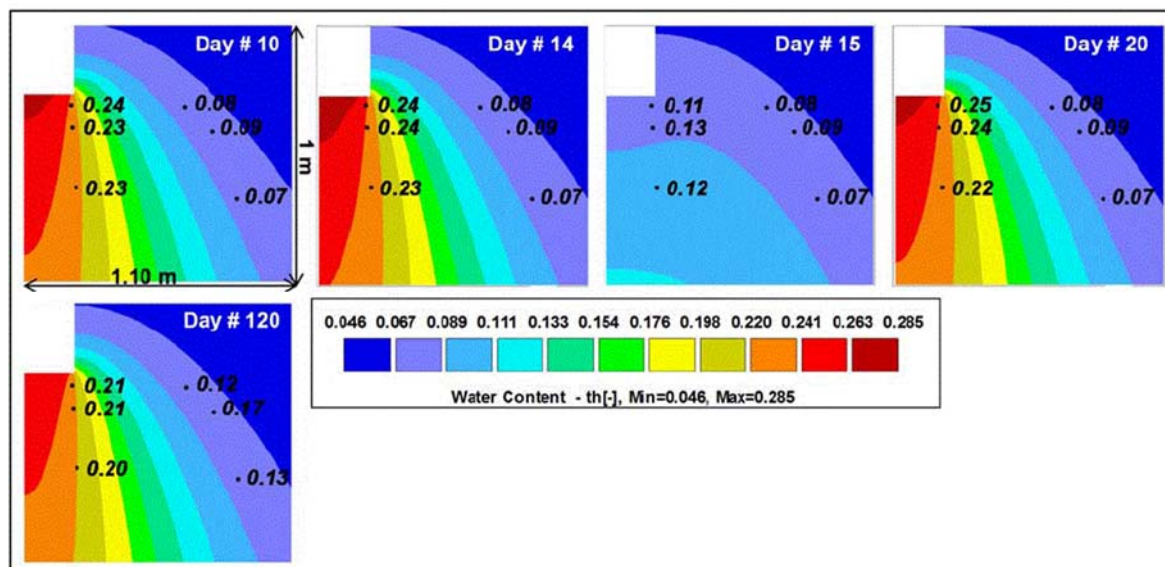


Figure 22 Close-up view of model output at several times, showing a predicted time series of soil water content from the HYDRUS model. Superimposed on the model results are point measurements. Note, MAR commenced on Day 6.

Predicted soil moisture contents over time for the six observation points are compared to soil moisture data logged with probes in Figure 23. The timing of changes in soil moisture at different observation points are predicted fairly well by the model based on the initial Spearwood Sand hydraulic properties. There is variability in the soil moisture contents measured along the length of the gallery at the North, Middle and South Probe locations due to flow that the cross-sectional model cannot reproduce as it assumes homogeneity perpendicular to the plan of the cross-section. Predicted soil moisture contents at the observation points located 5, 15 and 40 cm below the infiltration gallery are similar to the measured data. During the first 20 days, the model reproduces the observed data from the Middle Probe locations at 5, 15 and 40 cm depths below gallery better than at the North and South locations. Thereafter, predicted soil moisture contents are generally higher than the observed data from the Middle probes during infiltration and lower than the observed data from the Middle probes during no flow events. For the Offset Probe at 5 cm relative to the base of the gallery, predicted soil moisture contents reproduce the variations in the observed data until Day 77 (17-Dec. 2013). Thereafter, the observed soil moisture contents increase considerably (e.g. 0.08 to 0.15 for the Offset probe located 5 cm below the gallery). Similar trends are shown for the deeper Offset probes (Figure 23), although the timing of the rapid increase in soil moisture is progressively later depending on the depth of the probe.

It is important to note that at the time of significant increase in soil moisture around Day 77 in the model, the total suspended solids in the wastewater inflow to the gallery increased well above average: sampling conducted between 6-December and 17-December (Day 65 and 76 in the model) yielded an average TSS of 37 mg/L. The filtering out of suspended solids from the wastewater as it passed through the Spearwood Sand would have altered the hydraulic properties. Moreover, a new pump was installed 20-December 2013 (Day 80 in the model), which reduced the frequency of interruptions in the flow of treated wastewater for the MAR trial. As a more consistent volume of wastewater recharged the site over the remaining months, it appears that there was greater lateral spread of wastewater through the soil profile, resulting in steadily increasing soil moisture at the Offset probe locations at depths 5, 15 and 40 cm relative to the base of the gallery. At this time, the soil hydraulic properties may have altered significantly as described in Figure 18, possibly leading to clogging beneath the gallery which facilitated lateral flow. One would anticipate that this behaviour would continue if the MAR experiment operated longer than the 5 month period. The model failed to reproduce the rising trend in soil moisture detected in the probes at the Offset probe location after a period of higher than average TSS and the installation of a new supply pump due most likely to changes in soil hydraulic properties that developed. In contrast, predicted soil moisture below the gallery at the North, Middle and South probe locations were generally higher than the observed data despite a relatively continuous supply of wastewater to the site, suggesting movement of soil water laterally away from these probes located below the gallery.

The introduction of a new set of soil hydraulic properties to the model on Day 70 based on the retention curve in Figure 17 was tested, but failed to provide a satisfactory match to the observed data: predicted soil moisture contents were significantly higher, but it was difficult to reproduce the timing as the properties were likely to have altered gradually over time and perhaps in a non-uniform spatial pattern. Further modelling of time-dependent changes in hydraulic properties could attempt to estimate changes in hydraulic properties in relation to cumulative wastewater volume or total suspended solids.

A model using hydraulic properties derived from post-experiment soil moisture retention data for the entire 160 day period was tested and the results over-estimate the soil moisture contents (e.g. Observation point #2; Figure 24). This suggests that further modelling should involve time-dependent changes in hydraulic properties; however to develop such a model will require greater sampling beneath the gallery to establish the dimensions of the zones with altered properties through time.

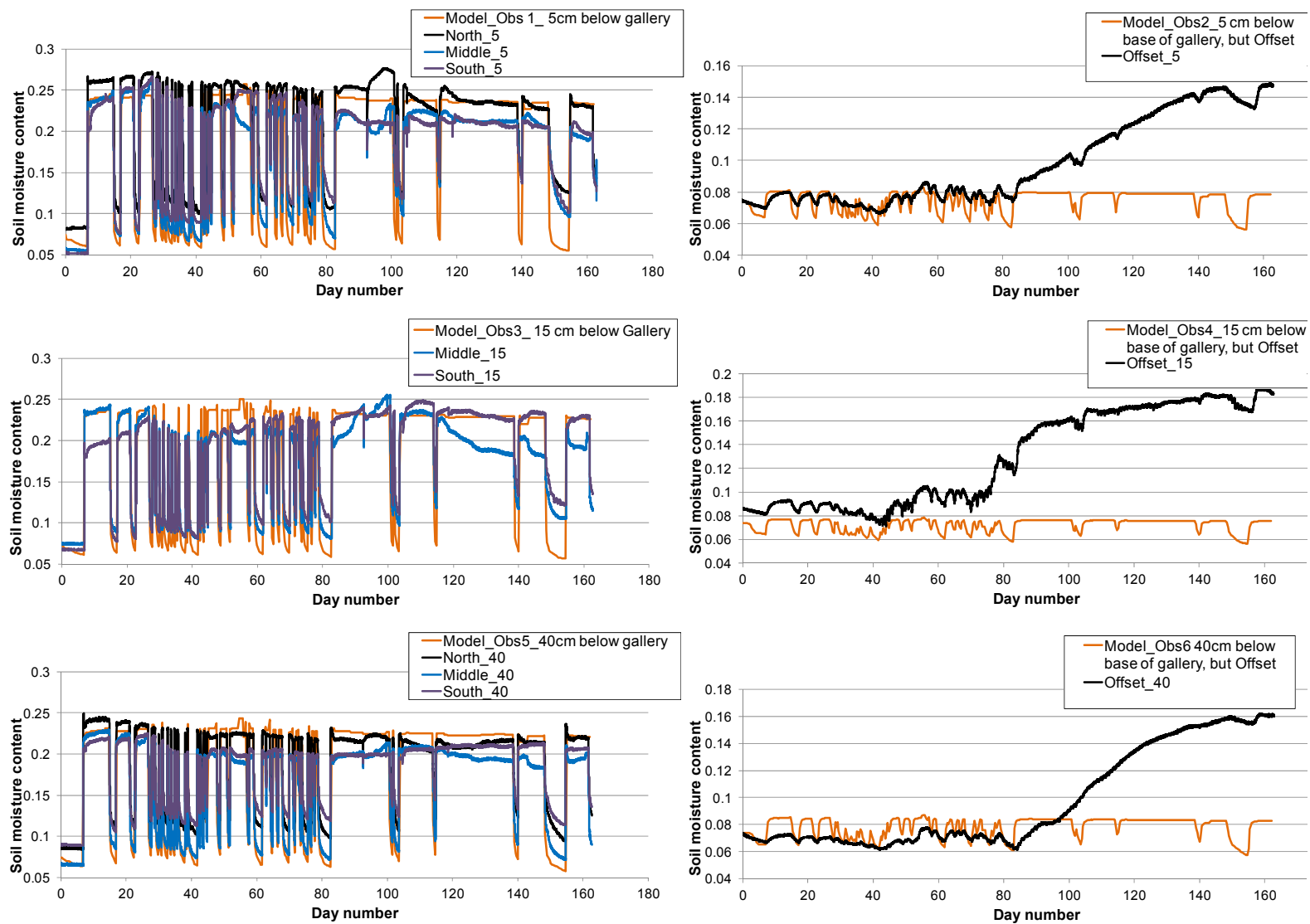


Figure 23 Comparison of HYDRUS model results and observed data from soil moisture probes. The hydraulic model is based on soil hydraulic properties derived from the analysis of soil moisture retention data from Vermooten (2002) for Perth, Western Australia.

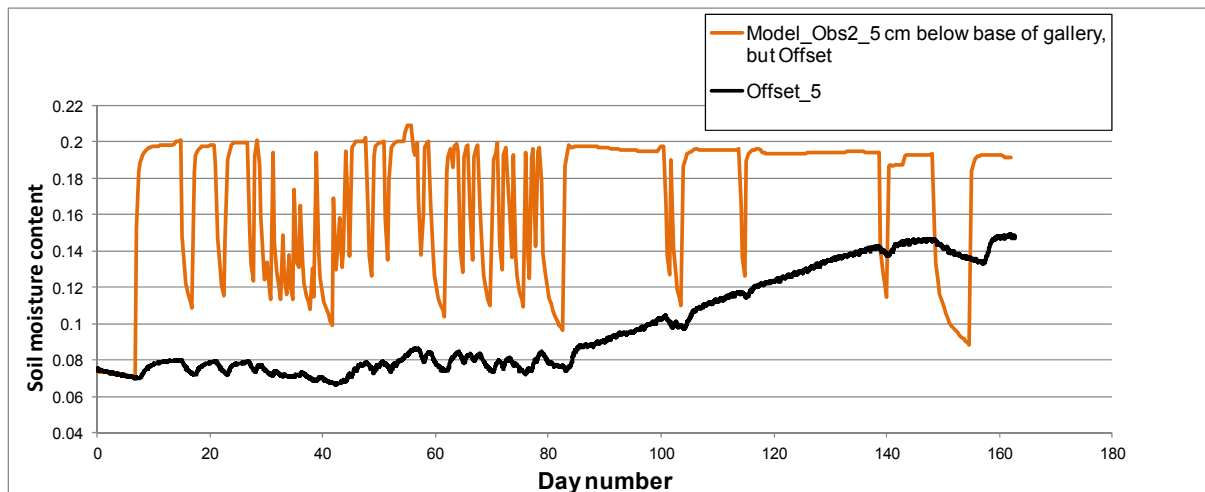


Figure 24 Comparison of Hydrus model results and observed data from monitoring the Offset probe located 5 cm below the base of the gallery. Soil moisture retention data to underpin the hydraulic model were obtained by analysing Spearwood samples collected from the Floreat MAR site, post-experiment.

Geochemistry

The average water quality for the infiltration gallery source water is shown in Table 4 in comparison the pre-infiltration groundwater quality in the two nearby monitoring bores, MB1 (up-gradient) and MB2 (down-gradient). These bores were designed with small screens (1 m long) and were located within approximately 1 m of the maximum groundwater level (Table 2 and Figure 15) to intercept the infiltrated wastewater plume.

The 5 mg/L target for total suspended solids (TSS) was exceeded on some occasions. TSS ranged from <1 to 52 mg/L and was 10.4 mg/L on average based on 33 samples collected between 10-October 2013 and 4-February 2014. Reliable pre-treatment (filtration) to ensure the source water meets the TSS target would be required to manage clogging in an operational filtration gallery. While minor clogging may have occurred in the gallery the TSS load did not appear to influence the hydraulic performance of the gallery to a significant degree.

Background groundwater is typical of the unconfined aquifer and with the major ion chemistry, Ca-Na-HCO₃-Cl influenced by the calcareous sand/limestone aquifer and the coastal location with similar composition for the background (FLBGRND1 and FLBGRND2) and the up-gradient (MB1) monitoring locations (Figure 25). The down-gradient monitoring location (MB2) initially had similar major ion chemistry, however following MAR groundwater chemistry at MB2 was influenced by the source water transitioning towards the Na-Cl dominated influent (Figure 25).

The major ion chemistry also indicates that the source water was the major contributor to groundwater at MB2. Previously, Bekele *et al.* (2011) used potassium as a conservative tracer for source water in this system. An abrupt change in the MB2 potassium concentration occurred approximately five weeks after commencing MAR (Figure 26b). Based on these potassium concentrations, the groundwater in MB2 was 15% source water on 12/11/2013, increasing to 100% source water on 4/12/2013. Other major ions, for example chloride (Figure 26a) also show increasing proportions of recycled water at MB2, though changes are more gradual from initiation of MAR until 100% on 4/12/2013. Bekele *et al.* (2011) found that the source water contributed greater than 80% in a bore 4 m up-gradient. However in the current study the source water only contributed a maximum of 17% to the groundwater measured at MB1, 5 m up-gradient of the infiltration gallery.

Table 4 Infiltration gallery source water quality (October 2013-March 2014). Source water is secondary effluent from Subiaco Sewage Treatment Plant with addition filtration. All parameters in mg/L except pH (-) and EC ($\mu\text{S/cm}$).

mg/L unless given	Source water			MB1	MB2
	No. of samples	Mean	Standard deviation	20/6/13*	20/6/13*
pH (pH units)	36	7.0	0.4	7.5	7.5
Electrical conductivity (EC) ($\mu\text{S/cm}$)	39	1195	80	1170	1020
Total suspended solids	33	10	12	<1	3
Temperature ($^{\circ}\text{C}$)	26	24	3	21	-
Dissolved oxygen	23	3	2	4.9	6.5
Alkalinity as CaCO_3	32	124	12	262	261
Chloride	42	269	26	175	151
Sulfate	42	44	6	57	49
Sodium	42	214	17	116	104
Calcium	42	30	2	104	101
Magnesium	42	6.1	2.1	17	16
Potassium	42	27	2	7.9	7.9
Nitrate-N	37	1.6	1.6	7.0	9.1
Total dissolved N	14	8.9	2.7	8.4	10.8
Phosphate-P	42	4.3	2.1	-	-
Total dissolved P	32	5.3	1.9	<0.01	<0.01
Dissolved organic C	36	26	25	7.4	2.7

*pH, EC, TSS, DO, alkalinity, TDP from 14/8/13

The slower breakthrough behaviour of potassium relative to chloride and sodium indicates that potassium may be retained on cation exchange sites within the soil profile. The sharp breakthrough of potassium may be related to the filling of the available exchange sites before leaching. The behaviour of these ions indicates that recharge with recycled water resulted in the displacement of ambient groundwater to at least 2 m down-gradient of the infiltration gallery.

While the calcium (Figure 26c) and alkalinity/bicarbonate concentrations in groundwater in MB2 shift towards recycled water concentrations, however remained above that expected from conservative mixing alone. Based on the average source water quality, the calcite saturation index ($\text{SI}_{\text{Calcite}}$) was -1.4, whereas the ambient groundwater was in equilibrium with calcite. This suggests that the passage of the source water through the unsaturated zone, especially below a depth of 7.5 m where the average calcite contents is 30% (Bekele *et al.* 2011), resulted in calcite dissolution and the buffering of calcium and bicarbonate concentrations relative to the source water concentrations.

Prior to the field experiment, groundwater in close proximity to the infiltration gallery (MB1, MB2) was higher in nitrogen than the background monitoring bores (FLBGRND1 and FLBGRND2) and the source water, possibly due to impacts of localised land use between the background bores and the monitoring bores (Figure 26e). The nitrate concentration in MB2 decreased toward the influent concentration (Figure 26e), however there was no evidence of nitrate removal. Nitrate concentrations in MB1 behave much differently to MB2 rising to 31 mg-N/L at the end of the trial. This exceeds the historical TN range for the treatment plant (Table 1) and considering that the groundwater only comprises a maximum of 17% of the source water at this location, the nitrate is unlikely to be derived from the recycled water. Addition of nutrient for plant growth trials conducted in a shade house ~30 m up-gradient of the trial site is the likely source of the nitrate. Groundwater sampling eight months after completion of the trial indicate that nitrate concentrations at MB1 were still elevated with respect to the

pre-trial concentrations (Figure 26e), while most other parameters measured returned to pre-trial concentrations.

Phosphorus remained below 0.01 mg/L in all groundwater, despite the breakthrough of source water to MB2. This is consistent with removal by adsorption to iron and aluminium oxides or precipitation as calcium phosphates during infiltration. The aquifer's capacity for adsorption is not infinite and adsorption can also be reversed, thus adsorption cannot be relied upon to permanently remove phosphorus during wastewater infiltration.

Dissolved organic carbon concentrations were variable in the source water and groundwater (Figure 26d). A peak in the influent concentration of 75 mg/L DOC on 5/11/2013 was evident in groundwater from MB2 as a reduced peak of 30 mg/L on 12/11/2013. However, as groundwater in MB2 at this time was only around 15% source water, the reduction in the magnitude of the DOC peak can be attributed to dilution without any evidence for biodegradation. This is supported by the information gleaned from the fluorescence excitation-emission matrices (EEMs) (see following section).

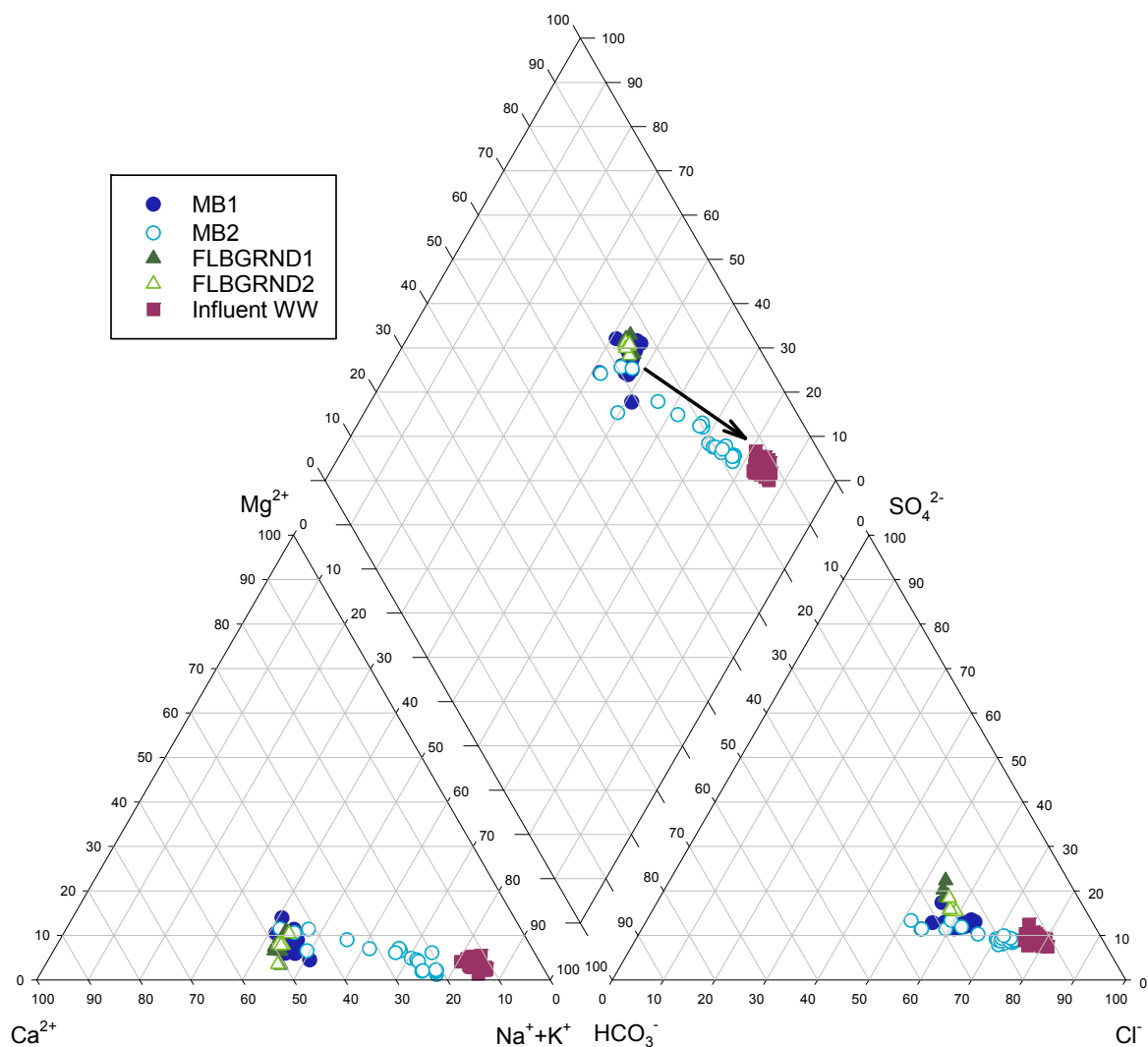


Figure 25 Piper diagram illustrating the transition in major ion chemistry (shown by arrow) in the groundwater down-gradient of the infiltration gallery (MB2) from ambient groundwater (FLBGRND1, FLBGRND2, MB1) toward the infiltration gallery source water (Influent WW).

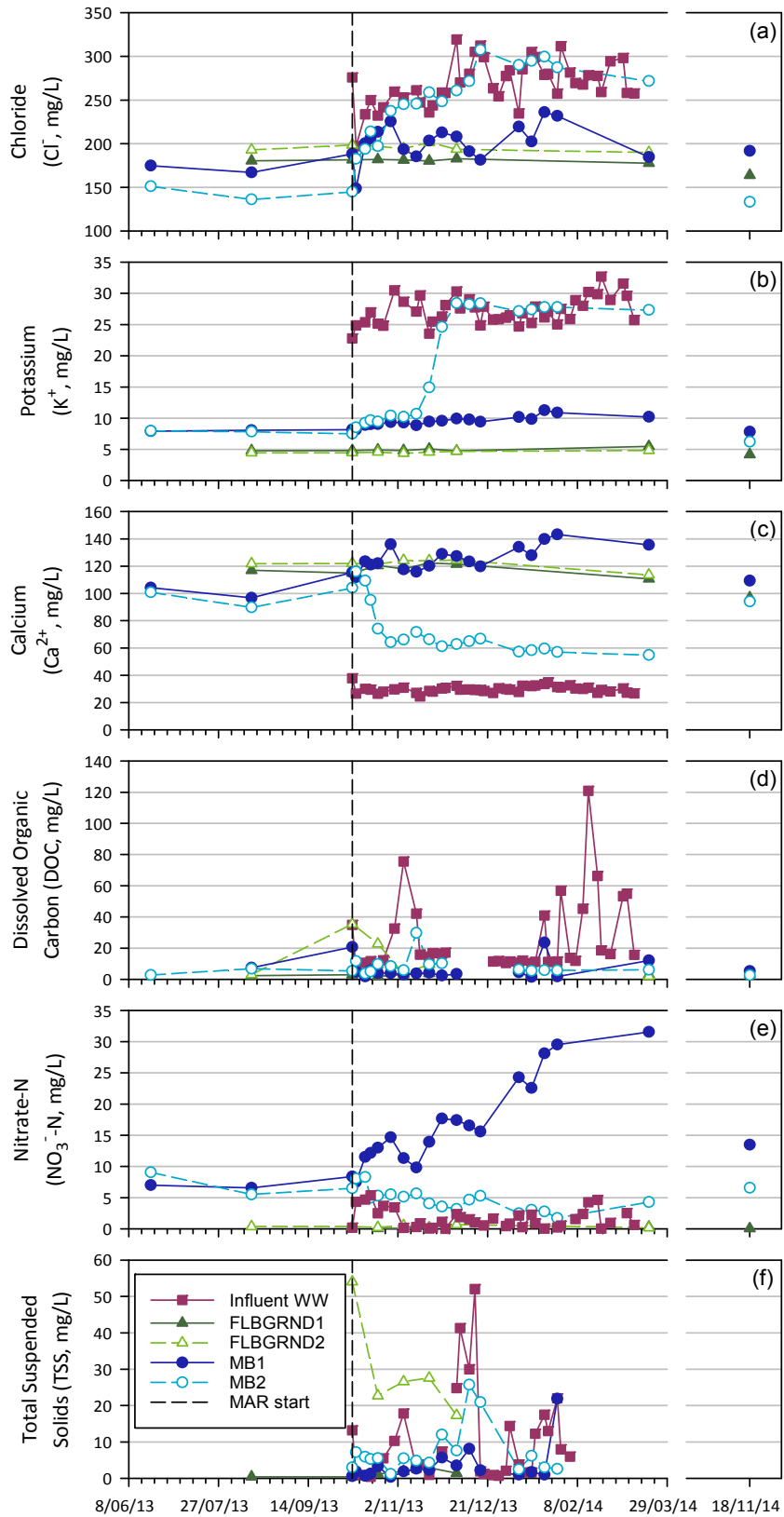


Figure 26 (a) Chloride, (b) potassium, (c) calcium, (d) dissolved organic carbon (DOC), (e) nitrate-N, and (f) total suspended solids concentrations in the infiltration gallery source water (Influent WW), groundwater down-gradient from the infiltration gallery (MB2) and ambient groundwater (FLBGRND1, FLBGRND2, MB1).

Dissolved organic carbon characterisation

Fluorescence excitation-emission matrices (EEMs) have the potential to distinguish different types of organic compounds in water. Fluorescence spectroscopy involves exciting the organic compounds with light at a particular wavelength and measuring the light emitted from the sample with a number of scans making up an excitation-emission matrix. Peaks in the EEMs, fluorophores, have been associated with humic and fulvic acids, proteins and their constituent amino acids such as tyrosine and tryptophan (Henderson *et al.* 2009; Hudson *et al.* 2007). Fluorescence EEMs have been used to identify different organic matter sources based on the characteristics of organic matter terrestrial or marine origin (e.g. Parlanti *et al.* 2000) as well as the relative reactivity based on the relationship between refractory humic and fulvic acids and more labile protein/amino acid components (e.g. Hood *et al.* 2007; McKnight *et al.* 2001; Petrone *et al.* 2011).

The infiltration of recycled water through the unsaturated (vadose) zone has the potential to alter the composition of the organic matter as the biodegradability of the constituent components differs. Initial testing of using fluorescence as a technique to distinguish recycled water dissolved organic carbon from natural dissolved organic carbon were conducted for the influent recycled water (secondary treated, Influent WW), the two background bores (FLBGRND1 and FLBGRND2) and the monitoring bores up-gradient (MB1) and down-gradient (MB2) of the infiltration gallery for samples taken on 19/11/2013. The DOC concentration groundwater samples from these bores were 15.8, 3.8, 9.5, 4.2 and 29.7 mg/L, respectively. After filtering through 0.45 µm cellulose acetate filters, the fluorescence EEMs were determined following the method of Petrone *et al.* (2011). Briefly this involves measuring the fluorescence intensity at a range of emission wavelengths between 300 and 600 nm (2 nm increments) following excitation at wavelengths between 240 and 450 nm (5 nm increments). The samples were diluted to an optical density of 0.05 at 254 nm to minimise inner filter effects (Green and Blough, 1994). The EEMs were corrected for instrument bias (Variab Cary Eclipse) and a blank (Milli-Q water) to eliminate matrix effects. Finally the samples were normalised using the Raman water peak at excitation wavelength of 350 nm with the fluorescence intensity expressed in Raman units.

Figure 27 shows the EEMs measured for the groundwater and recycled water. Peaks relating to different fluorophores, A – humic-like, C – fulvic- and humic-like, and T1 and T2 – tryptophan-like, have been labelled in each figure. The up-gradient groundwater, background bores and MB1, generally showed an overall lower intensity emission than that recycled water and MB2, reflecting the lower dissolved organic carbon concentrations. Groundwater samples up-gradient were dominated by humic-like fluorescence (A) with a less intense C peak. This strongly distinguished it from the influent recycled water which had a more intense C peak as well as tryptophan-like T1 and T2 peaks indicating that more labile organic matter components were present. These tryptophan-like peaks have been used extensively to trace wastewater derived organic matter (Henderson *et al.* 2009; Hudson *et al.* 2007), thus are a strong indicator of the presence of organic matter from the recycled water in groundwater at MB2. Although the samples tested were obtained before complete wastewater breakthrough at MB2 the strong similarity of EEMs between MB2 and the influent recycled water and the presence of the more labile organic matter components suggests that little biodegradation was occurring in the unsaturated zone. The difference in the fluorescence intensity supports the breakthrough of some recycled water at MB2 and results from the mixing of the ambient groundwater and infiltrated recycled water.

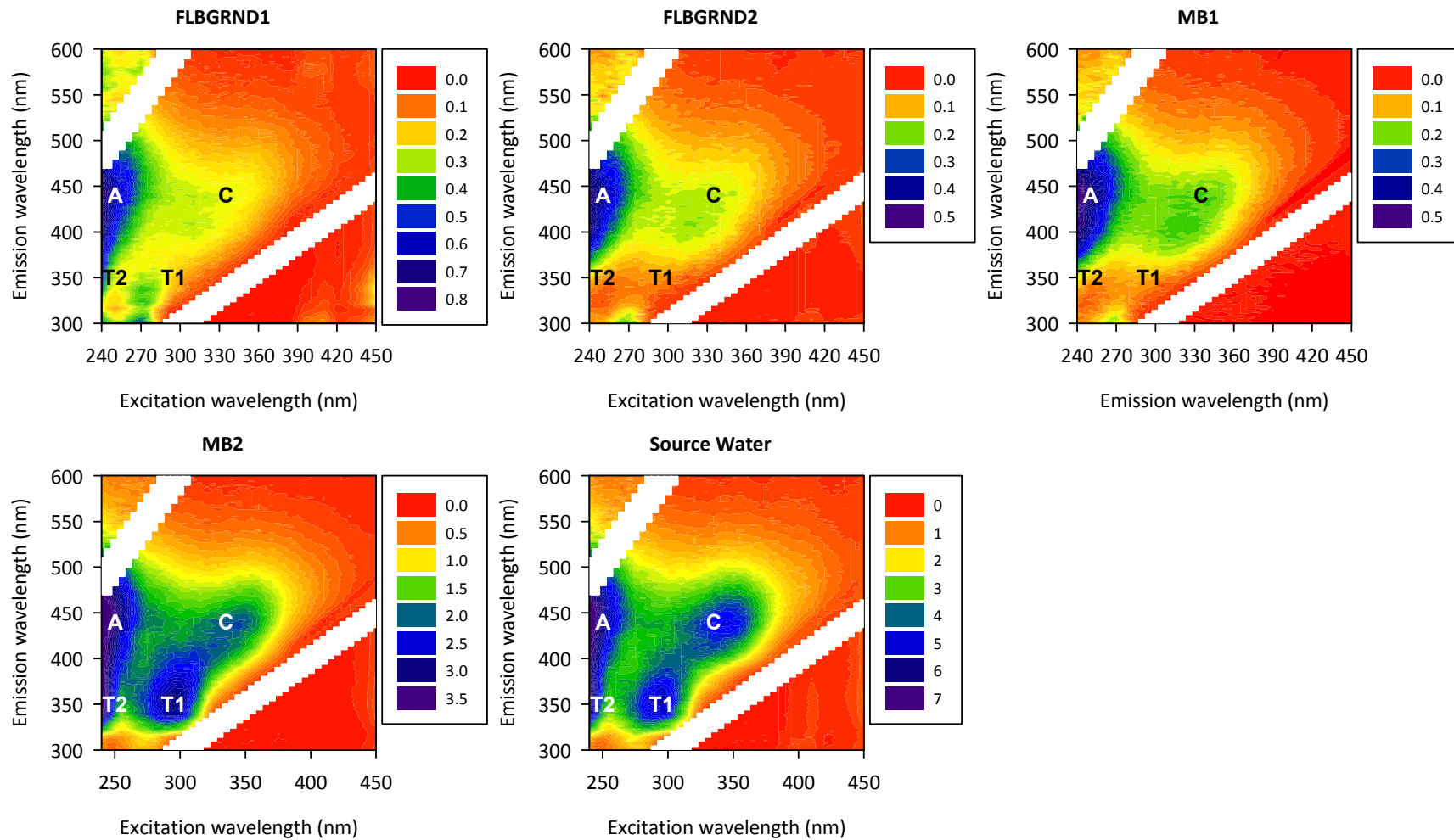


Figure 27 Fluorescence excitation-emission matrices (EEMs) of dissolved organic carbon for: groundwater sampled from the background bores (FLBGRND1 and FLBGRND2), up-gradient monitoring bore (MB1), down-gradient monitoring bore (MB2) and influent recycled water (Source Water), where A = humic-like, C = humic- and fulvic-like, T1 and T2 = typtophan-like fluorescence. The colours represent the fluorescence intensity expressed in Raman units. Note the different fluorescence intensity scales are used to enable comparison of samples. The white areas mask the Rayleigh scatter peaks of water.

Microbial communities

The total microbial cell counts in the infiltration galleries before infiltration were $6.5 \times 10^6 \pm 7.7 \times 10^6$ cells/g of soil. After infiltration the cell numbers in the crate samples were $2.2 \times 10^7 \pm 2.2 \times 10^7$ cells/g. The cell numbers in the adjacent samples after infiltration were $8.9 \times 10^6 \pm 3.8 \times 10^6$ cells/g (Kaksonen *et al.* 2015).

The microbial community structure was analysed for the recycled water (influent to galleries), soil sampled during the installation of the infiltration gallery (six locations on base and sidewall) and during decommissioning of the infiltration gallery, two locations beneath the gallery (at 0-0.5 cm (root mat), 0.5-1.0 cm, 1-2 cm, 5-10 cm and 10-20 cm depth below the gallery base) and two locations adjacent to the gallery (40-50 cm below the gallery base) (Kaksonen *et al.* 2015).

Eighteen bacterial families were identified in the recycled water infiltrated in the galleries ranging from 1% to 28% relative abundance, with *Comamonadaceae* (26-28%), *Burkholderiales* (14-15%), *Solimonadaceae* (10-12%) and *Sphingobacteriaceae* (8-9%) as the dominant bacterial families (Kaksonen *et al.* 2015). These bacterial families have been associated with wastewater treatment systems utilising activated sludge which is used in the Subiaco STP (Wang *et al.* 2012; Wu *et al.* 2013; Zhang *et al.* 2012). While these bacterial families were present in the soil post-infiltration they occurred at much lower relative abundances, *Comamonadaceae* (1-7%), *Burkholderiales* (0-8%), *Solimonadaceae* (1-5%) and *Sphingobacteriaceae* (0-3%) (Figure 28). Aside from *Burkholderiales* which increased in abundance following infiltration (initially 0-1%) the other bacterial families present in the soil did not increase substantially due to the recycled water infiltration, indicating that the recycled water related bacterial families did not outcompete the indigenous soil bacteria during infiltration at the field site (Kaksonen *et al.* 2015).

The diversity of the bacterial families 2% or higher relative abundance in the soil both before (37) and after (33) infiltration was higher than in the recycled water (12). A shift in the community structure was observed between samples obtained before and after infiltration. For example the relative abundance was higher prior to infiltration for *Hyphomicrobiaceae* (1-14% before and 1-4% after), *Oxalobacteraceae* (1-14% before and 0-4% after) and *Caulobacteraceae* (0-6% before and 0-1% after) as shown in Figure 28 (Kaksonen *et al.* 2015). Potentially this may be related to members of these families being adapted to the low nutrient conditions (Abraham *et al.* 2014; Baldani, *et al.* 2014a; Oren and Xu 2014) and being out competed following the infiltration of high nutrient recycled water.

Following infiltration of recycled water the relative abundance of the following bacterial families increased: *Rhodospirillaceae* (2-6% before and 2-12% after), unknown *Alphaproteobacteria* (0-1% before and 3-14% after), *Nitrospiraceae* (1-5% before and 2-11% after), *Rhodocyclaceae* (0-3% before and 0-9% after) as shown in Figure 28 (Kaksonen *et al.* 2015). The increase in these bacterial families was likely in response to the increase organic carbon supply (chemoorganotrophic *Rhodospirillaceae* and *Rhodocyclaceae*), nitrite supply (oxidation by *Nitrospiraceae*), and potentially related to nitrate reduction (*Rhodospirillaceae* and *Rhodocyclaceae*) in response to the increased nitrate availability provided anaerobic microenvironments were present in the soil (Baldani, *et al.* 2014b; Daims 2014; Oren 2014). The presence of *Flavobacteriaceae* (0-15%) and especially at high relative abundances in one root mat sample (0-5 mm, $56 \pm 5\%$) (Kaksonen *et al.* 2015) also supports the use of organic carbon as the utilisation of macromolecules such as polysaccharides and protein is a common feature of many members of this bacterial family (McBride 2014).

The shifts observed in the bacterial family abundances following infiltration of recycled water in the infiltration gallery resulted mainly from changes in the soil chemical conditions with the supply of organic carbon and nitrogen rather than the proliferation of bacteria introduced with the influent recycled water.

The dominant archaeal family in the treated wastewater was methanogenic *Methanoregulaceae* (48-58 %), with minor populations of methanogenic *Methanocellaceae* (1-13 %), *Methanomicrobiales* (0-4 %), *Methanobacteriaceae* (0-3 %), *Methanosaetaceae* (1-2 %), ammonia oxidising *Nitrososphaeraceae* (0-2 %), and symbiotic *Cenarchaeaceae* (0-2 %). The archaeal communities in

the infiltration galleries were mostly dominated by ammonia oxidising *Nitrososphaeraceae* (15-99 %), although in some samples symbiotic *Cenarchaeaceae* (0-78%) and methanogenic *Methanomassiliococcaceae* (0-71 %) were more abundant. Some samples also contained minor populations of methanogenic *Methanobacteriaceae* (0-2 %) and *Methanocellaceae* (0-1 %). The overall diversity of archaeal families with ≥ 2 % relative abundance in the wastewater and Floreat infiltration galleries was rather low (Kaksonen *et al.* 2015).

The eukaryotic community in the treated wastewater was heavily dominated by fungi with *Spizellomycetaceae* (87%) and *Testudinaceae* (3-6%) being the only families identified with over 2% relative abundance (Kaksonen *et al.* 2015). The samples taken from the infiltration gallery before infiltration and the adjacent samples from 140-150 cm distance of the gallery after infiltration had lower overall diversity of eukaryotic families with over 2% abundance than the samples taken from the crates after infiltration. Higher relative abundances of *Chromulinaceae* (algae), *Sordariomycetes* (fungi) and *Cercomonadidae* (protists) were detected in the samples before infiltration than after. *Chlorococcaceae* (algae), *Poaceae* (grass), *Oxytrichidae* ciliates (protozoa), *Amoebidiaceae* (protists), *Cryptomycota* (fungi), *Zoopagaceae* (fungi), *Pythiaceae* (oomycetes, fungus-like saprophytic and pathogenic organisms), *Vampyrellida* (protists), *Ichthyophonida* (parasitic protists), *Monhysteridae* (nematodes), *Lagenidiaceae* (oomycetes), *Monoblepharidales* (fungi), *Syllidae* (worms), *Kreyellidae* ciliates (protozoa), *Stemonitidae* (plasmodial slime molds), *Gigasporaceae* (fungi), *Cryptosporidiidae* (parasitic protists), *Corioliaceae* (fungi), *Paramoebidae* (protists), *Thaumatomastigidae* (protists), *Neocallimastigaceae* (fungi) and *Stephanoecidae* (protists) were relatively more abundant in the samples after infiltration than before infiltration. The four adjacent samples taken after infiltration had rather different eukaryotic communities and were dominated by *Dorylaimida* (nematodes), *Qudsianematidae* (nematodes), *Poaceae* (grass) or *Mortierellaceae* (fungi), respectively (Kaksonen *et al.* 2015).

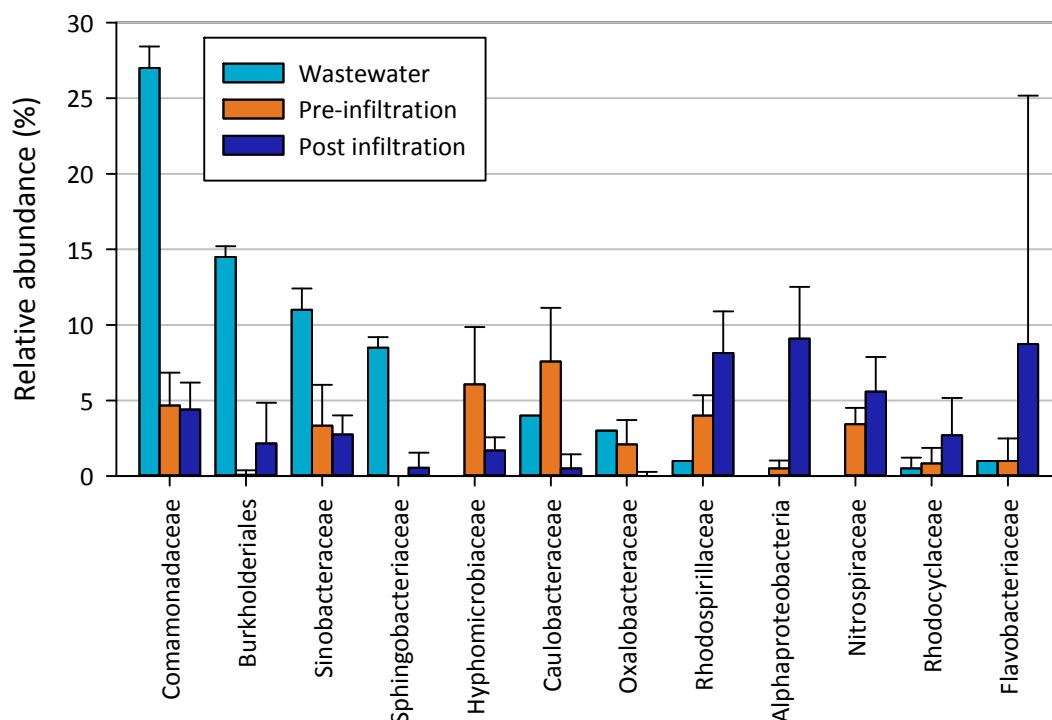


Figure 28 Relative abundance (mean) of selected bacterial families present in the filtered Subiaco wastewater and pre-infiltration and post-infiltration soil samples taken from the Floreat infiltration gallery. Error bars represent one standard deviation.

Floreat summary

Clogging

An infiltration gallery constructed of Atlantis Flo-Tank® modules in Spearwood Sand demonstrated that secondary treated wastewater can be used to recharge the aquifer at an average rate of at least 4 m/d over a 5 month period. A total of 750 kilolitres was recharged to the Tamala Limestone aquifer over this period (average rate of 6.7 kL/d). During the MAR trial, the groundwater levels only changed in response to the seasonal pattern of rainfall due to the highly conductive sand and limestone at this site. In contrast, infiltration experiments conducted using similar wastewater quality and application rates in columns filled with Spearwood Sand led to clogging and significantly reduced effluent outflows from 5 to 0.2 m/d after 3.5 weeks that led to wastewater ponding at the surface. Whilst the average recharge rate of wastewater was 4 m/d during the field experiment, changes occurred spatially in gallery wastewater levels and soil moisture contents surrounding the gallery after 14 weeks. These observations support the hypothesis that heterogeneous clogging developed locally within the gallery and promoted increased flow of wastewater laterally away from the gallery.

There is evidence that non-uniform flow and spatial variability developed in the soil moisture retention characteristics of Spearwood Sand at the Floreat field site at several locations at shallow depths relative to the base of the gallery due to wastewater infiltration. The majority of the samples collected below and adjacent to the gallery were not significantly (statistically) different from each other in terms of their soil moisture retention characteristics. Thus, a single hydraulic function was used to represent sand impacted by wastewater infiltration in a HYDRUS model developed for the site. A different soil moisture characteristic curve was needed to fit the data for Spearwood Sand unaffected by wastewater. This suggests that passage of wastewater through the sands near the base of the gallery variably added fine material and suspended solids from wastewater, thereby enabling the soil matrix to retain more moisture and lowered hydraulic conductivity affecting the direction of migration pathways for wastewater.

The HYDRUS model based on unaltered Spearwood Sand cannot reproduce the soil moisture data for the entire duration of the MAR trial. A steadily increasing discrepancy between modelled and observed soil moistures for the MAR trial was observed and correlated to just after a period of higher than average TSS and the installation of a new supply pump for wastewater that improved continuity of supply. These changes in water quality and the consistency of wastewater inflow would have likely promoted clogging. It is likely that the passage of wastewater through the sands near the base of the gallery variably added fine material and suspended solids from wastewater, thereby enabling the soil matrix to retain more moisture and lowered hydraulic conductivity affecting the direction of migration pathways for wastewater. A single soil moisture characteristic curve for the Spearwood Sand in the HYDRUS model cannot accurately reproduce the time-dependant spatially-varying changes in soil moisture that were observed over the 5 month field trial; instead, temporally varying hydraulic properties in response to changes in wastewater quality are needed to accurately predict soil moisture content and flow changes during MAR. Further modelling of time-dependent changes in hydraulic properties could attempt to estimate changes in hydraulic properties in relation to cumulative wastewater volume or total suspended solids.

Results from the column experiment relative to the field trial highlight the limitations of relying on a one-dimensional interpretation of flow to predict infiltration from a gallery in 2D or 3D. Whilst effluent outflow from columns is representative of vertical flow to the watertable in a MAR experiment, sediment-filled columns with predominantly uni-directional flow produce a high ratio of wastewater to sediment surface area and hence greater opportunity for trapping of particulates, biofilm growth and ultimately clogging that severely impedes outflow. This approach provides a minimum estimate of the time until clogging becomes problematic for recharge; however, it would be very unrealistic to extrapolate time estimates derived from column experiments to the field. Setting water quality objectives to avoid clogging based on column experiments could be unnecessarily restrictive.

Field trials of MAR using infiltration galleries are also not without drawbacks and present difficulties of extrapolating to a larger scale as demonstrated in the Floreat study: it was difficult to maintain

consistent inflows of wastewater due to malfunctioning of the equipment used to supply wastewater to the site and limited resources to address maintenance and equipment problems as they arose. To maintain a fairly consistent level of TSS required bi-weekly, if not more frequent monitoring and maintenance of the filtration equipment. Despite attempts to frequently maintain consistent wastewater inflow and filtration, TSS ranged from <1 to 52 mg/L (average of 8.7 mg/L) during the 5 month experiment. The field trial revealed changes in wastewater levels in the gallery and soil moisture contents surrounding the gallery after a period of higher than average TSS and the installation of a new supply pump, which inhibited intermittent drying. Consistent maintenance of a high ratio of wastewater to sediment surface area over the entire duration of the experiment would presumably lead to clogging within a shorter time frame than that observed in the Floreat field trial.

To extrapolate results from the Floreat field trial to new sites for MAR requires several caveats. It is anticipated that a gallery located in sands with similar hydraulic properties with no lateral restrictions to the outflow of wastewater could recharge the aquifer. To ensure satisfactory hydraulic performance, filtration equipment should be frequently monitored to maintain a target level of TSS of 5 mg/L or less. Based on this study, an infiltration gallery sized similarly and receiving wastewater of similar quality should provide satisfactory hydraulic performance for a minimum of 5 months. For comparison, Water Corporation typically operates a wastewater infiltration basin for 1-2 months with 1-4 months for pond maintenance. Allowing galleries to periodically dry may reduce clogging due to oxidation of organic material. Evaluation of recovery of hydraulic conductivity following drying is warranted to determine if this may prolong the effectiveness of infiltration galleries.

Groundwater quality

Changes in the quality of receiving groundwater from passage of wastewater through the Spearwood Sand and the underlying Tamala Limestone aquifer during the 5 month trial were assessed by comparing the concentrations in the treated wastewater entering the infiltration gallery with water sampled from a monitoring bore located 2 m down-gradient and slotted < 2 m below the watertable. Potassium was used as a conservative tracer to estimate the percentage of wastewater (source water) in groundwater sampled from the down-gradient monitoring bore. The predominant water type in the Tamala Limestone aquifer is Ca-Na-HCO₃-Cl. The infiltration of secondary treated wastewater gradually changed the composition of the receiving groundwater to that of the Na-Cl dominated source water. The proportion of source water in groundwater sampled from down-gradient increased to 100% after approximately 250 kL of wastewater recharge to the Tamala aquifer (after 60 days of the MAR experiment). The reduction in phosphate from passage of wastewater through the subsurface was 100%, whereas the reduction in Dissolved Organic Carbon (DOC) was 69% throughout the MAR trial. Changes in the groundwater concentrations of calcium, alkalinity and phosphorus suggest carbonate dissolution and phosphorus adsorption occurred during MAR, as reported previously by Bekele *et al.* (2011) for a field trial conducted over 39 months in an adjacent pair of galleries.

There was no evidence of nitrate removal. Aerobic conditions in the unsaturated zone and aerobic source water were not conducive to denitrification and an unexpected source of nitrate was discovered up-gradient from the MAR site. The concentrations of total dissolved nitrogen sampled from a down-gradient monitoring bore and the source water were approximately 8 mg/L.

Microbial communities

The total number of microbial cells in soil increased as a result of infiltration of treated wastewater in both column and infiltration gallery experiment. Deoxyribonucleic acid (DNA) sequence analysis showed clear differences in the bacterial communities in sand before and after infiltration. The presence of both bacterial families associated with the influent recycled water and increased abundance of native bacterial families may have contributed to the clogging observed in the columns (Kaksonen *et al.* 2015).

The dominant group of archaea in the Spearwood Sand used for the column studies was methanogens, with ammonia-oxidising archaea also being abundant. These two groups were also consistently observed in the column experiments. Methanogens represented the most dominant

archaeal families in the treated wastewater used in Floreat infiltration gallery with minor populations of ammonia oxidising and symbiotic archaea also present. Most of the soil samples from the Floreat infiltration gallery were dominated by ammonia oxidising archaea, although in some samples methanogens or symbiotic archaea were more abundant (Kaksonen *et al.* 2015).

Recommendations

1. Future studies should evaluate the recovery of hydraulic conductivity following drying to assess whether this would prolong the effectiveness of infiltration galleries.
2. To reduce the potential for future clogging,
 - TSS should be maintained below a target level of 5 mg/L and there should be routine supervision/monitoring of filtration equipment to ensure that TSS levels are below the target level;
 - The ingress of roots into the galleries should be prevented if at all possible by covering the top and sides of the galleries with geofabric, covering the overlying land surface to prevent re-vegetation above the buried infiltration galleries, and possibly applying herbicides (as commonly employed for maintenance of infiltration basins).
3. Due to uncertainty in quantifying the relationship between the amount of biodegradation and adsorption relative to source water quality, the results for phosphate and DOC concentration reductions arising from MAR using infiltration through the Spearwood Sand cannot be extrapolated beyond the limits of the experimental conditions tested (i.e. recharge volumes, rates; source water quality) at this time. Establishing new MAR schemes at a larger scale with higher recharge volumes will need to be intensively monitored.
4. Future studies should aim to quantify the relationship between the amount of water quality treatment (i.e. biodegradation and adsorption) relative to recharge volumes with similar source water quality to determine if there is an incremental relationship that can be used to extrapolate to new MAR schemes involving different recharge volumes and rates.
5. Investigation of changes in soil water retention characteristics due to MAR revealed changes in hydraulic properties that were likely due to changes in source water quality. To satisfactorily predict variably-saturated flow during the operation of a MAR scheme, greater attention is needed to maintain a consistent source water quality and/or determining a quantifiable relationship between the hydraulic properties and time-dependent changes in source water quality that increase solids trapped in the soil matrix and biofilm growth. This may involve a series of experiments using different water qualities and monitoring changes in soil water retention characteristics and possibly changes in the distribution of soil particle sizes.
6. With regard to column studies: in future, more attention to sizing of the columns (e.g. lysimeters instead of columns), and logistics to facilitate supplying large volumes of source water is needed to better represent field conditions and eliminate the potential for edge effects; for example, conducting the experiments at the WWTP, using a larger supply pipe.

Alice Springs Soil Aquifer Treatment

Soil aquifer treatment (SAT) is a method of managed aquifer recharge (MAR) in which the treated wastewater is intermittently placed in recharge basins, allowing for infiltration into the ground for the recharge of unconfined aquifers (Figure 29). As the water moves through the soil and the aquifer, it can undergo water quality improvements through physical, chemical and biological processes. The water is stored in the underlying aquifer for subsequent reuse, generally for irrigation water supplies. This is a favourable water resources management method in areas with high evaporation rates and sufficient land is available for basins.

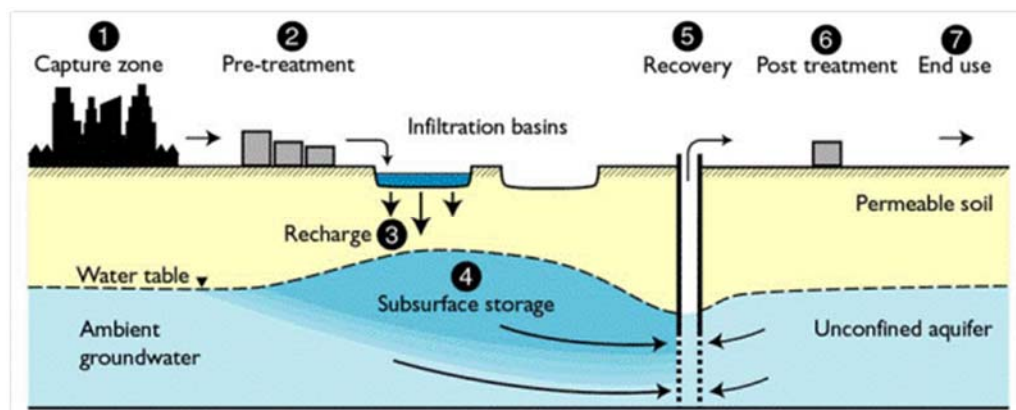


Figure 29 Soil Aquifer Treatment System infiltrating water to an unconfined aquifer (MAR Guidelines NRMCC-EPHC-NHMRC 2009).

As a result of movement of reclaimed water in the subsurface, SAT provides mechanical filtration of suspended particles. From a chemical point of view the method is particularly focussed on producing intermittent aerobic and anaerobic conditions in the soil under the basin. The alteration in redox conditions facilitates nitrogen removal via nitrification and denitrification and also removal of organic carbon from recycled water through mineralisation. Other constituents in wastewater such as pathogens, phosphorus, some organic chemicals (including polysaccharides and proteins) and trace metals can also be effectively removed during SAT. The chemical processes are accelerated by bacteria abundant in this environment.

The efficacy and sustainability of a SAT system is indicated by measurements of (1) infiltration rate and (2) removal of constituents, such as nitrogen, organic carbon and pathogens, from the reclaimed wastewater. Performance is influenced by an appropriate duration of drying and wetting cycles to maximise and sustain the hydraulic loading while also producing water of acceptable quality for its intended uses.

Potential operational issues of SAT sites include:

- Development of a clogging layer (“schmutzdecke”) due to entrapment of suspended solids, biofilm and algae growth, and precipitation of chemical substances, which adversely affects the hydraulic loading.
- Insufficient removal of substances (mostly organic carbon and inorganic nitrogen) which may lead to contamination of groundwater in an underlying aquifer.
- Vegetation growth in the recharge basins which can impact on the effectiveness of the drying cycles.

Site description

The Alice Springs Soil Aquifer Treatment (SAT) scheme is located at the Arid Zone Research Institute (AZRI) situated approximately 7 km south of Alice Springs towards the airport (Figure 30). The Water Reclamation Plant (WRP), where recharge water is produced, is situated next to Ilparpa Swamp adjacent Blatherskite Park. The alluvial aquifer system below the AZRI site extends from Heavitree Gap in the north to south of the airport. Alice Springs' water supply comes from the underlying aquifers of the Amadeus Basin extracted via the Roe Creek borefield located approximately 7 km south west of the SAT site. The area under investigation is characterised by desert climate, with very high evaporation rates and an annual average rainfall 284 mm (Figure 31, Station: 15590 Alice Springs Airport Lat: -23.80, Long: 133.89, elevation: 546 m, daily rainfall). However it should be noted that in 2009 there was only 77 mm rainfall followed by an above average wet year in 2010 with 769 mm. The remaining years 2008, 2011 to 2014 averaged 252±69 mm.

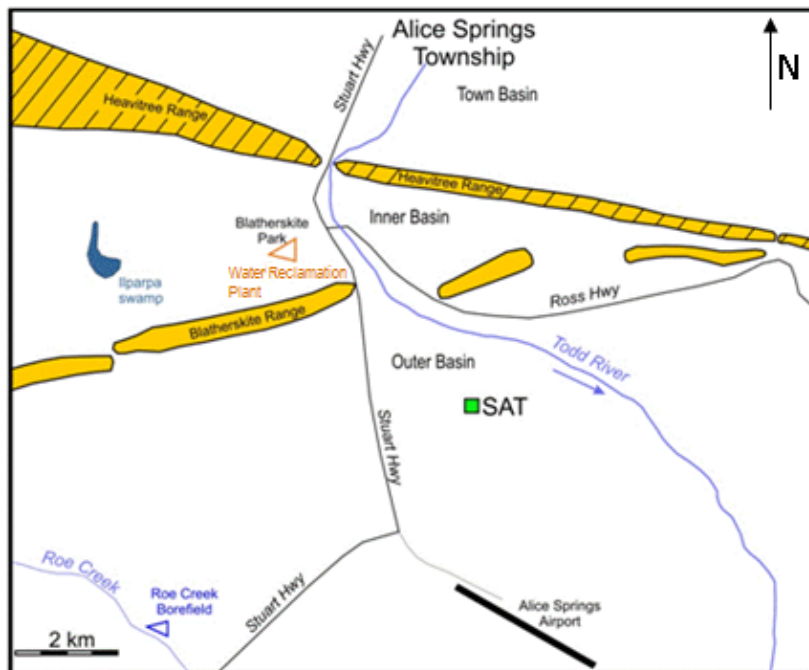


Figure 30 Location of the Alice Springs SAT scheme.

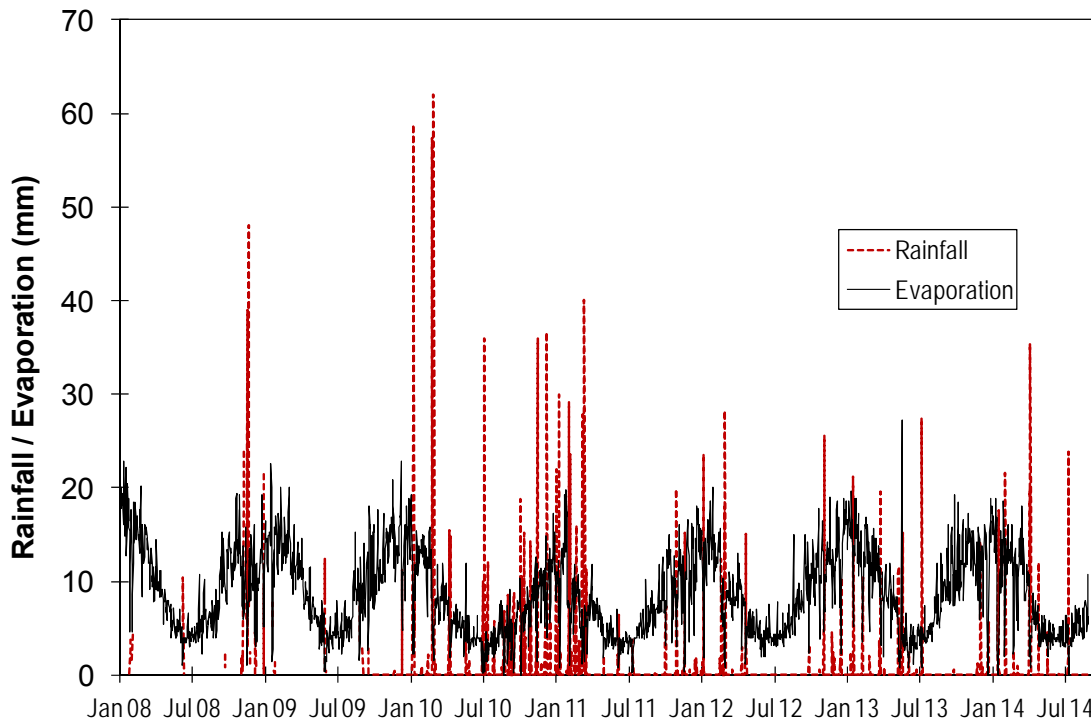


Figure 31 Daily Rainfall and evaporation at the Alice Springs Airport, Bureau of Meteorology Station #15590.

Sequence of development

The Alice Springs SAT project was conceived in 2000 at a workshop to (1) address overflows from the sewage treatment plant into Ilparpa Swamp and (2) reduce high demand on the deeper Mereenie Sandstone aquifer within the Amadeus basin, which has been a major source for potable, industrial and irrigation water for Alice Springs.

By 2004 field investigations were undertaken to select a site for the SAT operation and a feasibility study and environmental impact assessment were completed. This was followed by a public consultation phase and finally construction of the Dissolved Air Flotation (DAF) plant, the pipeline to deliver recharge water to the SAT basins, and completion of the SAT site in early 2008. After commissioning of the DAF plant the basins were first operated on 3 June 2008. Initially four recharge basins (named as RB1, RB2, RB3 and RB4) with a total area of 7,640 m² were available for recharge of recycled water (Figure 32). In December 2009 a fifth recharge basin (named as RB5) was commissioned increasing the total area to 10,300 m².

Historic data on the site performance indicated that by the end of 2009, within first 19 months of the site operation, when four basins of a total area of 7,640m² were operational, 317 ML of reclaimed wastewater was discharged through the system (Miotliński *et al.* 2010). This corresponds to 40 m hydraulic loading at an average rate of 70 mm/d over the total period of 575 days. Average infiltration rate in individual basins varied from 80 mm/d (RB4) to 350 mm/d (RB2), but inflow time lengths for these basins were not equal (Table 5, Figure 33). The average infiltration rate for the first four basins was 238 mm/d (Miotliński *et al.* 2010).



Figure 32 SAT basin RB1 during filling on 22 July 2009.

Table 5 Performance of four recharge basins operating in 2008 and 2009 and average/total performance of the SAT site.

Recharge basin	RB 1	RB 2	RB 3	RB 4	Total
Area (m ²)	1,928	1,880	1,964	1,868	7,640*
Inflow (days)	206	222	164	104	174*
Inflow (ML)	92.9	102.5	82.4	39.7	320.4 ⁺
Average infiltration rates (mm/d)	300	350	220	80	238

⁺ sum of all RBs, * mean value

Expansion of the basins started at the beginning of 2011. The operation of the first basin to be expanded, Basin B, commenced on 29/09/2011. This was followed by Basin A (18/11/2011), Basin C (16/12/2011), Basin D (18/08/2012), and Basin E (19/10/2012). The current configuration involves five recharge basins (A, B, C, D, and E) and a total area of 38,473 m². Basins A and B were established by expanding old basins 1 and 2, respectively; Basin C incorporates old basins 3 and 4; while Basin D is an expansion of the original basin 5. Basin E was established in an area that had not previously contained an infiltration basin (Figure 33). The construction of basins C, D, and E involved lighter machinery than that had been used previously to help prevent compaction of the basin floor. The floor of basin B was compacted by machinery during construction and this had a marked impact on infiltration rates.

Self-seeding vegetation (dominated by Love Grass, Bob Williams pers. comm.) has grown to cover the floors of the basins and at times this acts as a straw mulch. Woody vegetation is also present in Basin B and D, reaching a height of approximately 1.5 m. This tall, woody vegetation has made it difficult or impossible to access some sampling locations on occasion. Transects of vegetation were cleared for the geophysics survey in 2014, which also enabled access to all but one (D14) sampling locations during the final field sampling campaign in August 2014. A photographic record of changes in basin vegetation can be found in Appendix 4.



Figure 33 Expansion of old recharge basins 1, 2, 3, 4, 5 (highlighted), into basins A, B, C, D, E.

MAR system configuration

The current configuration of the Soil Aquifer Treatment basins consists of five recharge basins providing a total recharge area of 38,473 m². Basins A is 7,324 m², Basin B is 8,460 m², Basin C is 8,094 m², Basin D is 6,648 m² and Basin E is 7,947 m².

The source water for recharge is supplied from the Alice Springs Water Reclamation Plant (WRP). Treatment is provided by a series of lagoons, consisting of an initial facultative lagoon and a series of maturation ponds, followed by dissolved air flotation (DAF) (until the end of August 2013). The DAF treatment step was upgraded to dissolved air flotation and filtration (DAFF) and UV from 16 September 2013, to provide Class A Reclaimed Water and increase the potential for direct recycling.

Recharge targets a paleochannel of the Todd River, a Quaternary alluvial aquifer consisting of coarse grained sediments overlain by finer grained clayey silts, clays and sands (Knapton *et al.* 2004). At conception, recharge was intended to reduce environmental impacts associated with wastewater overflow while also augmenting the groundwater resource. Recovery of groundwater could be used for agricultural use or for non-potable domestic uses, possibly substituting for use of potable supplies, however to date no recovery has occurred.

Methods

Field-based experimentation was deemed as the most informative for the Alice Springs SAT site due to the variability in soil characteristics across the site. Initial attempts to undertake column studies found that initial hydraulic conductivity was altered due to soil dispersion or soil disintegration. The field program includes characterising the physical, chemical and microbiological properties of the schmutzdecke and soil profile within the basins; evaluating the character and reactivity of organic carbon and nitrogen in source water for SAT; and assessment of infiltration beneath the basins using geophysical techniques. Furthermore, commissioning of the upgrade to the Alice Springs Wastewater Treatment Plant from DAF to DAFF treatment in September 2013 provided an opportunity to assess the basin performance with an improved source water quality.

Infiltration rates

Volumes of recharge water released to individual infiltration basins were measured using water meters. Infiltration rate in each recharge basin was estimated from the water level measured by a pressure transducer located close to the inlet. The measurements were taken when the floor of the basin was fully covered with water, immediately after inflow had ceased. Infiltration rate is calculated from the following formula, neglecting evaporation, which is comparatively small in relation to the rate of infiltration:

$$I_p = \frac{\Delta h}{\Delta t} \quad \text{Equation 1}$$

where I_p – infiltration rate (mm/d)

Δh – change of water level in a basin (mm)

Δt – time over which the change in water level takes place (d).

The method of estimating infiltration rates gives approximate results. At the beginning of application when the soil is dry, change in soil moisture and above ground storage is a major component of the mass balance equation. Also there are many processes affecting water level in recharge basins that are not considered here. For example, the methods neither include losses due to evapotranspiration nor gains due to rainfall.

This report includes data up to and including 30 September, 2014.

Soil compaction tests

Soil compaction was evaluated using nuclear densometer and dynamic core penetrometer methods, carried out by Alice Materials Testing between July and November 2012. Sampling locations are shown in Figure 34. Fifteen nuclear densometer tests were completed, based on Australian Standards (AS1289 1.2.1, 5.8.1, 5.1.1, 2.1.1 and 5.4.1). This method is used to measure bulk density and moisture content of soils. The nuclear densitometer consists of two radioactive sources or emitters; namely, a gamma source for measuring density and a neutron source for measuring moisture content. The direct transmission mode of operation, which requires insertion of the source rod into the soil profile, is used for measuring density. The density reading recorded is an average value for the material between the surface and the source at the end of the rod. The source of the rod may be inserted into the soil profile at different increments, up to a maximum depth of 300 mm. The neutron source is located in the gauge itself, which uses a backscatter technique to measure the average moisture content of the top 10 cm of material beneath the gauge. The gauge calculates the moisture content, subtracts it from the soil's in-place (wet) density, and reports the soil's dry density. Densometer tests were undertaken for a depth interval of 0-150 mm at all locations. For six locations in Basins B and D the measurements were also taken for two additional depth intervals, 150-300 mm and 300-450 mm. Nine dynamic core penetrometers (DCP) tests were undertaken as described in the Australian Standard AS1289.6.3.2, whereby a 16 mm steel rod with a steel cone of 20 mm base diameter and 60° cone tip is attached. The 'DCP' is driven into the soil by a 9 kg hammer with a falling height of 510 mm. The accumulative number of blows and penetration depth is recorded during the operation.

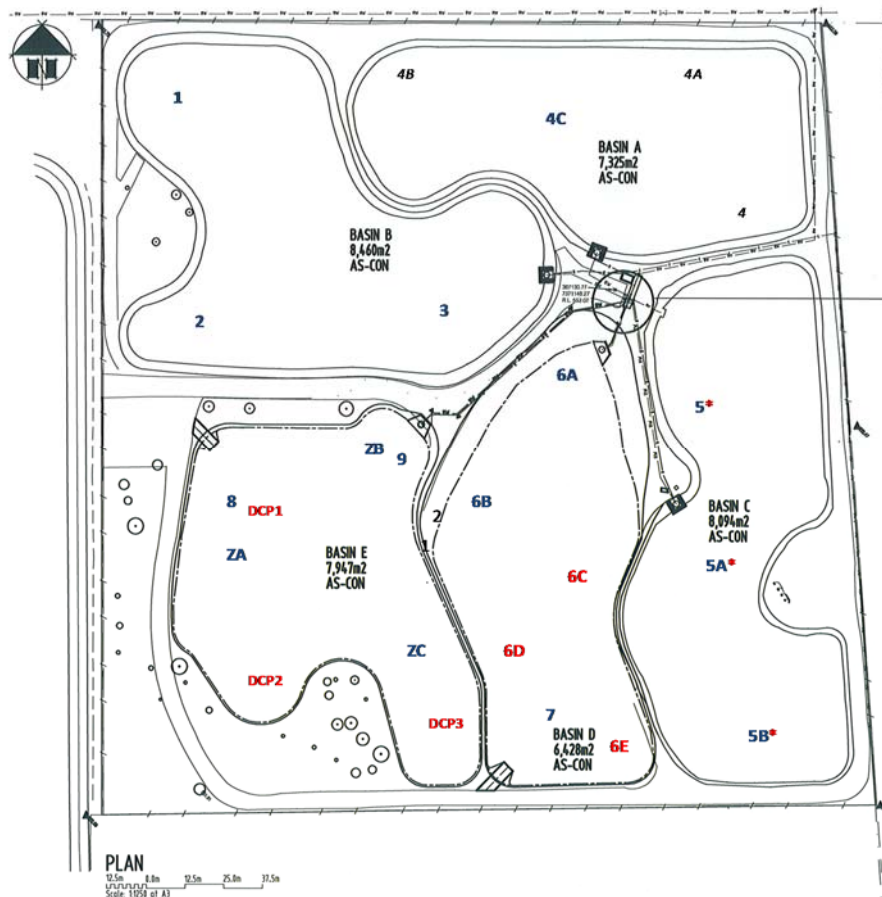


Figure 34 Sampling locations for geotechnical study. Nuclear densometer tests were done at locations: 4C in Basin A; 1, 2, 3 in Basin B; 5, 5A, and 5B in Basin C; 6A, 6B and 7 in Basin D; and 8, 9, ZA, ZB and ZC in Basin E. Cone penetrometers tests were done at locations 5, 5A, 5B in Basin B; 6C, 6D, 6E in Basin C and DCP1, DCP2, DCP3 in Basin E (Source: Alice Materials Testing).

Soil sampling and characterisation

Soil sampling was carried out at regular periods through the study focusing on the carbon and nitrogen concentrations in the soil profiles and surface layer (Table 6, Figure 35). Sampling included an annual round of surface sampling at designated locations in 2012, 2013 and 2014 as well as periodic profile samples up to a depth of 2 m. During October to November 2012 a series of samples were collected before and after basin wetting events in order to establish if there were any significant changes in chemical composition immediately following a wetting event. Table 6 summarises the sequence of soil sampling events undertaken at the Alice Springs SAT site through the study.

Undisturbed soil samples were collected for measurement of bulk density and water content using stainless steel bulk density rings or PVC rings pounded in with a rubber mallet. Disturbed soil samples were taken for other analyses using a hand trowel, chippette or PVC rings pounded in with a rubber mallet.

Samples for microbial analyses were taken from the top clogging layer (0-5 mm) in basins A, C and E on 30 July 2013. Another sampling campaign for microbial analyses was conducted on 3-8 August 2014, targeting 10-150 cm depth profiles in basins A and E. Samples for microbial analysis were refrigerated at 4°C prior to analysis at the CSIRO Waite and Floreat laboratories. Microbial analyses were conducted as described by Kaksonen *et al.* (2015).

Samples collected from the temperature logger locations in November 2013 were ground to <300 µm for analysis by the CSIRO mid infrared (MIR) laboratory. MIR can predict a wide range of chemical and physical soil properties that are closely related to the bulk properties of soil (clay, organic matter,

moisture content, cation capacity, mineralogy). Previous studies have been carried out by Gates *et al.* (2009) to assess the soil properties at the SAT site prior to any recharge operations.

Table 6 Summary of soil sampling events and equipment installation undertaken at the Alice Springs SAT site.

Date	Samples	Depth	Analysis
6-7 Jul 2012	21 samples / A1, A2, A3, A4, A5, A6, C14, C15, C16, C17, C18, C19, C20, C21*, 5(D)7, 5(D)8, 5(D)9, 5(D)10, 5(D)11, 5(D)12, 5(D)13	Surface 0-2.5 cm	TC, TN, CaCO ₃ Air dry soil moisture content
	9 samples / A1, A3, A6, C14, C18, C19, 5(D)7, 5(D)12, 5(D)13	5 cm depth x 5 cm diameter	Bulk density, water content
	Bulk sample/ Future Basin E location	Up to 0.5 m depth	For experiments & chemical analysis
2012, 22, 25 Oct, 2, 6, 13, 23 Nov, 27 Dec	Basin E – EA, EB & EC Basin C - CD	0-5 cm, 5-10 cm undisturbed using PVC rings 0-15 cm disturbed	
30 Jul – 2 Aug 2013	21 samples including: Repeat locations - A1, A2, A3, A4, A5, A6, D7,D8, D9 ^a , D12, D13, EA, EB & EC New locations - BA, BB, BC, D_14, D_15, ED, EE D10 and D11 – inaccessible due to vegetation Basin C inaccessible due to pond fill	Surface 0–2.5 cm depth	TC, TN, CaCO ₃ Air dry soil moisture content
	Profiles at A3, D15 and ED	2 m depth (10 cm increments)	TC, TN, CaCO ₃ Air dry soil moisture content
	Profile along test EM38 transect in Basin B	90 cm depth (15 cm increments)	TC, TN, CaCO ₃ Air dry soil moisture content
	Basins A, D and E – various locations mostly near inlets	Surface lay (1-5 mm thick)	Algal material and schmutzdecke for microbial analysis and SEM
25-29 Nov 2013	Temperature probes (T1 - T4) installed at locations A2, A3, A6 and ED + new locations T5, T6, T7 & in-situ probe near basin E inlet 'Mini diver' standing water level loggers installed in wells RN17937, 47, 42 and 99	T1 – T6 depths: 0, 10, 20, 40, 60 & 90 cm T7 depths: 10 & 40 cm Insitu Tprobe (ie can download thru cable connection) depths: 0,5,15,25,45,65,85 & 115 cm	
	3 samples from location T2 (A3) & location T6	10, 50 and 90 cm depth	Thermal properties (conductivity and capacity, Uni NSW) Air dry soil moisture content TC, TN, CaCO ₃ , pH, EC Chemical and physical properties by MIR
6-8 May 2014	EC5 soil moisture sensors installed to 4 depths at locations A3/T2 and ED/T4 Sensors connected to hobo dataloggers		

Date	Samples	Depth	Analysis
	8 samples from 4 depths during soil moisture sensor installation	25, 45, 65 and 95 cm	TC, TN, CaCO ₃ Air dry soil moisture content
3-8 Aug 2014	13 profiles at 5 locations each in basins A & E 1 location each in basins B, C & D	1.5 m depth (10 cm increments)	KCl soil extracts for NH ₄ -N, NO _x -N Air dry soil moisture content 20 g for possible microbial analysis
	Subsamples from A4, A6, AN (new), EE, ET6 & ET8	1.5 m depth (10 cm increments)	Microbial analysis
	31 samples / A1, A2, A3, A4, A5, A6, BA, BB, BC, C14, C15, C16, C17, C18, C19, C20, C21, D7, D8, D9, D10, D11, D12, D13, D14 ^a , D15, EA, EB, EC, ED, EE	Surface 0–2.5 cm depth	TC, TN, CaCO ₃ Air dry soil moisture content

*20 cm depth; ^a location stake missing, collected sample from comparable location

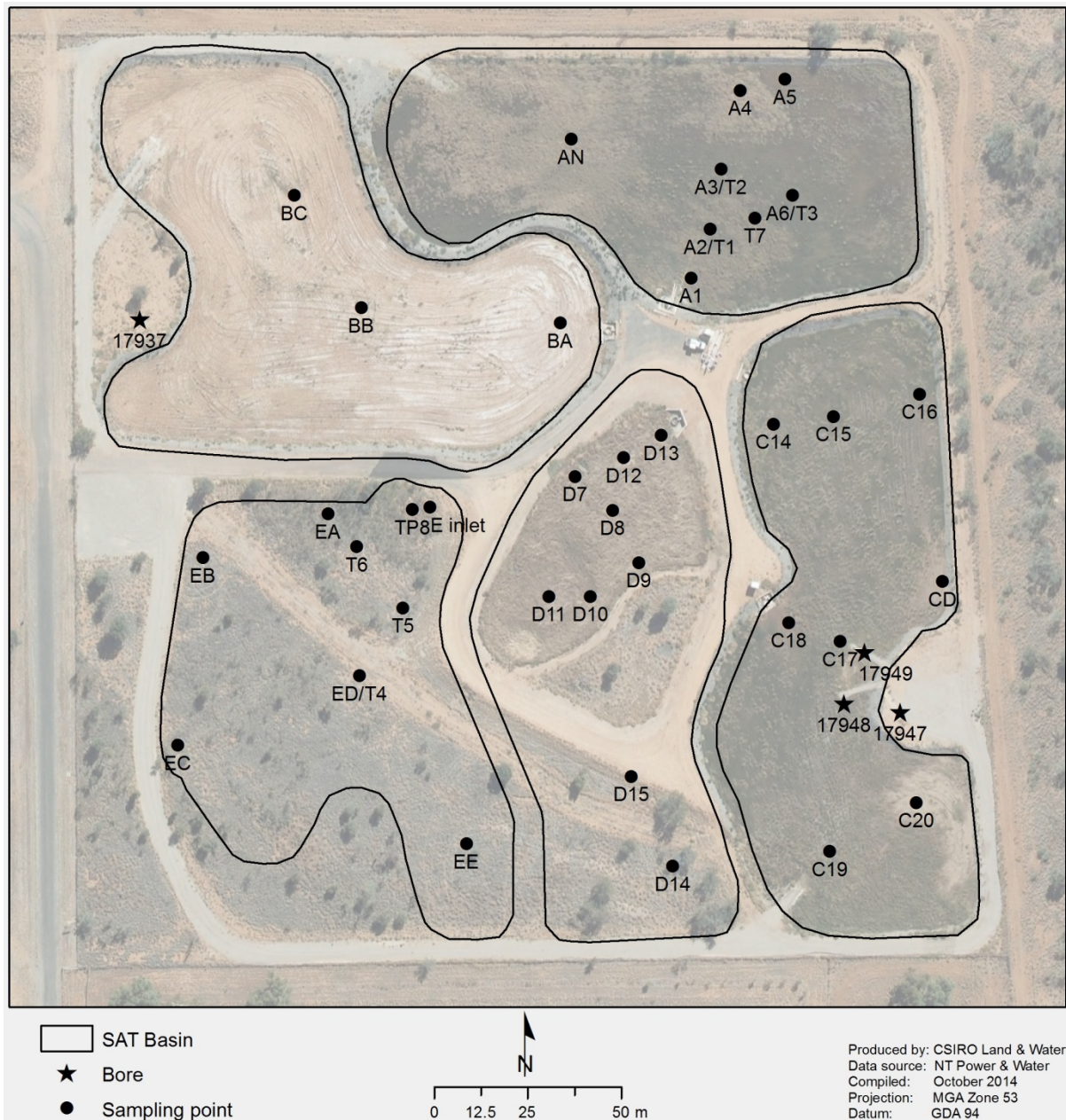


Figure 35 Overview of soil sampling, instrument locations and near basin monitoring bores used throughout the study.

Geophysical survey

In November 2013, CSIRO Earth Science and Resource Engineering conducted a preliminary geophysical survey at the Alice Springs SAT site, followed by a more comprehensive survey in August 2014.

In November 2013, after the basins had been dry for approximately 4 weeks (during plant works), thirteen time-domain EM (NanoTEM) quadrants were measured. Ten 20 x 20 m quadrants in basins A, E and C; one 20 x 20 m quadrant 50 m East of well RN17942; and two 10 x 10 m quadrants in Basin C (area had to be reduced due to interference from the power lines running along the eastern side of the site). A single line DC Resistivity across basins E and D was carried out, which intersected location ED and D9. It was difficult to position transects of sufficient length for resistivity across the basins as the access tracks between the basins interfered with the readings, also heavy vegetation cover required a track to be mowed using a mini bobcat to enable the resistivity line to be pegged in. All 'in basin' locations are shown in Figure 36.

In August 2014, 40 time-domain EM (NanoTEM) quadrants were measured, following the most recent wetting cycle (July 26 – August 2); 10 in Basin A, 9 in Basin B, 5 in basin D, 10 in Basin E (all 10 x 10 m) as shown in Figure 36, plus seven 20 x 20 m quadrants approximately 500 m SE of the site near well RN 17999 in a west to east transect. There was some overlap between the 2013 and 2014 NanoTEM quadrants measured in Basins A and E. A single line DC Resistivity across basins E and D was repeated and a CMD (electromagnetic conductivity meter) was used to map basins A, B, C and E to 6 m depth. NanoTEM survey locations down-gradient of the basins are shown in the SAT Project Monitoring Bores map, located in Appendix 6.

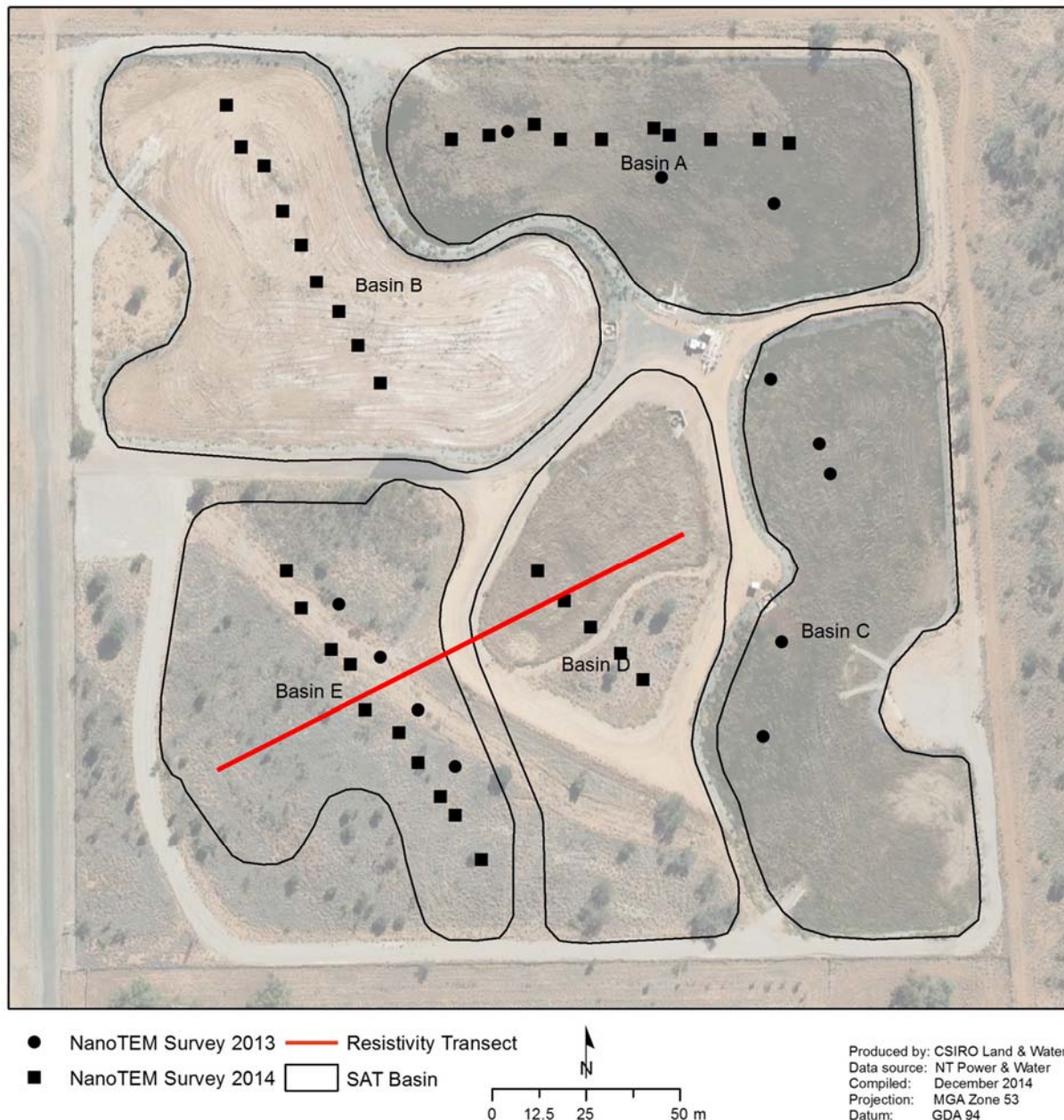


Figure 36 Geophysical survey locations November 2013 and August 2014; black circles represent NanoTEM quadrants in 2013 and black squares represent NanoTEM quadrants in 2014. The red line represents DC Resistivity run in 2013 and repeated in 2014.

Thermal probes

On 26 November 2013 eight 'thermal probes' (multi point temperature loggers) were installed across Basins A and E (T1-T7 and TP8 in Figure 35). Each of the thermal sensors (buttons) were downloaded and then reset in May and August 2014. In May 2014 soil moisture sensors were

installed and soil samples were collected. The soil moisture sensors (Decadon EC H₂O EC-5) were installed at depths of 20, 45, 60 and 90 cm below the base of the basin at locations in basin A (A3/T2) and basin E (ED/T4). Each set of 4 sensors was connected to a Hobo Micro Station logger. Soil samples were also collected at each depth to enable comparison between the gravimetric water content and the volumetric water content readings from the sensors. The soil moisture data from the Hobo data logger was retrieved in August 2014.

Six of the thermal probes (T1–T6) consisted of a 1.5 m rod with 6 iButton® temperature loggers embedded in the side of the rod at 0, 10, 20, 40, 60, and 90 cm depths from the base of the basin. One short probe of 1 m length (T7) had buttons installed at 10 and 40 cm depths. Probes T1-7 were recovered to download data from each logger. The ‘TP8’ probe with 8 buttons installed at 0, 5, 15, 25, 45, 65, 85, 115 cm was able to be downloaded in-situ. Each of the buttons was programmed to record data at 30 minute intervals (with no roll-over) to provide up to 4 months of data upon retrieval of the probe. A 20% failure rate of the buttons was evident in May 2014. Due to the reduced number of operating buttons, probes were reinstalled at locations T1, T2, T3, T4 and T6, with buttons at 10, 20, 40, 60, and 90 cm depths from the base of the basin.

Water quality

Water quality data for the Alice Springs Reclamation Plant, the SAT recharge water, groundwater quality and groundwater level data was provided by Power and Water Corporation. Groundwater was collected at quarterly intervals from wells up-gradient, at the basins and down-gradient (2008 to 2014). Locations of the groundwater bores are shown in Appendix 6. Routine monitoring of recharge water was undertaken on a monthly basis. Additional monitoring was undertaken by Power and Water Corporation for this study, to evaluate the reactivity of organic carbon (measured as biodegradable dissolved organic carbon, BDOC) within the source water for SAT.

Samples were collected from various stages within the wastewater treatment process (Table 7 and Figure 37) on four sampling events; 13/8/2013, 24/9/2013, 25/8/2014 and 22/9/2014). Table 8 outlines the analysis suite, with additions to the routine sampling program identified in bold text.

Table 7 Sample locations in Alice Springs Reclamation Plant used to evaluate nutrient reactivity.

Sample location	Location code
Inlet sewer	Saa001
Outlet facultative pond AN4	Saa005
Outlet facultative pond AN2/3	Saa010
Outlet maturation pond A5	Saa020
Outlet maturation pond A4	Saa030
Outlet maturation pond A2	Saa025
Combined pit (before A6 & A7)	SASPD01
Wet well 1 (source to DAF)	Saa040
Wet well 2 (source to DAF)	Saa045
Outlet of DAF (prior to chlorination)	RASPT001

Table 8 Analysis suite to evaluate nutrient reactivity.

Suite	Lab
EC, pH, temp, DO, turbidity	Field parameters
NH ₃ -N free, NH ₃ -N organic, NO ₃ -N, NO ₂ -N, TN (calculated), TP, FRP, Chlorophyll a , alkalinity	NT lab as per routine sampling, with additional parameters
BDOC, TOC, DOC, UV₂₅₄ (filtered), E.Coli	AWQC
Fluorescence EEM†	CSIRO

Bold parameters are in addition to parameters already included in routine wastewater analysis

†Fluorescence EEM – research tool to characterise the nature of the organic matter

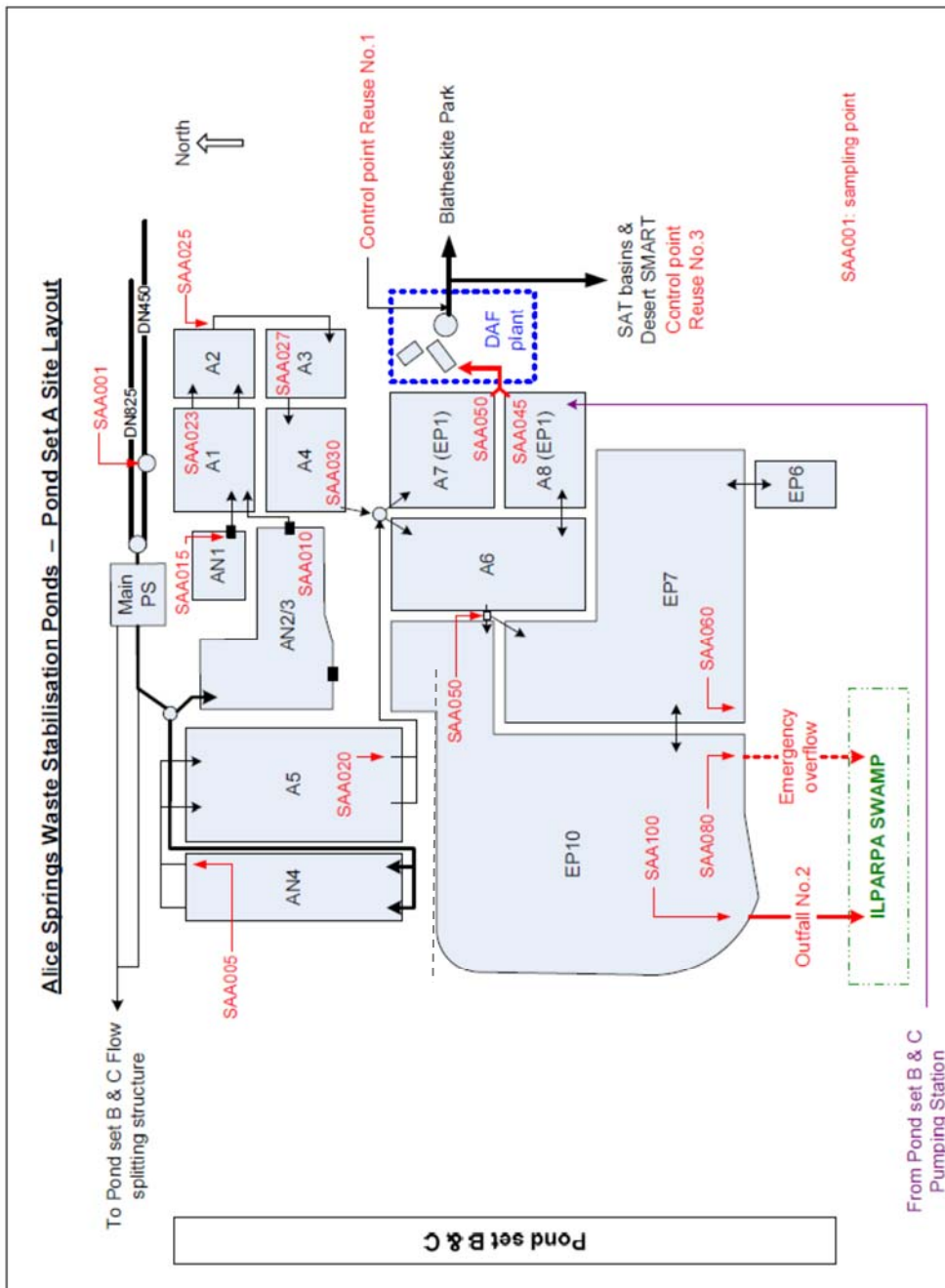


Figure 37 Stream A of Alice Springs Waste Stabilisation Ponds.

SAT Basin operation

Influence of drying time

Average infiltration rates for Basins D and E (Table 9) were typically higher than in the original smaller basins regardless of source water treatment (238 mm/d Table 5), while Basins A, B and C exhibited similar or higher infiltration rates with DAFF treated source water. The

There is an indicative trend for higher infiltration rates with longer drying, illustrated for Basins A and C in Figure 38 and for Basins D and E in Figure 39. Nonetheless Basin D and E are still infiltrating at significantly higher rate than Basins A and C. Drying and wetting times of less than 1 day were excluded from analysis of their influence on hydraulic performance as these do not represent standard basin operation. Short infill periods make stable infiltration rate calculations difficult.

The relationship between infiltration rate and wetting interval varied between the two pairs of similarly performing basins, Basins A and C (Figure 40) and Basins D and E (Figure 41). Basins D and E were generally empty in less than 4 days, while Basins A and C needed up to 7 days to empty. Basins were operated on a time cycle encompassing both the wet and dry intervals. As a result drying times were diminished as wetting intervals increased and therefore insufficient drying time resulted in a reduction in infiltration rate.

Table 9 Summary of infiltration rate, drying time and wetting time (average±standard deviation) for basins based on source water treatment (DAF or DAFF). Basin B with DAF treated source water was not included due to the impact of soil compaction on infiltration rate.

Basin	DAF treated source water				DAFF treated source water			
	n	Infiltration rate (mm/d)	Drying time (d)	Wetting time (d)	n	Infiltration rate (mm/d)	Drying time (d)	Wetting time (d)
A	57	170±100	7±3	4±1	17	250±100	10±2	3±2
B	Impacted by soil compaction				16	200±30	10±8	2±1
C	46	140±50	8±5	4±1	14	250±100	10±6	3±1
D	30	500±200	12±8	2±1	15	1000±400	10±5	3±1
E	16	550±460	12±8	2±1	19	760±520	11±6	3±1

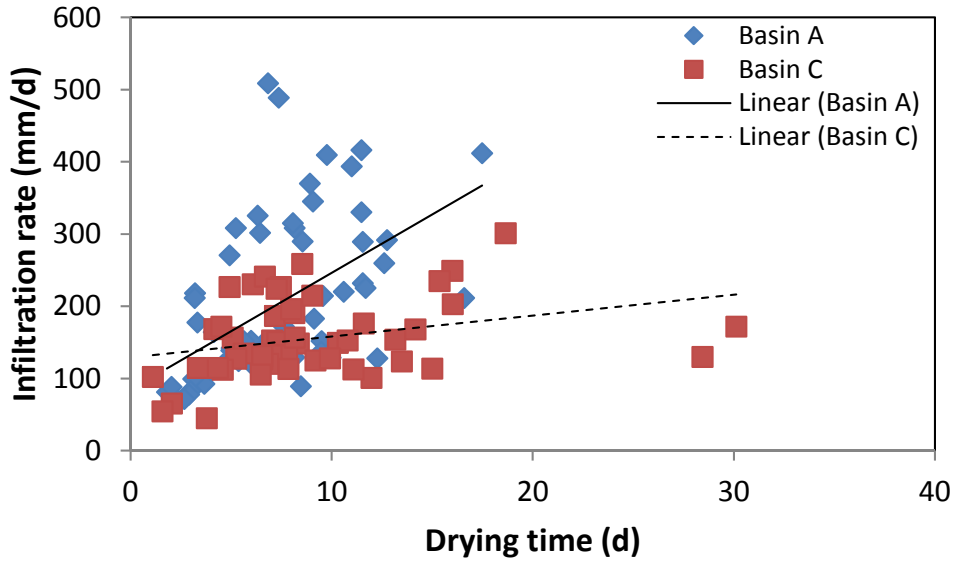


Figure 38 Relationship between infiltration rate and drying time for Basins A and C.

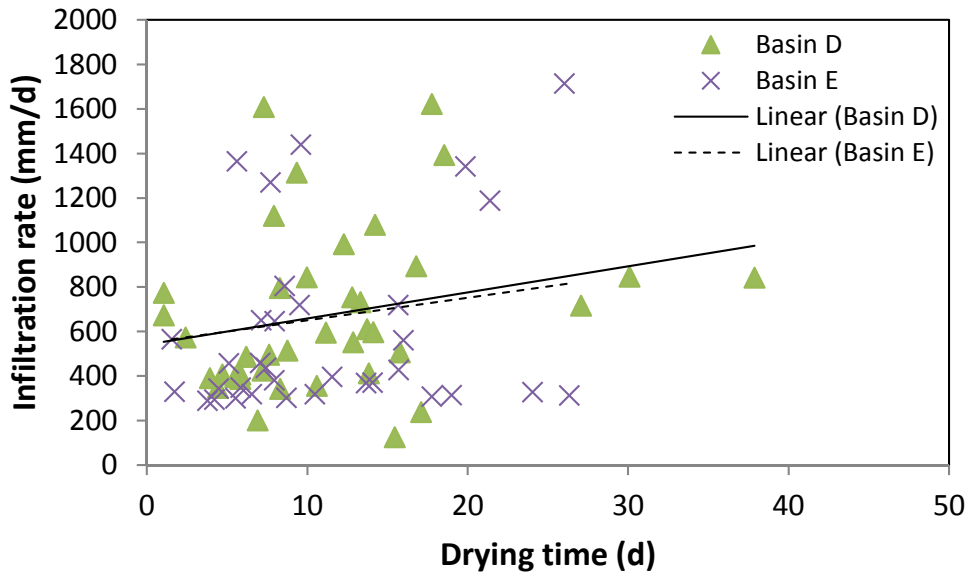


Figure 39 Relationship between infiltration rate and drying time for Basins D and E.

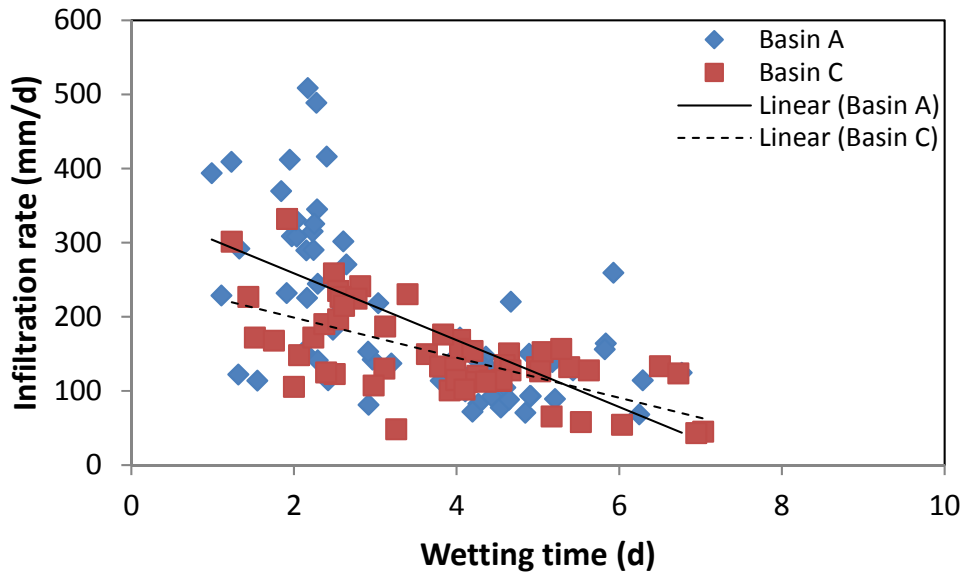


Figure 40 Relationship between infiltration rate and wetting time for Basins A and C.

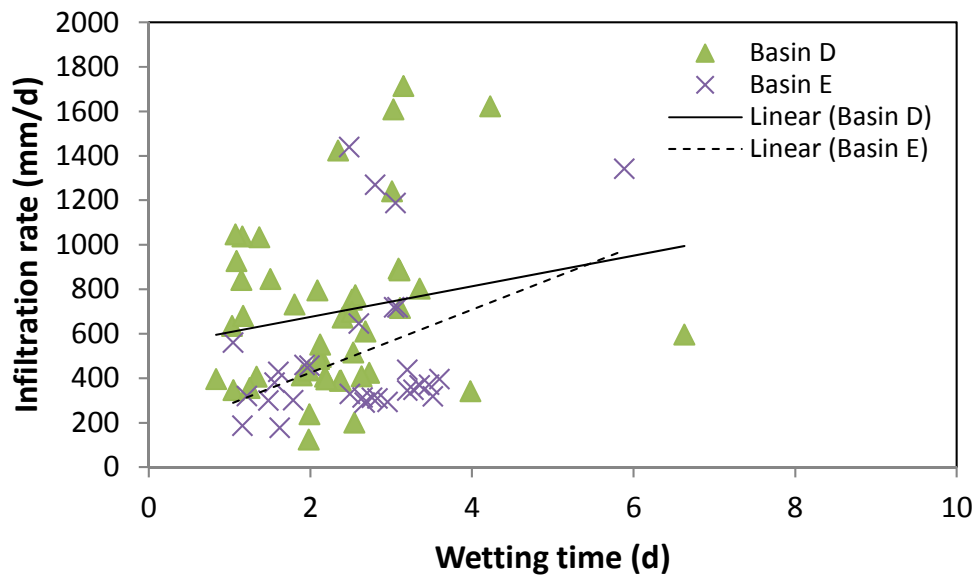


Figure 41 Relationship between infiltration rate and wetting time for Basins D and E.

Bouwer *et. al.* (1974; 1980) made some observations from the Flushing Meadows infiltration project (Phoenix, Arizona) that are very relevant to the Alice Springs SAT site:

- Vegetation can improve infiltration rates through soil structure improvement, but it can also act as mulch in winter and prevent drying.
- Drying periods should be extended in winter; recommended 10 days drying in summer and 20 days in winter.
- Vegetation can contribute to N uptake and stimulate denitrification.
- It's not worth preventing vegetation growth unless it increases mosquito problems or interferes with cleaning or flow-control devices.
- Maintenance can be achieved by an extended dry period or a surface clean (if warranted).

Based on the observed infiltration rates and information from the literature, the following suggestions are made for operation of the Alice Springs SAT basins:

- Evaluate the benefit of an extended drying period, especially for basins A and C with the lowest infiltration rates.
- Important for Basin C, use guidance on an acceptable bed surface to determine when to refill or aim to dry for at least 20 days (one-off) Breton (2009) (Appendix 5). This may include a regular (1-2 daily) inspection and documentation of Basin C floor to determine the general rule for drying time in winter.
- Increase drying period for all basins to a minimum of 5 days, preferably up to 10 days in winter. This may require a change in current operational procedures. A critical limit for infiltration rate (e.g. 200 mm/d) or a percentage decline in infiltration rate could be used to trigger a change in operational regime such as a longer drying interval.
- Maintain the maximum length of the filling period without breaching the 7 day limit for standing water as an increased wetting period will assist with obtaining anoxic conditions needed for N reduction. For Basins D and E this may allow a longer filling period of 3-4 days. For Basins A and C, if there is some recovery in infiltration rate the filling period may be able to remain at 2 days.

Hydraulic performance

Hydraulic performance of the SAT basins was influenced by the hydraulic properties of the soil beneath the basins and by soil clogging mechanisms, including formation of an algal mat, microbial growth, chemical precipitation and filtration of suspended solids. The effects of algal growth and biofilm formation can be reversed through basin drying where sufficient time is provided for these deposits to crack and expose fresh soil surfaces. Remediation of physical and chemical clogging requires removal of the clogging layer.

From June 2008 to September 2014 a total of approximately 2,580 ML reclaimed wastewater was delivered from the WRP plant to the SAT basins (Figure 42). The current, expanded basin configuration has received 1470 ML equating to approximately 1.9 ML/d, which is sufficient to meet the initial target volume for recharge of 600 ML/yr. Reclaimed water use for irrigation of Blatherskite Park consumes 1-3 ML/d and reduces the volume of water available for recharge.

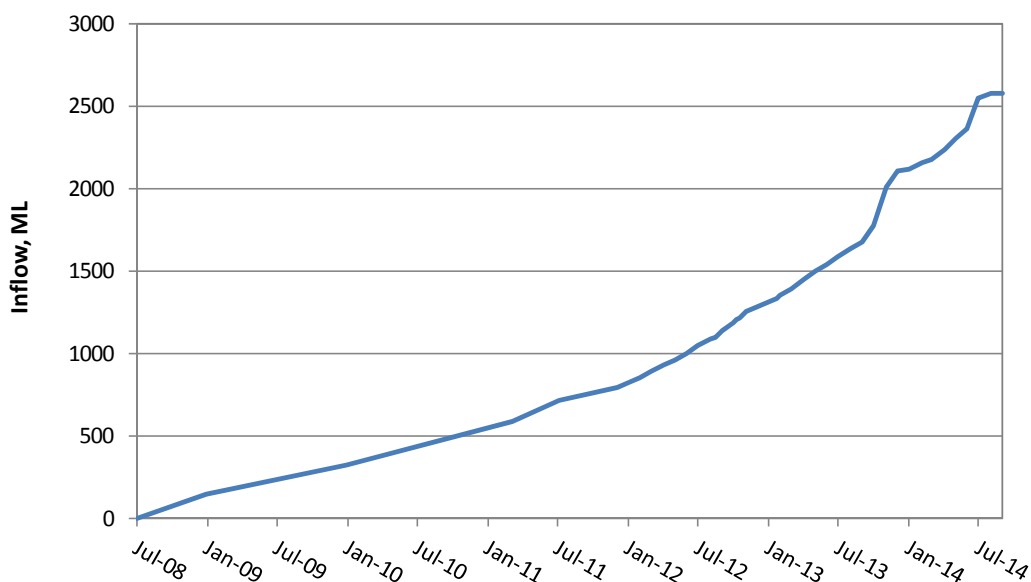


Figure 42 Total volume of water released to the SAT system in its history (Jun 2008- Sep 2014).

During 2013 a filtration plant was constructed at the DAF plant to upgrade the treatment step to DAFF. Between 21/8/13 and 25/9/13 there was minimal flow to the basins due to the final construction phase of the new plant and any flow that did occur went to Basin B. After this a period of preliminary testing of the new plant began, however the SAT site meters were out of operation. Volumes to the SAT basins were estimated from the total volume of water leaving the WRP (via the AZRI meter), which may have resulted in some overestimation of volumes going to the site at times. There were also occasions when all the water was going to SAT and no water to Blatherskite Park, which explains the significant increase in inflow (2 – 5 times) during this period. There was also a significant stoppage period from 13/11/13–7/12/13 due to lack of coagulant for the treatment plant.

Since the major expansion of the basin, most of the reclaimed water was released to Basin A (62 kL/m²), followed by Basin D (54 kL/m²), Basin C (41 kL/m²), Basin E (38 kL/m²) and Basin B (26 kL/m²) (Figure 43). It is immediately striking that the inflow to the Basin B is less than other basins, likely due to compaction by heavy earthworks on levelling the basin after it had been constructed, as discussed later. Also flow to basin B stopped in May 2013 to have a valve replaced at the inlet.

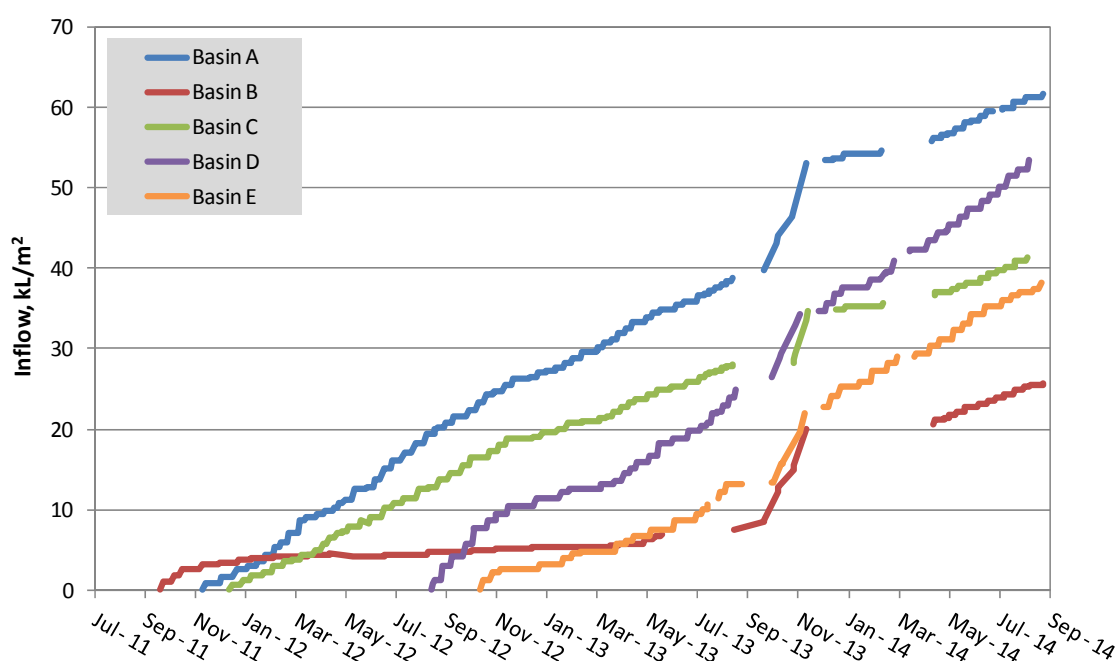


Figure 43 Volumes of recharge water released to the individual basins from October 2011 to September 2014. Interruptions in inflow for all basins relate to treatment plant stoppages (August 2013, November 2013) and loss of data (March 2014). Additional interruptions in inflow for Basin B represent periods when the basin was not in use.

The graphs with calculated infiltration rates (Figure 44-Figure 48) should be interpreted as follows:

1. Each infiltration event has an infiltration rate estimated from a decline of water level over time from the cessation of inflow. This infiltration rate was plotted on the horizontal axis (time) at the time when the water pressure transducer within the basin reached a value of zero.
2. Length of the immediately preceding wetting period is also plotted at the same time. The wetting period is the time from the opening of the inlet valve delivering water to a basin to the moment when the basin water transducer reached a value of zero.
3. Length of the preceding drying period is also plotted at the same time as the infiltration rate and length of wetting period for a particular recharge event.
4. In general, a high infiltration rate correlates with a short length of a wetting period. This is because the soil moisture storage change that occurs at the beginning of the wetting period has not had sufficient time to stabilise before the inflow valve is shut off. As a result, spikes in infiltration rates that are not sustained are not considered to accurately represent the performance of the basin.

Calculated infiltration rates in Basin A varied from 80 mm/d to 500 mm/d (Figure 44). Initially they were oscillating around 200 mm/d to 300 mm/d, similar to what had been observed in the old basin 1. Around August 2012, infiltration rates stabilised around 130 mm/d, but in July and August 2013 declined to approximately 80 mm/d. This decline in infiltration rate coincided with marginally higher wetting periods (5 days compared with the average of 3 days), but generally shorter drying intervals (< 5 days, compared to the average of 8 days). In Basin A it was also observed that vegetation acted as a mulch during winter, with the plant matter lying flat over the basin surface, reducing drying potential. It is recommended that drying periods should be extended during winter (15-20 days). After the stoppage associated with the treatment plant upgrade (September 2013) infiltration rates increased to 300-400 mm/d (250 mm/d on average). This can be explained by a reduction in clogging, due to improvement in the quality of recharge water applied, but also to drying times consistently >5 days which resulted when infiltration rates increase.

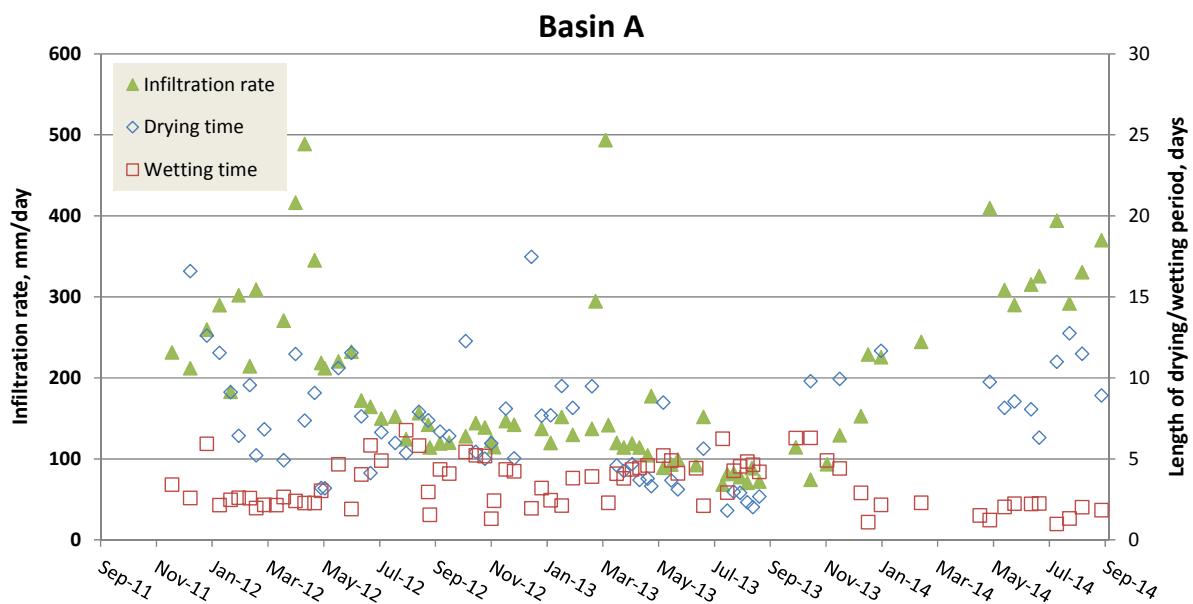


Figure 44 Infiltration rates and lengths of drying and wetting cycles in Basin A.

Calculated infiltration rates in Basin B started from 220 mm/d, but rapidly declined to below 50 mm/d (Figure 45; note the scale on the axes is variable in Figure 44-Figure 48). The dramatic decline in infiltration rate was caused by the use of heavy machinery during levelling of the basin floor, which compacted the basin floor (discussed in 'Compaction tests' section). Ploughing and seeding of grass in March 2012 did not help to restore the infiltration rate. However an improvement in infiltration rate was evident after approximately 50% of the floor material was turned over to a depth of 700 mm prior to the fill in March 2013. After this floor turn over, the infiltration rate has been approximately 100-150 mm/d, corresponding to an average wetting time of 4 days and a variable drying interval of <1 to 144 days. There has also been significant vegetation growth in Basin B since the July 2013, with most of the basin being covered in tall bushes by November 2013 (Appendix 4). As seen for Basin A, the infiltration rate in Basin B improved after the upgrade to the WRP, achieving around 200 mm/d in late 2014. Drying time in the corresponding period was around 10 days.

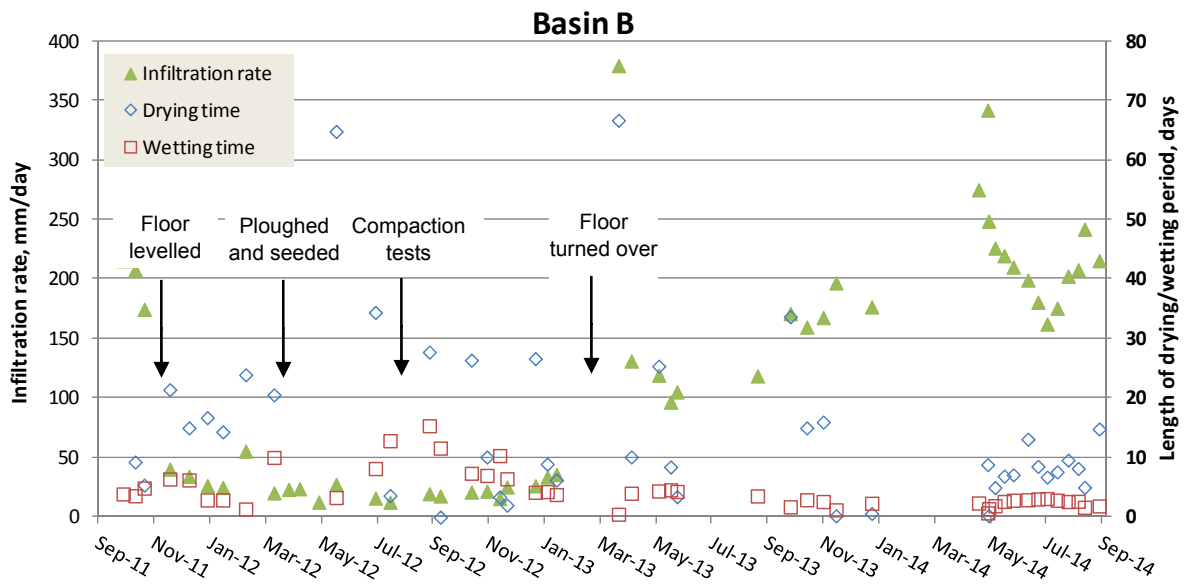


Figure 45 Infiltration rates and lengths of drying and wetting cycles in Basin B.

Calculated infiltration rates in Basin C varied from 60 to 330 mm/d (Figure 46). Initially, the infiltration rate oscillated around 150 mm/d and then stabilised at 125 mm/d. Notably, the infiltration rate dropped to 50 mm/d from July to September 2013, possibly due to mulching effect of vegetation in the winter months and short drying times. Conversely in warmer months infiltration rates could be improved via increased root growth of the vegetation, improving soil structure and the drying of the vegetation mat which is across much of the basin. Infiltration rate improved to approximately 250 mm/d after the WRP upgrade in September 2013, however a gradual decline is observed yet again through the cooler months in 2014. Recent wetting and drying intervals have been 3 and 10 days on average, respectively.

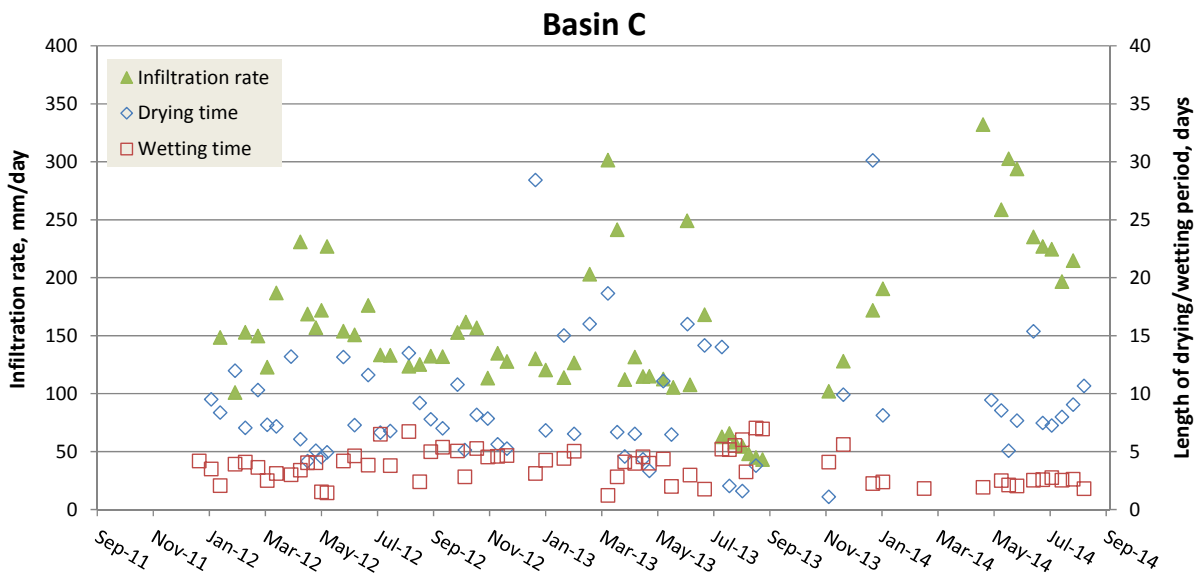


Figure 46 Infiltration rates and lengths of drying and wetting cycles in Basin C.

The old Basin 5, which was operating from December 2009 to July 2012, exhibited infiltration rates from about 150 to > 600 mm/d. The highest rates were attributed to short wetting intervals (<2 d). A similar pattern in infiltration rate was observed in the expanded Basin D (Figure 47). With DAF treated source water, infiltration rates were typically 600-1,400 mm/d (average 500 mm/d) corresponding to average wetting and drying intervals of 2 and 12 days respectively. The impact of the WRP upgrade

on infiltration rate was also evident in this basin, with the average infiltration rate increasing to 1000 mm/d, corresponding to wetting and drying intervals of 3 and 10 days respectively.

Basin E has also illustrated higher infiltration rates than Basins A, B and C, on average 550 mm/d with DAF treated source water and 760 mm/d following the WRP upgrade to DAFF treatment. The average wetting and drying intervals were 2 and 12 days respectively with DAF treated source water and more recently 3 and 11 days with DAFF treated source water.

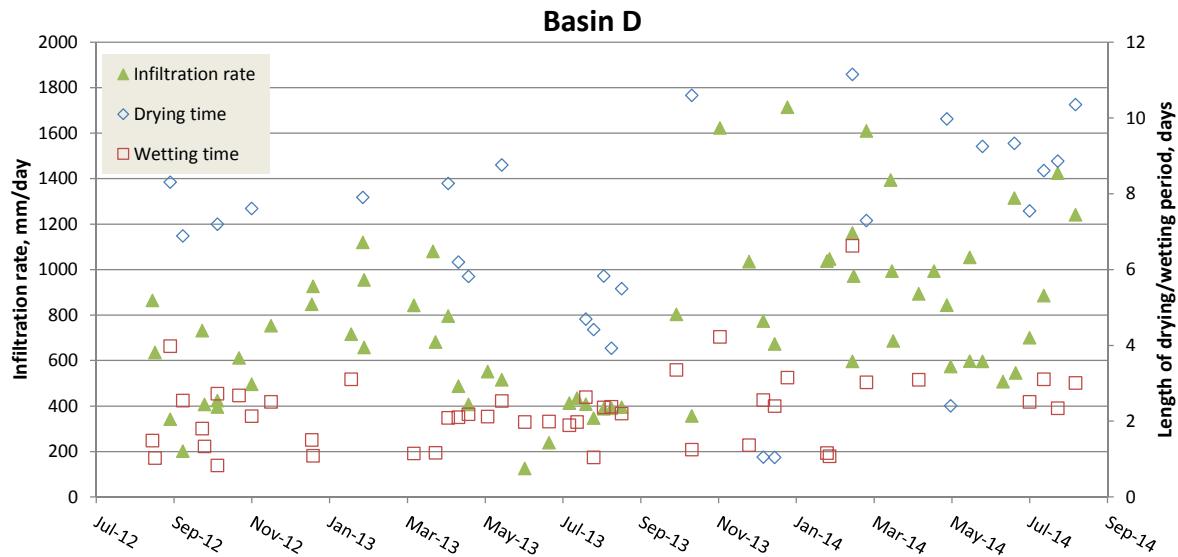


Figure 47 Infiltration rates and lengths of drying and wetting cycles in Basin D.

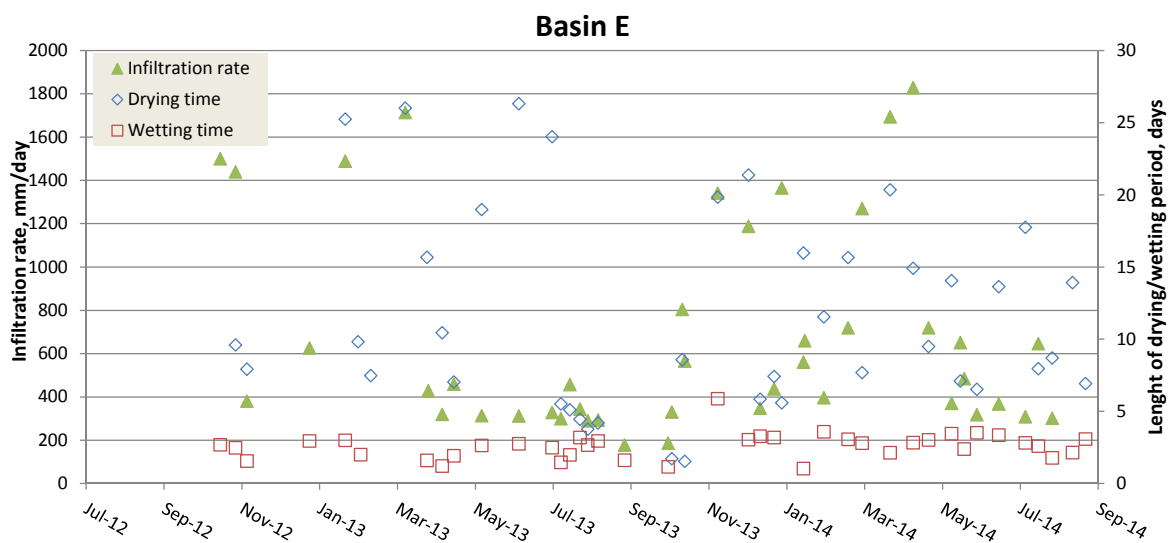


Figure 48 Infiltration rates and lengths of drying and wetting cycles in Basin E.

Prior to the WRP upgrade, there were warnings that infiltration rates would decline with time as evident in the two oldest basins, A and C, where rates declined from >200mm/d to around 100 to 130mm/d. Infiltration rates improved after September 2013, suggesting the quality of recharge water was an importance influence on basin performance. Table 9 compares the average infiltration rate, drying time and wetting time for the basins based on source water treatment DAF or DAFF. The upgrade to DAFF treatment increased the average infiltration rate for each of the four basins, which in turn decreased the wetting time or time to empty and lengthened the drying time.

Basin construction has a large bearing on the maximum infiltration rates achievable, which was illustrated by the performance of Basin B where the infiltration rate plummeted from 200 mm/d to ~25 mm/d due to basin floor levelling with heavy equipment which caused soil compaction.

Thermal Fluxes

Gunatunge (2014) assessed heat as a tracer to quantify the infiltration taking place in the recharge basins by applying a 1-D heat transport model to multi-level temperature measurements. The method required pre-processing in order to extract the diurnal signal but is capable of calculating temporal variations in infiltration. The raw thermal data from the temperature arrays T2 (Basin A), T6 (Basin E) were compared (refer to Figure 35 for locations) for the estimation of point-specific heat derived infiltration fluxes. Data was filtered using 'dynamic harmonic regression analysis' to calculate thermal diffusivity and thermal front velocity using methods from McCallum *et al.* (2012) and Luce *et al.* (2012). The thermal front velocity was converted to Darcy flux using laboratory thermal parameters and porosity. In order to constrain the heat derived fluxes, whole-basin infiltration were also calculated based on the mass balance equation:

$$I = Q + P - E - \partial S \quad \text{Equation 2}$$

where,

I is volume of infiltration from the Basin, Q is discharge volume into the Basin, P is precipitation, E is evaporation and ∂S is the change in storage which relates to the change in water level. Calculated infiltration rates for eight recharge events between May and July 2014 varied between 250 and 500 mm/d in Basin A and between 300 and 650 mm/d in Basin E.

Figure 49 and Figure 50 summarise the overall flux comparison from locations T2 (Basin A) and T6 (Basin E) from 10 May to 3 August 2014. The analytical solution of the heat transport model was less reliable to interpret flux for short discharge events. In general, the heat derived fluxes were generally lower than the flux estimated by the basin mass balance method, but variations were consistent between the two methods. Due to the variable infiltration rates between basins, the soil moisture data indicated the saturated periods of the shallow sediments lasted longer at T6 (Basin E) than at T2 (Basin A). A nearby location in Basin E (T8; data not shown) revealed an infiltration regime quite distinct from that at T6 despite only 20 m separation between them. Thus, the heat derived fluxes at different locations in the MAR basins have given a further insight into the spatially heterogeneous and dynamic infiltration that takes place.

In order to study the spatial and temporal infiltration patterns, temperature data has to be obtained at a higher spatial resolution. These low cost multi-level temperature arrays could be deployed to collect sufficient temperature depth profiles to provide a picture of whole basin infiltration at variable depths. These results could be used to identify and remedy areas of low hydraulic conductivity facilitating better basin management.

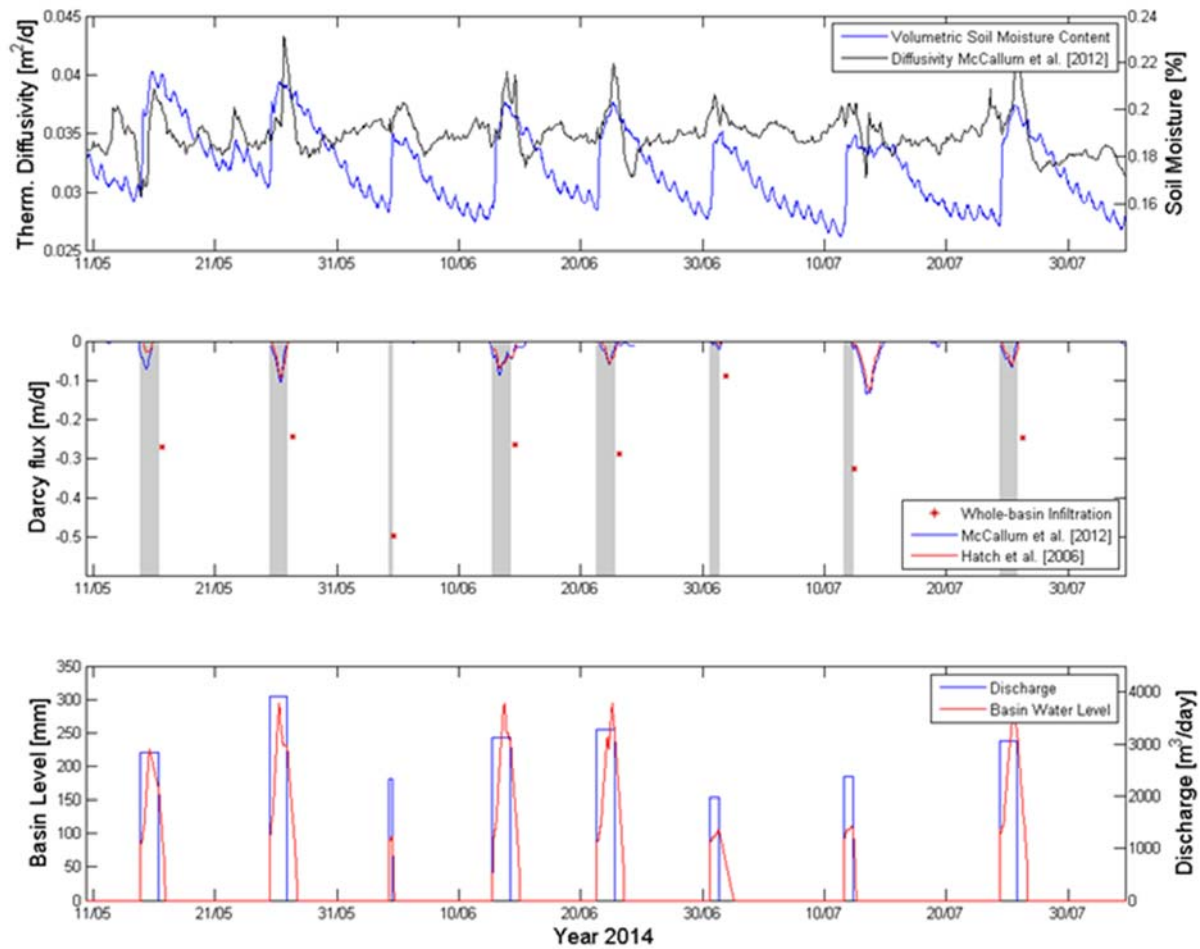


Figure 49 Overall flux comparison at T2 (Basin A) (Gunatunge 2014). The grey shaded area denote recharge events.

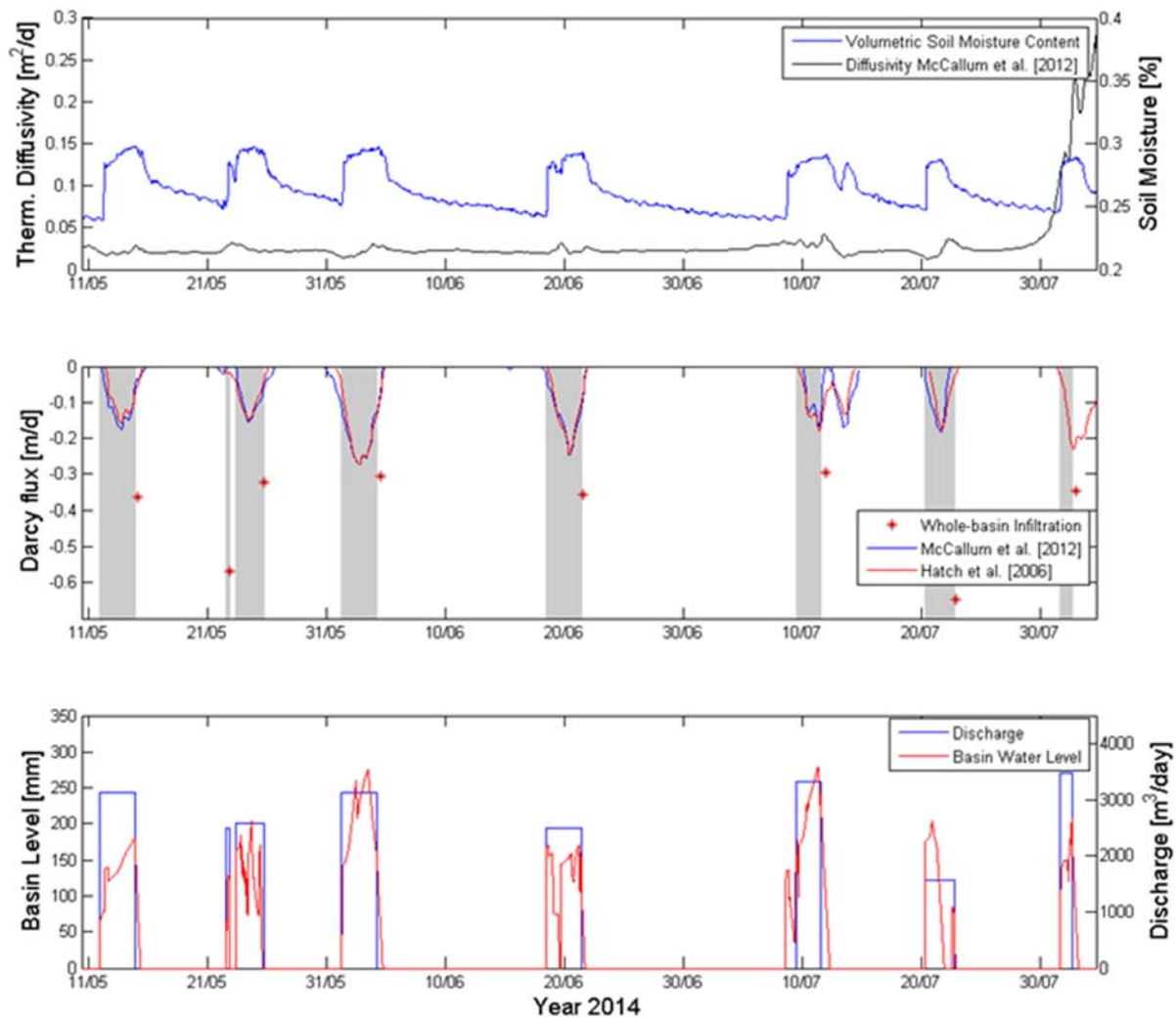


Figure 50 Overall flux comparison at T6 (Basin E) (Gunatunge 2014). The grey shaded area denote recharge events.

Recharge water quality

An overview of recharge water quality is presented in Figure 51, which highlights the impact of the WRP upgrade to include DAFF treatment on nutrient concentrations. Following the treatment change, the concentrations of turbidity, BOD, reduced forms of nitrogen ($\text{NH}_3\text{-N}$ free and organic) and phosphorus were typically lower while oxidised nitrogen ($\text{NO}_3\text{-N}$) tended to increase. Pérez-Paricia (2000) recommends targets to minimise clogging of turbidity <5 NTU, <10 mg/L TSS and TOC <10 mg/L. Following DAFF treatment, the source water for SAT complies with these targets. TOC is not shown in Figure 51 as monitoring data was limited to the lifetime of this project.

To date the removal of nitrogen via the Soil Aquifer Treatment (SAT) basins has been limited and independent review of the operation by an expert in this field (Peter Fox, Arizona State University) suggested this may be limited by the nature of the organic carbon in the source water for recharge. If the labile or easily biodegradable organic carbon is removed during wastewater treatment, there may not be sufficient labile organic carbon in the SAT source water to stimulate denitrification in the subsurface. Therefore the quality of wastewater through the Alice Springs Wastewater Treatment Plant was evaluated to see if plant operation could influence the portion of reactive organic carbon in the source water for SAT.

The majority of BOD was removed within the facultative ponds, declining from an average of 220 mg/L BOD in raw sewage to ~ 80 mg/L BOD after the facultative ponds. Transit through a series of ponds followed by DAF and DAFF treatment resulted in further removal to approximately 8 mg/L BOD

in DAF and 1 mg/L BOD in DAFF (excluding outliers during commissioning phase), presumably through removal of suspended organic matter, as algae.

Samples collected in August and September of 2013 and 2014 (Table 10-Table 12) revealed that organic carbon was predominantly in particulate form in raw wastewater and throughout each of the two treatment trains until DAF or DAFF treatment where DOC was predominant (~90%). DAFF treatment commenced on 16 September, 2013 and therefore the DAFF plant was still being optimised at the time of the 24/9/13 sampling event. The reactivity of DOC, reported as biodegradable dissolved organic carbon (BDOC) decreased significantly throughout the treatment process from greater than 80% in the raw wastewater to 50% or less in the SAT source water where BDOC was less than 5 mg/L. The BDOC reduction from raw wastewater to SAT source water was approximately 90%. This reduction in lability of organic matter was largely achieved in the facultative ponds, where BDOC was reduced by 70-80%. Given that the majority of labile DOC removal occurred in the first of a series of ponds, it is unlikely that a reduced residence time through the entire pond system would significantly increase the DOC reactivity.

The C:N ratio of organic matter was low in both the raw wastewater and the SAT source water (Table 10), due to its origin from microbial sources, which are nitrogenous (Page *et al.* 2001). Nitrogen in the SAT recharge water was present as ammonium, organic nitrogen and nitrate. After DAF treatment the average ammonium, organic nitrogen and nitrate concentrations were 11 mg/L, 2 mg/L and 1 mg/L, respectively. As discussed earlier the nutrient concentrations were altered with upgrade to DAFF, which resulted in average ammonium, organic nitrogen and nitrate concentrations of 4 mg/L, 1.5 mg/L and 2 mg/L, respectively.

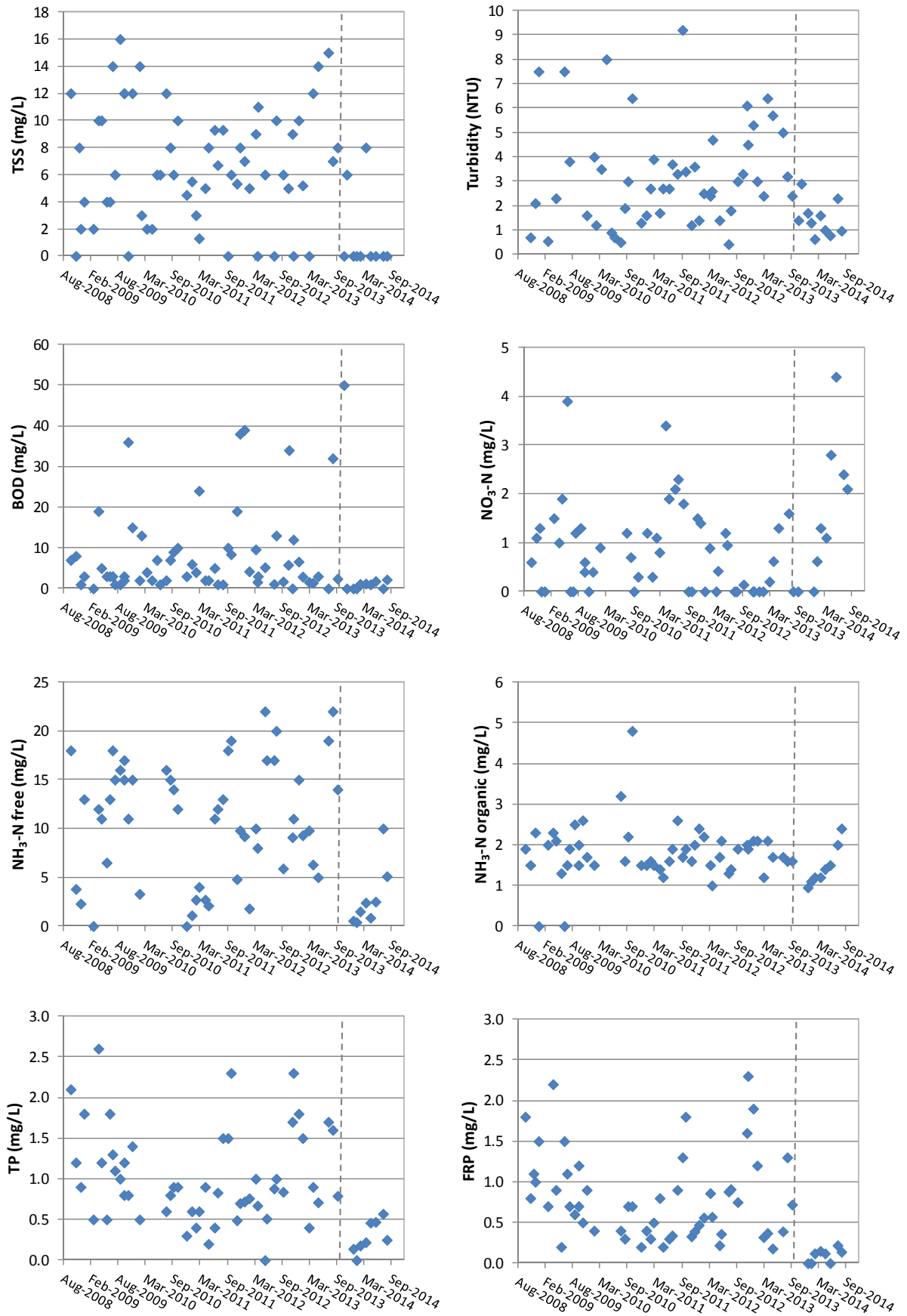


Figure 51 Water quality of recharge water sampled at the SAT site. The vertical dashed line marks the WRP upgrade to DAFF treatment in September 2013.

Table 10 Water quality for raw wastewater and source water for SAT basins.

mg/L unless stated	Raw (Saa001)				SAT source water (RASPT001)			
	13/8/13	24/9/13	25/8/14	22/9/14	13/8/13	24/9/13	25/8/14	22/9/14
EC (µS/cm)	1410	1570	1440	1320	1700	1810	1680	1670
pH (pH units)	9.04	9.12	8.18	8.39	8.41	8.31	7.49	7.43
Temp (°C)	24.3	26.7	23.9	25.4	17.5	20.4	18.0	21.9
DO	0.5	<0.5	5.6	3.2	3.3	2.9	-	5.8
Turbidity (NTU)	158	166	-	-	7	2	-	-
Alkalinity as CaCO ₃	450	500	440	410	410	380	250	140
BOD	180	180	170	110	<1	16	<1	<1
NH ₃ -N free	64	65	44	48	25	22	5.4	0.55
NH ₃ -N organic	17	16	12	11	2.3	2.4	3.1	2.2
NO ₂ -N	<0.10	<0.10	<0.10	<0.10	<0.10	0.8	2.5	<0.10
NO ₃ -N	<0.10	<0.10	<0.10	<0.10	<0.10	0.2	2.0	2.4
TN	81	81	56	59	27	25	13	5.2
FRP	6.4	5.8	4.1	3.8	0.9	<0.1	<0.1	0.3
TP	9.3	8.6	5.1	6.2	1.4	0.2	0.3	0.4
TOC	131	69	58.3	48	10.4	-	9.3	9.6
DOC	49	33	18	19	9.6	11	8.3	9.0
BDOC	43	41	35	28	4.8	2.7	1.0	3.1
UV ₂₅₄ (filtered) (%)	43	41	52.6	47.7	71	70	77	64
<i>E. Coli</i> (cfu/100 mL)	1.9x10 ⁷	1.3x10 ⁷	1.2x10 ⁷	1.3x10 ⁷	2.5x10 ²	15	<1	<1
Chlorophyll <i>a</i> (µg/L)	20.8	10.8	<0.1	8.2	12.2	42.6	8.1	0.61
C:N	0.60	0.41	0.32	0.33	0.35	0.45	0.98	3.3

C:N=DOC/(NH₃-N free+NH₃-N organic); TKN

Table 11 Water quality for wastewater train A1.

mg/L unless stated	Facultative pond AN4 (Saa005)				Maturation pond A5 (Saa020)				A Train distribution chamber (SASPDC01)				Wet well 2 (Saa045)			
	13/8/13	24/9/13	25/8/14	22/9/14	13/8/13	24/9/13	25/8/14	22/9/14	13/8/13	24/9/13	25/8/14	22/9/14	13/8/13	24/9/13	25/8/14	22/9/14
EC (µS/cm)	1660	1770	1660	1690	1640	1700	1530	1800	1850	1780	1540	1860	1670	1790	1500	1790
pH (pH units)	8.57	8.83	7.58	7.57	9.33	10.14	8.86	8.33	9.4	9.34	8.72	8.4	9.03	9.09	9.24	9.24
Temp (°C)	17.3	20.7	14	19.4	17.4	19.7	16.1	18.1	17.5	20.4	15.5	18.3	17.7	20.2	15.6	18.7
DO	1.3	0.7	-	5.7	3.3	0.9	-	9.5	5	0.5	11	7.7	2.2	1.2	16	7.4
Turbidity (NTU)	110	123	-	-	150	232	-	-	96	73	-	-	146	113	-	-
Alkalinity as CaCO ₃	400	460	470	440	370	340	430	470	400	350	420	470	720	450	390	340
BOD	86	130	63	54	68	77	33	35	44	65	27	58	190	83	33	30
NH ₃ -N free	21	32	33	31	5.8	1.1	13	25	6.6	7.4	12	25	28	23	7.8	3.5
NH ₃ -N organic	18	22	18	22	16	21	18	14	11	10	18	19	180	17	17	11
NO ₂ -N	<0.10	<0.10	<0.10	<0.10	0.89	1.8	0.29	<0.10	0.41	0.74	0.35	<0.10	<0.10	<0.10	0.42	0.23
NO ₃ -N	<0.10	0.12	<0.10	<0.10	0.19	1.1	0.21	<0.10	0.37	0.71	0.33	<0.10	<0.1	<0.10	0.51	0.11
TN	39	54	51	53	22	25	32	39	18	19	31	44	208	40	26	15
FRP	3.7	0.18	2.1	<0.1	1	0.56	2	2.8	1.6	0.7	1.9	3.8	2.3	4.5	1.4	0.91
TP	6.1	7	6.9	7	3.7	3.2	6.5	7	4.5	2.1	6.3	8.6	73	6.8	4.7	3.4
TOC	125	51	61	65	56	35	34	53	34	-	33	58	108	31	29	28
DOC	12	15	15	13	16	14	23	22	17	18	23	21	15	17	18	19
BDOC	10	9.7	11	5.5	5.8	2.6	14	17	6.1	2.0	7.4	22	5.5	7.8	5.5	7.1
UV ₂₅₄ (filtered) (%)	60	63	44	58	60	56	47	38	59	64	62	36	56	51	51	46
<i>E. Coli</i> (cfu/100 mL)	3.9x10 ⁵	1.6 x10 ⁵	1.5x10 ⁵	2.3x10 ⁶	3.9x10 ³	4.8x10 ²	5.4x10 ³	2.3x10 ⁴	1.7 x10 ³	1.1 x10 ⁴	4.4x10 ³	1.8x10 ⁴	3.4 x10 ³	2.1x10 ²	2.4x10 ²	17
Chlorophyll a (µg/L)	2930	1620	<0.1	143	2390	2340	1320	1220	1440	1020	1210	1050	2440	1830	1990	1350
C:N	0.31	0.28	0.30	0.24	0.73	0.63	0.75	0.55	0.97	1.0	0.76	0.48	0.072	0.43	0.75	1.3

C:N=DOC/(NH₃-N free+NH₃-N organic); TKN; DAFF from 16 September 2013.

Table 12 Water quality for wastewater train A2.

mg/L unless stated	Facultative pond AN2/3 (Saa010)				Maturation pond A2 (Saa025)				Maturation pond A4 (Saa030)				Wet well 1 (Saa040)			
	13/8/13	24/9/13	25/8/14	22/9/14	13/8/13	24/9/13	25/8/14	22/9/14	13/8/13	24/9/13	25/8/14	22/9/14	13/8/13	24/9/13	25/8/14	22/9/14
EC (µS/cm)	1810	1940	1710	1820	1870	980	1790	2010	1860	1850	1710	1940	1650	1780	1620	1800
pH (pH units)	9.01	8.6	8.53	8.06	8.82	8.97	8.41	8.48	9.37	9.38	8.86	8.66	9.56	9.20	9.12	9.31
Temp (°C)	17.3	20.6	16	19.6	16.7	19.8	14.8	17.4	17.6	20.2	16.5	18.6	16.4	19.3	14.6	17.9
DO	2.8	0.9	13	7.0	1.6	1.0	12	8.0	2.5	0.9	13	8.2	2.8	0.5	17	7.6
Turbidity (NTU)	103	287	-	-	152	236	-	-	84	71	-	-	80	94	-	-
Alkalinity as CaCO ₃	500	530	440	450	460	450	450	480	390	350	380	430	370	430	360	330
BOD	140	210	41	120	73	76	27	50	54	58	16	34	55	75	73	23
NH ₃ -N free	30	36	32	30	21	17	23	28	7.2	8.2	11	19	7.6	20	5.0	1.5
NH ₃ -N organic	96	52	16	32	30	16	20	16	19	13	11	13	14	15	21	10
NO ₂ -N	<0.10	<0.14	<0.10	<0.10	<0.10	<0.10	0.13	<0.10	0.44	0.74	0.21	<0.10	0.27	<0.10	0.34	0.31
NO ₃ -N	<0.10	0.14	<0.10	<0.10	<0.10	<0.10	<0.10	<0.10	0.3	0.71	0.24	0.11	<0.10	<0.10	0.22	0.13
TN	126	88	48	62	51	33	43	44	27	23	22	32	22	35	27	12
FRP	1.8	2.4	3.1	3.3	3.2	1.7	3.1	2.8	1.5	0.65	1.5	3.9	1.0	3.2	0.79	0.55
TP	1.5	13	6.2	8.5	8.6	6.3	6.8	6.6	4.7	2.2	3.7	5.4	3.3	5.2	4.9	2.3
TOC	89	171	42	50	39	31	34	34	34	21	25	30	34	28	26	30
DOC	12	14	16	24.2	13	14	11	15	16	13	12	23	21	15	17	15
BDOC	8.4	13	14	5.9	5.5	3.5	7.0	5.0	5.5	1.8	4.4	8.9	8.4	10	5.4	6.9
UV ₂₅₄ (filtered) (%)	61	54	36	52	63	60	56	55	60	63	50	47	55	53	48	48
<i>E. Coli</i> (cfu/100 mL)	20	49	2.6x10 ⁵	4.6x10 ⁵	8.7 x10 ³	2.3x10 ²	1.8x10 ⁴	6.5x10 ⁴	2.0x10 ⁵	1.8x10 ⁵	4.1x10 ²	28	-	2.9x10 ²	68	21
Chlorophyll a (µg/L)	1540	2240	1080	2820	1140	1200	1950	1380	1370	1500	1210	982	1730	1910	4120	1860
C:N	0.095	0.16	0.32	0.39	0.25	0.42	0.25	0.34	0.61	0.61	0.54	0.72	0.97	0.43	0.65	1.3

C:N=DOC/(NH₃-N free+NH₃-N organic); TKN

Wastewater treatment resulted in an average BOD:N ratio of approximately 0.5, which is lower than generally reported for SAT schemes (Fox *et al.* 2001). Fox *et al.* (2001) reported that a BOD:N ratio greater than 3 is necessary to sustain nitrogen removal, while the majority of SAT schemes have a lower BOD:N ratio of 1. A BOD:N ratio of 1 can account for approximately 30% nitrogen removal via heterotrophic denitrification, assuming all the carbon present is available for denitrification. Thus the potential for nitrogen removal in the Alice Springs SAT basins via denitrification was limited by the BOD:N ratio of the source water.

Previous analysis of nutrient transformations at the Alice Springs SAT site reported that total nitrogen was attenuated by about 20% prior to the watertable (Miotlinksi *et al.* 2010). The mechanisms for removal of organic nitrogen were adsorption of ammonium to the soil profile, followed by oxidation to nitrate. Removal of nitrate can occur under anoxic conditions, by heterotrophic denitrification or the anammox process. However, aside from spikes of low oxygen concentration after the wetting period there was little evidence of anoxic conditions in the profile beneath the recharge basins (Miotlinksi *et al.* 2010).

Figure 52 shows the EEM spectrums for dissolved organic carbon along the wastewater treatment process, the Sewer inlet (raw wastewater), facultative pond AN 2/3, maturation pond A2, maturation pond A4, DAFF source water and the SAT source water. Peaks relating to different fluorophores, A – humic-like, C – fulvic- and humic-like, and T1 and T2 – tryptophan-like, have been labelled. The raw wastewater shows protein-like fluorescence (T1, T2) and the treatment process resulted in an increase of humic- and fulvic- like fluorescence corresponding to a decrease in protein-like fluorescence.

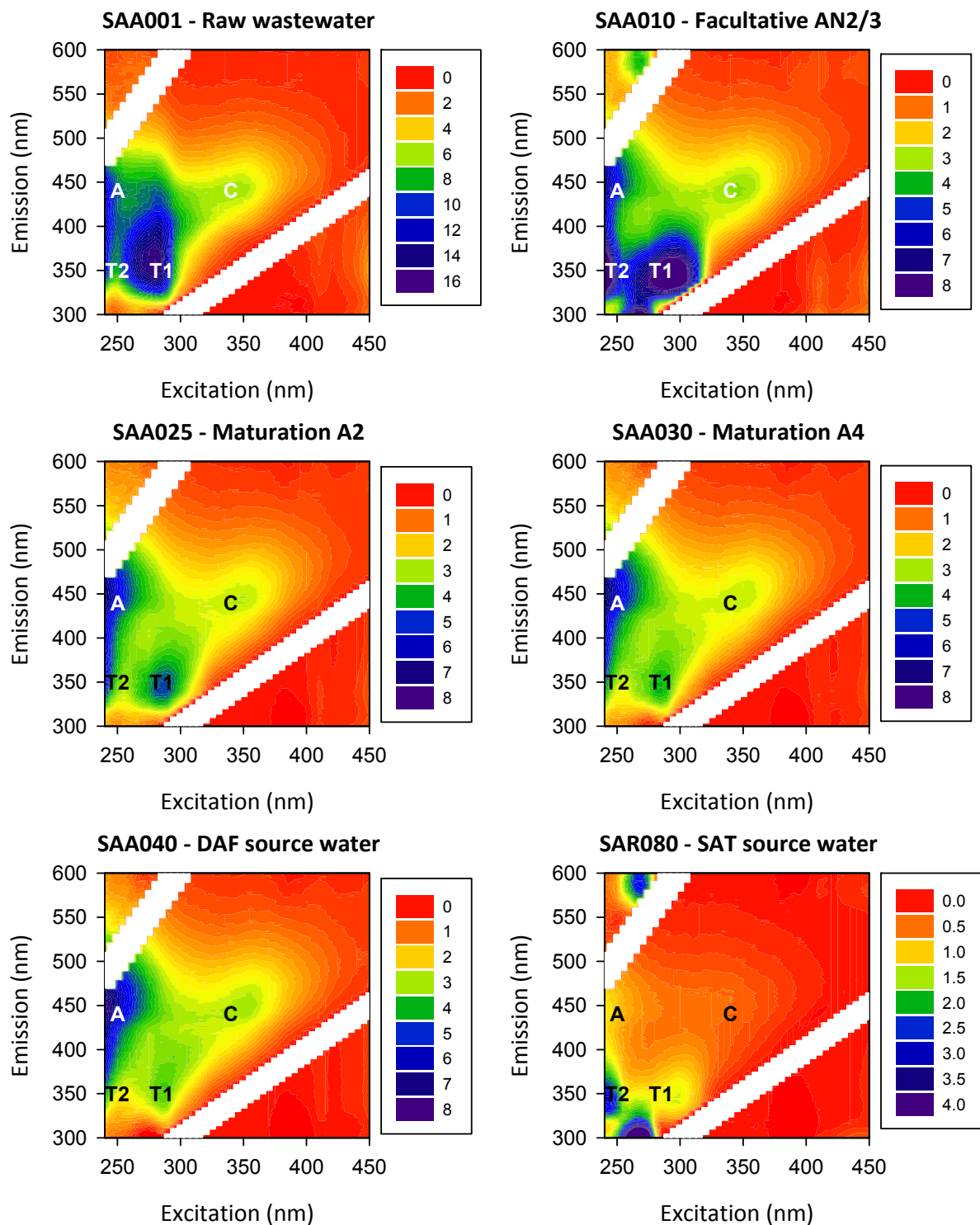


Figure 52 Fluorescence excitation-emission matrices (EEMs) of dissolved organic carbon during wastewater treatment for: sewer inlet (Saa001), facultative pond AN2/3 (Saa010), maturation pond A2 (Saa025), maturation pond A4 (Saa030), DAFF source water (Saa040) and SAT source water (Sar080) sampled in September 2014, where A = humic-like, C = humic- and fulvic-like, T1 and T2 = typtophan-like fluorescence. The colours represent the fluorescence intensity expressed in Raman units. Note the different fluorescence intensity scales are used to enable comparison of samples. The white areas mask the Rayleigh scatter peaks of water.

Soil and groundwater characterisation

Compaction tests

A high density ratio determined using a nuclear density tensiometer indicates soil compaction. Basins B and C had higher density ratios (>85%) in the 0-150 mm interval than the remaining basins (Table 13). In Basin B, the density ratio remained high throughout the profile with the highest measurements in the 150-300 mm interval. This is consistent with compaction contributing to the low infiltration rates observed. Density ratios were consistently below 85% throughout the profile in Basins D and E where lighter machinery was used during the construction.

The results from the dynamic cone penetrometers are shown in Figure 53. Basin C and D measurements were taken during winter (August), when soil was relatively moist while Basin E measurements were taken in November, when temperature was warmer (Figure 31) and soil drier. In general the measurements from Basin E suggest lower compaction compared with samples from Basins D and C, in spite of the fact the experiment was performed in much drier soil. The higher the numbers of blows per 50 mm increment, the 'denser' the soil.

Table 13 Density ratio (%) determined at various depths for locations in Figure 34 (Source: Alice Materials Testing).

Sample location ID	Basin	Sample date	Density ratio (%)			
			0-150 mm	150-300 mm	300-450 mm	450-600 mm
4C	A	12/9/12	77.0	n/a	n/a	n/a
1	B	26/7/12	89.0	94.5	88.0	n/a
2	B	"	77.0	84.0	75.0	n/a
3	B	"	88.5	92.0	89.0	n/a
5	C	"	86.0	n/a	n/a	n/a
5A	C	27/7/12	91.5	n/a	n/a	n/a
5B	C	"	88.0	n/a	n/a	n/a
6A	D	2/8/12	81.5	n/a	n/a	n/a
6B	D	"	75.0	n/a	n/a	n/a
7	D	16/7/12	76.5	73.5	65.0	78.0
8	E	"	68.5	68.5	72.0	73.0
9	E	"	71.0	67.0	68.0	69.5
ZA	E	12/9/12	71.5	n/a	n/a	n/a
ZB	E	"	72.0	n/a	n/a	n/a
ZC	E	"	69.0	n/a	n/a	n/a

n/a = depth interval not applicable for this sample location ID

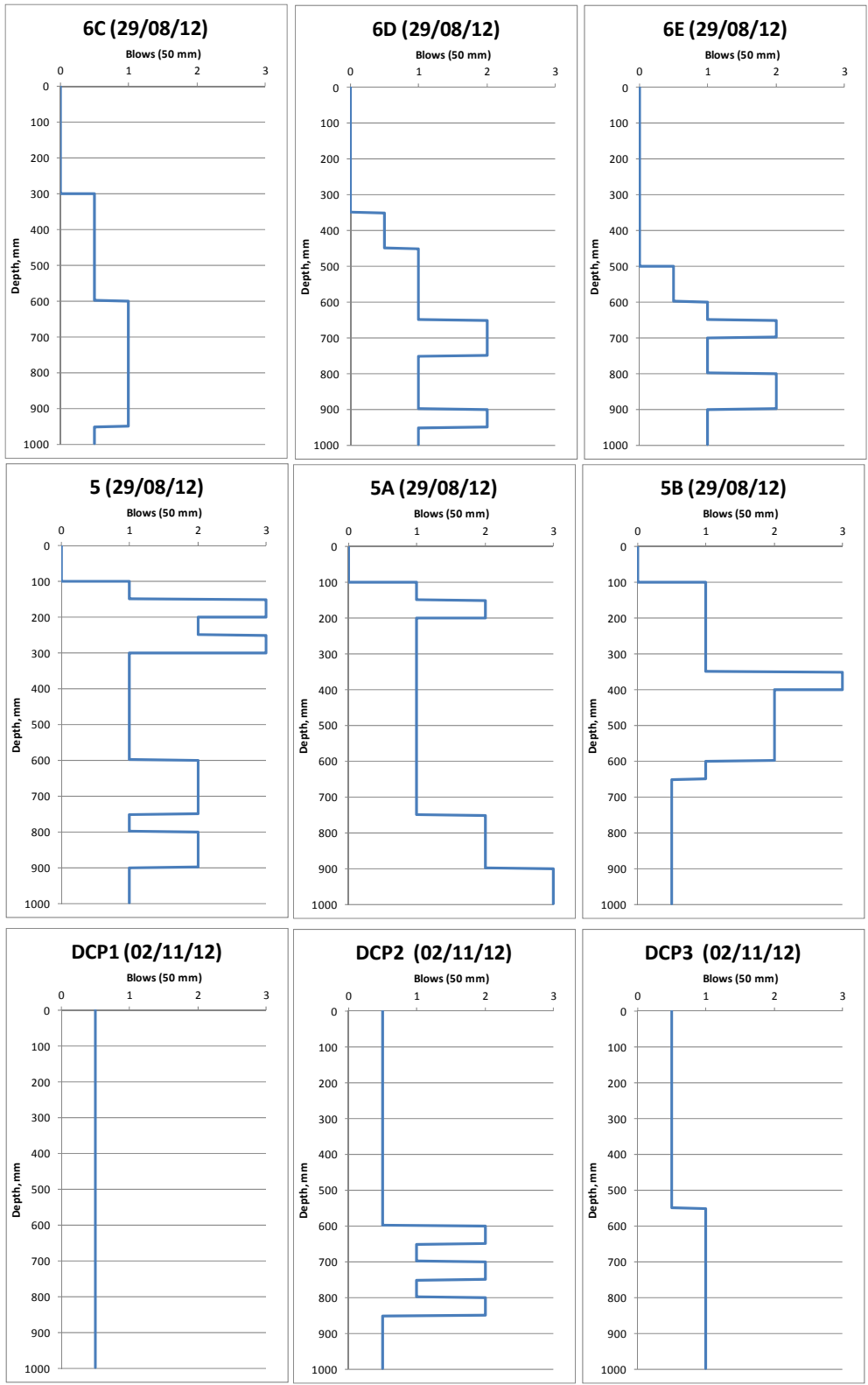


Figure 53 Dynamic cone penetrometers results for Basin D (6C, 6D, 6E), C (5, 5A, and 5B) and E (DCP1, DCP2, DCP3) (Source: Alice Materials Testing).

Basin soil profiles

The top soil (upper 0.2 m) consisted largely of brown silt and clay, with the profile to 2 m depth a mix of loamy sand to sandy clay loam until the predominantly sandy profile was reached below 2 m depth, though this was shallower in parts of the basin. There were even lenses of sand dispersed around the 1.0 to 1.2 m depths in parts along with more clay dominated lenses of clay/loam.

In July 2012 and 2013 surface samples were collected for bulk density and water content from Basin A, Basin C, Basin D (old Basin 5), a location within the extended area of future Basin E (July 2012) and 9 months after infiltration in Basin E (July 2013). The average values of bulk density varied from 1.60 to 1.82 g/cm³, and the average soil moisture content from 13 to 20 % (Table 14). However the water content of the surface layer in Basins A, C and D (5) was a function of when the last infiltration occurred and therefore is not indicative of the true soil texture.

Table 14 Average basin bulk density at 0 – 5 cm and water content at 0 – 2.5 cm depth for samples collected July 2012 and July-August 2013.

Basin/location	Number of samples	Bulk Density (g/cm ³)	Water content (%)
Basin A	5	1.82±0.08	14.7±1.2
Basin C	3	1.81±0.04	13.4±1.6
Basin D (5)	6	1.71±0.06	18.2±5.8
Basin E	3	1.60±0.11	20.1±3.4

During the July to August 2013 field trip, soil samples were also collected to 2 m depth (at 0.1 m intervals) from locations A3, D15 and ED (middle of basins A, D and E). In May and August 2014, five profiles each from locations in basins A and E plus one each from basins B, C and D (approximately 20 m from the inlet) were collected to a depth of 1.5 m. Comparing profiles from 2014 to 1.5 m depth (shown in Figure 54), there appears to be a higher soil moisture layer around the 1.0 to 1.3 m depth in the profile for Basin A, C, E and to a lesser extent in Basin D. This could indicate the presence of a more clay dominated layer or lens that retains water, in comparison to the rest of the profile where loamy sand/sandy loam was present. Basin A showed spatial variability in water content (large error bars in Figure 54) in the upper 0.5 m of the profile, whereas Basin E exhibited more variability between 1.0 to 1.3 m depth. The sandy lithology was evident at around the 1.4 to 1.5 m depth.

Soil textures also were determined using the ribboning technique (McDonald *et al.* 1990) (Table 15-Table 16) and this showed there were significant variations across the Basins A and E in the upper 1.5 m interval. This level of detail in the variability of the soil texture was not reported in the original Costean Trench results, which differentiated between sand and loamy sand to sandy clay loam (Figure 55). There does appear to be a greater proportion of sandy loam in the Basin E profiles compared with Basin A profiles with a higher proportion of sandy clay loam present, which corresponds with the different infiltration rates between the two basins.

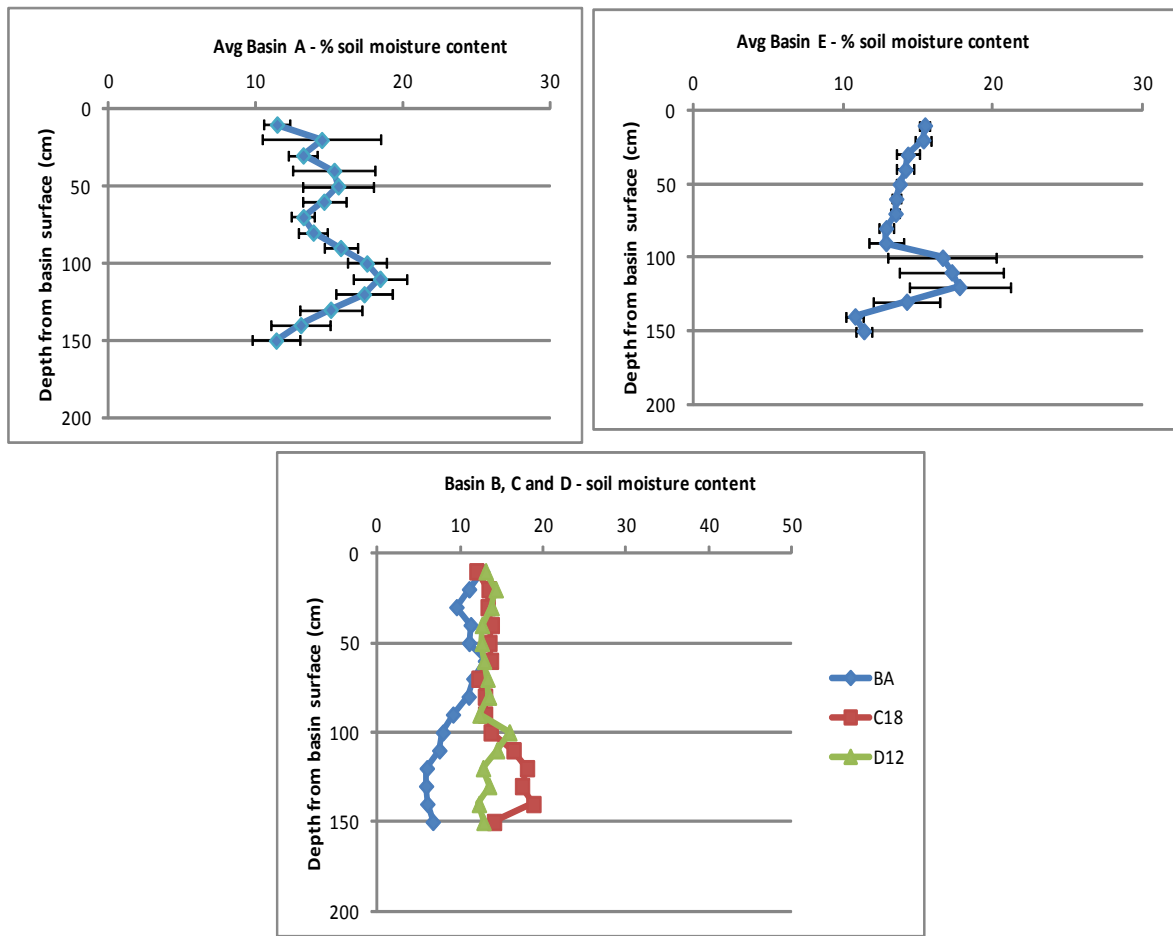


Figure 54 Average soil moisture to 1.5 m depth in basin A and D and at locations BA, C18 and D12 from samples collected in 2014.

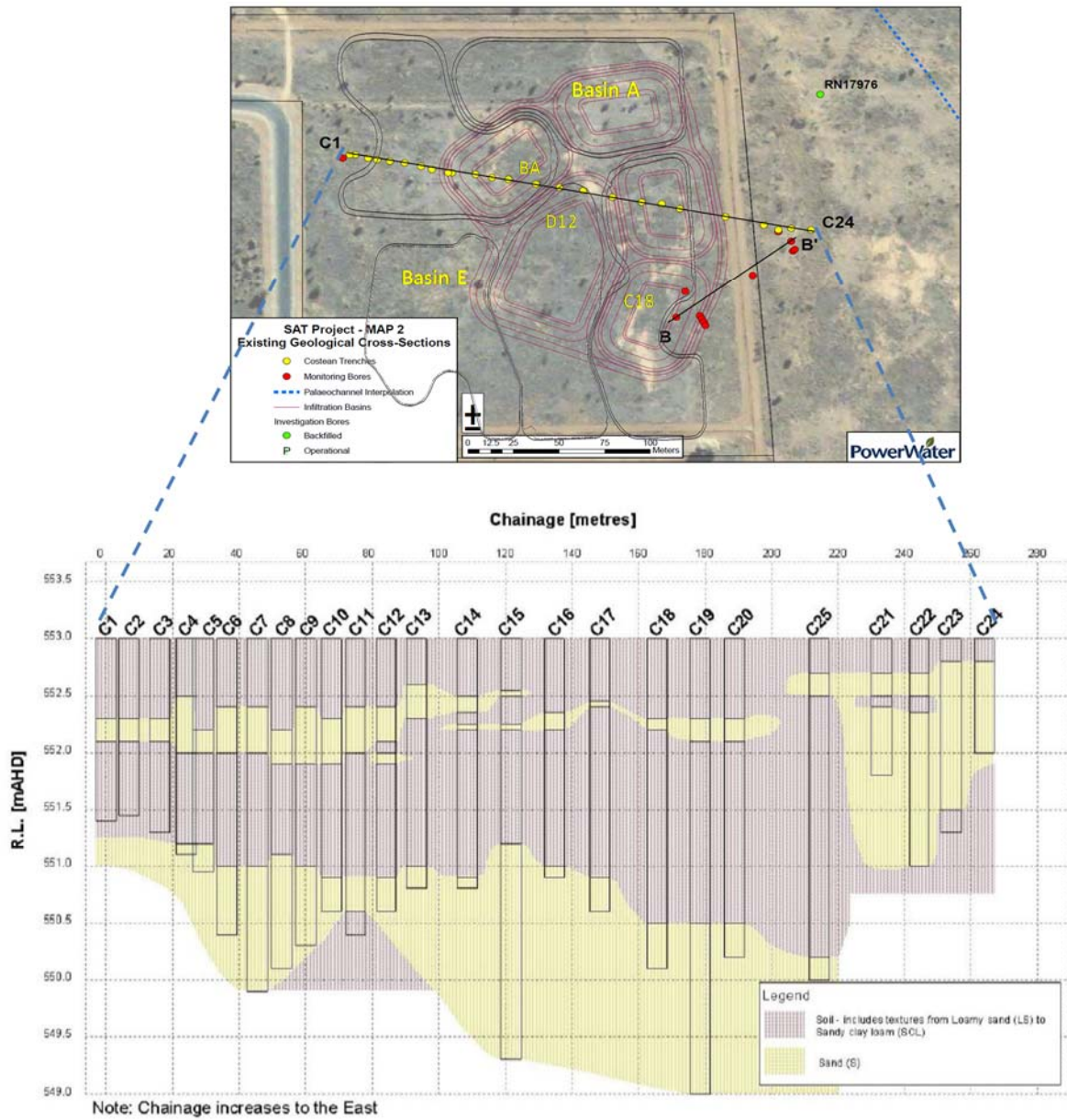


Figure 55 Soil texture previously determined by Costean Trench (C1-C24) (Knapton and Lennartz 2005).

Table 15 Soil texture variability in Basin A.

Depth	A2	A3	A4	A6	AN
10	Loamy sand	Sandy loam	Loamy sand	Loamy sand	Loamy sand
12	"	"	"	"	"
30	"	Sandy clay loam	"	"	Clay sand
40	"	"	Sandy loam	"	"
50	Light sandy clay loam	"	"	"	"
60	"	Light sandy clay loam	"	Sandy clay loam	Light sandy clay loam
70	"	"	"	"	"
80	"	"	"	"	"
90	Sandy clay	"	Light sandy clay loam	"	"
100	"	Sandy clay	"	"	Sandy clay loam
110	"	"	"	Sandy clay	"
120	"	"	"	"	"
130	Sandy loam	Light sandy clay loam	"	Light sandy clay loam	Sandy loam
140	"	"	Loamy sand	"	"
150	"	Sandy loam	"	Sandy loam	"

Table 16 Soil texture variability in Basin E.

Depth	EC	ED	EE	T6	T8
10	Sandy loam	Sandy loam	Loamy sand	Light sandy clay loam	Sandy loam
12	"	"	"	"	"
30	"	"	"	"	"
40	Light sandy clay loam	"	Sandy loam	"	Loamy sand
50	"	"	"	Clay sand	"
60	"	"	"	"	"
70	"	"	"	"	"
80	Sandy loam	Light sandy clay loam	"	"	"
90	"	"	"	Light sandy clay loam	Light sandy clay loam
100	"	Sandy clay loam	"	"	"
110	Loamy sand	"	"	"	Sandy clay loam
120	"	"	"	"	"
130	Sand	"	Loamy sand	Loamy sandy	"
140	"	Loamy sand	"	"	Sandy loam
150	"	"	"	"	"

Soil carbon and nitrogen

Comparisons can be made between soil samples collected from the top 2.5 cm layer in 2012, 2013 and 2014 (Figure 56). Basin B in 2012 and Basin C in 2013 were not accessible as water was still draining from the basin. Basins A, C and D had carbon present in organic and inorganic forms on the surface, whereas calcium carbonate was not present in Basins B and E. Precipitation of calcium carbonate on the basin surface is induced by photosynthesis of algae (Bouwer 1980). Suspended algae, filtered and trapped on the bottom of the basin can grow when exposed to sunlight. This alone will contribute to clogging, but will also lead to adsorption of carbon dioxide from the recharge water and a rise in pH which subsequently induces precipitation of calcium carbonate further cementing the clogging layer (possibly also metal oxides). The decrease in calcium carbonate content on the surface of Basin D over time may indicate that the amount of algae reaching the basin also declined with time.

The highest organic carbon content was found on the surface of Basin D, but it was highly variable. In July 2012, the Basin D had not yet been expanded; it was still in the Basin 5 configuration (Figures 33 and 35) with approximately a third of the surface area of the final Basin D. All seven sample locations from this time were located within 40 to 50 m of the inlet. In 2013 and 2014, two more locations were added which were in the southern half of the completed Basin D (~ 100 to 150 m away from the inlet).

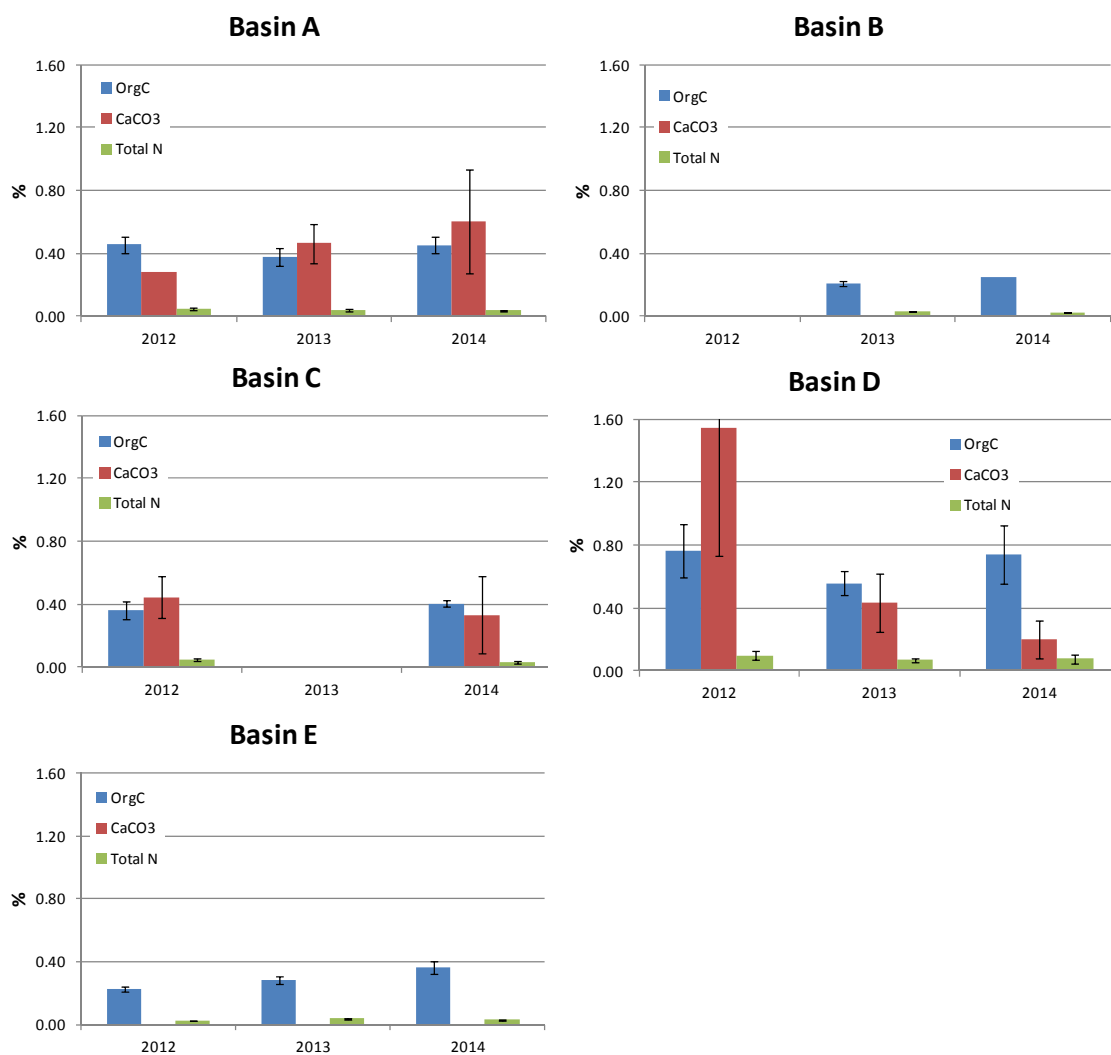


Figure 56 Comparisons of organic carbon (OrgC), calcium carbonate (CaCO₃) and total nitrogen (Total N) in the top 2.5 cm layer over three successive years.

There has been a marginal increase in carbon (organic carbon and carbonate) on the surface of Basin A with time and also an increase in organic carbon on the surface of Basin E, which can contribute to clogging. In contrast, Basin B, C and D have not shown an increase in carbon on the basin surface with time. Overall, this suggests that the schmutzdecke is not developing rapidly and can be appropriately managed for an extended period of time through appropriate drying and wetting cycles.

The concentration of nitrogen species in soil water beneath the SAT basins indicated that reduced nitrogen, as ammonium was dominant, aside from Basin D where nitrate was the dominant nitrogen species (Figure 57). There was a marginal increase in nitrate concentration between 0.8 and 1.3 m below the surface in most basins.

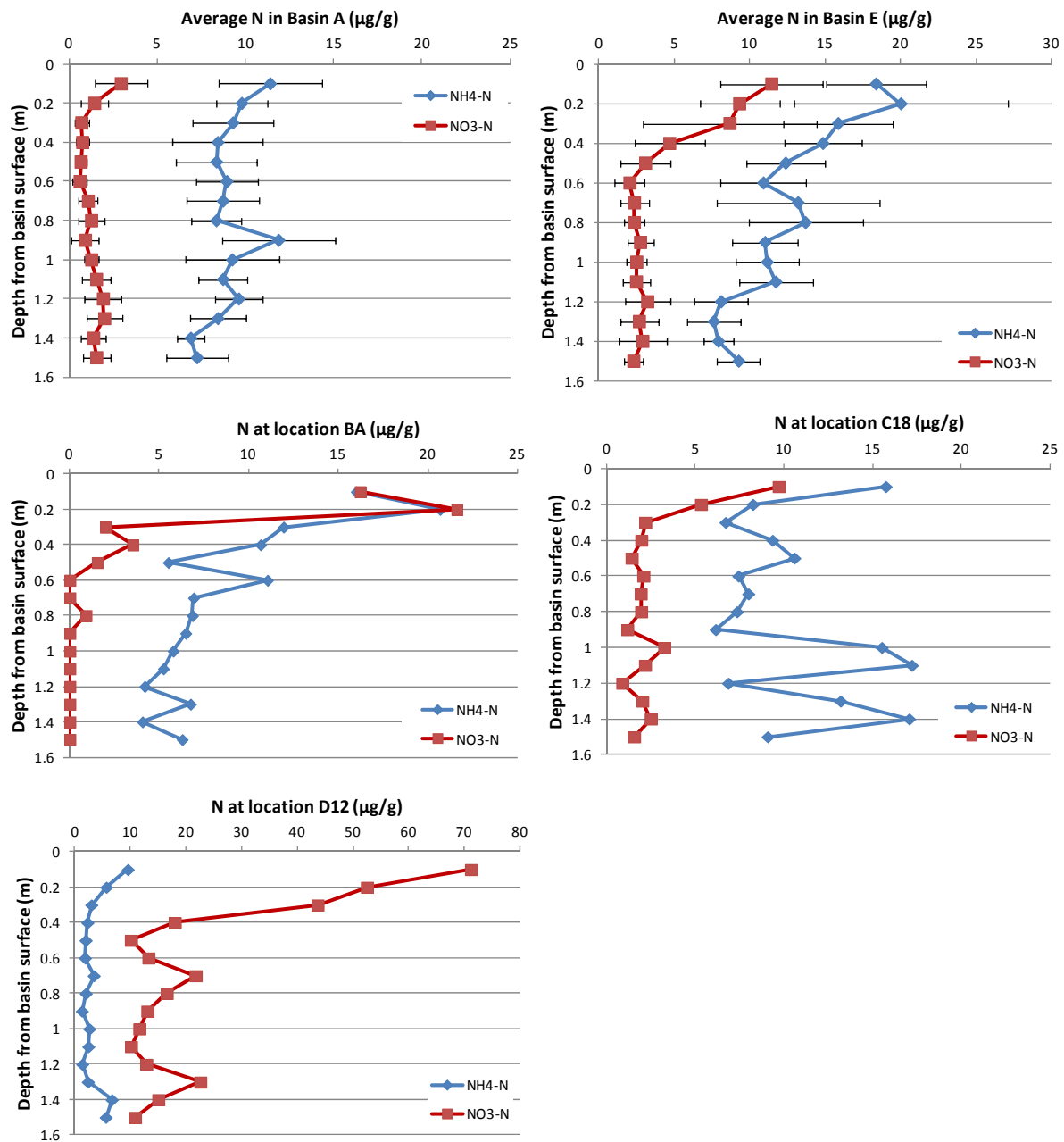


Figure 57 Nitrogen species (NO₃-N and NH₄-N) determined on KCl soil extracts from soil profiles beneath the basins. An average of multiple samples is presented for Basins A and E and individual profiles for Basins B, C and D (locations BA, C18 and D12).

Microbial communities

Microorganisms with potential for denitrification and ANaerobic AMMonium OXidation (anammox) were detected using DNA-based methods throughout the soil profile down to 1.5 m depth in basins A and E (Kaksonen *et al.* 2015). Greater knowledge of the abundance of these species relevant for nitrogen removal has implications for wastewater treatments that alter the concentrations of electron donors. Anammox bacteria convert ammonium and nitrite directly to N₂ anaerobically and do not require organic carbon or other electron donors unlike denitrifying bacteria, which reduce nitrate to N₂ with the input of suitable electron donors. Since DAFF treatment reduced the concentration of labile dissolved organic carbon in wastewater, this was likely to limit the activity of denitrifying bacteria.

Several bacterial families were detected in basin A and E shallow (S: 10-50 cm) and deep (D: 90-130 cm) depth profiles using DNA sequencing. The most dominant described families in A were *Comamonadaceae* and *Nitrospiraceae* (both average 4% relative abundance) and in basin E *Oxalobacteraceae* and *Comamonadaceae* (both average 7% relative abundance). An unknown bacterial taxa iii1-15 was found in the shallow and deep samples at a higher abundance (3-15%). *Nitrospiraceae*, *Syntrophobacteraceae* and *Flavobacteriaceae* were found in higher abundance in the samples from basin A (2-8%, 1-4% and 0-9%, respectively) than in basin E (1-5%, 0-2% and 0-3%, respectively). *Comamonadaceae*, *Solimonadaceae*, *Rhodocyclaceae*, *Nocardiaceae* and *Rhodospirillaceae* were found in higher abundance in the samples from basin E (4-11%, 1-16%, 0-17%, 0-13% and 2-9%, respectively) than in basin A (2-7%, 1-3%, 0-5%, <1% and 2-6%, respectively). *Actinomycetales*, *Gaiellaceae* were more dominant in deep (0-5% and 1-7%, respectively) than shallow (0% and 0-2%, respectively) depths, whereas *Rhodocyclaceae*, *Cytophagaceae*, *Geobacteraceae* and *Opitutaceae* were more dominant in shallow (2-17%, 1-6%, 0-3% and 1-3% respectively) than deeper (0-6%, 0-2%, 0% and 0-1%, respectively) depths (Kaksonen *et al.* 2015).

Two archaeal families were found to be the most dominant at all sites, ammonia oxidising *Nitrososphaeraceae* (19-73%) and methanogenic *Methanomassiliicoccaceae* (7-77%). The highest abundance of both families were found in the Deep depth profiles. A third family, symbiotic *Cenarchaeaceae*, was found in abundance at all basin A samples (2-37%) and several basin E samples (0-31%). The overall diversity of archaeal families in Alice Springs MAR site was rather low (Kaksonen *et al.* 2015).

The most abundant eukaryotic family in all basin A samples and depths was *Chlorophyceae* (algae) (7-49%). Other dominant families in A4D samples were fungi *Pezizales* (8-10%) and *Chytridiomycota* (9-13%). *Hypotrichia* protozoa was noted in high abundance at the A4S (43-45%) and A6S (30%) samples. *Enoplea* nematodes were in high abundance (18-19%) in the shallow ANS samples while *Sordariomycetes* (fungi) (24-42%) and *Cercomonas* (protists) (13-26%) were in higher abundances in the deeper AND samples (Kaksonen *et al.* 2015). In Basin E samples, *Liliopsida* (plant) was in high abundance in deep samples EED (32%) and ET6D (24-27%), but was absent in all basin A samples. Basin ET8D had the highest abundance of *Monohysteridae* (nematodes) (34%) while ET8S samples had a high abundance of *Dorylaimidae* (nematodes) (22-28%) and *Mononchidae* (nematodes) (9-14%). In shallow EES and ET6S samples *Sordariomycetes* (fungi) (16-28% and 11%, respectively) was abundant. *Pythium* (oomycetes) was also relatively abundant in deeps samples EED (19-23%), ET6D (4-15%) and shallow sample EES (15%) (Kaksonen *et al.* 2015).

Schmutzdecke characterisation and microbial communities

Samples of accumulated algal material and schmutzdecke were collected from in Basin A, D and E in July 2013. Samples collected near the inlet of the basins appeared to be an accumulation of algae and organic matter from the source water (Figure 58a), often quite wet and gelatinous with some evidence of a drier crust developing over time. Samples collected from further into the basins were from areas of dried out schmutzdecke ~1-3 mm thick (Figure 58b).

SEM/EDX imaging of dried out schmutzdecke from location A5 in Basin A revealed a mixture of clay, quartz and organic material with some amorphous iron oxyhydroxide (Figure 59 and Figure 60). In contrast, moist material collected from the inlet of Basin A was mainly algae, possibly including

cyanobacteria (Figure 61), with some detection of aluminium that could originate from its use as a coagulant in wastewater treatment.

The total microbial cell counts in the samples obtained from the top layers of basins A, C and E were $1.1 \times 10^9 \pm 0.5 \times 10^9$ cells/g (4 samples), $7.2 \times 10^8 \pm 5.3 \times 10^8$ cells/g (4 samples) and $0.9 \times 10^9 \pm 1.2 \times 10^9$ cells/g (8 samples), respectively. The high variation for basin E is due to the fact that the cell numbers were much higher in sampling sites E1 and E2 ($1.8 \times 10^9 \pm 1.1 \times 10^9$ cells/g) than in sites EC and EE ($8.0 \times 10^5 \pm 3.5 \times 10^5$ cells/g). The yields of extracted DNA from the top layers of basins A, C and E were $8.6 \times 10^3 \pm 2.5 \times 10^3$ ng/g, $5.5 \times 10^3 \pm 1.9 \times 10^3$ ng/g and $8.5 \times 10^3 \pm 8.2 \times 10^3$ ng/g, respectively. The yields of extracted DNA from the sample cores for the upper layer (10-50 cm depth) and lower layer (90-130 cm depth) for basin A were $6.4 \times 10^2 \pm 1.2 \times 10^2$ ng/g and $1.4 \times 10^2 \pm 5.0 \times 10^1$ ng/g (averages of 12 pooled samples), respectively and for basin E $9.0 \times 10^2 \pm 1.9 \times 10^2$ ng/g and $1.9 \times 10^2 \pm 6.1 \times 10^1$ ng/g (averages of 12 pooled samples), respectively (Kaksonen *et al.* 2015).

The most dominant bacterial family in the top layer of Basin A was *Pseudomonaceae* (21-39% relative abundance). Other abundant families were *Rhodocyclaceae* (6-18%), *Gammaproteobacteria* (6-9%) and *Comamonadaceae* (5-8%). Site A1 had additionally abundant populations of *Rikenellaceae* (13%) and *Chromatiaceae* (8%), which were only represented by 0-1% and 1-3% of the bacteria in site A2 (Kaksonen *et al.* 2015).

In Basin C site C1 top layer the most abundant families were *Pseudomonaceae* (24-26%), *Rhodocyclaceae* (16-19%) and *Oxalobacteraceae* (15%), whereas in site C2 most abundant families were *Porphyromonadaceae* (15-19%) and *Caulobacteraceae* (14-20%) (Kaksonen *et al.* 2015).

In Basin E top layer, the abundance of various families varied between different sampling sites. The highest abundances for individual sites were detected for *Rhodocyclaceae* (1-28%), *Gammaproteobacteria* (2-27%), *Porphyromonadaceae* (0-25%), *Rikenellaceae* (0-18%), *Caulobacteraceae* (2-16%), *Comamonadaceae* (4-15%), *Pseudomonaceae* (4-12%), *Oxalobacteraceae* (2-12%), *Sphingobacteriaceae* (1-12%) and *Bacteroidales* (0-12%) (Kaksonen *et al.* 2015).

A number of the bacterial families detected in the top layer of the Alice Springs MAR site harbour species that can reduce nitrate (e.g. families: *Pseudomonaceae*, *Rhodocyclaceae*, *Comamonadaceae*, *Caulobacteraceae*, *Rhodospirillaceae*, *Xanthomonadaceae* and *Helicobacteraceae*). Some families contain nitrogen fixing species (e.g. *Oxalobacteraceae* and *Rhodobacteraceae*). Some of the families harbour pathogenic species (e.g. families *Pseudomonaceae*, *Porphyromonadaceae*, *Sphingobacteriaceae*, *Aeromonadaceae*, *Sphingomonadaceae*, *Helicobacteraceae*) (Kaksonen *et al.* 2015).

The most dominant archaeal family in basin A at the sampling sites close to the water inlet was methanogenic *Methanosarcinaceae* (10-37 % relative abundance). Other minor populations were observed for uncultured *Micrarchaeles* (1-3 %), and methanogenic *Methanoregulaceae* (0-1 %). In basin C at sites close to the inlet methanogenic *Methanosarcinaceae* (0-4%) were detected with other populations representing either unknown archaeal or families with less than 1 % relative abundance. In basin E, sampling sites E1 and E2 close to the inlet, methanogenic families *Methanosarcinaceae* (21-52 %) and *Methanoregulaceae* (0-5 %) and members of uncultured *Micrarchaeles* (2-5 %) were most dominant, whereas at sites EC and EE further away from the inlet, ammonia-oxidising *Nitrososphaeraceae* (2-8 %) was the dominant family. The areas near the basin inlets are likely to be saturated with water longer periods of time (thus allowing strictly anaerobic methanogens to grow) than the areas further away from the inlets, where aerobic ammonia-oxidisers can convert ammonia to nitrate (Kaksonen *et al.* 2015).

The eukaryotic communities in Basins A and C top layers were heavily dominated by *Scenedesmeaceae* (algae) (69-96% and 20-92% for Basins A and C, respectively). Other abundant families in basin A were *Tobrilidae* (nematodes) (0-12%) and *Tephritidae* (fruit flies) (0-16%), and in basin C *Chromulinaceae* (algae) (0-43%), *Chlorellaceae* (algae) (0-39%) and *Tobrilidae* (nematodes) (0-29%).

Depending on the sampling site, the highest abundances in Basin E top layer were detected for the following eukaryotic families: *Tobrilidae* (nematodes) (0-66%), *Viridiraptoridae* (protists) (0-42%), *Chlorellaceae* (algae) (4-31%), *Scenedesmaceae* (algae) (0-29%), *Mononchidae* (nematodes) (0-25%) and *Diplogastridae* (nematodes) (0-22%) (Kaksonen *et al.* 2015).



Figure 58 a) Accumulated matter near inlet of basin; and b) dried schmutzdecke on surface of basin.

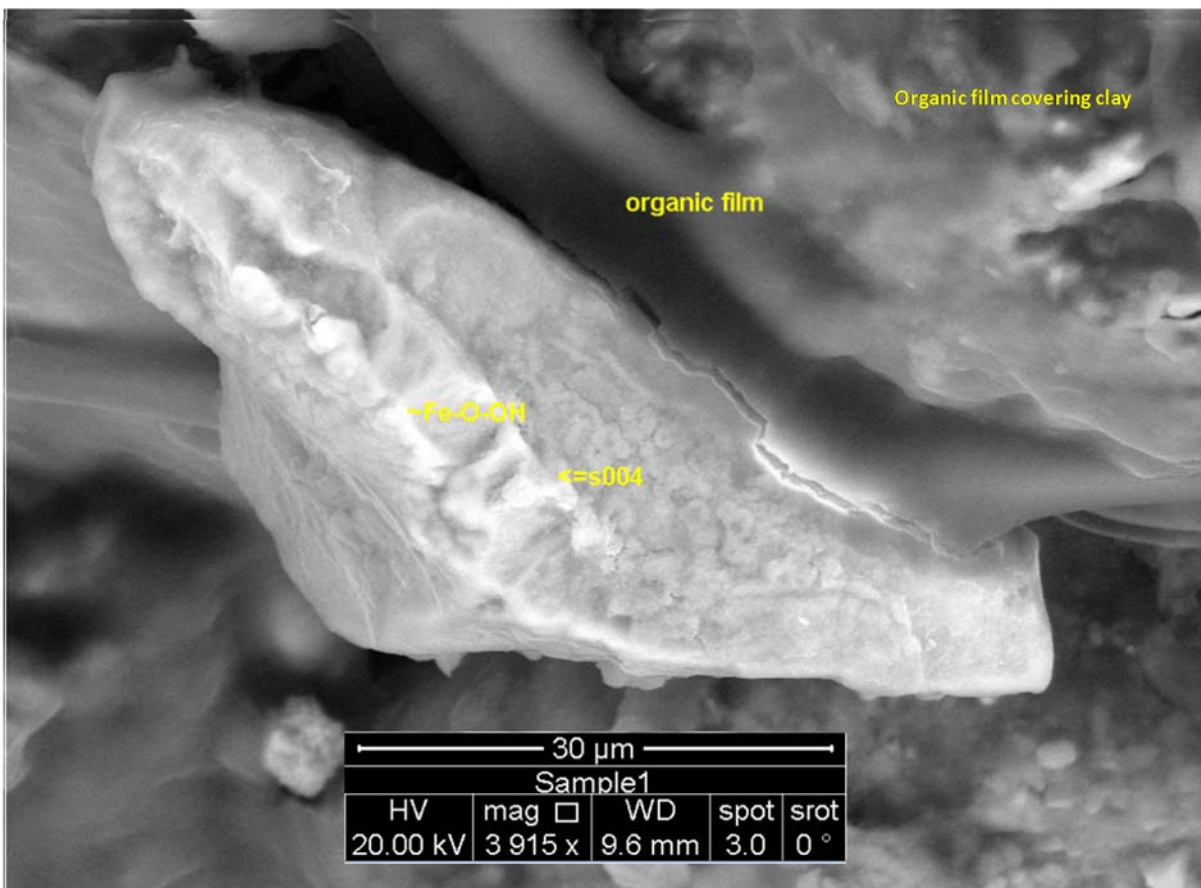


Figure 59 SEM image of schmutzdecke from Basin A (location A_5) indicating the presence of iron oxyhydroxide and organic material.

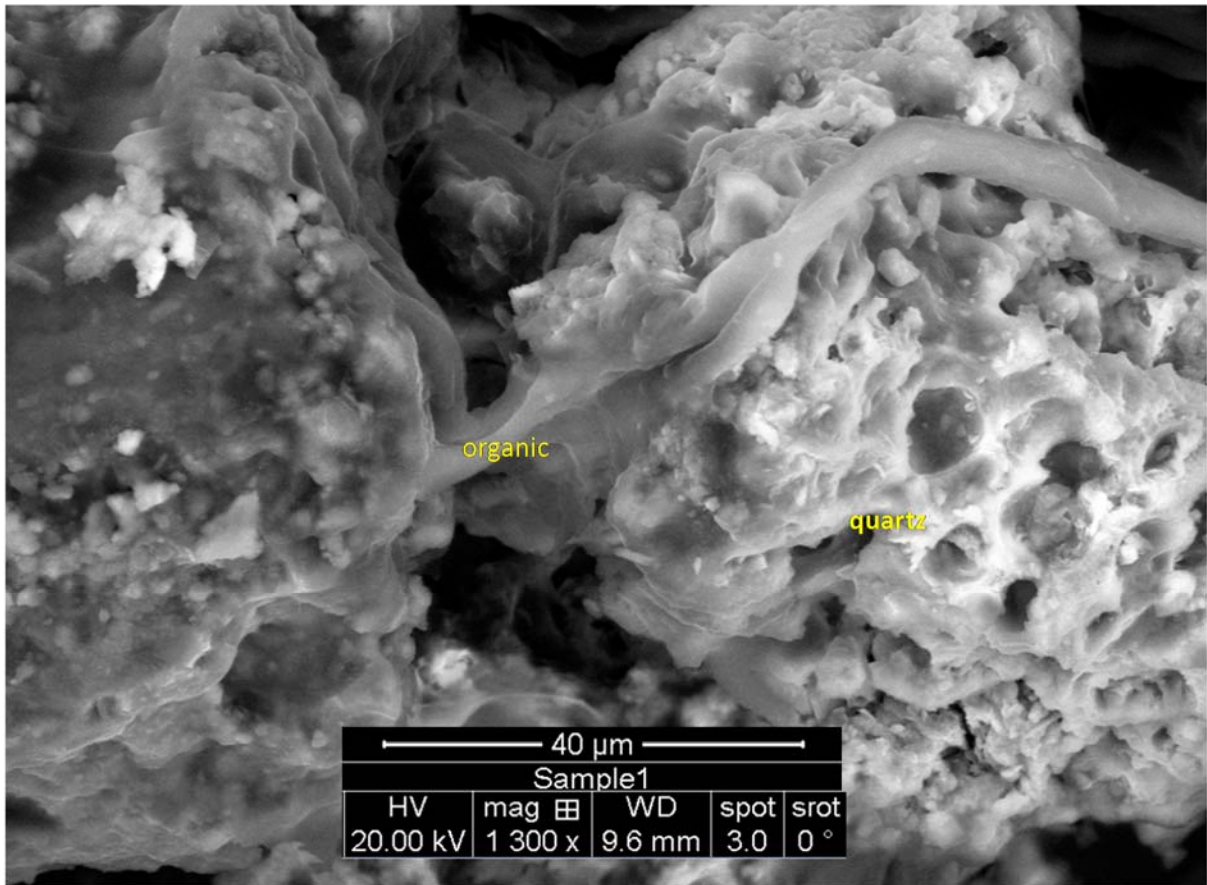


Figure 60 SEM image of schmutzdecke from Basin A (location A_5) indicating the presence of quartz and organic material.

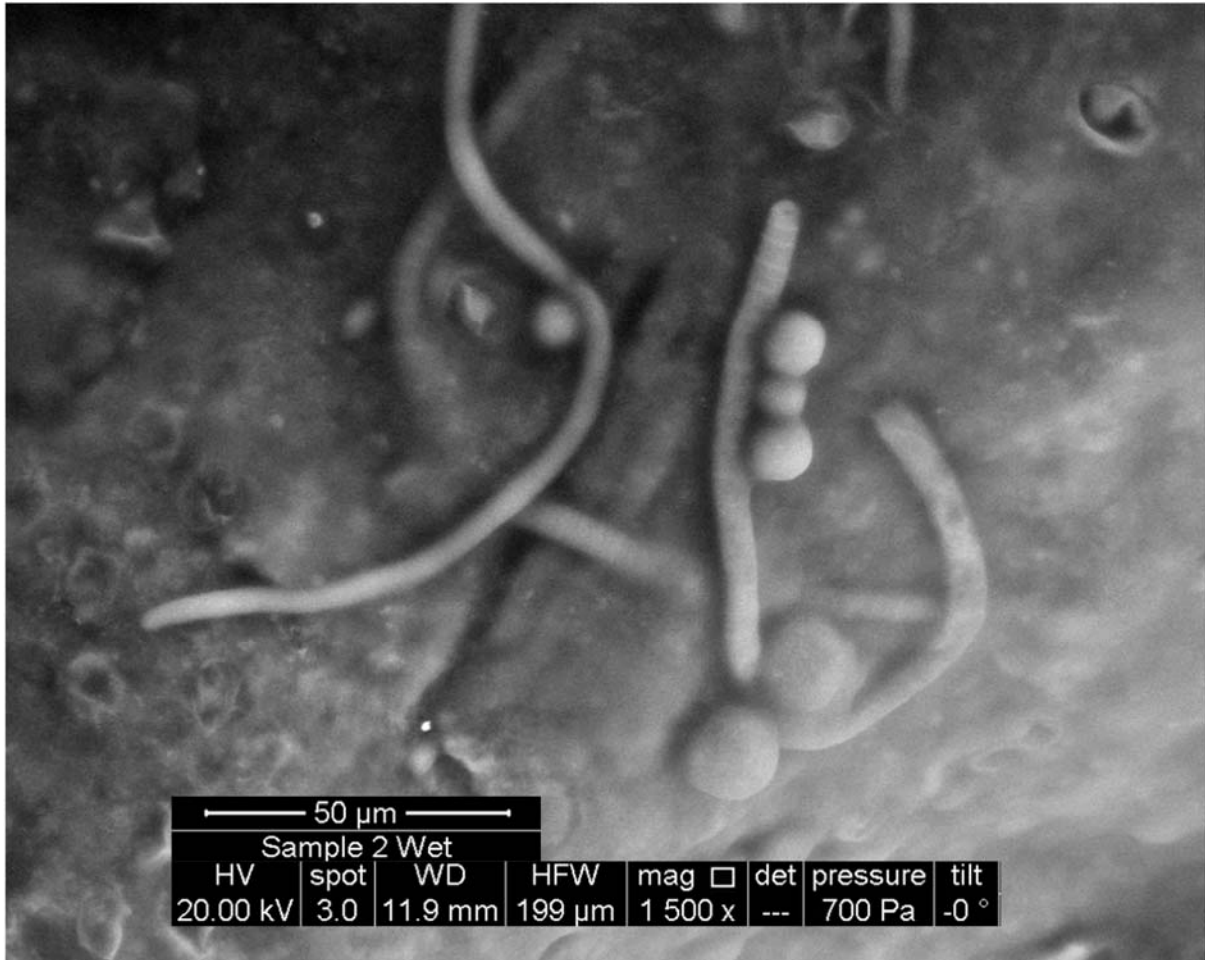


Figure 61 SEM image of accumulated algal material from the inlet of Basin A.

Geophysical characterisation

Groundwater flow beneath the SAT basins was interpreted with time-domain EM (NanoTEM). Figures from all transects run during 2013 and 2014 can be found in Appendix 6, with a detailed report to be published by Cahill *et al.*, which will assess all the results of the geophysical surveys. For this report we will focus on Basins A and E as they have been intensively monitored in other investigations (soil sampling, thermal monitoring, microbial analysis). Figure 62 shows the two NanoTEM transects run in Basins A and E in August 2014, after they had been recently infiltrated (previous week). The unsaturated zone (>12 m) had been fully flushed with recharge water as indicated by the blue area of lower conductivity.

The areas of lower conductivity below the watertable potentially indicate areas of more rapid drainage through alluvium to the palaeochannel. These are marked by an arrow on the image. It can be observed there appears to be greater areas of moisture retention beneath Basin A compared with Basin E, with the water in Basin A needing to move horizontally across less well-drained subsoil. The likely presence of finer grained subsoil could relate to the lower average infiltration rates observed in Basin A compared with Basin E.

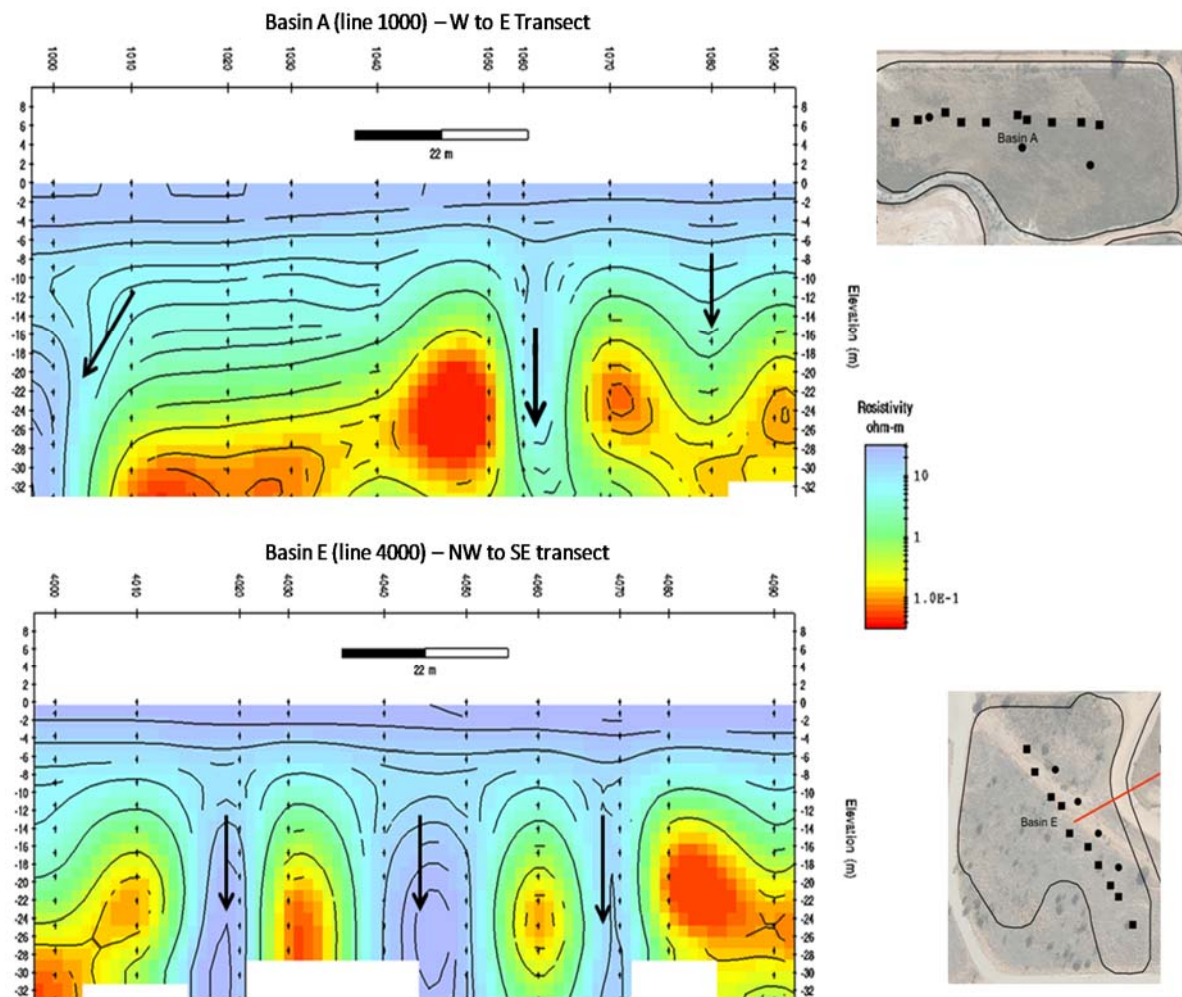


Figure 62 Groundwater flow beneath Basins A and E interpreted from time-domain EM (NanoTEM).

The CMD grids and line (Figure 63) displays the conductivity approximately 6.0 to 6.5 m below the surface, following the most recent wetting cycle, 26 July – 2 August. The range of conductivity was not large, between 15 and 35 mS/m, however there were differences between the basins which corresponded to their variable infiltration rates. Basin A showed an area of higher conductivity located in the 'older part' of the basin (previously basin 1), whereas the expanded areas to the west and north east were lower in conductivity. The newest Basin E, showed a relatively uniform coverage of conductivity in comparison. Though the thermal studies and soil sampling also showed there was variability in Basin E profiles, a higher predominance of loamy sands and sands was observed, especially below the 1 m mark. The lower conductivities appeared to run through the centre of the basins in a SE direction with the lowest conductivities observed in the southern end of the basin complex.

The resistivity model showed a relatively uniform cross section, reflecting the more even distribution of infiltration across Basins D and E observed (higher resistivity corresponds with lower conductivities), though there was an area of possible higher resistivity observed near the 90 m mark as marked (Figure 63) on the transect, which could correspond to a flow channel.

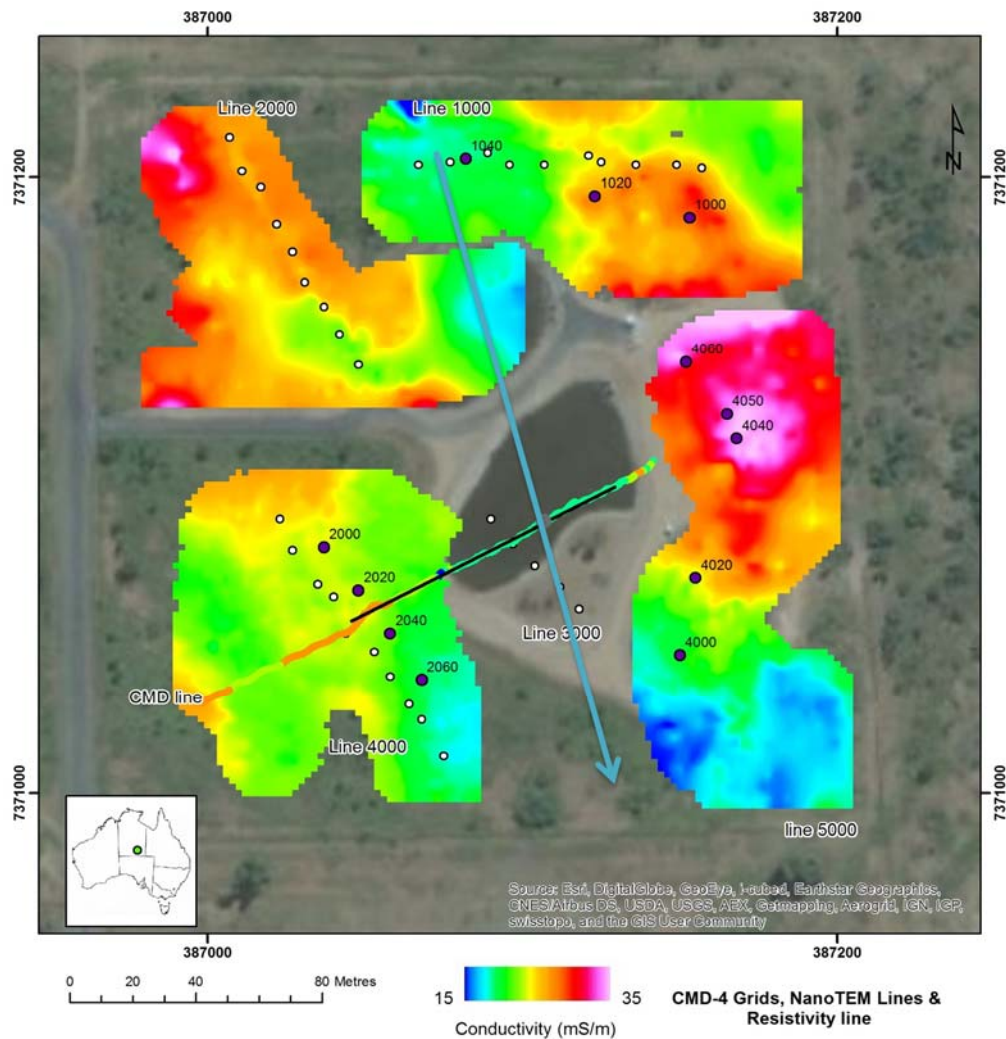


Figure 63 Interpreted CMD (apparent electromagnetic conductivity) survey results for Basins A, B, C and E at 6-6.5 m depth below basin surface after recent wetting (week prior) August 2014. The black line shows the location of the resistivity transect and this line represents the location of high resistivity at surface and at 10 m depth. The blue line represents groundwater flow which occurs at a depth of ~20m. The arrow represents a possible flow direction based on lower conductivities on Lines 1000, 3000 and the resistivity transect and the interpolated groundwater hydraulic gradient.

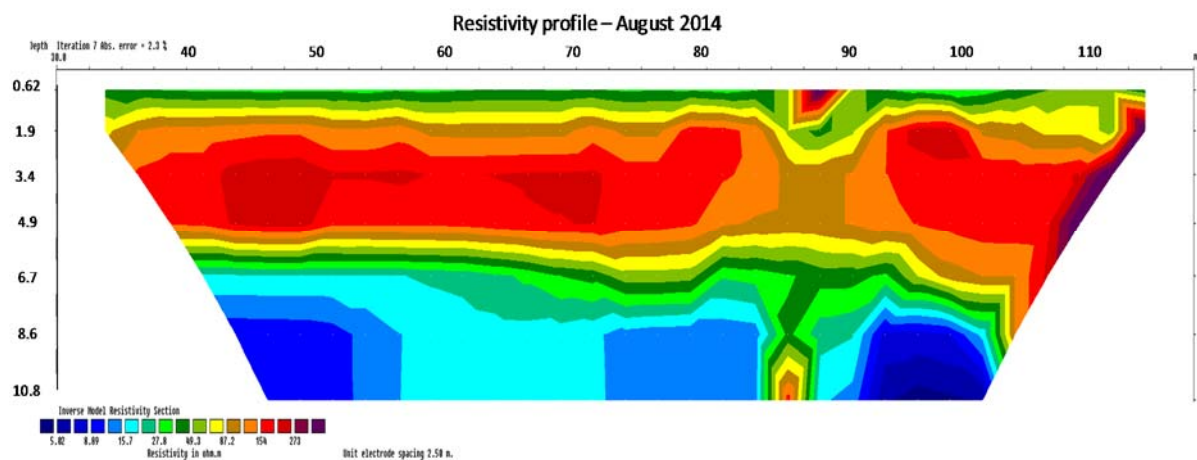


Figure 64 Resistivity transect across Basins E and D.

Groundwater quality and level response

Available electrical conductivity (EC) and chloride concentrations in RN17942, shown in Figure 65- Figure 66 (200 m down-gradient of the SAT site) illustrated freshening in response to infiltration that was comparable to on site monitoring bores (RN17947 and 17949). The trend for nitrate-N was extremely variable (Figure 67), though this may be related to how soon after an infiltration event samples have been collected as well as preservation and storage times prior to lab analysis. Despite this, the concentration in the down-gradient bore 17942 (200 m) was comparable to that in the on-site bore 17947. Down-gradient bores 17999 (500 m) and 17932 (1000 m) were showing lower nitrate concentrations until 2013, but by 2014 full breakthrough of the nitrate plume was evident, indicating that the SAT scheme does result in some increase in nitrate concentration in the groundwater. After the treatment upgrade, nitrate concentrations declined considerably in the on-site observation well RN17947 and this decline also appeared to be reflected 200 m down-gradient at RN17942. Based on the quality of DAFF treated source water, groundwater down-gradient from the SAT operation could be expected to have an EC of around 1700 $\mu\text{S}/\text{cm}$ (~ 1000 mg/L TDS) and nitrate-N concentration of approximately 5 mg/L (based on September 2014 data).

Dissolved organic carbon (DOC) (Figure 68) levels in the individual wells appear to have remained relatively stable over time, though there was more variability in the 17947 piezometer closest to the basin. DOC concentrations in groundwater were higher in the monitoring bores closest to the basins (17947 and 17949), at ~ 2 mg/L, while DOC in groundwater 200 m down-gradient (17942) was ~ 1.5 mg/L and at 500 m and 1000 m down-gradient was ~ 1 mg/L. Figure 69 shows the EEM spectrums measured for groundwater sampled in June 2014. Groundwater from bores 17938 (600 m up-gradient) and 17936 (1000 m down-gradient) displayed similar spectrum. There were minimal (A) humic peaks and no presence of (C) fulvic- and humic like fluorescence, which were present in the recharge water as shown in Figure 52 location SAR080, which suggests no impact from DOC in the recharge water at these bores as yet. In bores 17947 (on site) and 17942 (200 m down-gradient) the (C) fluvic- and humic like fluorescence was most prominent at the basin and was also present at the 200 m well, indicating the influence of the SAT recharge water (Figure 52), which supports the groundwater chemistry.

The stable isotopes of water appear also indicated that on site and down-gradient bores were impacted by recharge, with groundwater plotting along the same evaporation line as the recharge water (Figure 70). Stable isotopes indicated the presence of recharge water 1000 m down-gradient which was not apparent with some of the less sensitive environmental tracers. Also although chloride and electrical conductivity have decreased at RN17938 600 m up-gradient the isotopic data did not show a change, suggesting that there were natural local variations in ionic strength of groundwater. Head can naturally increase without the transmission of solutes to this location.

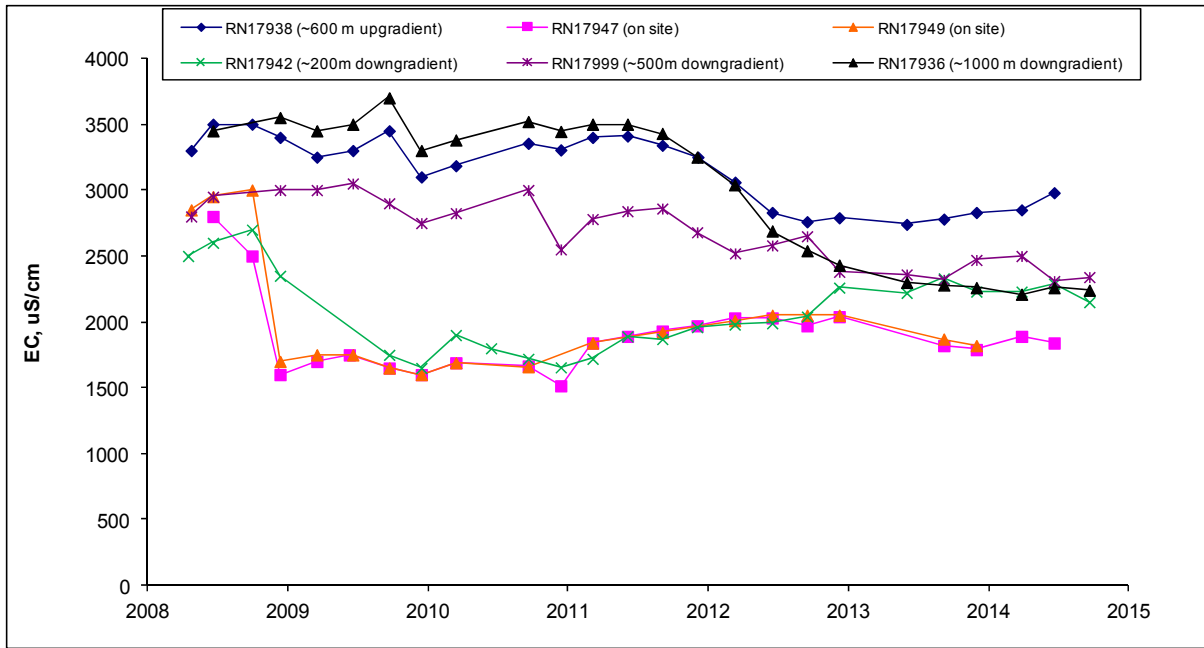


Figure 65 Salinity (EC) in groundwater monitoring bores in response to SAT operation.

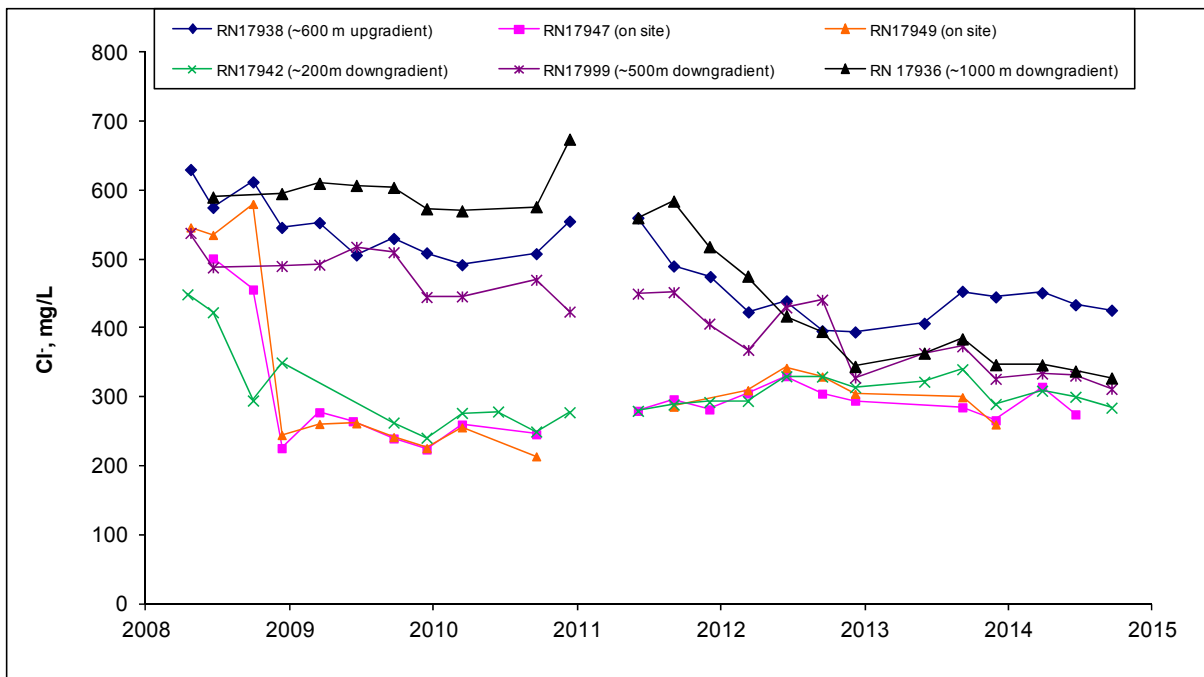


Figure 66 Chloride concentrations in groundwater monitoring bores in response to SAT operation.

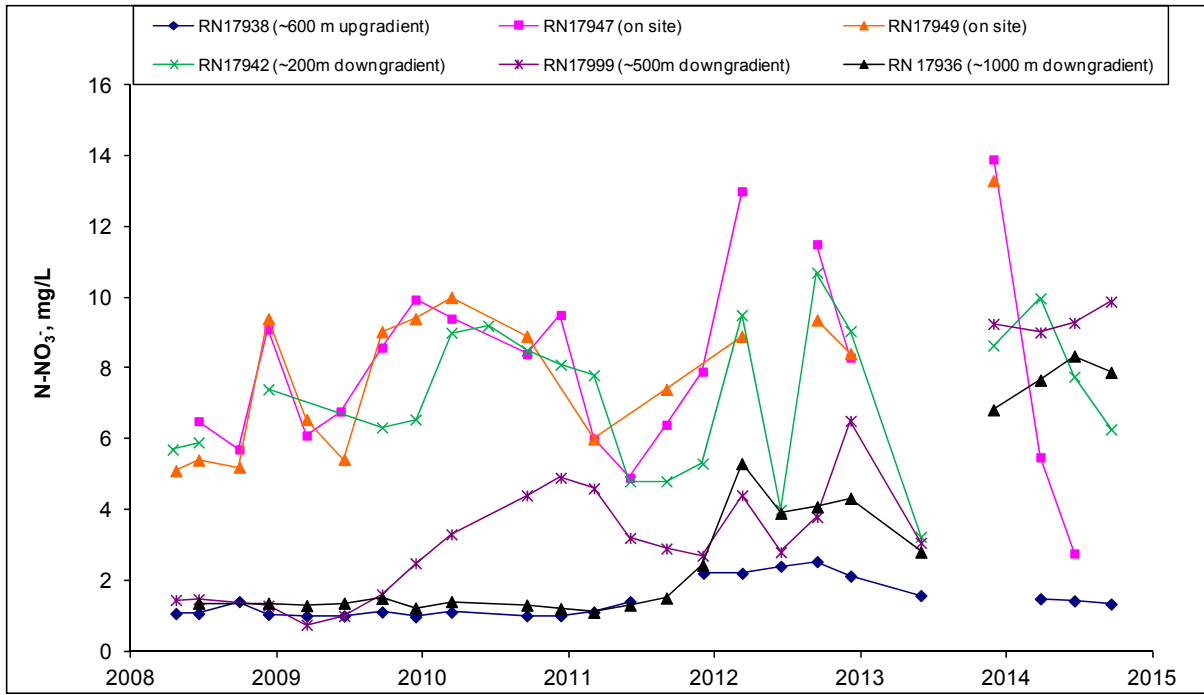


Figure 67 Nitrate-N and concentrations in groundwater monitoring bores in response to SAT operation.

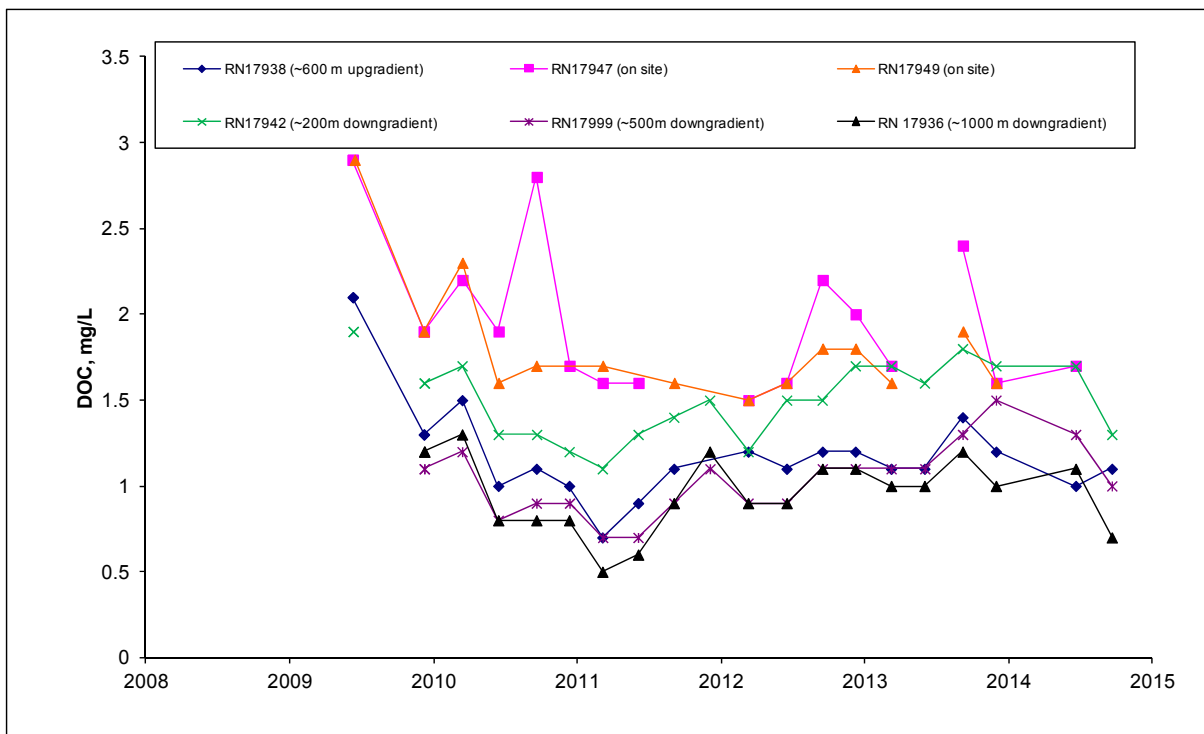


Figure 68 Dissolved organic carbon (DOC) concentrations in groundwater monitoring bores in response to SAT operation.

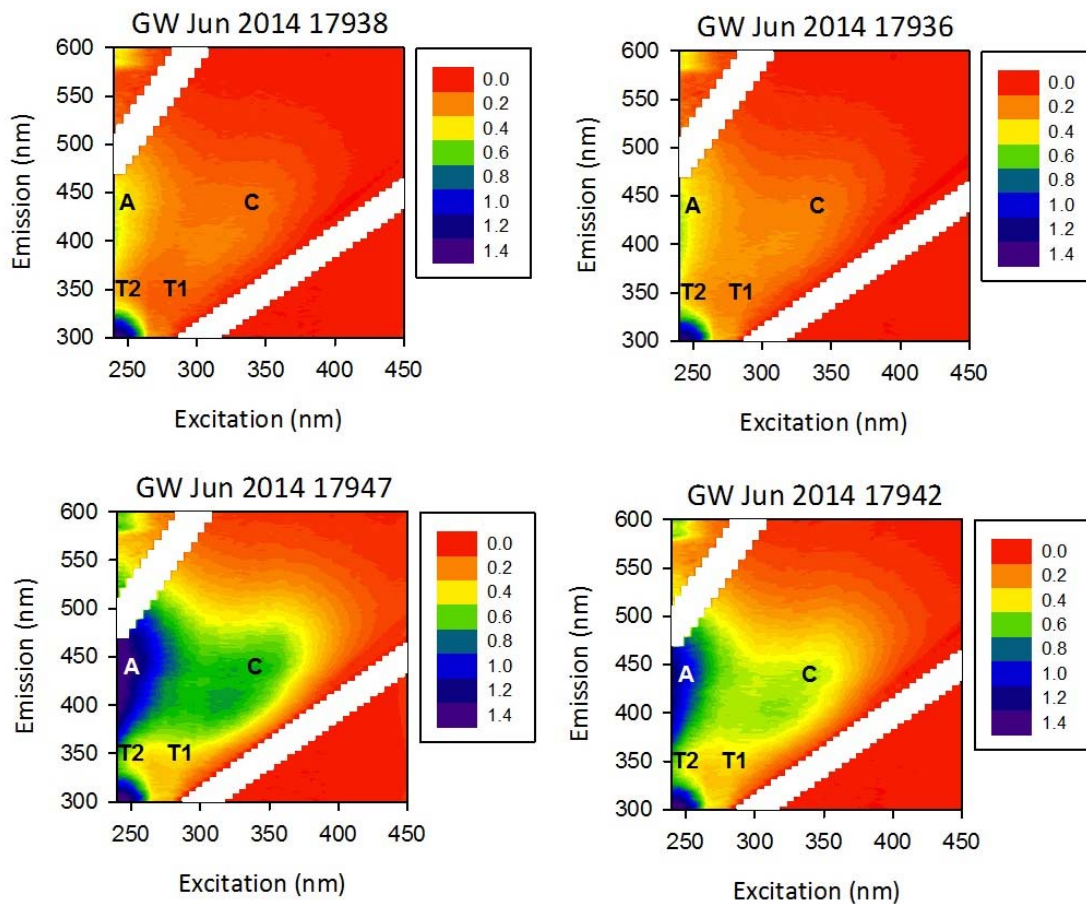


Figure 69 Fluorescence excitation-emission matrices (EEMs) of dissolved organic carbon in groundwater for: RN17938 (600 m up-gradient), RN17936 (1000 m down-gradient), RN17947 (on site) and RN17942 (200 m down-gradient) sampled in June 2014, where A = humic-like, C = humic- and fulvic-like, T1 and T2 = typtophan-like fluorescence. The colours represent the fluorescence intensity expressed in Raman units. Note the different fluorescence intensity scales are used to enable comparison of samples. The white areas mask the Rayleigh scatter peaks of water.

Standing water levels have also been monitored on a quarterly basis throughout the duration of the trial. Levels plotted as mAHD are shown in Figure 71 for monitoring bores up-gradient of the SAT operation (RN18252, 17939 and 17938); in Figure 72 for down-gradient monitoring bores (RN17942, 17999, and 17936); and in Figure 73 for near basin paleochannel monitoring bores (RN17937, 17948 and 17949) plus near basin piezometers (17947, 17946, 17945 and 17944). The basin piezometers, 17947 and 17946 which intersected the saturated zone, paralleled the open hole monitoring bores (17937, 17948 and 17949). Piezometer 17945, showed a response to individual infiltration events on those occasions when levels were measure near an event. Piezometer 17944 recorded dry throughout the study, indicating the localised basin water mound had not reached this depth (2-6 m BGS) in the unsaturated zone.

It is observed that water levels remained relatively stable in the paleochannel until 2010. Following expansion of the basins in 2011 the water level steadily increased on site and down-gradient of the basins. The up-gradient bores also showed an increase in water level from 2010, however these appear to have been influenced largely by the higher than average rainfall in 2010, with a total of 769 mm, compared with annual average of 284 mm. The levels in the majority of up-gradient bores have been dropping back down to background levels, but bore RN17938 was showing the hydraulic influence of the expanding basin plume with levels stabilising rather than dropping from 2011 onwards. Table 15 summarises the relative changes in water levels from the start of the trial in 2007 to 2014 (end of the MARRO project). The rise in water level observed down-gradient of the basins illustrates the positive impact of the SAT scheme on water resources.

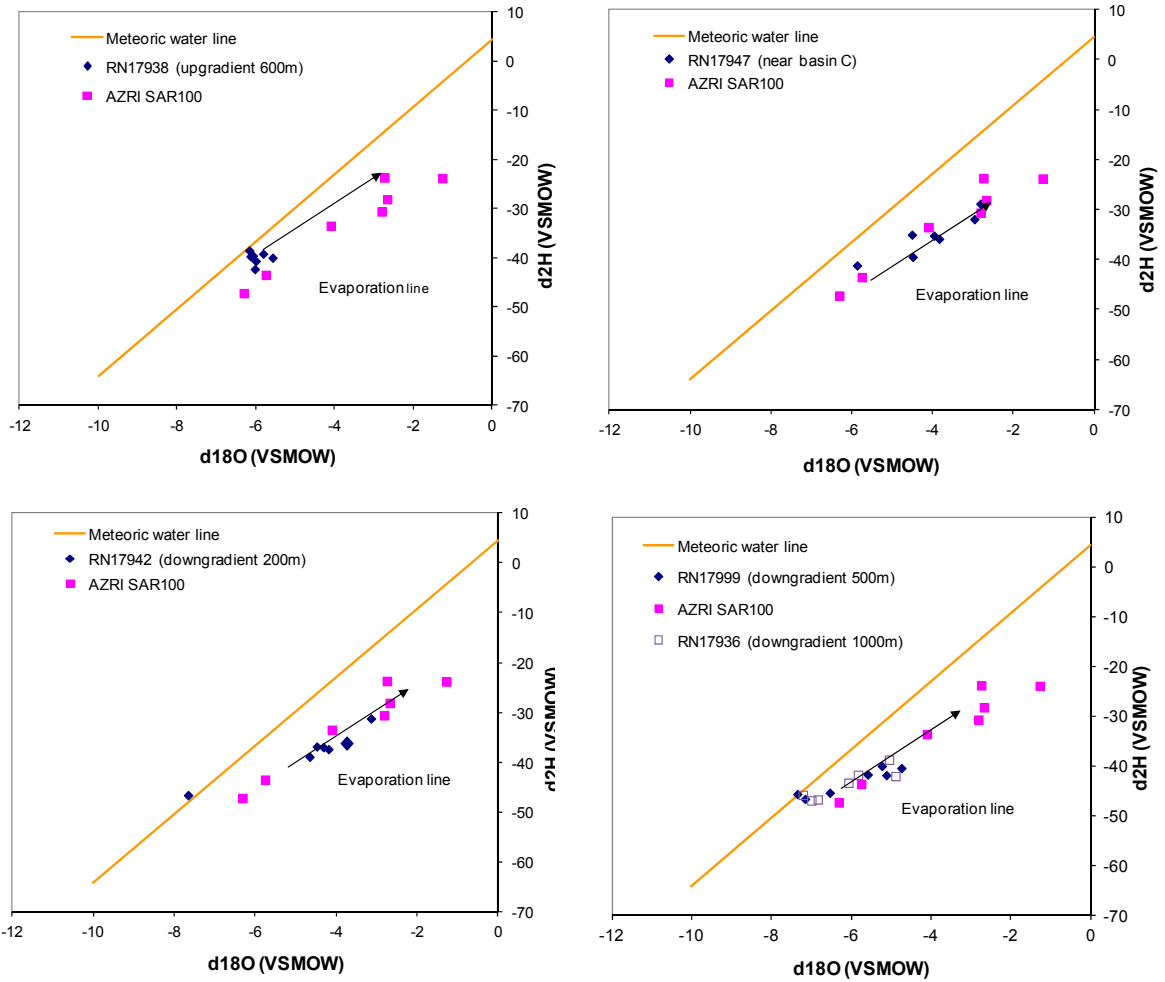


Figure 70 Average annual stable isotopes of water in groundwater sampled from April 2008 to December 2014 compared to the recharge water (AZRI SAR100) and the meteoric water line.

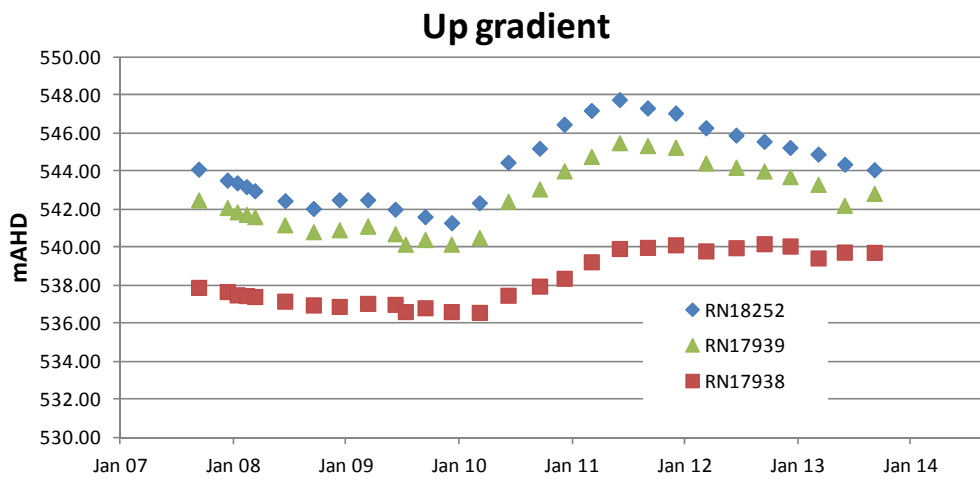


Figure 71 Groundwater levels (mAHD) of monitoring bores up-gradient from the SAT basin operation.

Down gradient

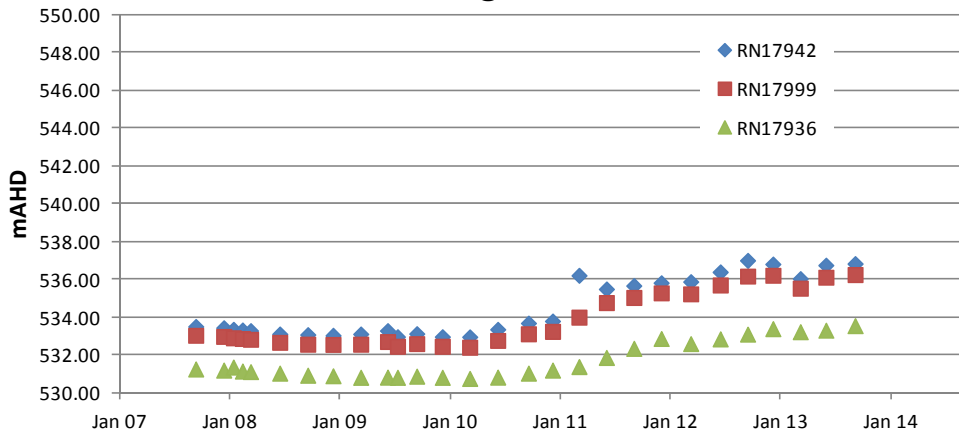


Figure 72 Groundwater levels (mAHd) of monitoring bores down-gradient from the SAT basin operation.

At Basin

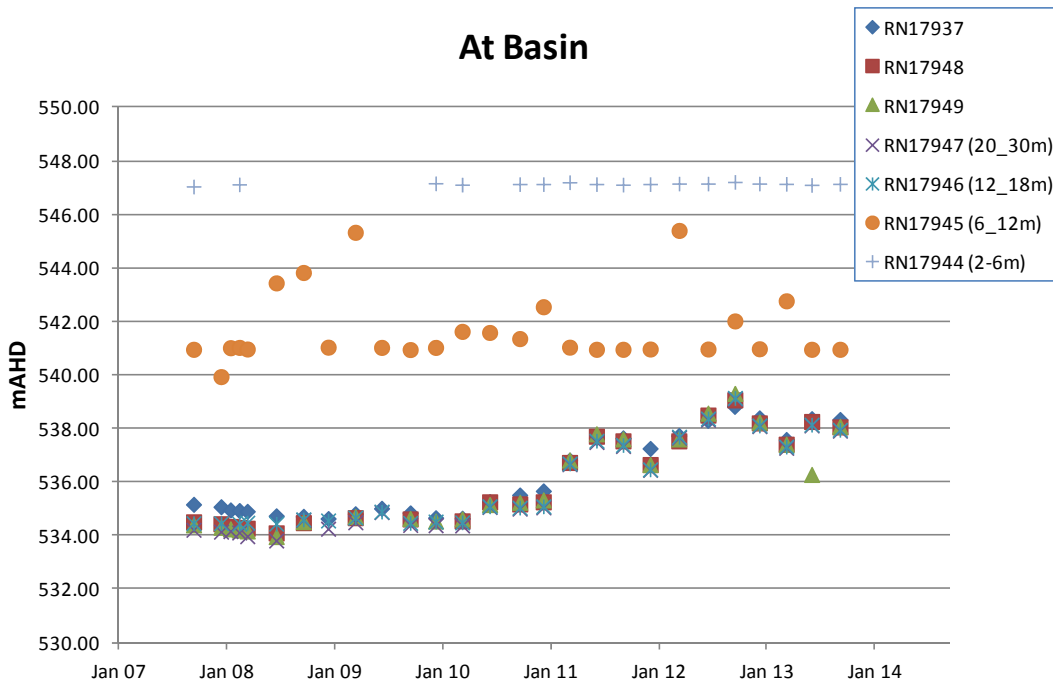


Figure 73 Groundwater levels (mAHd) of open hole monitoring bores next to Basin B and in Basin C during SAT operation.

Table 17 Relative change in paleochannel groundwater levels (Δm) measured from before start of infiltration in June 2007 to September 2013.

Up-gradient monitoring bores (distance from basins)	Δm	Monitoring bores at basins	Δm	Down-gradient monitoring bores (distance from basins)	Δm
RN18252 (1500 m)	-0.03	RN17937	3.17	RN17942 (200 m)	3.32
RN17839 (1000 m)	0.34	RN17948	3.55	RN17999 (500 m)	3.21
RN17838 (500 m)	1.85	RN17949	3.68	RN17936 (1000 m)	2.29

Alice Springs summary

Clogging

From June 2008 to September 2014 a total of approximately 2,580 ML reclaimed wastewater was delivered from the WRP plant to the SAT basins. The current, expanded basin configuration has received 1,470 ML equating to approximately 1.9 ML/d, which is sufficient to meet the initial target volume for recharge of 600 ML/yr. Assuming a conservative infiltration rate of 200 mm/d over the infiltration area of approximately 38,000 m², suggests the basins are not currently used to their full capacity and they may be able to recharge around 7.6 MLD.

Operational data for the SAT basins during winter highlighted the impact of insufficient drying periods on infiltration rates. Vegetation can act as mulch in winter and prevent drying and as a result drying periods should be extended in winter. While a winter drying interval of 5 to 10 days has been suggested, the preferred strategy would be to use the basin surface condition to inform operation, as previously recommended by Breton (2009). It is also recommended that an appropriate strategy is developed for management of vegetation growth in the basins.

Implementation of filtration as an additional pre-treatment step improved the quality of recharge water to the SAT basins, reducing nutrient concentration and turbidity through greater removal of algae and coagulant. This improvement in the quality of recharge water resulted in higher infiltration rates in all basins. However, the impact was most pronounced in the poorest performing basins where infiltration rates had declined to <100 mm/d prior to the improvement in source water quality.

The variability in performance was largely influenced by the soil profile beneath the basins. Spatially distinct zones of higher infiltration and laterally gradational changes in infiltration were detected using geophysical methods and recharge water temperature as a tracer. Factors affecting the spatial variations were the chemistry and mineralogy of the SAT basin soils, type and quantity of carbon present and the interrelationship with algae at the basin floor which contributed to clogging both directly and indirectly through calcite precipitation.

Groundwater quality

Groundwater on site and down-gradient from the Alice Springs SAT scheme was influenced by the recharge operation. Chloride and electrical conductivity indicated freshening of the groundwater, with EC reaching that of the fresher source water at around 1700 $\mu\text{S}/\text{cm}$ (~1000 mg/L TDS). Nitrate concentrations in groundwater were variable especially in the immediate vicinity of the basins, but did indicate an increase in response to recharge with breakthrough being detected at the 1000 m down-gradient well. Since the WR{ upgrade, nitrate in SAT source water has declined, groundwater nitrate concentrations has declined at the SAT site and this appears also to be conveyed on to 200 m down-gradient. There was no evidence of denitrification nor decline in DOC beneath the basins largely due to the recalcitrant nature of the organic material following wastewater treatment. Stable isotopes of water have been shown to be effective tracers in tracing the movement of the recharge plume.

It is recommended that groundwater quality is assessed against water quality targets for beneficial use. Freshening may enhance the opportunity to use groundwater down-stream of the SAT scheme.

Microbial communities

Microorganisms with potential for denitrification and anammox were detected throughout the soil profile down to 1.5 m depth in Basins A and E (Kaksonen *et al.* 2015). As the anammox reaction does not require organic carbon, the removal of nitrogen in the subsurface is not entirely dependent on the availability of labile organic carbon, which is low after DAFF treatment.

A large number of bacterial families were detected in the top layer and depth profiles of the infiltration basins with DNA sequencing. These included families harbouring aerobic and anaerobic bacteria, and chemoorganotrophs, chemolithotrophs and phototrophs. A number of the detected bacterial families can contribute to the biogeochemical cycling of nitrogen by oxidising ammonia, reducing nitrate or

nitrite or fixing nitrogen. Members of some families are common in human and animal digestive tracts and some contain pathogenic species. The most abundant bacterial families identified in three of the basins can reduce nitrate (e.g. *Pseudomonaceae*, *Rhodocyclaceae*) and harbour pathogenic species (e.g. *Pseudomonaceae*). Deeper in the soil profiles (at 10-50 cm and 90-130 cm depths) the most abundant bacterial families were *Oxalobacteraceae*, *Comamonadaceae* and *Nitrospiraceae*. Some members of *Oxalobacteraceae* family can fix nitrogen, some members of *Comamonadaceae* reduce nitrate and some members of *Nitrospiraceae* family can oxidize nitrite. Some members of the *Oxalobacteraceae*, *Comamonadaceae* families are pathogenic (Kaksonen *et al.* 2015).

The archaeal families in the soil samples obtained from the top layer of the Alice Springs MAR site were dominated by methanogens at the sites close to the water inlets, whereas the sites further away from the inlets were dominated by ammonia-oxidising archaea. Ammonia oxidising and methanogenic families were also dominant in the depth profiles at 10-50 cm and 90-130 cm depths of the basins (Kaksonen *et al.* 2015).

The eukaryotic communities in the top clogging layer of the Alice Springs MAR site were heavily dominated by algae. Other abundant families in the top layer were worms, fruit flies and protists. The most abundant families in the depth profiles were algae, plants, with also large populations of fungi, protists, worms and oomycetes (Kaksonen *et al.* 2015).

Recommendations

1. Develop a protocol for basin construction and maintenance that will not result in compaction of the basin floor and negatively impact on hydraulic performance. This protocol should address the management of vegetation in the basins. While vegetation can enhance infiltration through soil structure improvement, vegetation was observed to act as a mulch which prevented adequate drying of the basin surface.
2. Ensure drying times are adequate to allow desiccation of the clogging layer under the range of climatic conditions and vegetation growth experienced. Preferably this would be based on judgement of an acceptable bed surface prior to filling. However, practically this may require setting routine drying intervals, such as 10 days in summer and 20 days in winter. It is recommended that the minimum drying period is five days. Ongoing analysis of hydraulic performance would allow a critical limit for infiltration rate (e.g. 200 mm/d) or a percentage decline in infiltration rate to be used to trigger a change in operational regime such as a longer drying interval.
3. Maintain the maximum length of the filling period without breaching the seven day limit for standing water as an increased wetting period will assist with obtaining anoxic conditions needed for nitrogen reduction while also maximising the use of the recharge basins.
4. Evaluate the hydraulic and water quality impacts of the SAT operation, which has recharged over 2.6 GL recycled water, against the impacts predicted in the pre-commissioning investigations to ensure the scheme is adequately managed. This evaluation would encompass a review of the current monitoring programs.
5. Compare the down-gradient groundwater quality to water quality targets for a range of potential beneficial uses to demonstrate the benefit of the SAT operation and encourage recovery of groundwater for subsequent use.
6. If additional nitrogen removal is deemed necessary, undertake an experimental program to assess the feasibility of adding biodegradable dissolved organic carbon to the source water for recharge.

References

- Abraham, W.-R., Rohde, M. and Bennisar, A. (2014). The Family *Caulobacteraceae*. In 'The Prokaryotes: Alphaproteobacteria and Betaproteobacteria'. (Eds E. Rosenberg, E. DeLong, S. Lory, E. Stackebrandt and F. Thompson) pp. 179-205. (Springer Berlin Heidelberg).
- Baldani J., Rouws L., Cruz L., Olivares F., Schmid M. and Hartmann A. (2014a). The Family *Oxalobacteraceae*. In 'The Prokaryotes: Alphaproteobacteria and Betaproteobacteria'. (Eds E. Rosenberg, E. DeLong, S. Lory, E. Stackebrandt and F. Thompson) pp. 919-974. (Springer Berlin Heidelberg).
- Baldani, J., Videira, S., dos Santos Teixeira, K., Reis, V., de Oliveira, A., Schwab, S., de Souza, E., Pedraza, R., Baldani, V. and Hartmann A (2014b). The Family *Rhodospirillaceae*. In 'The Prokaryotes: Alphaproteobacteria and Betaproteobacteria'. (Eds E. Rosenberg, E. DeLong, S. Lory, E. Stackebrandt and F. Thompson) pp. 533-618. (Springer Berlin Heidelberg).
- Bastian, L.V. (1996). Residual soil mineralogy and dune subdivision, Swan Coastal Plain, Western Australia. *Australian Journal of Earth Sciences* 43, 31-44.
- Bekele, E., Toze, S., Patterson, B., Devine, B., Higginson, S., Fegg, W. and Vanderzalm, J. (2009). Chapter 1 - Design and operation of infiltration galleries and water quality changes. In: Determining requirements for managed aquifer recharge in Western Australia. CSIRO: Water for a Healthy Country National Research Flagship Report.
- Bekele, E., Toze, S., Patterson, B., Fegg, W., Shackleton, M., and Higginson, S. (2013). Evaluating two infiltration gallery designs for managed aquifer recharge using secondary treated wastewater. *Journal of Environmental Management* 117, 115-120.
- Bekele, E., Toze, S., Patterson, B. and Higginson, S. (2011). Managed aquifer recharge of treated wastewater: Water quality changes resulting from infiltration through the vadose zone. *Water Research* 45, 5764-5772.
- Bouwer, H., Rice, R. C. and Escarcega, E. D. (1974). High-Rate Land Treatment I: Infiltration and Hydraulic Aspects of the Flushing Meadows Project. *Water Pollution Control Federation* 46(5), 834-843.
- Bouwer, H., Rice, R. C., Lance, J. C. and Gilbert, R. G. (1980). Rapid-infiltration research at Flushing Meadows Project, Arizona. *Water Pollution Control Federation* 52(10), 2457-2470.
- Breton, M. (2009). Alice Springs Soil Aquifer Treatment; Operational review and hydraulic performance. Master of Hydrogeology and Groundwater Management Thesis, University of Technology, Sydney.
- Brearley, J. (2010). Report on Recycled Effluent Filter Trials – Subiaco WWTP August 30, 31 and 1 September 2010. Water Corporation report. 11pp.
- Cresswell, H. (2002). The soil water characteristics, Chapter 4. In: Soil physical measurement and interpretation for land evaluation. McKenzie, N., Coughlan, K. and H. Cresswell (Eds). Australian Soil and Land Survey Handbook Series, CSIRO Publishing, p. 59-84.
- Daims, H. (2014), The Family *Nitrospiraceae*. In 'The Prokaryotes: Other Major Lineages of Bacteria and the Archaea'. (Eds E. Rosenberg, E. DeLong, S. Lory, E. Stackebrandt and F. Thompson) pp. 733-749. (Springer Berlin Heidelberg).
- DER (2014). 'Subiaco Wastewater Treatment Plant Licence - Environmental Protection Act 1986 (Licence Number: L4726/1991/15).' Department of Environment Regulation, Perth, Western Australia. (<http://www.der.wa.gov.au/our-work/licences-and-works-approvals/current-licences>).
- Dillon, P., Pavelic, P., Page, D., Beringen, H. and Ward, J. 2009. Managed aquifer recharge: An introduction. Waterlines Report Series No. 13, National Water Commission, Canberra, February 2009.

- Fox, P. *et al.* (2001). An investigation of soil aquifer treatment for sustainable water reuse. AWWA Research Foundation and American Water Works Association.
- Gates, W., Janik, L., Pavelic, P., Dillon, P., and Barry, K. (2009). Characterisation of the physical and geochemical properties and infrared spectra of five soil cores at the AZRI site near Alice Springs, Northern Territory. CSIRO Water for a Healthy Country Report. <http://www.clw.csiro.au/publications/waterforahealthycountry/2009/wfhc-characterisation-AZRI-site.pdf>
- GHD (2011). Report for Perry Lakes Managed Aquifer Recharge Project, Concept Design of Proposed Infiltration Galleries, Report for the Town of Cambridge.
- Green and Blough (1994). Optical-absorption and fluorescence properties of chromophoric dissolved organic-matter in natural-waters. *Limnology and Oceanography* 39, 1903-1916.
- Gunatunge, S. (2014). Natural heat as a tracer to quantify water infiltration for managed aquifer recharge. Honour thesis Bachelor of Civil Engineering, The University of New South Wales.
- Henderson, R.K., Baker, A., Murphy, K.R., Hambly, A., Stuetz, R.M., Khan, S.J. (2009). Fluorescence as a potential monitoring tool for recycled water systems: A review. *Water Research* 43 (4):863-881. doi:10.1016/j.watres.2008.11.027.
- Hood, E., Fellman, J., Edwards, R.T. (2007). Salmon influences on dissolved organic matter in a coastal temperate brown-water stream: An application of fluorescence spectroscopy. *Limnology and Oceanography* 52 (4):1580-1587. doi:10.4319/lo.2007.52.4.1580.
- Hudson, N., Baker, A. and Reynolds, D. (2007). Fluorescence analysis of dissolved organic matter in natural, waste and polluted waters - A review. *River Res. Appl.* 23 (6):631-649. doi:10.1002/rra.1005.
- Jacups, S., Kurucz, N., Whitters, R. and Whelan, P. (2011). Habitat modification for mosquito control in the Ilparpa Swamp, Northern Territory, Australia. *Journal of Vector Ecology*, 36(2):1-8.
- Kaksonen, A.K., Puzon, G.J., Wylie, J., Morgan, M., Walsh, T., Barry, K.E., Donn, M.J., Bekele, E., Vanderzalm, J.L. and Dillon, P.J. (2015). Managed Aquifer Recharge and Recycling Options (MARRO): Microbial aspects. CSIRO: Water for a Healthy Country National Research Flagship Report.
- Knapton, A., Jolly, P., Pavelic, P., Dillon, P., Barry, K., Mucha, M. and Gates, W. (2004). Feasibility of a Pilot 600 ML/yr Soil Aquifer Treatment Plant at the Arid Zone Research Institute. Department of Infrastructure Planning and Environment Technical Report 29/2004.
- Knapton, A. and Lennartz, R. (2005). Alice Springs Water Reuse Scheme Soil Aquifer Treatment Project AZRI Site Investigations. Department of Infrastructure Planning and Environment Technical Report 29/2005.
- Kuever J. (2014). The family *Syntrophobacteraceae*. In 'The Prokaryotes – Deltaproteobacteria and Epsilonproteobacteria'. (Eds E. Rosenberg, E. DeLong, S. Lory, E. Stackebrandt and F. Thompson) pp. 289-299. (Springer Berlin Heidelberg).
- Li, D., Alidina, M., Ouf, M., Sharp, J., Saikaly, P., and Drewes, J. (2013). Microbial community evolution during simulated managed aquifer recharge in response to different biodegradable dissolved organic carbon (BDOC) concentrations. *Water Research* 47(1), 2421-2430.
- Luce, C.H., Tonina, D., Gariglio, F., Applebee, R., 2013. Solutions for the diurnally forced advection–diffusion equation to estimate bulk fluid velocity and diffusivity in streambeds from temperature time series. *Water Resources Research* 49 (1), 488–506.
- McCallum, J.L., Cook, P.J., Berhane, D., Rumpf, C. and McMahon, G.A. (2012) Quantifying groundwater flows to streams using differential flow gaugings and water chemistry. *Journal of Hydrology* 416, 118-132.
- McArthur, W.M and E. Bettenay (1974). Development and distribution of the soils of the Swan Coastal Plain, Western Australia. Soil Publication No. 16, CSIRO, Australia, 55 pp.

- McBride, M.J. (2014). The Family *Flavobacteriaceae*. In 'The Prokaryotes: Other Major Lineages of Bacteria and the Archaea'. (Eds E. Rosenberg, E. DeLong, S. Lory, E. Stackebrandt and F. Thompson) pp. 643-676. (Springer Berlin Heidelberg).
- McFarlane, D., Smith, A., Bekele, E., Simpson, J. and Tapsuwan, S. (2009). Using treated wastewater to save wetlands impacted by climate change and pumping. *Water Science & Technology* 59(2), 213-221.
- McIlroy, S.J. and Nielsen, P.H. (2014). The family *Saprospiraceae*. In 'The Prokaryotes: Other Major Lineages of Bacteria and the Archaea'. (Eds E. Rosenberg, E. DeLong, S. Lory, E. Stackebrandt and F. Thompson) pp. 863-889. (Springer Berlin Heidelberg).
- Mualem, Y. (1976). A new model for predicting the hydraulic conductivity of unsaturated porous media. *Water Resources Research* 12(3), 513-522.
- McDonald, R.C., Isbell, R.F., Speight, J.G., Walker, J. and Hopkins, M.S. (1990). Australian soil and land survey field handbook. CSIRO.
- McKnight DM, Boyer EW, Westerhoff PK, Doran PT, Kulbe T, Andersen DT (2001). Spectrofluorometric characterization of dissolved organic matter for indication of precursor organic material and aromaticity. *Limnology and Oceanography* 46 (1):38-48.
- Miotlinski, K., Barry, K, Dillon, P. and Breton, M. (2010). Alice Springs Soil Aquifer Treatment Project – Hydrological and Water Quality Monitoring 2008-2009 Report. Water for a Healthy Country Flagship Report, May 2010. <http://www.clw.csiro.au/publications/waterforahealthycountry/2010/wfhc-Alice-Springs-SAT-monitoring.pdf>
- National Water Commission. (2014). National performance report 2012-13: urban water utilities. NWC, Canberra.
- NETAFIM™ (n.d.) Manual disc filters technical [Internet], NETAFIM USA <http://www.netafimusa.com/landscape/products/disc-filters-tech>, accessed January 2014.
- NRMMC–EPHC–AHMC (2006). Australian Guidelines for Water Recycling: Managing Health and Environmental Risks (Phase 1). Natural Resources Ministerial Management Council, Environment Protection and Heritage Council and Australian Health Ministers' Conference, Canberra.
- Oren, A. (2014) The Family *Rhodocyclaceae*. In 'The Prokaryotes: Alphaproteobacteria and Betaproteobacteria'. (Eds E. Rosenberg, E. DeLong, S. Lory, E. Stackebrandt and F. Thompson) pp. 975-998. (Springer Berlin Heidelberg).
- Oren, A., Xu, X.-W. (2014). The Family *Hyphomicrobiaceae*. In 'The Prokaryotes: Alphaproteobacteria and Betaproteobacteria'. (Eds E. Rosenberg, E. DeLong, S. Lory, E. Stackebrandt and F. Thompson) pp. 247-281. (Springer Berlin Heidelberg).
- Page, D.W., van Leeuwen, J.A., Spark, K.M., Drikas, M. and Mulcahy, D.E., (2002). Effect of alum treatment on the trihalomethane formation and bacterial regrowth potentials of natural and synthetic waters, *Water Research* 36, 19, 4884-4892.
- Page, D.W., van Leeuwen, J.A., Spark, K.M. and Mulcahy, D.E. (2001). Tracing terrestrial compounds leaching from two reservoir catchments as input to dissolved organic matter (DOM). *J. Mar. Freshwater Res.* 52(2), 223-233.
- Parlanti, E., Worz, K., Geoffroy, L. and Lamotte, M. (2000). Dissolved organic matter fluorescence spectroscopy as a tool to estimate biological activity in a coastal zone submitted to anthropogenic inputs. *Org. Geochem.* 31 (12):1765-1781.
- Parsons, S., Dillon, P., Irvine, E., Holland, G. and Kaufman, C. (2012). Progress in managed aquifer recharge in Australia. Waterlines Report Series No. 73, National Water Commission, Canberra, March 2012.

- Pavelic, P., Dillon, P.J., Mucha, M., Nakai, T., Barry, K.E. and Bestland, E. (2011). Laboratory assessment of factors affecting soil clogging of soil aquifer treatment systems. *Water Research* 45, 3153-3163.
- Pérez-Paricio, A. (2000). Integrated modelling of clogging processes in artificial groundwater recharge. Ph.D. Thesis, Technical University of Catalonia (UPC).
- Petrone, K.C., Fellman, J.B., Hood, E., Donn, M.J., Grierson, P.F. (2011). The origin and function of dissolved organic matter in agro-urban coastal streams. *Journal of Geophysical Research-Biogeosciences* 116:G01028. doi:10.1029/2010jg001537.
- Power and Water Corporation (2013). Alice Springs Waste Stabilisation Ponds Asset Summary (January 2013). D2012/15902.
- Rümmler, J., Bekele, E. and Toze, S. (2005). Preliminary hydrogeological characterisation for proposed covered infiltration galleries at CSIRO Laboratory, Floreat, Western Australia. CSIRO: Water for a Healthy Country National Research Flagship, Canberra.
- Salama, R. B., Silberstein, R. and Pollock, D. (2005). Soils characteristics of the Bassendean and Spearwood sands of the Gngangara Mound (Western Australia) and their controls on recharge, water level patterns and solutes of the superficial aquifer. *Water Air and Soil Pollution: Focus* 5, 3-26.
- Šejna, M., Šimůnek, J., and R. van Genuchten (2013). HYDRUS software version 2.02.0720. Released 31/8/2013. Downloaded from www.hydrus3d.com.
- Silberstein, R., Barr, A., Hodgson, G., Pollock, D., Salama, R. and Hatton, T. (2009). A vertical flux model for the Perth groundwater region. Department of Water, Hydrogeological record series no. HG33, Perth, Western Australia.
- Šimůnek, J., M. Th van Genuchten and M. Šejna (2011). The Hydrus software package for simulating the two- and three-dimensional movement of water, heat, and multiple solutes in variably-saturated porous media. Technical Manual, Version 2.0, PC Progress, Prague, Czech Republic, 258pp.
- Smith, A. J., Massuel, S. and Pollock, D. W. (2011). Geohydrology of the Tamala Limestone Formation in the Perth region: Origin and role of secondary porosity. CSIRO: Water for a Healthy Country National Research Flagship. 63 pp.
- Tapsell, P., Newsome, D. and Bastian, L.(2003). Origin of yellow sand from Tamala Limestone on the Swan Coastal Plain, Western Australia. *Australian Journal of Earth Sciences* 50, 331-342.
- Thomas, B. and Bennett M. (2010). \$2.0m to help fill drying lakes. *West Australian*, 27/10/2010.
- Vanderzalm, J. Tapsuwan, S., Pickering, P., Arnold, N., Bekele, E., Barry, K., Donn, M., McFarlane, D. and Dillon, P. 2015, Managed Aquifer Recharge and Recycling Options (MARRO): Case study compilation, Australian Water Recycling Centre of Excellence.
- van Genuchten, M. Th. (1980). A closed-form equation for predicting the hydraulic conductivity of unsaturated soils. *Soil Science Society of America Journal*. 44, 892-898.
- van Genuchten, M. Th, Leij, F.J., and S.R. Yates (1991). The RETC code for quantifying the hydraulic functions of unsaturated soils. Version 1.0. EPA Report 600/2-91/065, U.S. Salinity Laboratory, USDA-ARS, Riverside, California.
- van Genuchten, M. Th, Šimůnek, J., Leij, F.J., and M. Šejna (2009). RETC software version 6.02 released 13/02/2009. Code for quantifying the hydraulic functions of unsaturated soils. Downloaded September 2014 from www.hydrus3d.com
- Vermooten, S., (2002). Impact of land use on groundwater resources of the Gngangara mound. Internal Report. CSIRO Land and Water.
- Water Corporation (2009). Subiaco Wastewater Treatment Plant. Water Corporation, Perth.

Water Corporation (2013). Esperance Wastewater Services Upgrade [Internet], Water Corporation <http://www.watercorporation.com.au/water-supply-and-services/ongoing-works/esperance-wastewater-services-upgrade>, accessed January 2014.

Wang X.H., Hu M., Xia Y., Wen X.H., Ding K. (2012). Pyrosequencing Analysis of Bacterial Diversity in 14 Wastewater Treatment Systems in China. *Applied and Environmental Microbiology* 78, 7042-7047.

Willems, A. (2014). The family *Comamonadaceae*. In 'The Prokaryotes: Alphaproteobacteria and Betaproteobacteria'. (Eds E. Rosenberg, E. DeLong, S. Lory, E. Stackebrandt and F. Thompson) pp. 777-851. (Springer Berlin Heidelberg).

Wu, D.L., Shen, Y.H., Ding, A.Q., Mahmood, Q., Liu, S., Tu, Q.P. (2013). Effects of nanoscale zero-valent iron particles on biological nitrogen and phosphorus removal and microorganisms in activated sludge. *Journal of Hazardous Materials* 262, 649-655.

Zhang, T., Shao, M.-F. and Ye, L. (2012). 454 Pyrosequencing reveals bacterial diversity of activated sludge from 14 sewage treatment plants. *ISME Journal* 6, 1137-1147.

Appendix 1 Floreat experimental plan as executed

Title: Impediments to the adoption of infiltration galleries for MAR with recycled water: field investigation of measures to minimize clogging and aid nutrient removal

Elise Bekele, Michael Donn, Peter Dillon and Don McFarlane

Objectives

A new infiltration gallery at the CSIRO Floreat Laboratories site will be established to improve our understanding of factors that may have limited the adoption of infiltration galleries for MAR in sandy deposits with recycled water in the past. These factors include (i) the impact of clogging on the hydraulic performance, (ii) negligible removal of nutrients, and (iii) operational aspects that limit the long-term operation of the galleries (e.g. the ingress of plant roots within the galleries). The field-based study will yield insight into spatial variations in infiltration zone conditions, in particular the degree of saturation and the redox condition achieved and clogging potential from the removal of suspended solids, biomat formation and mineralogical changes that may not be apparent at the scale of 1-D column studies.

The study will be undertaken in conjunction with laboratory experiments and HYDRUS modelling to achieve the following objectives:

1. use HYDRUS software and information on biofilm development obtained through the initial column experiments to develop a preliminary model of infiltration below the gallery to inform the experimental design;
2. refine the HYDRUS model with experimental data collected during the study to improve its predictive capability;
3. identify changes in the unsaturated/saturated profile below the gallery during the course of monitoring soil moisture conditions whilst testing different infiltration rates; this includes determining how long it takes for saturated conditions to be established, and determining temporal changes in the proportion of water infiltrating vertically and laterally;
4. compare with the column study (1-D) to identify differences in hydraulic performance that may assist with evaluating the benefits and limitations of relying on columns studies for system design;
5. determine the attenuation of nutrients (N, P) and dissolved organic carbon in relation to saturation and redox conditions by monitoring the influent recycled water before it enters the galleries, in groundwater sampled up-gradient and down-gradient from the galleries, and changes to soil characteristics;
6. evaluate the potential for nitrogen removal via denitrification to be enhanced through supplemental carbon, initially undertaken as a pilot laboratory study;
7. determine the physical, chemical and microbiological composition of samples collected from areas where clogging is identified.

Background

Previous experience from operating infiltration galleries was obtained during the Floreat Infiltration Galleries trial, which operated for 39 months, beginning in October 2005 (Bekele *et al.* 2011, 2013).

Hydraulic Performance

- recycled water was delivered to a central discharge chamber and flowed laterally out through short (<1 m) sections of PVC pipe on either side into Atlantis® Flo-tank modules;
- The total suspended solids level of recycled water supplied to the galleries was quite variable (mean of 7.5 mg/L; standard deviation of 7.0 mg/L; Bekele *et al.* 2009);

- water level measurements were not made at different locations within the gallery, hence recycled water may not have been evenly distributed throughout the gallery as it infiltrated;
- nominally 1 m/d of infiltration through the base of the gallery was maintained over a period of up to 2-3 years;
- testing at a higher rate (between 2.9 and 3.8 m/d; 3.5 m/d on average) in one of the galleries over a two month period produced rising water levels in the central discharge chamber, indicative of clogging.

Chemistry/Water Quality Transformations

- reductions of 30% for phosphorus and 51% for total organic carbon were achieved by passage of recycled water through up to 10 m of unsaturated thickness at an infiltration rate of 1 m/d;
- aerobic recycled water and aerobic conditions in the vadose zone were not conducive for denitrification (total N in recycled water remained unchanged despite passage through the vadose zone);
- nitrification occurred in the vadose zone with nitrate produced by the oxidation of ammonia and organic nitrogen.

CSIRO Modelling Study for Perry Lakes

- an alignment of galleries was modelled, covering an infiltration area of 1,300 m²;
- preliminary steady-state modelling by CSIRO suggested an infiltration rate of 4 m/d would raise groundwater levels under Perry Lakes by 1 m compared with current levels (McFarlane et al 2009);
- the steady-state modelling also predicted that an infiltration rate of 5 m/d would produce a watertable rise under Perry lakes of the same order of magnitude, and would raise groundwater levels under Herdsman Lake and Mabel Talbot Reserve located 1.5 to 2 km up-gradient, respectively from the proposed galleries at Perry Lakes.

GHD Modelling Study for Perry Lakes

- GHD recommended 1.2 m/d of infiltration through the base of the galleries covering a total infiltration area of 2,500 m² based on transient groundwater flow modelling;
- this would, “restore the periodic presence of water in both West and East Lake with limited discharge of infiltrated treated wastewater into the southern parts of both lakes” (GHD 2011);
- GHD assumed that the infiltration galleries would have an operational efficiency of 80% to account for a number of individual galleries being rested to enhance aerobic conditions (GHD 2011).
- GHD recommended that the scheme have a safety margin of 30%, hence a design flow rate of 5 ML/d, equivalent to an infiltration rate of 2 m/d through the base of the gallery.

Water Corporation Testing of Amiad Filters for Perry Lakes

- Filter trials, utilising AMIAD supplied equipment, were conducted on Subiaco STP final effluent over 3 days in August and September 2010 (Brearley 2010; GHD 2011);

- Final effluent total suspended solids (TSS) over the trial period never exceeded 20 mg/L (Brearley 2010);
- The testing indicated that two-stage pressure media filtration using the media/NEX sand filter combination could guarantee an output TSS of 5 m/L based on a final effluent TSS of no more than 20 mg/L entering the filter. If such a filtration combination was utilised, final effluent turbidity would need to be automatically monitored to shut down the filter plant for periods when TSS in excess of 20 mg/L occurred (Brearley 2010).

Methods/Materials

Assumptions

- 1) Power for treating and pumping recycled water to the site is to be the responsibility of the Water Corporation at no cost to CSIRO.
- 2) Approval from CSIRO Corporate property to modify the paddock is forthcoming when requested.
- 3) DEC/DOW approvals are forthcoming when requested and may require supplying an environmental risk assessment.
- 4) It is unlikely that recovery of recycled water from the aquifer will be required given the adjoining property and previous experience with the risk assessment for Perry Lakes; hence there is no need to purchase and operate an extraction pump.

Unsaturated Flow Modelling

- HYDRUS software will be used to develop a preliminary, two-dimensional model of the Floreat infiltration gallery based on soil moisture characteristics data obtained from the site;
- 2-D modelling will aid in estimating saturated conditions surrounding the gallery to assist with the placement of monitoring equipment;
- clogging rates obtained from the laboratory column study will be used to develop a 2-D model that will be used to analyse the hydraulic performance during operation of the infiltration galleries.

Gallery Site Design

As depicted in Figure 74, a linear configuration of Atlantis Flo-Tank® modules will be used to minimize the proportion of horizontal flow parallel to the ends of the gallery. An external contractor will be consulted regarding rejuvenation of the telemetered skid at CSIRO and the installation of the slotted pipe network to evenly distribute recycled water to the tank modules. The design intended for the new gallery is different from the original FIG operation, which had a 50 m² infiltrative surface area and operated over a three year period. The new gallery will operate over a shorter time frame of several months with a total infiltrative surface area of 1.7 m². It also differs in that the focus is on small scale spatial variability in infiltration within the gallery and will involve evaluating higher infiltration rates with a higher quality of source water quality than the original FIG operation.

- 6 Atlantis Flo-Tank® modules with a total infiltrative surface area of 1.7 m²
- dimensions of each tank are L=685 mm; H =450 mm; W=408 mm
- gallery buried to a depth of 500 mm below ground surface (Figure 75)
- Geofabric material to prevent sand from entering the top of the modules and a portion of the sides (Figure 75)

- A network of slotted pipes that will supply recycled water at an evenly distributed rate to the 6 Atlantis Flo-Tank® modules.
- Two groundwater bores constructed of 50 mm-diameter PVC will be installed for monitoring water quality and water levels. One bore will be positioned approximately 5 m east of the gallery for sampling groundwater that is hydraulically up-gradient from the gallery; another bore will be located approximately 2 m west of the gallery for sampling groundwater down-gradient.
- Temporary fencing to prevent sheep from entering the site, which is an existing paddock

Source and Inflow Rates of Recycled Water

The quality of recycled water will be typical of what the Water Corporation would consider for a managed aquifer recharge site. As described earlier, the Water Corporation conducted testing of filters for the Perry Lakes proposal which indicated that a total suspended solids (TSS) content of less than 5 mg/L could be produced using a two-stage pressure media filtration given the feed treated wastewater has a TSS of less than 20 mg/L (Brearley 2010). A TSS of less than 5 mg/L was the design criteria for the proposed filtration system for Perry Lakes (GHD 2011). This will be achieved using unchlorinated recycled water from the Subiaco STP that has passed through media filtration.

The sand filter skid used for the original trials will be renovated and retrofitted to provide the required filtration of unchlorinated recycled water from the Subiaco STP. Whilst the target for TSS is ≤ 5 mg/L, maintaining a low level of TSS will depend on the reliability of pumps to supply the source water and regular maintenance and cleaning of the filtration unit. The system will be designed to minimise faults and downtime, and the Water Corporation will provide advice to CSIRO to ensure the skid is appropriate. The staff at Subiaco Wastewater Treatment Plant (WWTP) will provide the first response in the event of a supply disruption [advised by CSIRO] or a fault message from the skid. The Subiaco STP staff will then advise CSIRO if the fault cannot be corrected or supply cannot be resumed.

There are renovations planned at the Subiaco STP, which may limit the duration of the infiltration experimentation to a period of 5 months. Infiltration will commence in early October 2014, using an infiltration rate of 5 m/d until clogging occurs (Table 18). Infiltration experiments will continue until early March 2014, or earlier if there is repeated clogging leading to potential overflow of recycled water.

Table 18 Inflow rates for supplying recycled water to the Atlantis Flo-Tank® modules calculated based on the surface area of the gallery base and the target infiltration rate.

Atlantis Flo-Tank® module surface area (m ²)	Number of tanks	Nominal infiltration rate (m/d)*	Inflow rate (kilolitre/d)	Comments
0.279	6	2	3.35	Initial rate. If ponding does <u>not</u> occur, then the rate will be increased.
0.279	6	3.5	5.87	Intermediate rate
0.279	6	5	8.38	Recommended by CSIRO steady-state modelling

* This assumes infiltration only through the base of the gallery

Monitoring of Fluxes

The former telemetered skid for controlling the inflow of recycled water will be rejuvenated and used to regulate and monitor the inflow. Although the settings will be adjusted to a specified rate of inflow, a float-switch in the gallery may be required to automatically shut off the inflow if there is potential for overflow (Figure 76). Any changes in inflow will be monitored and these data will be downloaded regularly to a database.

Monitoring of Saturated/Unsaturated Conditions

As described earlier, unsaturated zone flow modelling with HYDRUS 2-D will be used to aid in deciding the placement of equipment for monitoring saturated conditions. A preliminary plan, showing the minimum number of monitoring points and the arrangement of equipment is shown in Figure 77. Refer to Appendix 2 for the final arrangement of monitoring equipment.

- water level probes will be installed at North, Middle and South locations within the gallery;
- soil moisture probes (MP406 probes from ICT) will be positioned at different depths below the base of the gallery. Several sets will be under the gallery and at least another set of probes at different depths will be down-gradient to monitor lateral flow as shown in Figure 77;

Monitoring of Water Quality

Nitrogen and phosphorus are the main nutrients of concern with the infiltration of wastewater. Attenuation may potentially occur within the infiltration zone immediately below the gallery and with passage through the vadose zone. Organic carbon, whilst not recognized as an environmental hazard for water recycling (NRMCC-EPHC-AHMC 2006), is a major factor influencing microbial community structure (Li *et al.* 2013) and may influence potential denitrification rates and thus will be included in the water quality monitoring. To determine whether attenuation is occurring water quality will be monitored at a number of locations, including

- the influent recycled water stream before it enters the gallery;
- the groundwater up-gradient of the gallery to provide background concentrations;
- the groundwater immediately down-gradient of the gallery; and
- potentially leachate from the unsaturated zone beneath the gallery (depending on whether collection is possible).

Samples will be collected from the bores in Table 2. MB1 and MB2 samples will be collected twice weekly, whereas the background bores may be sampled less frequently. The following parameters will be analysed:

- *Physiochemical parameters* – pH, electrical conductivity, turbidity, dissolved oxygen, temperature, redox potential, total suspended solids
- *Nutrients and organic carbon* – dissolved organic carbon, total dissolved N, nitrate-N, ammonium-N, dissolved organic N, total dissolved P, soluble reactive P
- *Major ions* – Ca^{2+} , Mg^{2+} , Na^+ , K^+ , Cl^- , SO_4^{2-} , HCO_3^- , plus Al, Fe and Mn

These parameters will provide a direct measure of nutrient attenuation and a way to trace the recycled water following infiltration.

Destructive Sampling of Gallery Site after Infiltration

Following termination of the infiltration experiments, a more invasive analysis will be conducted. Sediment sampling from the infiltrative surface will commence to identify the potential cause(s) of clogging. The determination will be based on measurements that are similar to those performed on

the columns during destructive sampling. This may also include analysis of the phosphorus sorption occurring within the vadose zone soil profile.

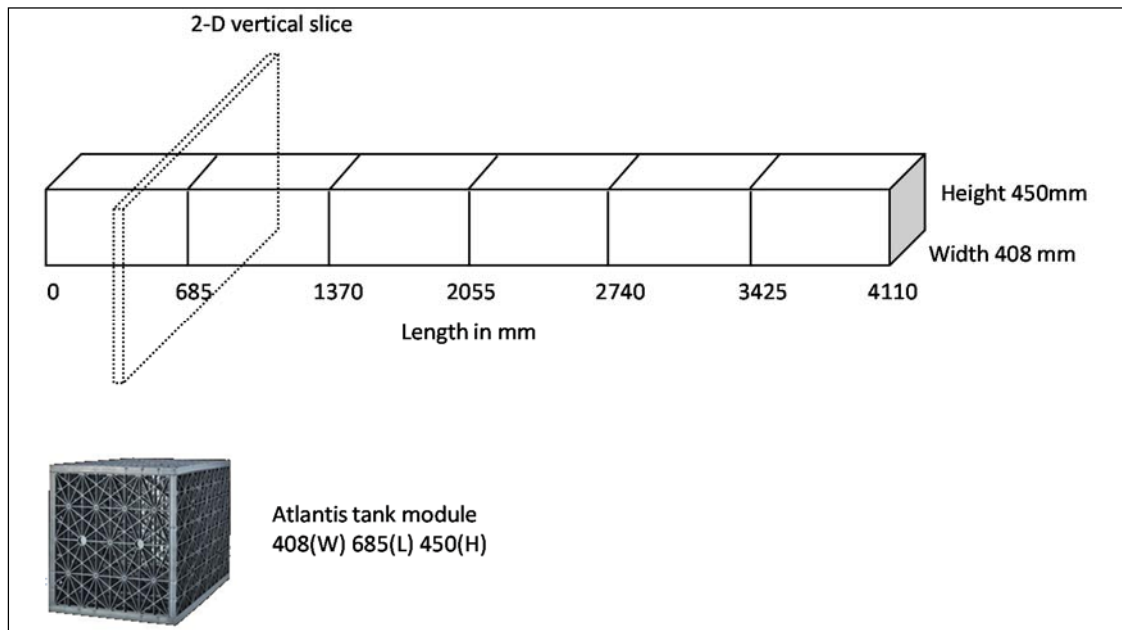


Figure 74 Schematic of proposed installation of six Atlantis Flo-Tank® modules. The dimensions of the linear gallery are approximately 4.0 m by 0.4 m. Vertical slices taken along the long dimension of the gallery will be used for HYDRUS modelling.

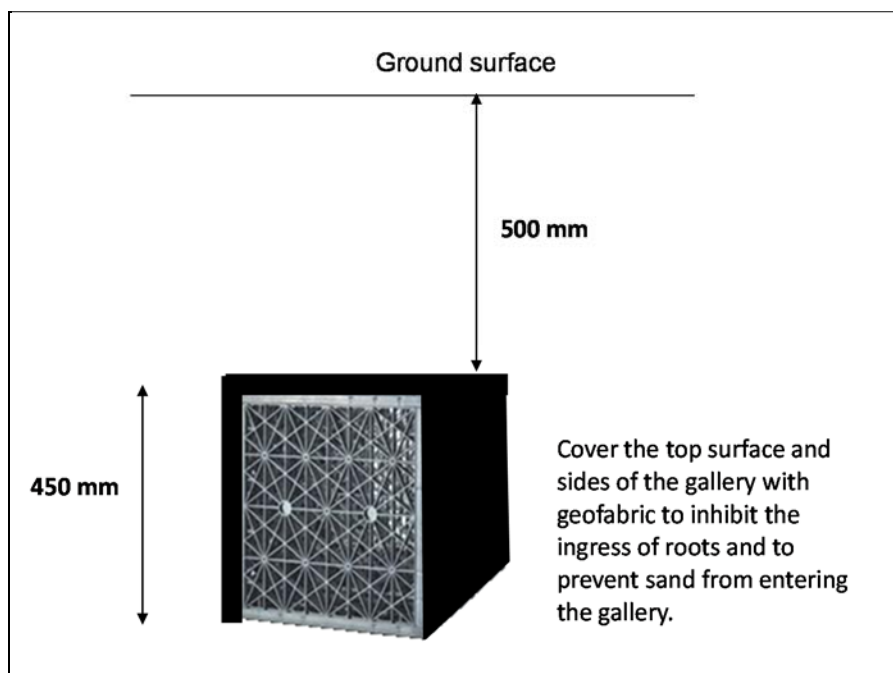


Figure 75 Cross-section view of an Atlantis Flo-Tank® modules below the ground surface depicting the excavation depth and details for the placement of geofabric.

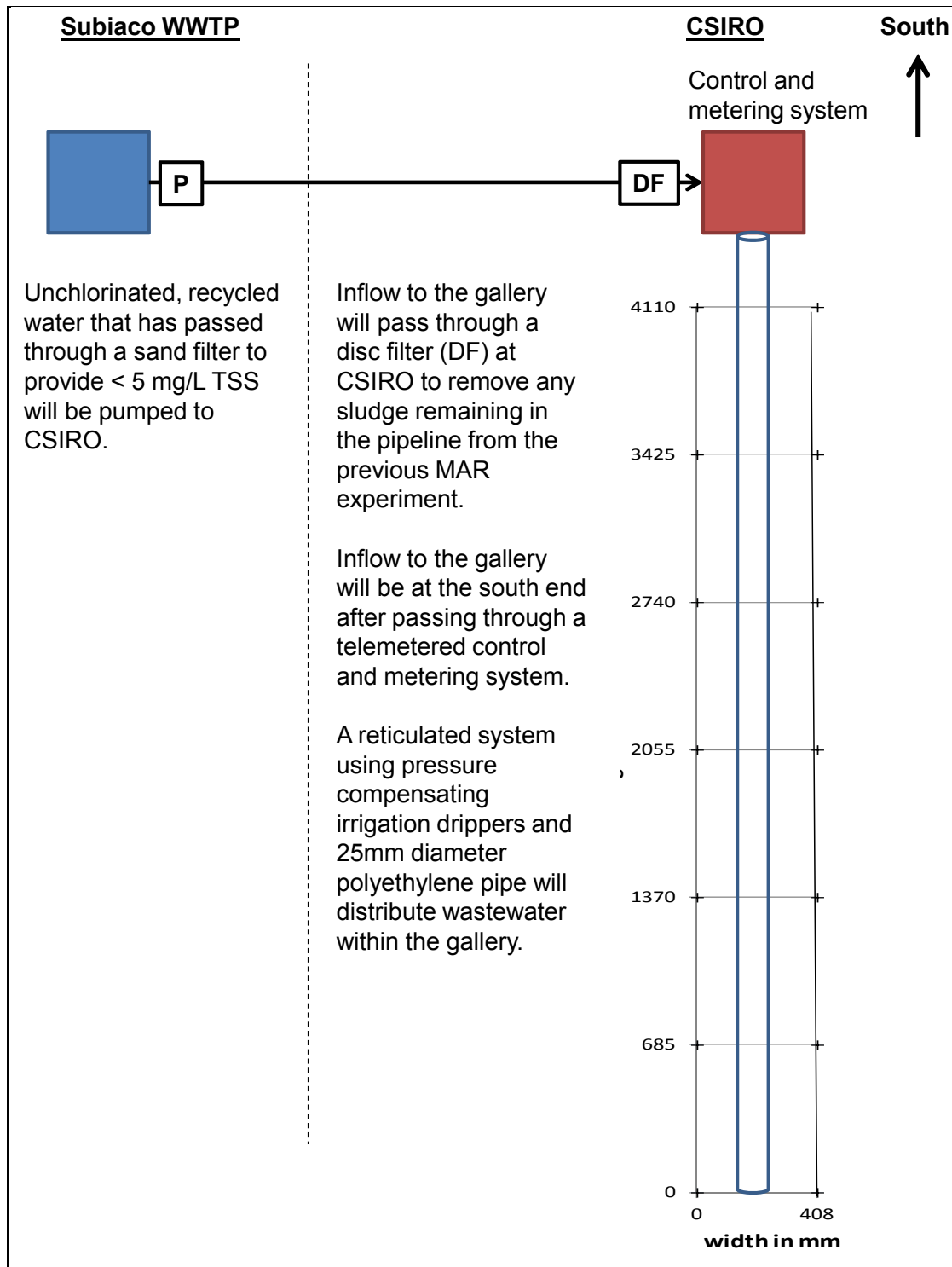


Figure 76 Plan view of the field installation at CSIRO relative and the connection to Subiaco STP.

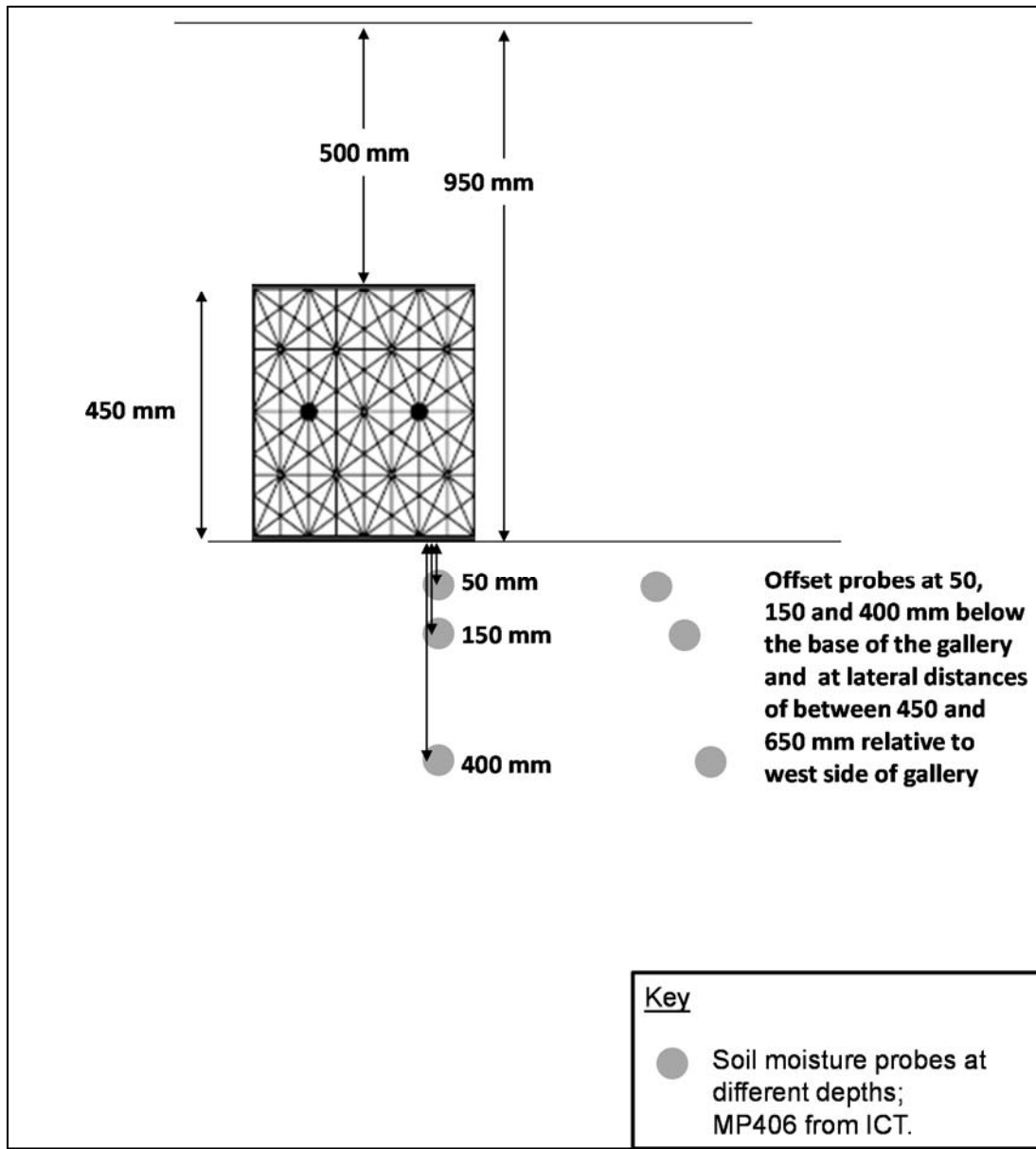


Figure 77 Cross-section view depicting the placement of soil moisture probes relative to the base of the gallery. For the probes directly under the gallery, the lateral distances relative to the edge of the gallery are approximate and varied (~2 to 4 cm) for the North, Middle and South sets of probes and the three depths.

Appendix 2 Floreat MAR site installation and dismantling

This section describes how the Floreat infiltration gallery and monitoring equipment were installed and later dismantled at the close of the experiment. Prior to installing the gallery at the CSIRO site, approval to commence the MAR study was obtained from regulatory agencies, including the Department of Water, Department of Health and the Department of Environmental Conservation/EPA. The experimental plan and clarification of existing underground services was discussed with CSIRO's Corporate Property (CP) and approval was granted to embark on the field project. One of the requirements stated by CP is that the gallery be removed and ground level restored once the project has ended. CSIRO HSE approved documents were submitted for the field work to commence.

Installation of the Floreat MAR site

The services of a contractor (CHS Engineering) were engaged to develop the site in two stages. During Stage 1 (29th to 31st July 2013), CHS pressure tested the pipeline between Subiaco STP and the experimental site at the CSIRO sheep paddock and replaced broken components (e.g. air relief valves) and repaired cracks in the pipeline. During repair of a section of cracked pipe, the contractor observed sand and a sticky sludge within the pipeline. Although CHS performed a thorough flush of the pipeline, there were concerns that if cracks develop during the experiment (e.g. from the weight of heavy vehicles parked above the buried pipeline on the road verge), sand could enter the pipeline. Also noted by CHS was that the sticky sludge remaining in the pipeline from the previous MAR experiment could become dislodged. As these occurrences could lead to blockage of the dripper system for dispersing treated wastewater within the gallery, a small add-on filter was purchased and installed near where the old pipeline enters the field site, but before the connections to new components supplying wastewater to the new gallery. The new filter is an ARKAL disc filter (2" Dual) that requires manual cleaning (fortnightly or more frequently as needed). The disc filter consists of flat, diagonally grooved plastic rings stacked together to form the filter element. As influent wastewater is pumping into the filter and pressure increases, the water compresses the disc rings and the water is then forced to flow through the grooves of the disc rings where debris is trapped (Figure 78). The particular filter recommended for the drippers has a mesh size of 80 and micron rating of 200 μm ; the latter refers to the groove spacing.

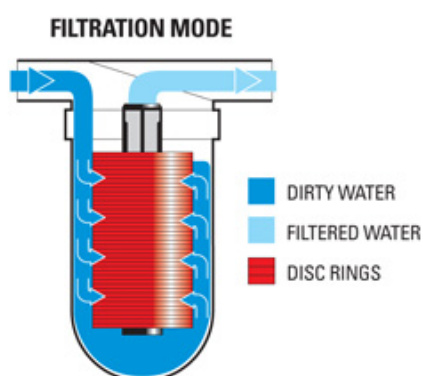


Figure 78 ARKAL manual disc filter showing mode of filtration (Source: NETAFIM™, <http://www.netafimusa.com/landscape/products/disc-filters-tech>).

As significant repairs and modifications to the pre-existing infrastructure were required throughout August 2013, CHS were not able to commence Stage 2 (excavation and installation of the new gallery) until 17th September. During excavation of the trench, the Atlantis Flo-Tank® modules were assembled (6 tank sub-sections end-to-end) and the reticulated system for dispersing treated wastewater was fitted into place (Figure 80). The reticulated system uses Netafim™ pressure

compensating irrigation drippers and 25mm diameter polyethylene pipe. The drippers selected for the study have a nominal flow rate of 8.5 L/hour and working pressure range of 50 - 400 kPa.



Figure 79 Trench excavation for the infiltration gallery (top) and assembly of the reticulated system for dispersing treated wastewater within the Atlantis Flo-Tank® modules (bottom).

Small sections of the Atlantis® modules were cut away to make space for the reticulated system to pass through laterally. Three lengths of poly pipe were used to disperse the wastewater from a 4-way joiner at the inflow (south) end of the gallery (Figure 80) and 42 Netafim™ pressure-compensating drippers were pierced into the pipe at fairly regular intervals (4). The reticulated system within the Atlantis® modules was tested with potable water above-ground before placing the system within the trench.



Figure 80 Close up view of the south end of the gallery, showing the inflow poly pipe connecting to three sections of poly pipe, each approximately 10 cm apart. This photo was taken before the 42 Netafim drippers were inserted and shows the gallery upside down. Three lengths of poly pipe pass laterally through incisions in the partitions within the Atlantis® modules and are terminated at the distal end of the gallery (4m to the north). The pipes were cable-tied to the top panels on the underside of the tanks.

Fourteen drippers were inserted at an average distance of 27 cm apart along each of the 3 pipes. Figure 81 shows the final arrangement of 42 drippers. The number drippers were calculated to provide an application of 5 m/d and spacing designed to spatially distribute the flow over the extent of the gallery base (411 cm x 40.8cm). The bottom panels of the Atlantis® modules were not used in the assembly of the gallery (Figure 80) to allow wastewater to drip directly onto the soil surface within the trench and to enable the development of the biofilm layer (Schmutzdecke) at the soil surface without interference from the plastic tank. This also enables more efficient soil sampling at the conclusion of the experiment.

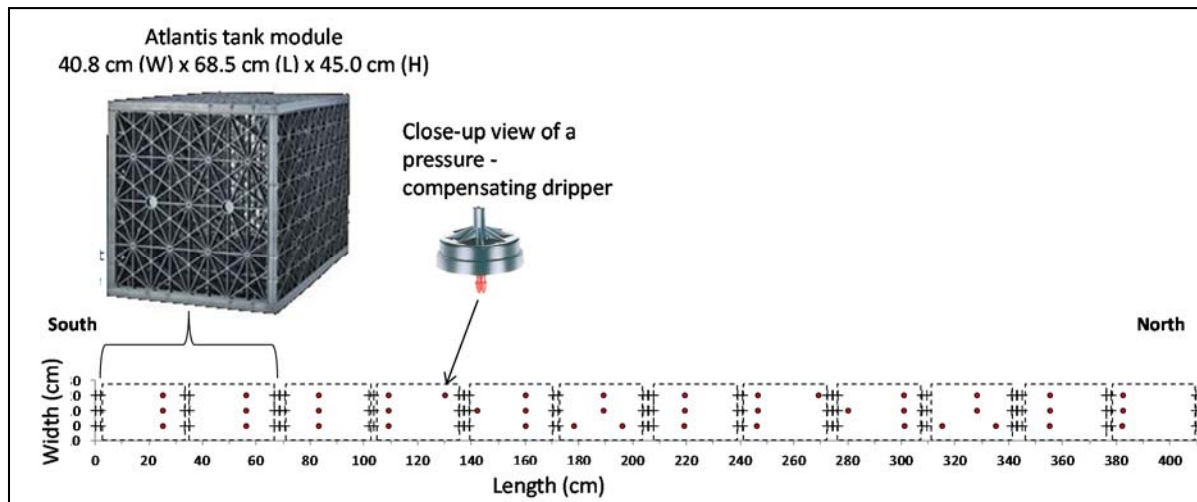


Figure 81 Arrangement of Netafim™ pressure-compensating drippers within the Atlantis Flo-Tank® modules. The image shows the placement of drippers relative to the internal partitions within each of the 6 tanks that were assembled.

Prior to installation of the tanks and other monitoring equipment, 6 soil samples were collected for microbial analysis. These were collected in pairs from the sidewall of the trench and the base level of the gallery, approximately 105 cm below ground (Figure 82).

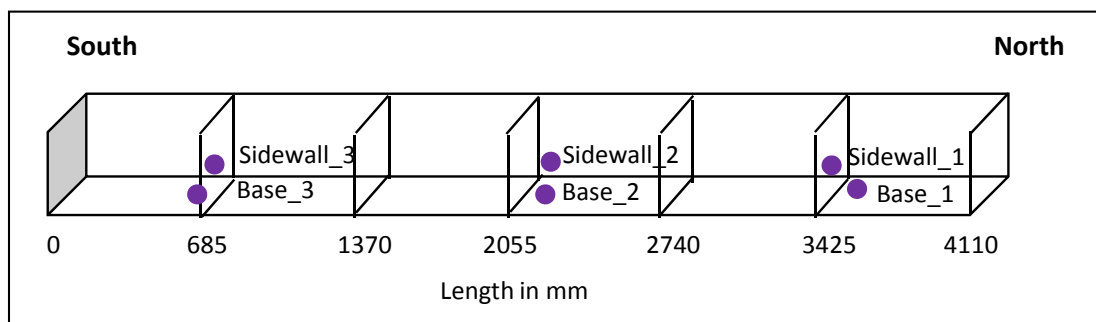


Figure 82 Locations where microbial samples were collected prior to MAR.

To monitor water-levels within the gallery, 50mm diameter PVC pipes were inserted at 4 locations along the gallery. Three of these contain water level loggers (Odyssey capacitance probes) recording at 30 minute intervals. These are referred to as Gall_N, Gall_M and Gall_S (Figure 83). During routine monitoring of the site, water levels are measured with a manual probe inserted into the unlogged access tube.

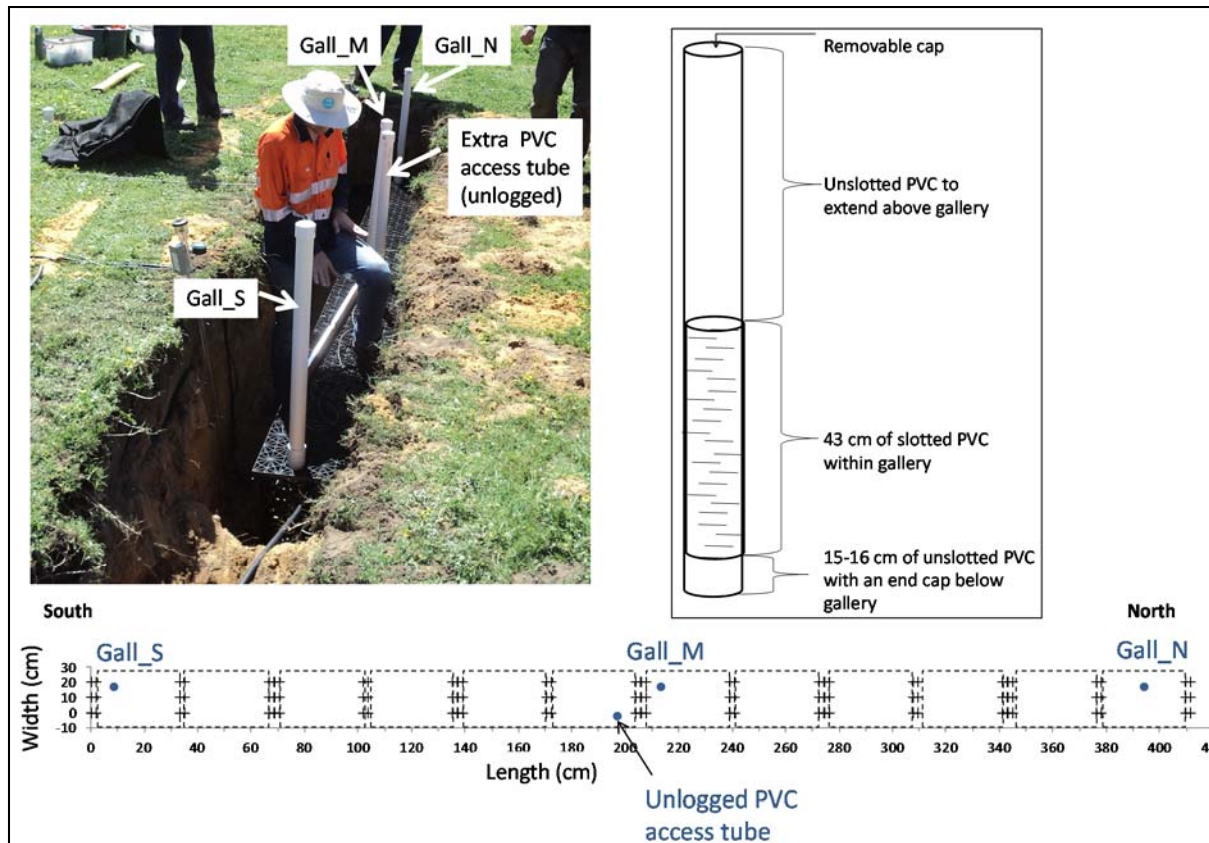


Figure 83 Locations of water level logging within the infiltration gallery. The diagram on the right (not to scale) shows the design of the PVC tubes used to monitor water levels in the gallery. Geofabric (not shown) was used to cover the top and upper few cm of the gallery to lessen the opportunity for roots to grow into the gallery.

Twelve standing wave soil moisture probes (MP406, ICT International) were installed in sets of 3 at depths of 5 cm, 15 cm and 40 cm below the base level of the gallery, which was at approximately 105 cm below ground. Three sets of probes were installed beneath the gallery by lateral insertion from a sidewall along the west side created by trenching deeper than the base level of the gallery (Figure 84 and Figure 85). The last set of 3 probes was installed west of the gallery at distances of approximately 45 cm to 65 cm relative to the west edge of the gallery. These were installed by augering at an angle to each of the desired depths below ground (110 cm, 120 cm and 145 cm below ground surface). The sensors were inserted at the base of the augered hole and backfilled with soil removed during augering. The sensors were connected to a Campbell logger (CR1000) and measurements recorded at 15 minute intervals. Following the installation, logging of soil moisture commenced approximately one week prior to commencing the MAR trial to monitor background conditions.

Tensiometers were borrowed and tested in the lab, but failed to provide reliable results once installed in the ground and were dropped from the monitoring program as the soil moisture probes provided sufficient information.



Figure 84 Michael Donn standing on a spare Atlantis® plate to distribute his weight while installing the soil moisture probes below the intended base level of the gallery. The foot plates indicate the approximate location of the gallery relative to the sensors. He is standing at a depth of 105 cm below ground. Small temporary trenches were used to insert the probes laterally from the sidewall by first augering a hole using a small piece of PVC tubing (shown on the left) and which were then backfilled. Soil moisture probes at 5 cm, 15 cm and 40 cm below base level were installed at slightly offset positions to avoid side-wall collapse.

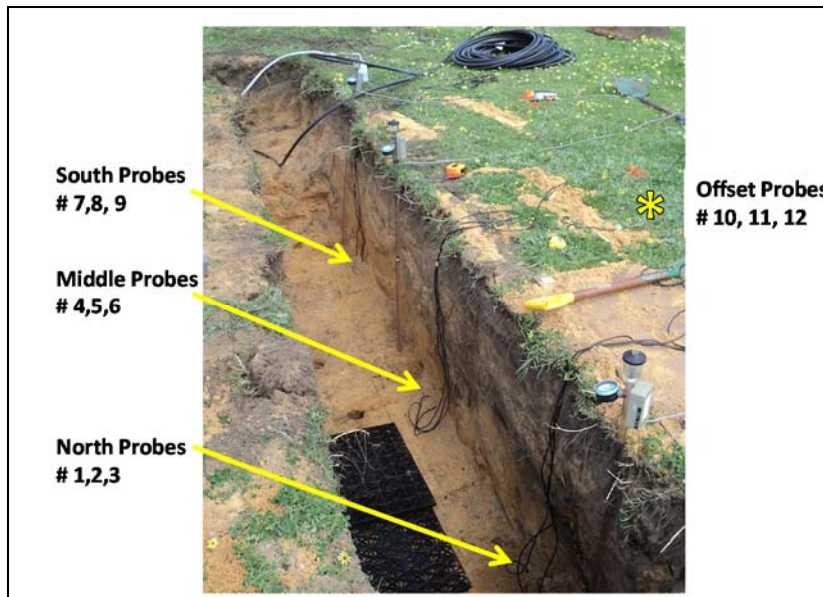


Figure 85 Placement of South, Middle and North soil moisture probes buried below the base level of the gallery with logging cables extending to the ground surface. The cables connect to a Campbell logger in a weather-proof box. Offset Probes # 12, 10 and 11 located 45, 55 and 65 cm, respectively west of the gallery were installed by augering at an angle to depths of 110, 120 and 145 cm, respectively below ground at roughly the position marked in the photo.

During excavation of the main trench for the gallery, charred material was observed and a charred tree branch was removed (Figure 86). It was decided not to relocate the trench as the site was otherwise fairly undisturbed and relatively uniform sand (Figure 87).



Figure 86 Close up view of charred material observed while developing the trench for the infiltration gallery.

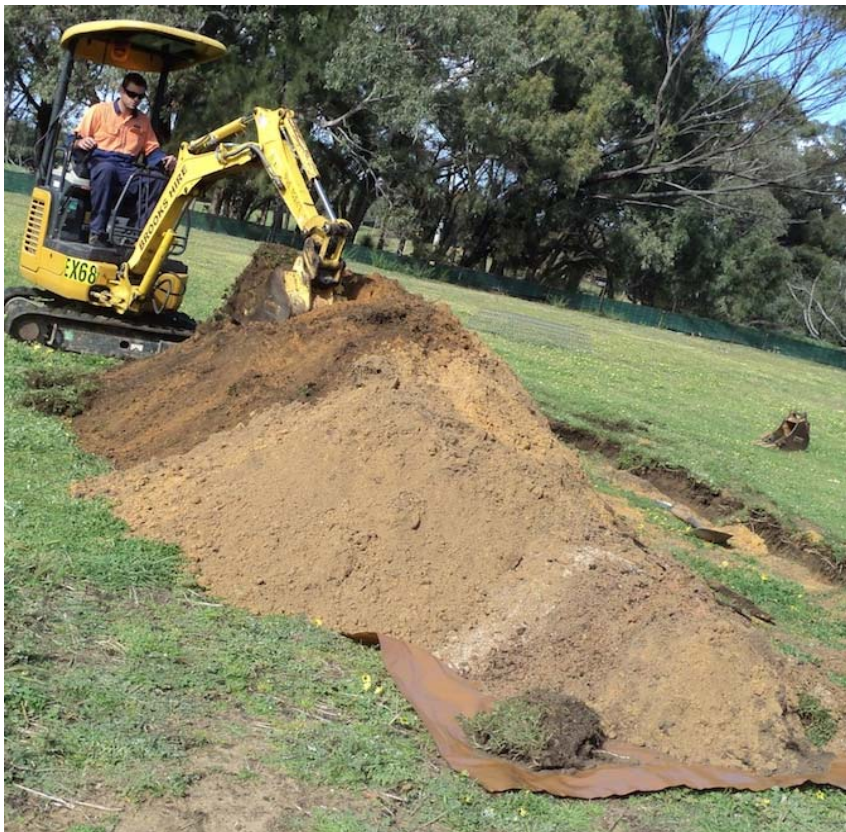


Figure 87 Sand removed from the trench during installation of the infiltration gallery.

Once the Atlantis Flo-Tank® modules were installed in the trench, geofabric was laid over the top and the sides of the tanks with small holes pierced in the fabric to accommodate the PVC water level monitoring tubes. The geofabric extended down the sides of the tanks to prevent sand from entering the gallery. Measurements of the depth to the top of the gallery relative to the ground surface

revealed slight differences (e.g. at the north end (64 cm), at the south end (59.5 cm), in the middle (58.5 cm)). The average depth to the top of the gallery below ground based on several measurements was 60.7 cm. The entire site was then backfilled with the previously excavated sand (Figure 88).

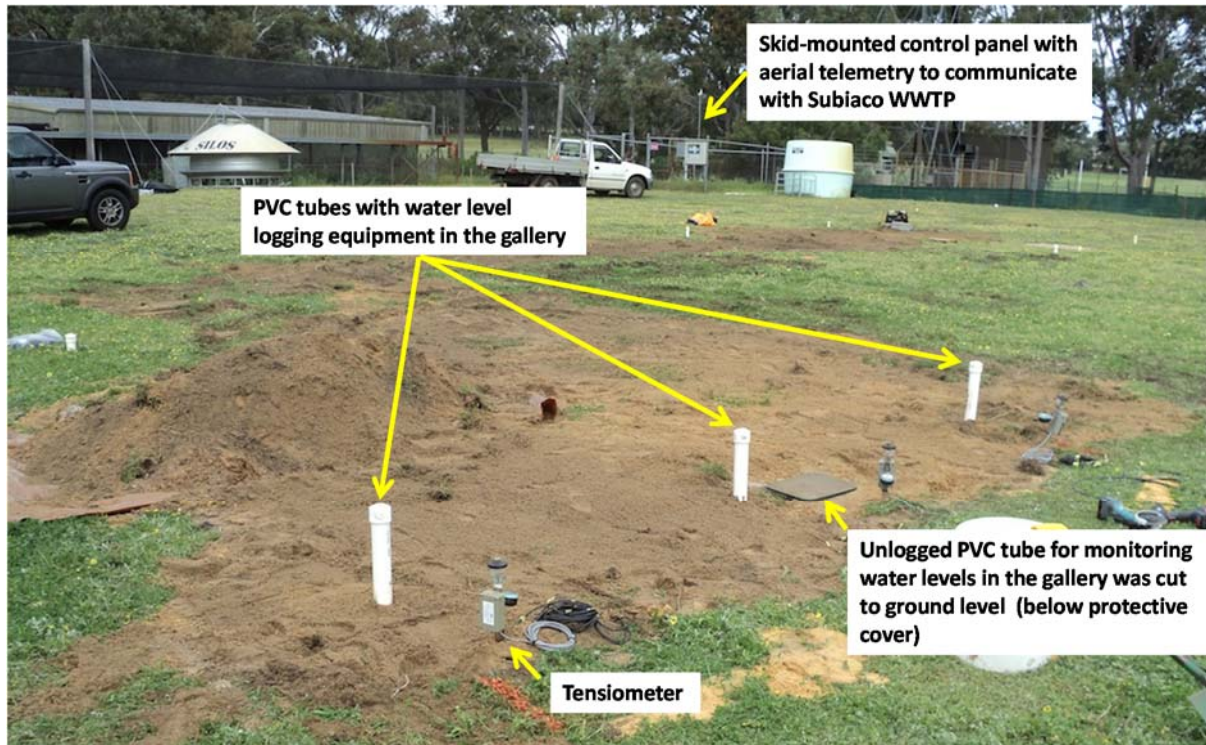


Figure 88 Backfilled site on 17-September 2013, showing the skid-mounted control system that regulates flow to the gallery. The PVC tubes for monitoring water levels are shown in the foreground. The tensiometers failed to provide reliable results once installed and are no longer being monitored. The grass has been allowed to grow back over the surface.

Dismantling of the Floreat MAR site

Dismantling of the Floreat infiltration gallery site was documented on March 11-13th, 2014, referred to as Days 1-3 below. We excavated to the top of the infiltration gallery on the first day and revealed the Atlantis Flo-Tank[®] modules, referred to as Crates below. We confirmed that geofabric had indeed been placed not only on top, but all the way over the sides. There were roots noted in the geofabric, particularly the underside of the geofabric facing into the gallery (Figure 89). The roots extended vertically down into the gallery from the geofabric covering the top of the gallery.



Figure 89 Photo of the excavated surface of the infiltration gallery and a close up of the roots embedded in the geofabric.

Roots were also holding the geofabric at the base. We started at the south end, intending to sacrifice crate 1 to be able to dig and apply dye tracer. We removed the cover on Crate 1 and noticed that one of the drippers was clogged. There was root mat under the gallery. Beneath the drippers that were working, there were indentations and a lack of root mat as the dripping action prevented enhanced growth.



Figure 90 View of crate 1 (numbered consecutively with respect to the south end of the gallery).

Since we did not remove the geofabric from the entire gallery prior stopping inflow and cutting the inflow pipe for better access, it is not known how many of the drippers were clogged, but there is some evidence of dripping based on slight indentations below where the drippers had been dripping.

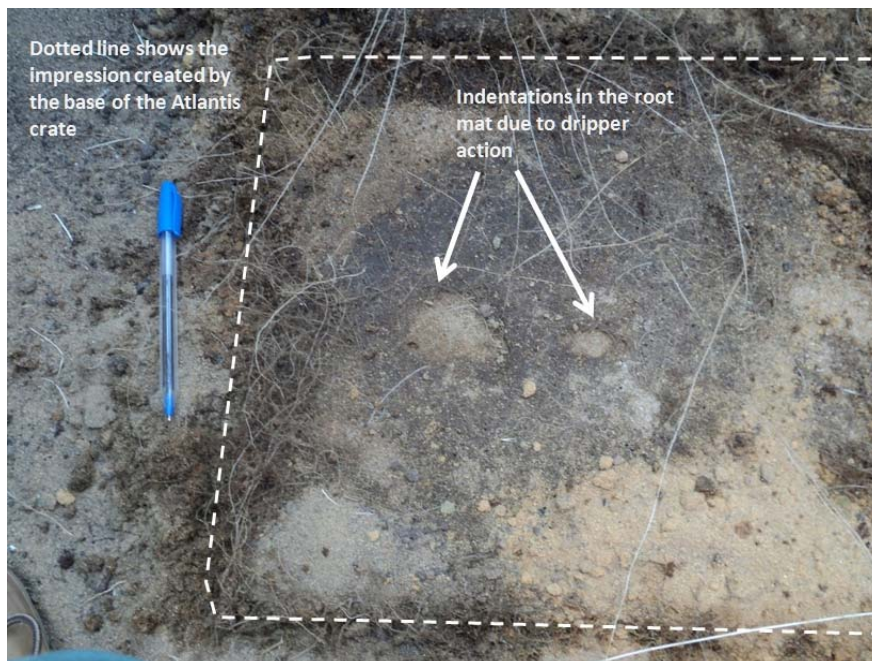


Figure 91 View of the soil layer below one of the crates.

We tried dye staining on day 2, but as the dye concentration was not strong enough, it had to be repeated on day 3. We cut out the inflow pipe to the gallery to make it possible to lift out the crates and sample sediments below them.

Sediments were sampled for soil moisture content. These were from the eastern sidewall of the trench at different depths relative to the top of the gallery. We commenced collection of samples for microbial analysis from beneath Atlantis® crate #2 relative to the south end. As shown in Figure 92 below Crate #2, the root mat was very thin (several mm).

Soil samples for other analyses were taken successively deeper below this location. The depth intervals for sampling were 0.5- 1 cm; 1-2 cm, 2-5 and 5-10. A microbial sample was collected at 5-10 cm. The soil was very mottled with organic material (Figure 93). The mottling disappeared at 8 cm depth below Crate #2.



Figure 92 Root mat sample collected for microbial analysis.



Figure 93 Discolouring or mottled appearance of soil below the gallery.

A similar set of samples were collected near the north end, below Crate #5 relative to the south end. The 5 cm x 5 cm section of root mat was taken approximately 16 cm south of Crate #5's north end and roughly the north-south mid-line of the crate. There appeared to be a greater amount of root growth at the north end compared to the south. The mottling disappeared at 4 cm depth below Crate #5. The depth intervals for sampling were 0.5- 1 cm; 1-2 cm, 2-5 and 5-10. A microbial sample was collected at 5-10cm.

During the excavation, we noticed wetter soil adjacent to, but above the base of the gallery. The height was about 20 cm above the base.

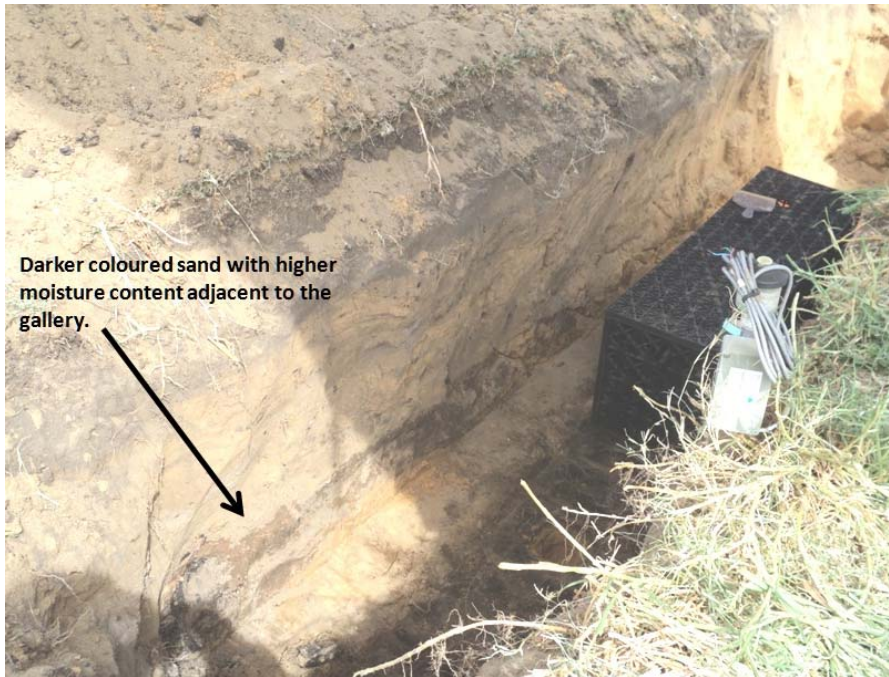


Figure 94 Variations in soil moisture content observed during excavation to remove the gallery.

On Day 3 (13/3/2014) of dismantling the site, 5 Litre of a 1 g/L Brilliant blue dye solution were applied via watering can in approximately 5 minutes: 40 seconds. We did not try to get the rate to be exactly like the previously applied rate of wastewater, which was on the order of 4.3 L/minute. The dye was applied to the area below Crate #4. After dye application, slices of soil were progressively removed from the north-facing wall, which immediately revealed a tree root and organic debris that was likely pre-existing and unrelated to wastewater. We took slices from the east-facing wall to try to avoid the tree root. It appears that matrix flow rather than preferential flow existed. The presence of the root did not enhance flow. Although flow appears to be predominantly vertical, there is some evidence of lateral from away from the east and west sides of Crate #4, but it was not possible to quantify the relative amount of lateral versus vertical flow as it may have depended on the distribution and quantity of dye applied over the surface.



Figure 95 Dye-stained surface showing darker coloured soil due to organic debris and fairly uniform (matrix) flow in the vertical direction.



Figure 96 Close-up view of the dye-stained profile looking south, following application of dye to the base of the gallery. Note the movement of dye laterally away to the east.

Appendix 3 Soil water retention characterisation of Spearwood Sand for the Floreat MAR site

Table 19 Bulk density and soil moisture retention characteristics for Spearwood Sand samples collected from the Floreat Infiltration Gallery site. Soil analyses were conducted by the University of Western Australia.

Sample ID	Sample Location and depth relative to the base of the gallery	Bulk density (g cm ⁻³)	Soil moisture retention characteristics					
			0.1 kPa	5 kPa	10 kPa	35 kPa	100 kPa	200 kPa
1a	Gallery South (0 to 10 cm)	1.504	0.4263	0.3884	0.1922	0.1544	0.0749	0.0332
1b		1.530	0.4091	0.3849	0.1968	0.1466	0.0730	0.0325
1c		1.531	0.3819	0.3700	0.1987	0.1427	0.0687	0.0326
2a	Gallery South (10 to 20 cm)	1.529	0.3599	0.3492	0.2070	0.1971	0.0521	0.0332
2b (repetition)		1.531	0.3768	0.3745	0.3373	0.0699	0.0509	0.0397
2c		1.530	0.4593	0.4084	0.2820	0.1196	0.0466	0.0321
3a	Gallery South (20 to 30 cm)	1.529	0.3623	0.3439	0.2645	0.0761	0.0435	0.0342
3b		1.536	0.3645	0.3486	0.2608	0.0713	0.0435	0.0318
3c		1.533	0.3681	0.3503	0.2512	0.0890	0.0460	0.0304
4a	Gallery South (50 to 100 cm)	1.529	0.3752	0.3523	0.2138	0.1176	0.0459	0.0332
4b		1.529	0.3438	0.3404	0.2417	0.0722	0.0441	0.0326
4c		1.530	0.3479	0.3364	0.2420	0.0782	0.0460	0.0401
5a	Gallery North (0 to 10 cm)	1.530	0.4094	0.4000	0.2303	0.2601	0.0521	0.0341
5b		1.529	0.3747	0.3600	0.2632	0.1819	0.0677	0.0472

5c		1.529	0.3983	0.3968	0.2296	0.1615	0.0719	0.0375
6a	Gallery North (10 to 20 cm)	1.530	0.4194	0.4345	0.3985	0.0807	0.0571	0.0474
6b		1.529	0.3408	0.4109	0.3753	0.0953	0.0664	0.0546
6c		1.529	0.3620	0.3740	0.3464	0.0799	0.0588	0.0478
7a	Gallery North (20 to 30 cm)	1.533	0.3434	0.3428	0.3192	0.0655	0.0468	0.0387
7b		1.529	0.3469	0.3510	0.3270	0.0657	0.0484	0.0396
7c		1.536	0.3444	0.3606	0.3319	0.0687	0.0525	0.0425
8a	Gallery North (50 to 100 cm)	1.531	0.3320	0.3474	0.3178	0.0726	0.0529	0.0401
8b		1.531	0.3243	0.3488	0.3203	0.0715	0.0511	0.0396
8c		1.530	0.3514	0.3599	0.3300	0.0769	0.0521	0.0417
9a	Adjacent South (0 to 10 cm)	1.466	0.3559	0.3673	0.3349	0.0580	0.0431	0.0352
9b		1.467	0.3671	0.3815	0.3207	0.0546	0.0404	0.0327
9c		1.463	0.3651	0.3747	0.3492	0.0594	0.0442	0.0347
10a	Adjacent South (10 to 20 cm)	--	0.3957	0.3719	0.2155	0.1055	0.0482	0.0300
10b		1.466	0.4011	0.3679	0.2080	0.1215	0.0481	0.0298
10c		1.463	0.4001	0.3714	0.2083	0.1050	0.0446	0.0321
11a	Adjacent South (20 to 30 cm)	1.529	0.3750	0.3647	0.2273	0.1022	0.0484	0.0411
11b		1.529	0.3948	0.3701	0.2279	0.1039	0.0467	0.0438
11c		1.529	0.3891	0.3697	0.2242	0.0970	0.0471	0.0318
12a	Adjacent North (0 to 10 cm)	1.464	0.4352	0.3979	0.2288	0.1136	0.0633	0.0343
12b		1.464	0.4607	0.4419	0.2568	0.1057	0.0459	0.0329
12c		1.466	0.3697	0.3579	0.2282	0.0576	0.0447	0.0320
13a	Adjacent North (10 to 20 cm)	1.467	0.4127	0.3812	0.2339	0.1028	0.0477	0.0363
13b		1.468	0.4019	0.3755	0.2193	0.0986	0.0503	0.0359
13c		1.465	0.4017	0.3724	0.2387	0.1251	0.0527	0.0384

14a	Adjacent North (20 to 30 cm)	1.461	0.4141	0.4009	0.2442	0.1447	0.0499	0.0293
14b		1.465	0.3886	0.3630	0.2245	0.1050	0.0506	0.0332
14c		1.466	0.4002	0.3630	0.2034	0.1354	0.0472	0.0318

Table 20 Summary of statistical P values from performing paired Student's t-test on groups of soil moisture retention characteristics from fourteen sampled locations at the Floreat infiltration gallery site, post-experiment. Abbreviations: G=Gallery; N=North; S=South; Adj=Adjacent; depth intervals relative to the base of the gallery.

	G_S 0-10 cm	G_S 10-20 cm	G_S 20-30 cm	G_S 50-100 cm	G_N 0-10 cm	G_N 10-20 cm	G_N 20-30 cm	G_N 50-100 cm	Adj_S 0-10 cm	Adj_S 10-20 cm	Adj_S 20-30 cm	Adj_N 0-10 cm	Adj_N 10-20 cm	Adj_N 20-30 cm
G_S 0-10 cm														
G_S 10-20 cm	0.76													
G_S 20-30 cm	0.37	0.03												
G_S 50-100 cm	0.19	0.02	0.45											
G_N 0-10 cm	0.24	0.51	0.15	0.07										
G_N 10-20 cm	0.60	0.51	0.08	0.12	0.90									
G_N 20-30 cm	0.77	0.44	0.52	0.48	0.44	0.01								
G_N 50-100 cm	0.76	0.42	0.53	0.47	0.42	0.02	0.90							
Adj_S 0-10 cm	0.88	0.60	0.39	0.40	0.55	0.00	0.45	0.53						
Adj_S 10-20 cm	0.19	0.17	0.60	0.30	0.11	0.33	0.95	0.96	0.81					
Adj_S 20-30 cm	0.35	0.10	0.45	0.11	0.14	0.27	0.94	0.95	0.78	1.00				
Adj_N 0-10 cm	1.00	0.67	0.20	0.13	0.48	0.48	0.70	0.69	0.83	0.20	0.20			
Adj_N 10-20 cm	0.68	0.29	0.24	0.08	0.25	0.40	0.83	0.82	0.99	0.07	0.07	0.47		
Adj_N 20-30 cm	0.58	0.32	0.32	0.12	0.15	0.44	0.84	0.83	0.98	0.06	0.24	0.65	0.96	

Appendix 4 Appearance of SAT basins over time

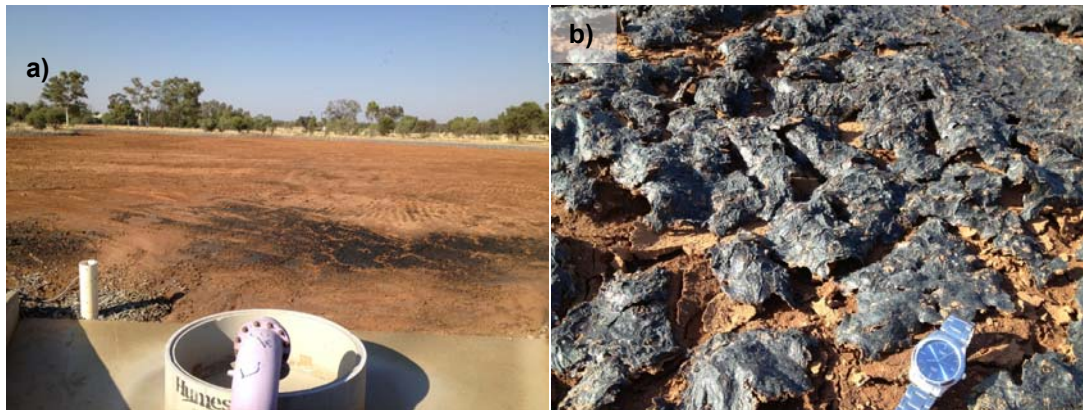


Figure 97 Basin E after the first infiltration event in 2012 showing a) the recharge water inlet and a pipe where the pressure transducer is installed and b) a black substance on the soil attributed to the presence of a water treatment polymer (photo 23/10/2012).



Figure 98 The inlet and pipes distributing recharge water in Basin A, which is covered with self-seeding Love Grass (*Eragrostis spectabilis*) (photo 23/10/2012).

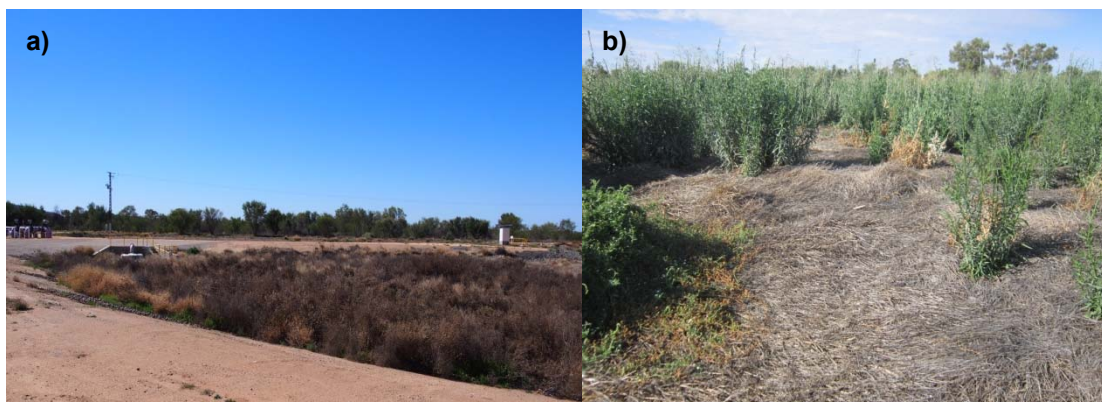


Figure 99 Vegetation in Basin D a) ~1.5 m high woody vegetation in July 2013 and b) spreading vegetation with channels forming in between for water flow in November 2013.

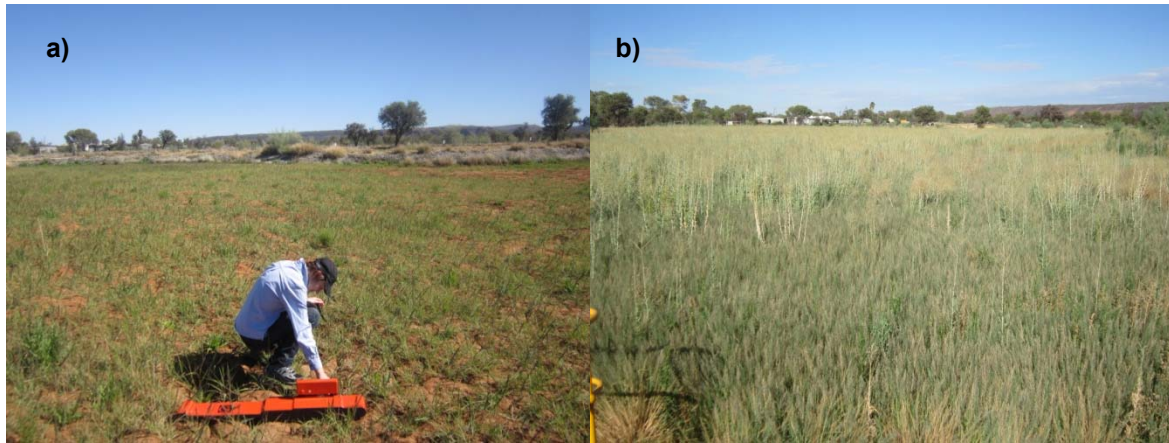


Figure 100 Basin B vegetation cover a) July 2013 b) November 2013.

Appendix 5 Guidance of SAT Basin operation (Breton 2009)

Breton (2009) provided guidance on the appearance of the basin surface prior to recharge (Figure 101-Figure 104).

	
<p>Figure 101 Best bed surface. Bare dry soil to 3 cm depth – deep cracking (Breton 2009).</p>	<p>Figure 102 Acceptable bed surface. Bare dry soil to 3 cm depth – small cracking – complete crumbling of clogging layer to brownish thin material (Breton 2009).</p>
	
<p>Figure 103 Tolerable bed surface. Bare dry soil to 3 cm depth – complete crumbling of clogging layer to flaky thin greenish material (Breton 2009).</p>	<p>Figure 104 Inadequate bed surface. Inefficient cracking – thick white greenish algae with fibrous texture that do not break down or crumble during drying period and cover most of the basin area – soil moist for extended periods (Breton 2009).</p>

Appendix 6 Geophysics results SAT basins

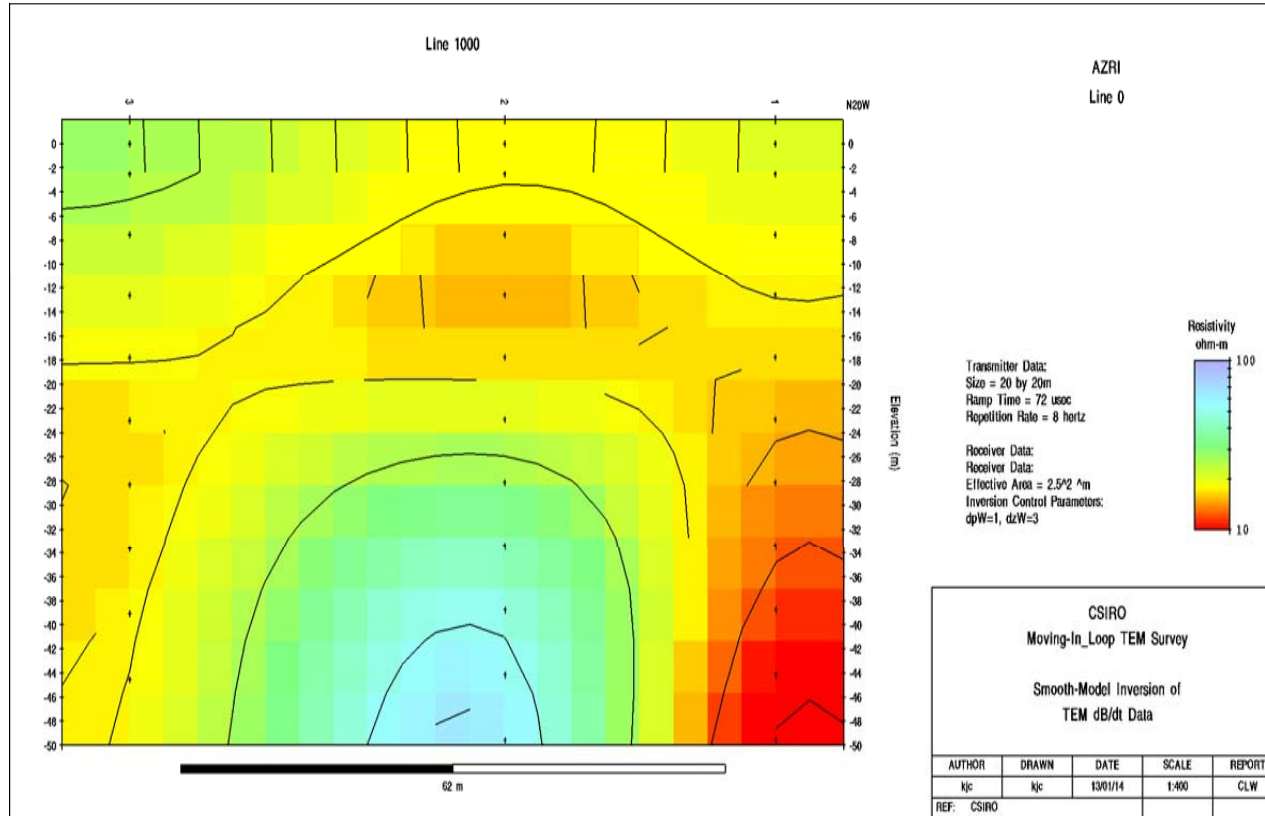


Figure 105 2013 Basin A (line 1000) 3 x 20m NanoTEM stations.

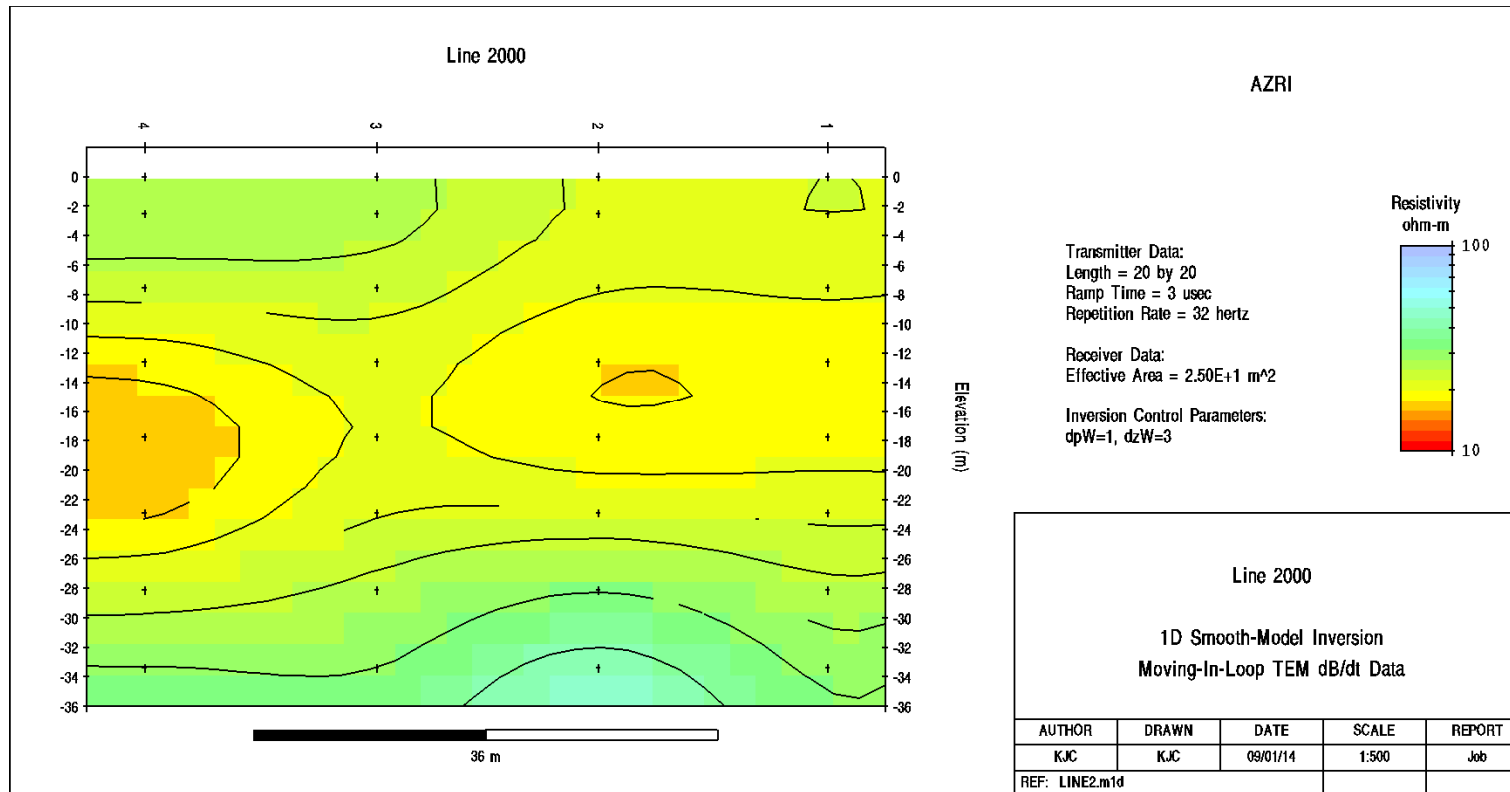


Figure 106 2013 Basin E (line 2000) 4 x 20m NanoTEM stations.

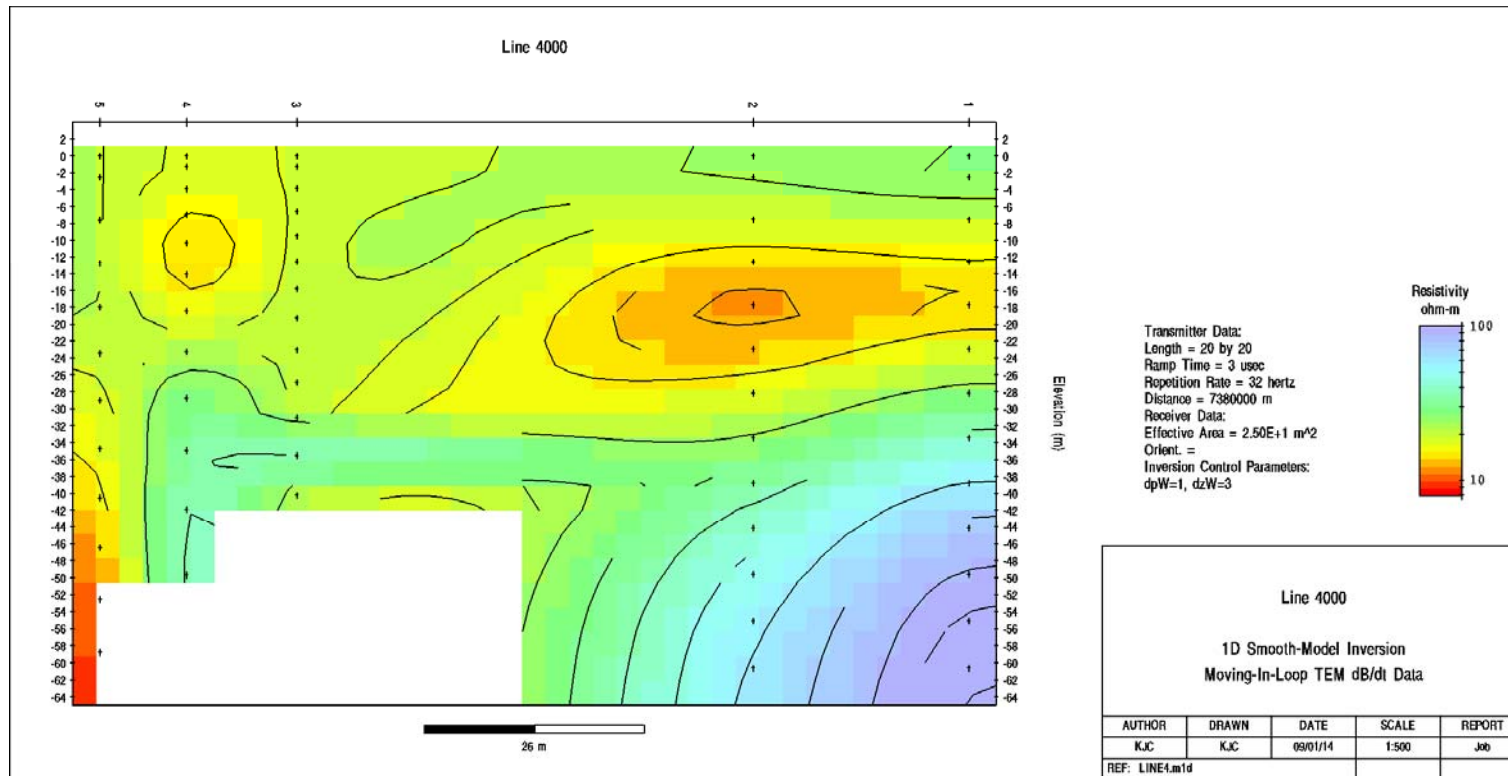


Figure 107 2013 Basin C (line 4000) 2 x 20m and 3 x 10m NanoTEM stations.

2013 approximately 200m down-gradient, near bore RN17942 (line 4000) 1 X 20m NanoTEM station; raw data not converted.

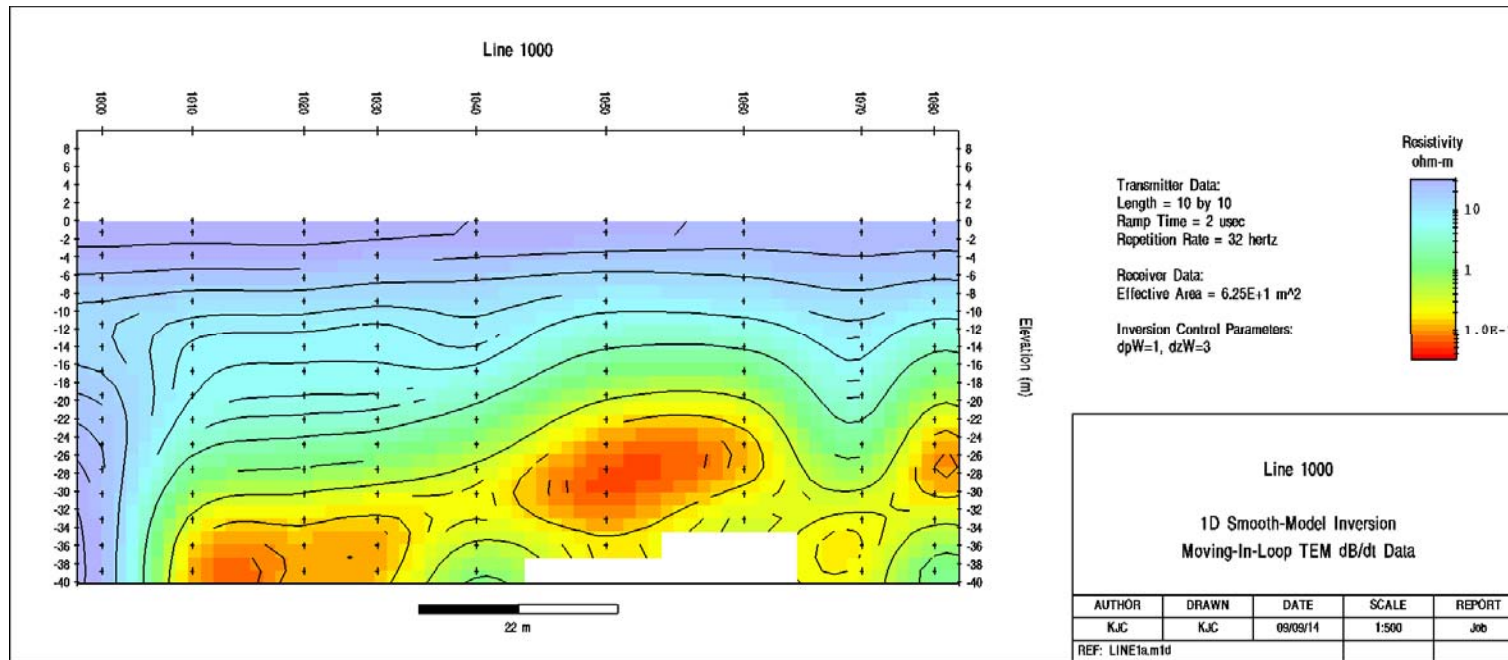


Figure 108 2014 Basin A (line 1000) 10 x 10m NanoTEM stations.

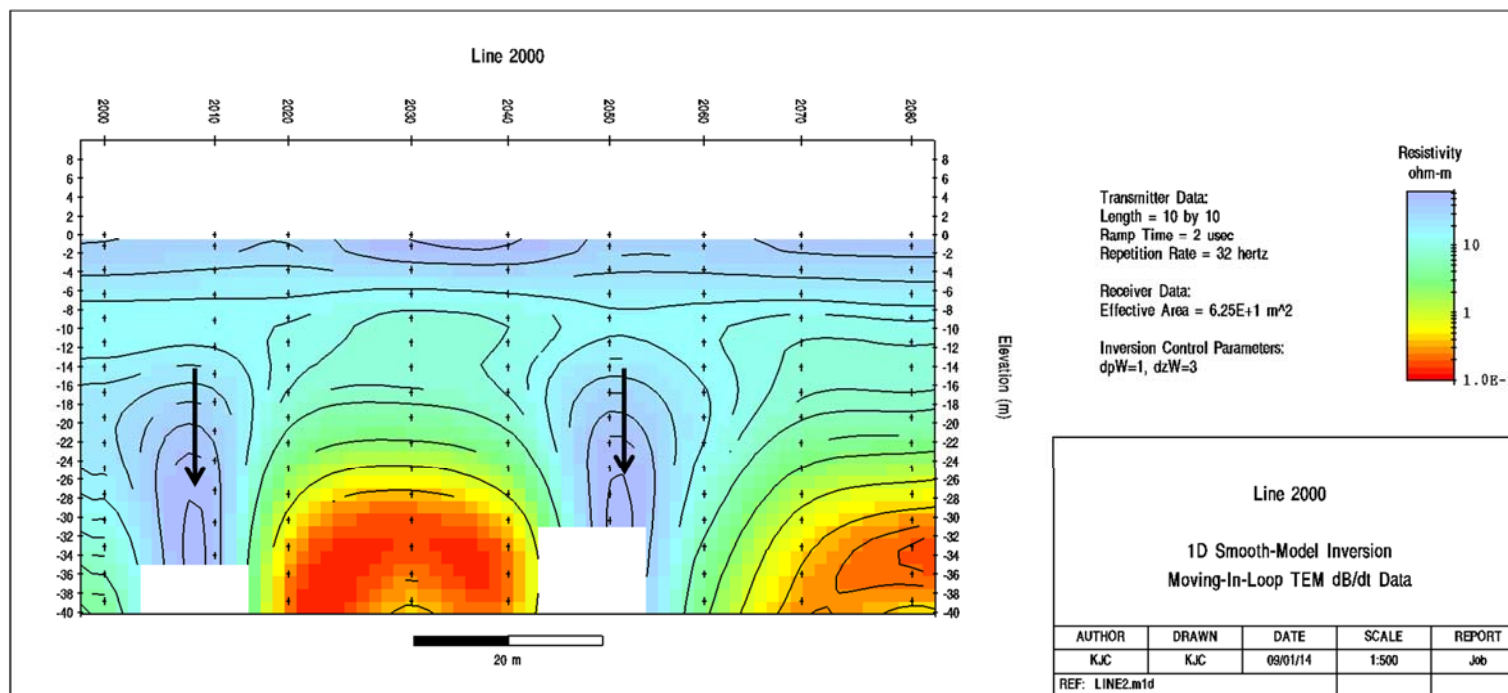


Figure 109 2014 Basin B (line 2000) 9 x 10m NanoTEM stations.

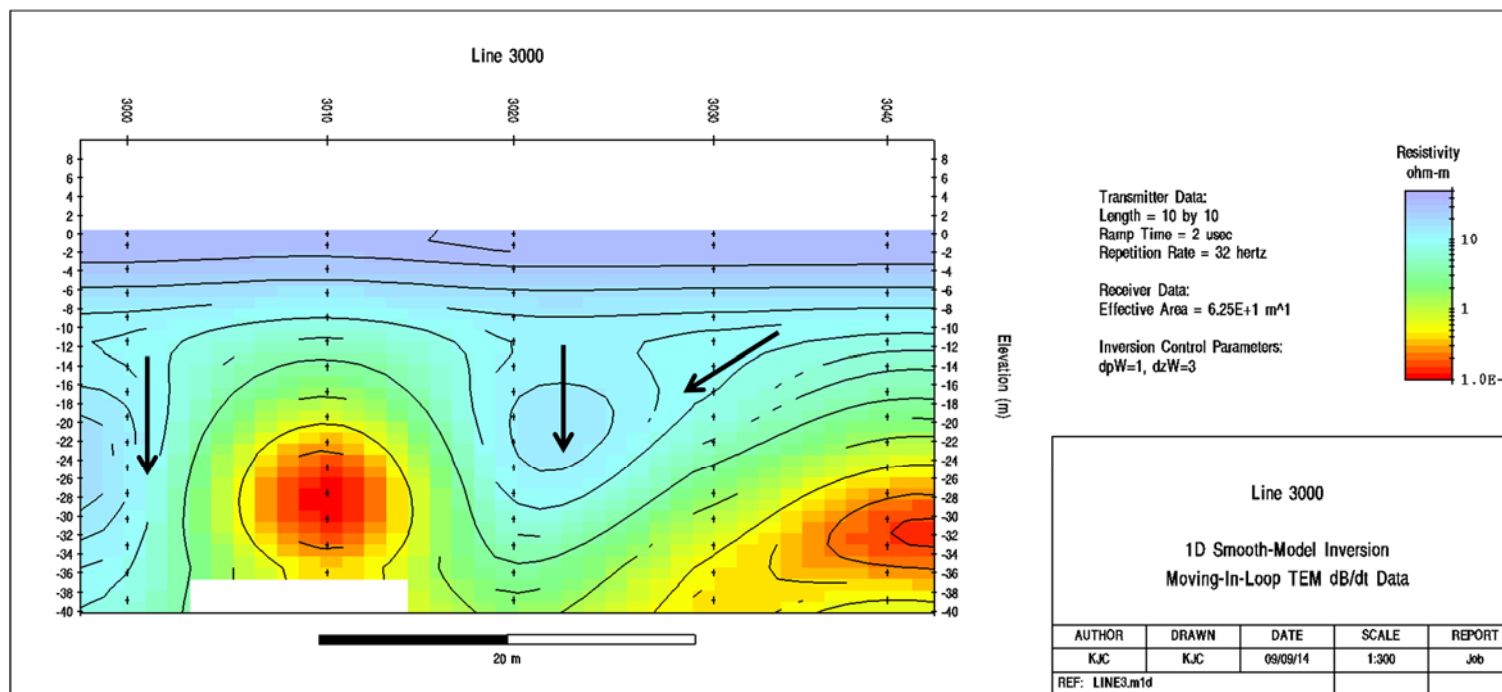


Figure 110 2014 Basin D (line 3000) 5 x 10m NanoTEM stations.

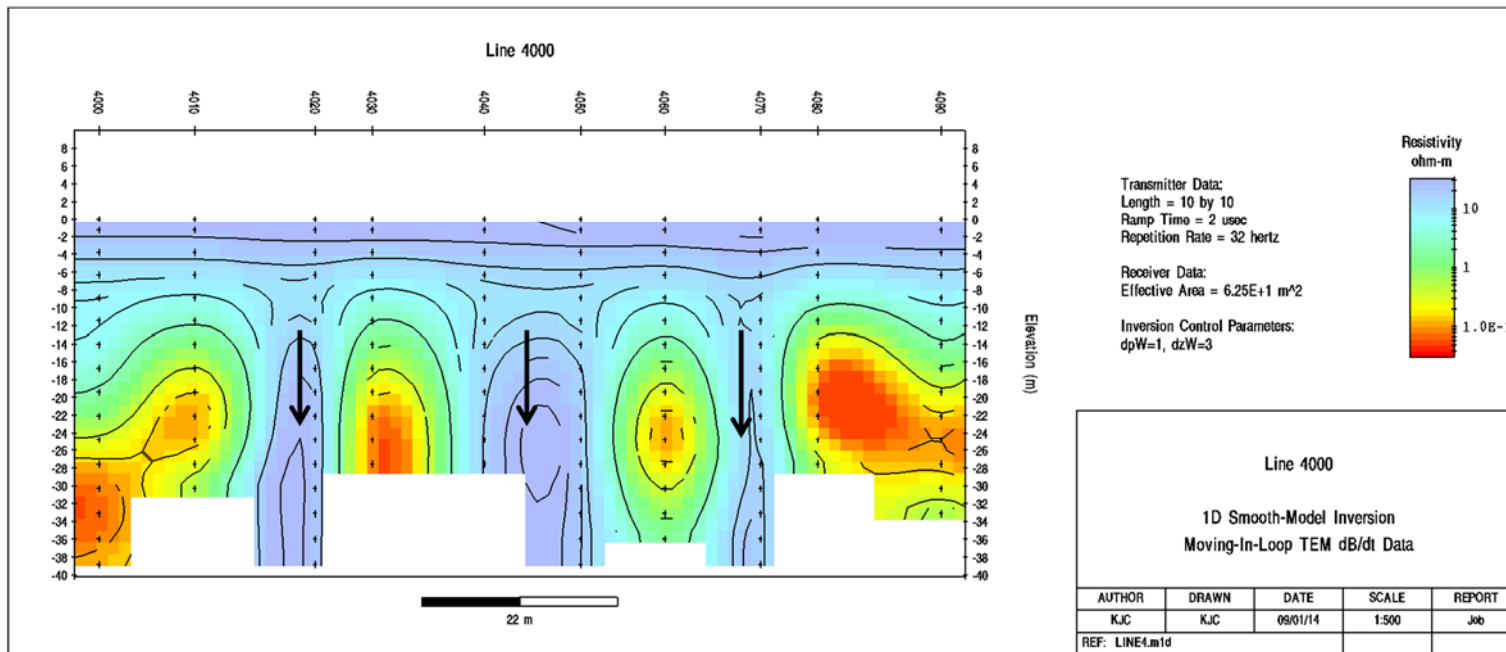


Figure 111 2014 Basin E (line 4000) 10 x 10m NanoTEM stations.

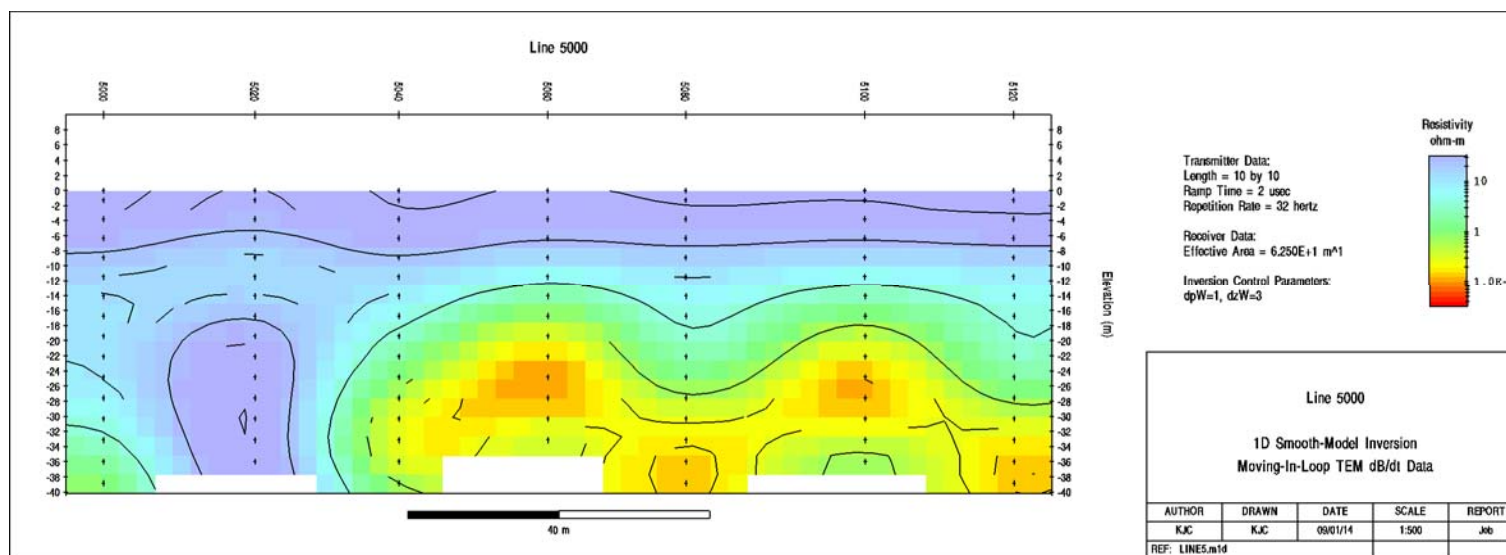


Figure 112 2014 approximately 500m down-gradient, near bore RN17999 (line 5000) 7 x 20m NanoTEM stations.

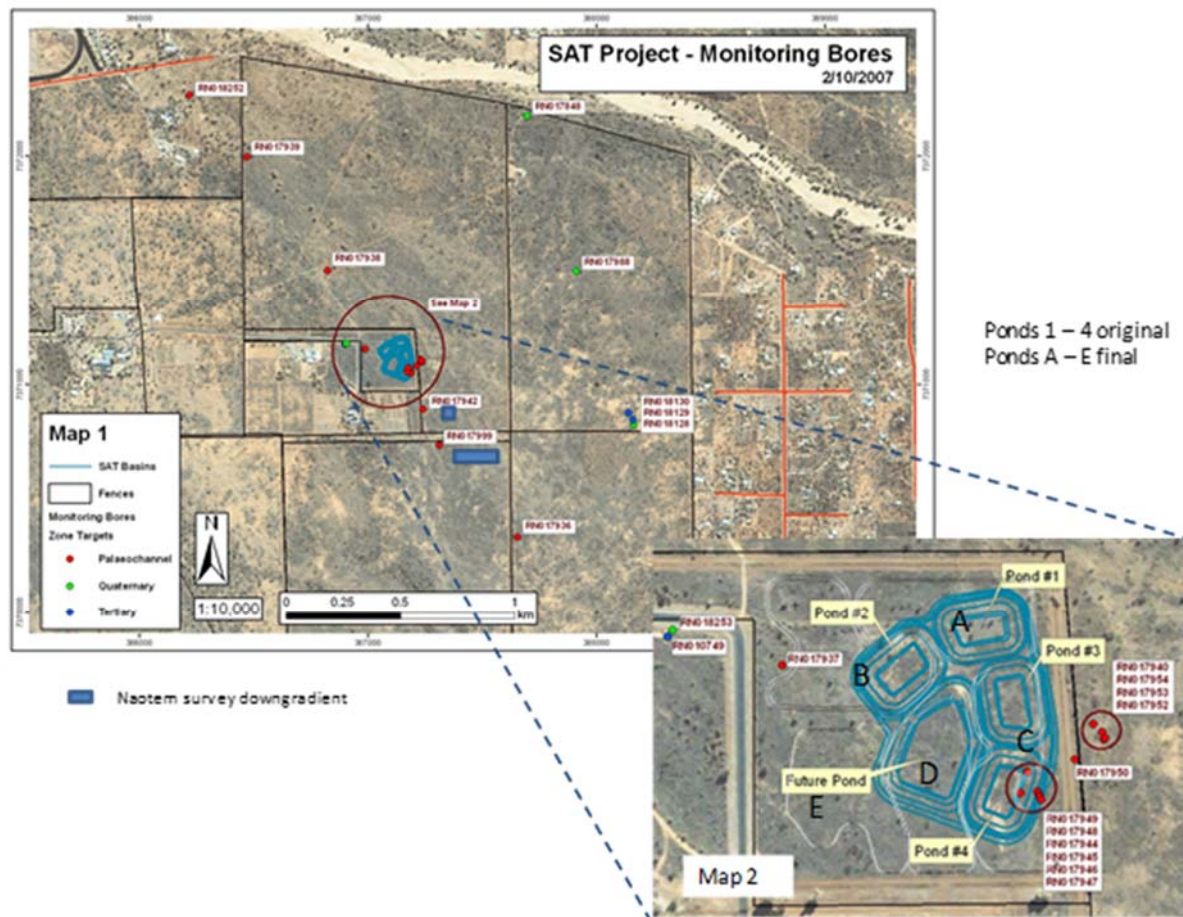


Figure 113 Map of project monitoring bores and locations of down-gradient NanoTEM survey